

Copyright is owned by the Author of the thesis. Permission is given for a copy to be downloaded by an individual for the purpose of research and private study only. The thesis may not be reproduced elsewhere without the permission of the Author.

**Functionalised Polythiophenes:
Synthesis, Characterisation and
Applications**

Amy Marisa Ballantyne

2005

Functionalised Polythiophenes: Synthesis, Characterisation and Applications

A thesis presented in partial fulfilment of the
requirements for the degree of

Doctor of Philosophy

in

Chemistry

at Massey University, Palmerston North
New Zealand

Amy Marisa Ballantyne

2005

Abstract

Conducting polymers display properties such as high conductivity, light weight and redox activity giving them great potential for use in many applications. Polythiophenes have proved to be particularly useful because they are readily functionalised and have good chemical stability. The purpose of this work was to investigate the effect of electron-withdrawing and electron-donating substituents on the synthesis and properties of polythiophenes.

Initial work entailed the synthesis of a series of styryl-substituted terthiophenes. Polymerisation of these materials using both chemical and electrochemical methods was found to produce predominantly short chain oligomers ($n < 4$) and insoluble material that could not be further processed.

An analogous series of styryl-substituted terthienylenevinylene materials were electrochemically oxidised for comparison to the terthiophene series. These materials were also found to produce predominantly dimer and short oligomers, but with the expected higher conjugation length than the corresponding terthiophene oligomers.

To enhance polymerisation and increase the solubility of the resulting materials, the polymerisation of styryl-terthiophenes with alkyl and alkoxy functionalities was investigated. The properties of the resulting polymeric materials were determined using electrochemistry, mass spectrometry, spectroscopy and microscopy. The alkoxy substituted polymer was found to have a longer average polymer length than the corresponding alkyl derivative ($\sim n = 11$ compared to $\sim n = 6$), but was less soluble (78% compared to 100%). It was found, however, that by increasing the alkoxy chain length from 6 carbons to 10 carbons, the solubility of the polymer could be increased to 97% without affecting the average polymer length. The alkoxy-substituted polymers were observed to be very stable in the oxidised, conducting state compared to the alkyl-substituted polymer, which appeared to be more stable in the neutral, non-conducting state. It was found that these soluble materials could be separated into

fractions of different length polymers by using sequential soxhlet extractions in different solvents.

Preliminary investigations were made into the suitability of these soluble oligomeric and polymeric materials for use in photovoltaic, actuator and organic battery applications and promising results were achieved for actuator and battery functions. In addition, the solubility of these materials allowed nano- and micro-structured fibre and fibril surfaces to be prepared for use in high surface area electrodes.

Acknowledgements

The last three years has been a journey on which I have met and worked with so many fantastic people and friends. I would like to take this opportunity to acknowledge these people who have generously given me their time, moral support and financial assistance.

Firstly, I would like to thank my supervisors Professor David Officer and Associate Professor Simon Hall. David, you have always been supportive and encouraging to me. Even with your hectic schedule, you have made time to see me and I really appreciate this. Simon, I am very grateful for your time and assistance, particularly during the arduous writing process. I would also like to acknowledge my '3rd' (lab) supervisor, Dr. Warwick Belcher, who started me off on this project and familiarised me in the lab.

I would like thank the Institute of Fundamental Sciences, Massey University, the Nanomaterials Research Centre, Massey University and the MacDiarmid Institute for Advanced Materials and Nanotechnology for my scholarships and funding for this project.

To the members of the NRC, past and present: Shannon Bullock, Wayne Campbell, Beatrice Eccles, Sonja Ensink, Sanjeev Gambhir, Daina Grant, Susan Habas, Ken Jolley, Fabio Lodato, Donna Macpherson, Giovanna Moretto, Yvonne Ting, Mark Vigneswaren, Klaudia Wagner, Pawel Wagner and Amy Watson. You have all helped me in some way, from synthesising materials used in this project, to advice, support and encouragement. Thank you.

I would like to thank the members of the IPRI at the UOW for their time and assistance, namely Professor Gordon Wallace, Chee Too, Caiyun Wang, George Tsekouras, Yanzhe Wu (Richard), Violeta Misoska, Phil Smugreski, Jun Chen and Peter Innis. I was always made to feel welcome and 'one of the bunch'.

I would like to thank Dr. Paul Dastoor and Chris McNeill at the University of Newcastle for their time, expertise and hospitality.

I would like to thank Doug Hopcroft at HortResearch for taking SEM images of my samples, Keith Gordon and Tracey Clarke from the University of Otago for useful discussions on computational chemistry of the compounds used in this study, and all the Massey University IFS staff for their help during the last few years.

Thank you to my friends, flatmates and family who have graciously accepted the emotional effects of the ups and downs of research and have supported me throughout. In particular, thank you to Graeme Ballantyne, Ingrid Dunckley and Giovanna Moretto for proof reading. A special thank you also to David Sherwin, who picked me up at the end of my first year, got me on track and supported me right to the end.

Finally, I would like to thank my parents, Graeme and Deborah Ballantyne, for the inspiration to start this project and the love and support to finish it. I love you both very much. 😊

Table of Contents

ABSTRACT	i
DECLARATIONS	iii
ACKNOWLEDGEMENTS	vi
TABLE OF CONTENTS	viii
LIST OF FIGURES	xii
LIST OF TABLES	xxv
LIST OF SYMBOLS	xxvi
LIST OF ABBREVIATIONS	xxviii
MONOMER ABBREVIATIONS	xxx

CHAPTER 1

INTRODUCTION.....	1
1.1 INTRODUCTION	1
1.2 CONDUCTING POLYMERS	2
1.3 THIOPHENE BASED POLYMERS	7
1.3.1 Polymerisation	7
1.3.2 Polymerisation methods	11
1.3.3 Effect of substituents on polythiophenes properties	13
1.3.4 Styryl-substituted polythiophenes	15
1.3.5 Alkyl and alkoxy substituents	18
1.3.6 Thienylenevinylene based conducting polymers.....	21
1.4 SCOPE OF WORK.....	22

CHAPTER 2

EXPERIMENTAL METHODS.....	23
2.1 ELECTROCHEMICAL TECHNIQUES	23
2.1.1 Introduction	23
2.1.2 Cell design.....	23
2.1.3 Electrochemical techniques	27
2.2 MALDI-TOF MASS SPECTROMETRY	33
2.2.1 Introduction	33
2.2.2 Instrumentation.....	33
2.2.3 Data acquisition and sample preparation.....	37

2.2.4	<i>Calculation of polydispersity</i>	39
2.3	¹ H NMR SPECTROSCOPY	40
2.4	UV-VIS-NIR SPECTROSCOPY	42
2.5	IMAGING TECHNIQUES	44
2.6	DEPOSITION TECHNIQUES.....	45
2.7	ELECTROSPINNING.....	47
2.8	PHOTOVOLTAICS DEVICES	48

CHAPTER 3

SYNTHESIS AND POLYMERISATION OF A SERIES OF STYRYL-SUBSTITUTED TERTHIOPHENES

50

3.1	INTRODUCTION	50
3.2	SYNTHESIS OF MONOMERS	52
3.3	POLYMERISATION USING CHEMICAL OXIDATION.....	53
3.3.1	<i>Polymerisation and reduction methods</i>	53
3.3.2	<i>Characterisation of soluble fractions</i>	55
3.3.3	<i>Attempted purification of dimer</i>	58
3.3.4	<i>Conclusions</i>	62
3.4	POLYMERISATION USING ELECTROCHEMICAL METHODS	63
3.4.1	<i>Introduction</i>	63
3.4.2	<i>Electrochemical growth</i>	63
3.4.3	<i>Characterisation of electrochemically deposited materials</i>	71
3.4.3.1	<i>Electrochemical characterisation</i>	71
3.4.3.2	<i>Analysis by UV-VIS-NIR spectroscopy</i>	79
3.4.3.3	<i>Scanning electron microscopy (SEM)</i>	85
3.5	CONCLUSIONS	90
3.6	EXPERIMENTAL.....	91
3.6.1	<i>Reagents and materials</i>	91
3.6.2	<i>Synthesis of styryl-substituted terthiophene</i>	91
3.6.3	<i>Polymerisation of styryl-substituted terthiophene monomers</i>	95
3.6.4	<i>Electrochemical synthesis</i>	97
3.6.5	<i>MALDI-TOF MS</i>	98
3.6.6	<i>UV-VIS-NIR spectroscopy</i>	99
3.6.7	<i>¹H NMR spectroscopy</i>	99
3.6.8	<i>SEM imaging</i>	99

CHAPTER 4

ELECTROCHEMICAL POLYMERISATION OF A SERIES OF STYRYL-SUBSTITUTED TERTHIENYLENEVINYLENES

100

4.1	INTRODUCTION	100
4.2	ELECTROCHEMICAL DEPOSITION	102
4.3	CHARACTERISATION OF FILMS	106
4.3.1	<i>MALDI-TOF MS characterisation</i>	106
4.3.2	<i>Cyclic voltammetry</i>	106
4.3.3	<i>UV-VIS-NIR spectroscopy</i>	110

4.4	CONCLUSIONS	116
4.5	EXPERIMENTAL	118
4.5.1	<i>Reagents and materials</i>	118
4.5.2	<i>Synthesis of materials</i>	118
4.5.3	<i>UV-VIS-NIR spectroscopy</i>	119
4.5.4	<i>MALDI-TOF MS</i>	119

CHAPTER 5

POLYMERISATION OF ALKYL- AND ALKOXY-SUBSTITUTED STYRYLTERTHIOPHENES	120
--	-----

5.1	INTRODUCTION	120
5.2	CHEMICAL POLYMERISATION OF OC ₆ DASTT	122
5.2.1	<i>Polymerisation and reduction procedure</i>	122
5.2.2	<i>Characterisation of the soluble fraction of polyOC₆DASTT</i>	124
5.2.3	<i>Improvement of the polyOC₆DASTT soluble fraction</i>	128
5.2.4	<i>Polymer separation according to chain length</i>	129
5.2.5	<i>Conclusions</i>	135
5.3	CHEMICAL POLYMERISATION OF C ₇ DASTT	137
5.3.1	<i>Introduction</i>	137
5.3.2	<i>Polymerisation and reduction</i>	137
5.3.3	<i>Polymer separation according to oligomer length</i>	140
5.3.4	<i>Conclusions</i>	144
5.4	CHEMICAL POLYMERISATION OF OC ₁₀ DASTT	146
5.4.1	<i>Introduction</i>	146
5.4.2	<i>Polymerisation</i>	146
5.4.3	<i>Polymer separation according to oligomer length</i>	151
5.4.4	<i>Conclusions</i>	157
5.5	ELECTROCHEMICAL POLYMERISATION	158
5.5.1	<i>Introduction</i>	158
5.5.2	<i>Electrochemical growth and post-growth analysis of polyC₇DASTT</i>	159
5.5.3	<i>Electrochemical growth and post-growth analysis of polyOC₆DASTT</i>	164
5.5.4	<i>Electrochemical growth and post-growth analysis of polyOC₁₀DASTT</i>	171
5.5.5	<i>Summary of electrochemically polymerised material</i>	181
5.6	CONCLUSIONS	182
5.7	EXPERIMENTAL	185
5.7.1	<i>Reagents and materials</i>	185
5.7.2	<i>Chemical synthesis</i>	185
5.7.3	<i>Electrochemical synthesis</i>	189
5.7.4	<i>MALDI-TOF MS</i>	190
5.7.5	<i>UV-VIS-NIR instrumentation and spectroelectrochemistry</i>	190
5.7.6	<i>SEM imaging</i>	190

CHAPTER 6

DEVICE FABRICATION AND ANALYSIS	192
---------------------------------------	-----

6.1	INTRODUCTION	192
-----	--------------------	-----

6.2	PHOTOELECTROCHEMICAL CELLS	194
6.2.1	<i>Introduction</i>	194
6.2.2	<i>Device assembly and materials</i>	196
6.2.3	<i>NMe₂STT oligomer films</i>	196
6.2.4	<i>PolyOC₁₀DASTT films</i>	198
6.2.5	<i>Styryl thienylenevinylene derivatives</i>	199
6.2.6	<i>Conclusions</i>	203
6.3	ELECTROMECHANICAL ACTUATORS	204
6.3.1	<i>Introduction</i>	204
6.3.2	<i>Testing procedures and terminology</i>	205
6.3.3	<i>Bilayer benders</i>	208
6.3.4	<i>Fibres</i>	215
6.3.5	<i>Free-standing film with incorporated wire</i>	219
6.3.6	<i>Conclusions</i>	224
6.4	BATTERIES	226
6.4.1	<i>Introduction</i>	226
6.4.2	<i>Cell construction, testing procedures and terminology</i>	228
6.4.3	<i>Analysis of electrodes</i>	229
6.4.4	<i>Charge/discharge characteristics</i>	231
6.4.5	<i>Cycle life</i>	233
6.4.6	<i>Conclusions</i>	234
6.5	MICRO- AND NANO-STRUCTURED SURFACES	225
6.5.1	<i>Introduction</i>	235
6.5.2	<i>Fibrils</i>	236
6.5.3	<i>Inverse opal and opal structures</i>	238
6.5.3.1	<i>Introduction</i>	238
6.5.3.2	<i>Platinum inverse opals (honeycomb structure)</i>	239
6.5.3.3	<i>Platinum, gold and ITO opals (bead structure)</i>	239
6.5.3.4	<i>Summary</i>	244
6.5.4	<i>Electrospinning</i>	245
6.5.5	<i>Conclusions</i>	247
6.6	CONCLUSIONS	258
6.7	EXPERIMENTAL PROCEDURES	260
6.7.1	<i>PEC devices</i>	260
6.7.2	<i>Actuator fabrication and experimental procedures</i>	261
6.7.3	<i>Details of battery fabrication and testing procedures</i>	263
6.7.4	<i>Fabrication and evaluation of nanostructures</i>	264

CHAPTER 7

CONCLUSIONS	259
-------------------	-----

BIBLIOGRAPHY	264
--------------------	-----

List of Figures

Number	Description	Page
1.1	A selection of polymers capable of exhibiting conductivity.	2
1.2	Relative conductivities of polythiophene and <i>trans</i> -polyacetylene in doped and undoped states.	3
1.3	Scheme showing the reversible p-doping (oxidation) and n-doping (reduction) redox processes of polythiophene, with the incorporation of required cation/anion species (X^+/A^-) to balance the charge of the polymer matrix.	3
1.4	(a) The semi-conducting, aromatic, neutral chain. (b) Formation of a polaron species. (c) The conducting, quinoidal, bipolaron species formed on further oxidation. $X = NH$ or S , $A^- =$ anion (e.g. Cl^- , ClO_4^-).	4
1.5	Energy level diagram showing the difference in band structure of a conducting polymer in the neutral state, and oxidised state with formation of polaron and bipolaron species.	5
1.6	(a) α/β positions on a thiophene ring, (b) $\alpha - \alpha$ coupling, (c) $\alpha - \beta$ coupling and (d) $\beta - \beta$ coupling.	7
1.7	Proposed mechanism for the polymerisation of thiophene.	8
1.8	Functionalisation of thiophene through the β positions.	8
1.9	Possible regioisomers formed by coupling of two, non-centrosymmetric monomer units: head-to-head (HH), head-to-tail (HT) and tail-to-tail (TT).	10
1.10	Examples of (a) regioregular and (b) regiorandom functionalised polythiophenes.	10
1.11	Potentiodynamic growth of terthiophene on a platinum disc electrode ($SA = 1.8 \text{ mm}^2$). Supporting electrolyte: 0.1 M TBAP/AN. Potential limits: 0/+900 mV. 9 cycles. Scan rate: 100 mV s^{-1} .	12
1.12	Synthetic polymerisation of functionalised thiophene using the grignard method.	12
1.13	Oxidative polymerisation of functionalised thiophene using iron(III) chloride.	13
1.14	Examples of (a) alkyl and (b) alkoxy spacers used to reduce steric hindrance of functional groups between thiophene units.	15
1.15	3-Aryl substituted polythiophene.	15
1.16	Styryl-substituted thiophene monomers investigated by Cutler.	16
1.17	Polyterthiophene functionalised through a vinyl linker.	17
1.18	Synthesis of vinyl-substituted terthiophene using Wittig reactions. $R = Ph-R$. $X = Br, Cl$ or I .	17

1.19	Examples of (a) crown ether and (b) polyether substituted styryl-terthiophene derivatives investigated by Grant.	17
1.20	(a) Terthiophene substituted with a tetraphenyl porphyrin (TPP) via a vinyl linker and (b) nitro-substituted styrylterthiophene synthesised and investigated by Cutler.	18
1.21	Supramolecular assembly of 3-hexylthiophene by interdigitation of alkyl chains.	19
1.22	Alkoxy substitution in the (a) 3,3''-positions and (b) 4,4''-positions on terthiophene monomers.	20
1.23	Thienylenevinylene derivatives. (a) poly(thienylenevinylene) and (b) poly(terthienylene-vinylene).	21
1.24	Styryl-substituted terthiophene ($m = 0$) and terthienylenevinylene ($m = 1$) materials investigated in this study.	22
2.1	Schematic of a three-electrode one compartment cell.	24
2.2	Illustration showing the linear and radial diffusion fields produced at standard electrodes ($SA: > 100 \mu\text{m}^2$) and disc microelectrodes.	25
2.3	Schematic of the Ag/0.01 M AgNO ₃ reference electrode and TBAP/AN salt bridge used in this study.	26
2.4	Variation of potential with time for cyclic voltammetry.	28
2.5	A CV of ferrocene, demonstrating a single reversible electron transfer process	28
2.6	Potentiodynamic growth of terthiophene on a platinum disc electrode ($SA = 1.8 \text{ mm}^2$). Supporting electrolyte: 0.1 M TBAP/AN. Potential limits: 0/+900 mV. 9 cycles. Scan rate: 100 mV s^{-1} .	29
2.7	Post-growth CV of OC ₁₀ DASTT on a Pt micro electrode ($SA: 10 \mu\text{m}^2$). Electrolyte solution: 0.1 M TBAP 1:1 AN:DCM. Potential limits: -500/+800 mV. Scan rate: 100 mV s^{-1} .	31
2.8	(a) A chronoamperogram with (b) the corresponding function of potential versus time.	32
2.9	Potentiostatic growth of polySTT on a Pt micro electrode ($SA: 10 \mu\text{m}^2$). Solvent: 1:1 AN:DCM. Potential held at -500 mV for 1 s, then stepped to 900 mV for 19 seconds.	32
2.10	Schematic of MALDI-TOF MS instrumentation.	34
2.11	Schematic illustrating the difference between the (a) linear and (b) reflection modes used in MALDI-TOF MS.	35
2.12	MALDI-TOF mass spectra of a poly(OC ₁₀ DASTT) sample (monomer $M_r = 662.48 \text{ g mol}^{-1}$). (a) Measured using reflectron mode. (b) Measured using linear mode. (c) Enlargement of a peak generated by the linear mode.	36
2.13	Dimerisation of terthiophene showing the loss in terminal protons.	40

2.14	Dimerisation of STT to form three different possible regioisomers: the HH isomer (generated by coupling through the 5 positions), HT isomer (coupling through the 5 and 5'' positions) and TT isomer (coupling through the 5'' positions).	41
2.15	Spectroelectrochemistry of 4,4''-bis(decyloxy-3'-nitro-2,2':5',2'')terthiophene obtained by Gambhir <i>et al.</i> ³¹ Reprinted by permission. A free-carrier tail is displayed at wavelengths above 700 nm.	43
2.16	Experimental setup for electrospinning.	47
2.17	Schematic diagram of a typical polymer photoelectrochemical cell structure consisting of an ITO/polymer/electrolyte/Pt sandwich structure. The interface between the polymer and liquid electrolyte are explicitly included to illustrate that the photovoltage is generated by the difference in standard electrode potential (work function) between the ITO-polymer interface and the polymer-electrolyte interface. Irradiation of the semiconducting polymer results in the formation of an exciton, which is separated at an interface. Reprinted with permission	48
2.18	Typical <i>I</i> - <i>V</i> curve of a photovoltaic device. <i>I</i> _{sc} is the short circuit current and <i>V</i> _{oc} is the open circuit voltage. <i>I</i> _{pp} is the current at peak power and <i>V</i> _{pp} is the voltage at peak power.	49
3.1	Substituents linked by (a) phenyl and (b) styryl moieties to polythiophene.	50
3.2	Structures of the five styryl-substituted terthiophene monomer derivatives investigated in this study.	51
3.3	Wittig reaction between a terthiophene aldehyde and phenyl substituted phosphonium salt for the synthesis of the substituted styrylterthiophene monomers used in this study.	52
3.4	Reaction procedure employed for the chemical polymerisation of styryl-substituted terthiophene derivatives.	53
3.5	The reversible doping (by iron(III) chloride or copper perchlorate) and dedoping (by washing with water or hydrazine) process of the polymer.	54
3.6	MALDI-TOF MS of crude, soluble fractions of chemically polymerised NMe ₂ STT, OMeSTT, STT, CNSTT and NO ₂ STT. Significant signals are labelled with oligomer length in terms of monomer units (<i>n</i>). Detection suppression limit: 320 Da.	57
3.7	¹ H NMR spectra (aromatic region) of NMe ₂ STT and the dimeric HH regioisomer produced by chemical oxidation.	59
3.8	¹ H NMR spectra (aromatic region) of styryl-15-crown-5 terthiophene, and the dimeric HH regioisomer that is produced by oxidation.	60
3.9	'Charge-trapping' over the two central thiophene rings and styryl substituents as exhibited by theoretical calculations.	61
3.10	CV of terthiophene monomer on a platinum disc electrode (SA = 1.8 mm ²). Supporting electrolyte: 0.1 M TBAP/AN. Potential limits: -1000/+1500 mV. Scan rate: 100 mV s ⁻¹ .	64
3.11	A possible mechanism to explain redox peaks (using thiophene for clarity) observed in the first scan of terthiophene derivatives.	65

3.12	CV scans of CNSTT, STT, OMeSTT and NMe ₂ STT on platinum disc electrodes (SA = 1.8 mm ²). Supporting electrolyte: 0.1 M TBAP/AN. Potential limits: -1000/+1500 mV. Scan rate: 100 mV s ⁻¹ .	66
3.13	CV of NO ₂ STT monomer on a platinum disc electrode (SA = 1.8 mm ²). Supporting electrolyte: 0.1 M TBAP/AN. Potential limits: -1000/+1500 mV. Scan rate: 100 mV s ⁻¹ .	66
3.14	Potentiodynamic growth of NMe ₂ STT on a platinum disc electrode (SA = 1.8 mm ²). Supporting electrolyte: 0.1 M TBAP/AN. Potential limits: 0/+900 mV. 9 cycles. Scan rate: 100 mV s ⁻¹ .	68
3.15	Potentiodynamic growth of OMeSTT on a platinum disc electrode (SA = 1.8 mm ²). Supporting electrolyte: 0.1 M TBAP /AN. Potential limits: +300/+750 mV. 9 cycles. Scan rate: 100 mV s ⁻¹ .	69
3.16	Potentiodynamic growth of STT on a platinum disc electrode (SA = 1.8 mm ²). Supporting electrolyte: 0.1 M TBAP /AN. Potential limits: +375/+900 mV. 9 cycles. Scan rate: 100 mV s ⁻¹ .	69
3.17	Potentiodynamic growth of CNSTT on a platinum disc electrode (SA = 1.8 mm ²). Supporting electrolyte: 0.1 M TBAP/AN. Potential limits: 0/+900 mV. 9 cycles. Scan rate: 100 mV s ⁻¹ .	70
3.18	Potentiodynamic growth of NO ₂ STT on a platinum disc electrode (SA = 1.8 mm ²). Supporting electrolyte: 0.1 M TBAP/AN. Potential limits: 0/+900 mV. 9 cycles. Scan rate: 100 mV s ⁻¹ .	70
3.19	Potentiostatic growth of STT on a Pt disc electrode (SA = 1.8 mm ²). Supporting electrolyte: 0.1 M TBAP/AN. Potential held at 0 mV for 10 s, then stepped to 900 mV for 290 s.	71
3.20	Post-polymerisation CV of NMe ₂ STT films polymerised (a) potentiodynamically and (b) potentiostatically. Electrode: platinum disc (1.8 mm ²). Electrolyte solution: 0.1 M TBAP/AN. Potential limits: 0/+900 mV. 15 cycles. Scan rate: 100 mV s ⁻¹ .	73
3.21	Post-polymerisation CVs of (a) potentiodynamically and (b) potentiostatically deposited oligoOMeSTT films. Electrode: platinum disc (1.8 mm ²). Electrolyte solution: 0.1 M TBAP/AN. Scan rate: 100 mV s ⁻¹ .	75
3.22	Post-polymerisation CVs of (a) potentiodynamically and (b) potentiostatically deposited oligoSTT films. Electrode: platinum disc (1.8 mm ²). Electrolyte solution: 0.1 M TBAP/AN. Potential limits: +375/+1200 mV. 5 cycles. Scan rate: 100 mV s ⁻¹ .	76
3.23	Post-polymerisation CVs of (a) potentiodynamically and (b) potentiostatically deposited oligoCNSTT films. Electrode: platinum disc (1.8 mm ²). Electrolyte solution: 0.1 M TBAP/AN. 5 cycles. Scan rate: 100 mV s ⁻¹ .	77
3.24	Post-polymerisation CVs of (a) potentiodynamically and (b) potentiostatically deposited oligoNO ₂ STT films. Electrode: platinum disc (1.8 mm ²). Electrolyte solution: 0.1 M TBAP/AN. 5 cycles. Scan rate: 100 mV s ⁻¹ .	78
3.25	Chromophores produced by styryl-substituted terthiophene derivatives.	81

3.26	UV-VIS-NIR spectra of a film of electrodeposited oligoNO ₂ STT in the oxidised (solid line) and neutral (dashed line) states.	82
3.27	UV-VIS-NIR spectra of a film of electrodeposited oligoCNSTT in the oxidised (solid line) and neutral (dashed line) states.	82
3.28	UV-VIS-NIR spectra of a film of electrodeposited oligoSTT in the oxidised (solid line) and neutral (dashed line) states.	83
3.29	UV-VIS-NIR spectra of oxidised films (solid lines) and neutral films (dashed lines) of OMeSTT deposited using potentiodynamic and potentiostatic methods.	83
3.30	UV-VIS-NIR spectra of films that were previously oxidised (solid lines) and neutral films (dashed lines) of NMe ₂ STT deposited using potentiodynamic and potentiostatic methods.	84
3.31	Spectroelectrochemistry of an electrochemically grown film of oligoSTT on ITO-coated glass. Potentials between 0.4 V and 1.1 V were applied in steps of 0.1 V.	84
3.32	SEM images of neutral and oxidised films of oligoNMe ₂ STT deposited onto ITO-coated glass using potentiodynamic methods. Magnification: x10000.	86
3.33	SEM image of an oxidised film of oligoOMeSTT deposited using potentiodynamic methods. Magnification: x10000.	86
3.34	Potentiostatically deposited films of STT oligomers. (a) Neutral film: x1400, inset: x70. (b) Oxidised film: x1400.	87
3.35	SEM images of oligoSTT films deposited using cyclic voltammetry. (a) Neutral film: x1000, inset: x5000. (b) Oxidised state: x2000 magnification.	87
3.36	SEM images of oligoCNSTT films deposited using a constant potential. (a) oxidised state, x10000 magnification, (b) neutral state, x5 000 magnification.	88
3.37	SEM images of oligoCNSTT films deposited using cyclic voltammetry. (a) oxidised state, x10000 magnification, (b) neutral state, x10000 magnification.	88
3.38	SEM image of a neutral oligoNO ₂ STT film deposited using a constant potential, x 10000 magnification.	89
3.39	SEM images of oxidised oligoNO ₂ STT films deposited by (a) potentiostatic and (b) potentiodynamic methods, x10000 magnification.	89
4.1	A polythienylenevinylene derivative	100
4.2	Terthienylenevinylene monomer derivatives.	101
4.3	Potentiodynamic growth of NO ₂ STV on a platinum micro electrode (SA = 10 μm ²). Monomer concentration: 5 mM. Supporting electrolyte: 0.1 TBAP/1:1 AN:DCM. Potential limits: -500/+800 mV. 15 cycles. Scan rate: 100 mV s ⁻¹ . Inset: first three cycles.	103

4.4	Potentiodynamic growth of CNSTV on a platinum micro electrode (SA = 10 μm^2). Monomer concentration: 5 mM. Supporting electrolyte: 0.1 TBAP/1:1 AN:DCM. Potential limits: -500/+800 mV. 15 cycles. Scan rate: 100 mV s ⁻¹ . Inset: first three cycles.	104
4.5	Potentiodynamic growth of STV on a platinum micro electrode (SA = 10 μm^2). Monomer concentration: 5 mM. Supporting electrolyte: 0.1 TBAP/1:1 AN:DCM. Potential limits: -500/+800 mV. 15 cycles. Scan rate: 100 mV s ⁻¹ . Inset: first six cycles.	104
4.6	Potentiodynamic growth of OMeSTV on a platinum micro electrode (SA = 10 μm^2). Monomer concentration: 5 mM. Supporting electrolyte: 0.1 TBAP/1:1 AN:DCM. Potential limits: -500/+800 mV. 15 cycles. Scan rate: 100 mV s ⁻¹ . Inset: first three cycles.	105
4.7	Potentiodynamic growth of NMe ₂ STV on a platinum disc electrode (SA = 1.8 mm ²). Monomer concentration: 5 mM. Supporting electrolyte: 0.1 TBAP /1:1 AN:DCM. Potential limits: 0/+800 mV. 15 cycles. Scan rate: 100 mV s ⁻¹ . Inset: first three cycles.	105
4.8	Post growth cycling of oligoNO ₂ STV deposited on a platinum micro electrode (SA = 10 μm^2). Supporting electrolyte: 0.1 TBAP/AN. Potential limits: -500/+800 mV. 10 cycles. Scan rate: 100 mV s ⁻¹ .	113
4.9	Post growth cycling of oligoCNSTV deposited on a platinum micro electrode (SA = 10 μm^2). Supporting electrolyte: 0.1 TBAP/AN. Potential limits: -500/+800 mV. 10 cycles. Scan rate: 100 mV s ⁻¹ .	108
4.10	Post growth cycling of oligoSTV deposited on a platinum micro electrode (SA = 10 μm^2). Supporting electrolyte: 0.1 TBAP/AN. Potential limits: -500/+800 mV. 10 cycles. Scan rate: 100 mV s ⁻¹ .	108
4.11	Post growth cycling of oligoOMeSTV deposited on a platinum micro electrode (SA = 10 μm^2). Supporting electrolyte: 0.1 TBAP/AN. Potential limits: -500/+800 mV. 10 cycles. Scan rate: 100 mV s ⁻¹ .	109
4.12	Postgrowth cycling of oligoNMe ₂ STV deposited on a platinum disc electrode (SA = 1.8 mm ²). Supporting electrolyte: 0.1 TBAP/AN. Potential limits: -500/+800 mV. 10 cycles. Scan rate: 100 mV s ⁻¹ .	110
4.13	UV-VIS-NIR spectrum of oligoNO ₂ STV electrodeposited onto ITO-coated glass and electrochemically oxidised (solid line) and reduced (dashed line).	112
4.14	UV-VIS-NIR spectrum of oligoCNSTV electrodeposited onto ITO-coated glass and electrochemically oxidised (solid line) and reduced (dashed line).	113
4.15	UV-VIS-NIR spectrum of oligoSTV electrodeposited onto ITO-coated glass and electrochemically oxidised (solid line) and reduced (dashed line).	113
4.16	UV-VIS-NIR spectrum of oligoOMeSTV electrodeposited onto ITO-coated glass and electrochemically oxidised (solid line) and reduced (dashed line).	114
4.17	UV-VIS-NIR spectrum of NMe ₂ STV electrodeposited onto ITO-coated glass and electrochemically oxidised (solid line) and reduced (dashed line).	114

4.18	Relationship between electron withdrawing/donating effect of the substituent and the wavelength maxima due to the $\pi \rightarrow \pi^*$ transition of the oligomer-chain chromophore for both terthiophene and thienylenevinylene derivatives.	115
5.1	Alkyl- and alkoxy-substituted styrylterthiophene monomers that were initially polymerised and investigated in this study.	121
5.2	Polymerisation of OC ₆ DASTT.	122
5.3	Possible structure created by the mesomeric effect of the oxygen on alkoxy substituted thiophene polymers.	124
5.4	MALDI-TOF mass spectrum of polyOC ₆ DASTT. Signals are labelled with the assigned oligomer length in terms of monomer units (<i>n</i>).	125
5.5	UV-VIS-NIR spectrum of the soluble fraction of polyOC ₆ DASTT in solution in the oxidised state (excess Cu(ClO ₄) ₂ , solid line) and neutral state (dashed line). The π - π^* band in the neutral state is labelled with its wavelength maximum.	126
5.6	CV of chemically polymerised OC ₆ DASTT, which has been cast as a film onto an ITO-coated glass electrode (~1 cm ²). Supporting electrolyte: 0.1 M TBAP/AN. Potential limits: -500/+1200 mV. 16 th to 20 th cycles. Scan rate: 100 mV s ⁻¹ .	127
5.7	Photograph of the monomer and solvent fractions as solutions in chloroform. (a) Monomer, (b) hexane, (c) acetone, (d) dichloromethane and (e) chloroform.	130
5.8	MALDI-TOF mass spectra of OC ₆ DASTT oligomer fractions extracted using hexane followed by acetone, dichloromethane and chloroform. Signals are labeled with the assigned oligomer length in terms of monomer units (<i>n</i>). <i>M_r</i> of monomer: 550.5 g mol ⁻¹ .	132
5.9	UV-VIS-NIR spectra of OC ₆ DASTT oligomer fractions separated by (a) hexane, (b) acetone, (c) DCM and (d) chloroform. Samples were measured in the oxidised state (excess Cu(ClO ₄) ₂ , solid line) and neutral state (dashed line) from solutions in chloroform.	134
5.10	UV-VIS-NIR spectra of neutral samples of OC ₆ DASTT oligomer fractions which have been separated using hexane, acetone, DCM and chloroform. The λ_{max} of the major $\pi \rightarrow \pi^*$ transition for each fraction is shown.	135
5.11	MALDI-TOF mass spectrum of poly(C ₇ DASTT). Signals are labelled with the assigned oligomer length in terms of monomer units (<i>n</i>).	138
5.12	UV-VIS-NIR spectra of polyC ₇ DASTT in the oxidised state (excess Cu(ClO ₄) ₂ , solid line) and neutral state (dashed line). The π - π^* bands in the neutral state are labelled with their wavelength maxima.	139
5.13	CV of a chemically polymerised C ₇ DASTT film, which has been cast onto an ITO-coated glass electrode (SA: ~1 cm ²). Supporting electrolyte: 0.1 M TBAP/AN. Potential limits: -500/+1200 mV. 5 cycles. Scan rate: 100 mV s ⁻¹ .	139

5.14	MALDI-TOF MS of C ₇ DASTT oligomer fractions extracted using methanol followed by hexane, acetone and dichloromethane. Signals are labelled with the assigned oligomer length in terms of monomer units (<i>n</i>). <i>M_r</i> of monomer: 546.5 g mol ⁻¹ .	141
5.15	UV-VIS-NIR spectra of C ₇ DASTT oligomer fractions separated by (a) methanol, (b) hexane, (c) acetone and (d) DCM. Samples were measured in the oxidised state (excess Cu(ClO ₄) ₂ , solid line) and neutral state (dashed line) from solutions in chloroform.	143
5.16	UV-VIS-NIR spectra of neutral samples of C ₇ DASTT oligomer fractions which have been separated using hexane, acetone and DCM. The λ _{max} of the π→π* transition for each fraction is shown.	144
5.17	C ₁₀ -dialkoxy styrylterthiophene (OC ₁₀ DASTT)	146
5.18	Reaction procedure employed for the polymerisation of OC ₁₀ DASTT	147
5.19	MALDI-TOF MS of polyOC ₁₀ DASTT. Signals are labelled with the assigned oligomer length in terms of monomer units (<i>n</i>).	147
5.20	UV-VIS-NIR spectra of polyOC ₁₀ DASTT in chloroform in the oxidised state (excess Cu(ClO ₄) ₂ , solid line) and neutral state (dashed line). The major λ _{max} for the π→π* absorbance is labelled.	148
5.21	CV of chemically polymerised OC ₁₀ DASTT, which has been cast as a film onto an ITO-coated glass electrode (~1 cm ²). Supporting electrolyte: 0.1 M TBAP/AN. Potential limits: -500/+1200 mV. 10 cycles. Scan rate: 100 mV s ⁻¹ .	149
5.22	MALDI-TOF mass spectra of OC ₁₀ DASTT polymer fractions extracted using hexane followed by acetone, dichloromethane and chloroform. Signals are labeled with the assigned oligomer length in terms of monomer units (<i>n</i>). <i>M_r</i> of monomer: 662.4 g mol ⁻¹ .	152
5.23	UV-VIS-NIR spectra of OC ₁₀ DASTT oligomer fractions separated by (a) hexane, (b) acetone, (c) DCM and (d) chloroform. Samples were measured in the oxidised state (solid line, oxidised using excess Cu(ClO ₄) ₂) and neutral state (dashed line) from solutions in chloroform.	154
5.24	UV-VIS-NIR spectra of OC ₁₀ DASTT oligomer fractions which have been separated using hexane, acetone, DCM and chloroform. The λ _{max} of the π→π* transition for each fraction is listed.	155
5.25	Cyclic voltammetry of OC ₁₀ DASTT oligomer fractions that have been cast onto a glassy carbon electrode (SA: 7 mm ²). Supporting electrolyte: 0.1 M TBAP/AN. Potential limits: -1000/+800 mV. 10 cycles. Scan rate: 100 mV s ⁻¹ . The average oligomer length in terms of monomer units (<i>n_{av}</i>) is displayed.	156
5.26	Growth CV of oligoSTT (5 mM) on a platinum microelectrode (SA: 10 μm ²). Electrolyte solution: 0.1 M TBAP/1:1 AN:DCM. Potential limits: -500/+900 mV. 15 cycles. Scan rate: 100 mV s ⁻¹ .	159
5.27	Growth CV of C ₇ DASTT (5 mM) on a platinum microelectrode (10 μm ²). Electrolyte solution: 0.1 M TBAP/1:1 AN:DCM. Potential limits: 0/+800 mV. 15 cycles. Scan rate: 100 mV s ⁻¹ .	160

5.28	Relationship between the current produced during the growth of C ₇ DASTT (measured at 0.8 V) and the cycle number.	161
5.29	Post growth cycling of polyC ₇ DASTT which has been deposited using cyclic voltammetry on a platinum micro electrode (SA: 10 μm ²). Supporting electrolyte: 0.1 M TBAP/AN. Potential limits: -500/+800 mV. 10 cycles. Scan rate: 100 mV s ⁻¹ .	162
5.30	Potentiostatic growth of C ₇ DASTT (5 mM) on a platinum micro electrode (SA: 10 μm ²). Solvent: 1:1 AN:DCM. Potential held at 0 mV for 1 s, then stepped to 700 mV for 29 seconds.	163
5.31	Post growth cycling of polyC ₇ DASTT, which has been deposited potentiostatically on a platinum microelectrode (SA: 10 μm ²). Supporting electrolyte: 0.1 M TBAP/AN. Potential limits: 0/+800 mV. 10 cycles. Scan rate: 100 mV s ⁻¹ .	164
5.32	Growth CV of OC ₆ DASTT (5 mM) of a platinum micro electrode (SA: 10 μm ²). Electrolyte solution: 0.1 M TBAP/1:1 AN:DCM. Potential limits: -500/+800 mV. Scan rate: 100 mV s ⁻¹ . The first scan is shown as an inset.	165
5.33	Post growth cycling of polyOC ₆ DASTT which has been deposited using cyclic voltammetry on a platinum microelectrode (SA: 10 μm ²). Supporting electrolyte: 0.1 M TBAP/AN. Potential limits: -500/+800 mV. 10 cycles. Scan rate: 100 mV s ⁻¹ .	166
5.34	Potentiostatic growth of OC ₆ DASTT (5 mM) on a platinum microelectrode (SA: 10 μm ²). Electrolyte solution: 0.1 M TBAP/1:1 AN:DCM. Potential held at -500 mV for 1 s, then stepped to 800 mV for 19 s.	167
5.35	Post growth cycling of polyOC ₆ DASTT which has been deposited potentiostatically on a platinum microelectrode (SA: 10 μm ²). Supporting electrolyte: 0.1 M TBAP/AN. Potential limits: -500/+800 mV. 10 cycles. Scan rate: 100 mV s ⁻¹ .	167
5.36	Growth CV of OC ₆ DASTT (5 mM) on an ITO-coated glass electrode (SA: ~1 cm ²). Electrolyte solution: 0.1 M TBAP/1:1 AN:DCM. Potential limits: -500/+800 mV. 5 cycles. Scan rate: 100 mVs ⁻¹ .	168
5.37	Post growth cycling of polyOC ₆ DASTT that has been deposited potentiodynamically on an ITO-coated glass electrode (SA: ~1 cm ²). Supporting electrolyte: 0.1 M TBAP/AN. Potential limits: -500/+800 mV. 10 cycles. Scan rate: 100 mV s ⁻¹ .	169
5.38	Potentiodynamically deposited films of OC ₆ DASTT oligomers on ITO-coated glass. (a) Neutral film: x1400, (b) Oxidised film: x1400 inset: x350.	170
5.39	MALDI-TOF MS of polyOC ₆ DASTT, which was polymerised by potentiodynamic deposition onto an ITO-coated glass electrode. Significant signals are labelled with oligomer length in terms of monomer units (<i>n</i>). Detection suppression limit: 1000 Da.	170
5.40	Growth CV of OC ₁₀ DASTT (5 mM) on a platinum microelectrode (SA: 10 μm ²). Electrolyte solution: 0.1 M TBAP 1:1 AN:DCM. Potential limits: -500/+800 mV. Scan rate: 100 mV s ⁻¹ .	171

5.41	Post growth cycling of polyOC ₁₀ DASTT which has been deposited potentiodynamically on a platinum microelectrode (SA: 10 μm ²). Supporting electrolyte: 0.1 M TBAP/AN. Potential limits: -500/+800 mV. 10 cycles. Scan rate: 100 mV s ⁻¹ .	172
5.42	Potentiostatic growth of polyOC ₁₀ DASTT (5 mM) on a platinum microelectrode (SA: 10 μm ²). Electrolyte solution: 0.1 M TBAP/1:1 AN:DCM. Potential held at -500 mV for 1 s, then stepped to 800 mV for 19 s.	173
5.43	Post growth cycling of polyOC ₁₀ DASTT which has been deposited potentiostatically on a platinum microelectrode (SA: 10 μm ²). Supporting electrolyte: 0.1 M TBAP/AN. Potential limits: -500/+800 mV. 10 cycles. Scan rate: 100 mV s ⁻¹ .	173
5.44	Spectroelectrochemistry of a potentiostatically deposited poly(OC ₁₀ DASTT) film on ITO-coated glass. The film was initially in a reduced state and was oxidised in steps of 0.1 V. Supporting electrolyte: 0.1 M TBAP/AN. Potentials are reported vs Ag/Ag ⁺ .	174
5.45	Growth CV of OC ₁₀ DASTT (5 mM) on an ITO-coated glass electrode (SA: ~1 cm ²). Electrolyte solution: 0.1 M TBAP/1:1 AN:DCM. Potential limits: -500/+800 mV. 5 cycles. Scan rate: 100 mVs ⁻¹ .	175
5.46	Post growth cycling of poly(OC ₁₀ DASTT) that has been deposited potentiodynamically on an ITO-coated glass electrode (SA: ~1 cm ²). Supporting electrolyte: 0.1 M TBAP/AN. Potential limits: -500/+800 mV. 10 cycles. Scan rate: 100 mV s ⁻¹ .	176
5.47	Potentiostatic growth of polyOC ₁₀ DASTT (5 mM) on an ITO-coated glass electrode (SA: ~1 cm ²). Electrolyte solution: 0.1 M TBAP/1:1 AN:DCM. Potential held at -500 mV for 1 s, then stepped to 800 mV for 19 s.	176
5.48	Post growth cycling of polyOC ₁₀ DASTT that has been deposited potentiostatically on an ITO-coated glass electrode (SA: ~1 cm ²). Supporting electrolyte: 0.1 M TBAP/AN. Potential limits: -500/+800 mV. 10 cycles. Scan rate: 100 mV s ⁻¹ .	177
5.49	SEM images of potentiodynamically deposited films of OC ₁₀ DASTT oligomers. (a) Neutral film: x1400, (b) Oxidised film: x1400.	178
5.50	SEM images of potentiostatically deposited films of OC ₁₀ DASTT oligomers. (a) Neutral film: x1400, (b) Oxidised film: x1400.	178
5.51	SEM images of (a/b) potentiostatically and (c/d) galvanostatically deposited polyOC ₁₀ DASTT films on ITO-coated glass. Images (b) and (d) are of the film edges formed at the solution/air interface. All images are displayed at x7000 magnification.	179
5.52	MALDI-TOF MS of polyOC ₁₀ DASTT, which was polymerised by potentiodynamic deposition onto an ITO-coated glass electrode. Significant signals are labelled with oligomer length in terms of monomer units (<i>n</i>). Detection suppression limit: 1000 Da.	180

5.53	MALDI-TOF MS of polyOC ₁₀ DASTT, which was polymerised by potentiostatic deposition onto an ITO-coated glass electrode. Significant signals are labelled with oligomer length in terms of monomer units (<i>n</i>). Detection suppression limit: 1000 Da.	180
5.54	MALDI-TOF MS of polyOC ₁₀ DASTT, which was polymerised by galvanostatic deposition onto an ITO-coated glass electrode. Significant signals are labelled with oligomer length in terms of monomer units (<i>n</i>). Detection suppression limit: 1000 Da.	180
6.1	Construction of a PEC cell.	196
6.2	<i>I</i> - <i>V</i> curve of a cast film of chemically dimerised NMe ₂ STT in the dark (thin line) and under illumination (thick line).	197
6.3	<i>I</i> - <i>V</i> curves of electrochemically grown films of styryl thienylenevinylene derivatives. (a) NMe ₂ STV, (b) OMeSTV, (c) CNSTV and (d) NO ₂ STV.	200
6.4	The relationship between the photovoltaic activity at <i>I</i> _{SC} (δI_{SC} , where $\delta I_{SC} = I_{light,SC} - I_{dark,SC}$) and the electron-withdrawing capability of substituents on films of thienylenevinylene oligomers.	201
6.5	<i>I</i> - <i>V</i> curve of a PEC device comprising a cast film of STV dimer.	202
6.6	Experimental setup using a Dual Mode Lever System for measuring electromechanical properties of a sample.	206
6.7	Schematic of a bender made by casting polymer as a solution in chloroform on a PVDF membrane strip.	207
6.8	CV of a cast polyOC ₁₀ DASTT film on a PVDF membrane substrate. Surface area of substrate: 7 mm ² . Amount of polymer cast: 15 µg. Supporting electrolyte: 0.1 M TPAP/AN. Ten cycles. Scan rate: 100 mV s ⁻¹ .	209
6.9	Absorbance of a polyOC ₁₀ DASTT film on PVDF (a) immediately after being cast from solution, (b) after electrochemical oxidation (+1 V vs Ag/Ag ⁺) and (c) after oxidation with iodine.	209
6.10	UV-VIS-NIR spectra of a cast polymer/PVDF strip which has been reduced and oxidised potentiostatically at -0.6V and +1.0 V. Supporting electrolyte: 0.25 M TBAPF ₆ /PC. A piece of platinum coil was used to wrap around the polymer/PVDF film to increase charge accessibility, and the potential was applied for 30 minutes.	211
6.11	Experimental setup for testing a polymer/PVDF strip. Electrolyte: 0.25 M TBAPF ₆ /PC electrolyte. Counter electrode: stainless steel mesh. Reference electrode: Ag/Ag ⁺ . The strip is shown in both an (a) reduced and (b) oxidised state.	212
6.12	Schematic showing the expansion of the polymer film on oxidation by incorporation of the anion, and contraction on reduction due to expulsion of the anion.	212
6.13	Chronoamperometry of polyOC ₁₀ DASTT/PVDF strip in 0.25 M TBAPF ₆ /PC. Oxidation potentials: switching from -0.6 V to 0.8 V. Reduction potentials: switching from 0.8 V to -0.6 V.	213

6.14	Correlation between the injected charge and the displacement of the free end of the film. The charge due to non-Faradaic process can be determined by extrapolation of the linear trend.	214
6.15	Schematic of fibres on which polyOC ₁₀ DASTT was deposited. (a) Hollow PVDF membrane fibre wrapped with a 50 µm platinum wire. (b) Hollow PVDF membrane fibre which has been sputter-coated with platinum and wrapped with a 50 µm platinum wire. (c) 250 µm wire wrapped in a 50 µm wire.	216
6.16	Actuation of a hollow PVDF membrane fibre (49 mm long) wrapped in a 50 µm wire and coated with polymer (39 µg mm ⁻¹). The force was held constant at 6 mN while the potential was alternated between -0.6 V and +0.8 V. The distance the fibre stretches and the current produced were measured.	217
6.17	Relationship between displacement and charge injected into a PVDF membrane fibre coated with polyOC ₁₀ DASTT during (a) reduction and (b) oxidation of one typical pulse. A negative charge is used to indicate reduction, a negative displacement to indicate contraction, a positive charge to indicate oxidation and positive displacement to indicate expansion.	218
6.18	Comparison of the rate of contraction/expansion during oxidation and reduction of one typical pulse. The slope represents the rate at which the fibre is expanding or contracting.	219
6.19	Free-standing film of polyOC ₁₀ DASTT incorporating a zigzagged (50 µm diameter) wire. Dimensions of film: 6 mm x 21 mm with a thickness of 81 µm. Mass = 16.1 mg.	220
6.20	Strain created by the polyOC ₁₀ DASTT film over time as it is doped (oxidised) and then dedoped (reduced at -0.6 V) to and from various oxidation potentials.	221
6.21	The effect of the oxidation potential on the strain measured after 5000 seconds of oxidation.	223
6.22	Relationship between the strain generated at different oxidation potentials and the electrochemical efficiency (EE).	223
6.23	Relationship between the isometric stress generated on the film and the charge density passed as the film is reduced. The film was pre-conditioned at +1V to obtain the fully expanded state and then isometric measurements were performed as the potential was switched to -0.6 V.	224
6.24	Schematic of the test cell used in this study.	228
6.25	SEM images of the electrodes. Anodes prepared by casting poly(OC ₁₀ DASTT) onto (a) Ni/Cu substrate (b) carbon fibre substrate. The blank substrates before polymer deposition are given for comparison as insets in the top right hand corner. (c) Cathode prepared by electrodeposition of polypyrrole on stainless steel mesh. Images are displayed at x400 magnification with insets at x100 magnification.	230
6.26	Cyclic voltammograms of polyOC ₁₀ DASTT cast on carbon fibre substrate and Ni/Cu substrate. Electrolyte solution: 60 mM TBAPF ₆ /PC. Scan rate: 10 mV s ⁻¹ .	231

6.27	Charge (A,C) and discharge (B,D) curves of cells with anodes comprising Ni/Cu substrate (A,B) and carbon fibre (C,D). The charge/discharge current density is 0.02 mA cm^{-2} .	232
6.28	Discharge capacities at different discharge current densities obtained for the Teflon cell using Ni/Cu and carbon fibre anode substrates.	233
6.29	Variation of discharge capacity with cycle number for cells with an anode comprising polyOC ₁₀ DASTT on Ni/Cu substrate and carbon fibre substrate. Current density: 0.02 mA cm^{-2} .	234
6.30	SEM images showing polyOC ₁₀ DASTT fibrils with a platinum film as a support. (a) Partially dissolved template and viewed from platinum coated side, and (b) cross-section of the fibrils with a polymer film on left and platinum film on the right.	237
6.31	CV of fibrils in a partially dissolved template with a platinum backing stuck on ITO coated glass. Supporting electrolyte: 0.1 M TBAP/AN. Scan rate: 100 mV s^{-1} .	238
6.32	Platinum inverse opals showing the honey comb structure. (a) x7500 and (b) x3000 magnification.	239
6.33	Platinum opal structures produced by sputter-coating the polystyrene opal with platinum. (b) opal showing predominantly body-centred cubic square-packing. (c) showing predominantly hexagonal close-packing with polymer coating.	241
6.34	AFM images of the underside of a platinum opal structure. (a) 3-dimensional image, (b) Height data and (c) deflection data. Scan size: $10.00 \mu\text{m}$.	242
6.35	(a) Gold opal surface on ITO-coated glass and (b) polyOC ₁₀ DASTT cast on a gold opal surface.	243
6.36	Edge of ITO opal structure on ITO-coated glass.	244
6.37	SEM images electrospun polyOC ₁₀ DASTT fibres.	246
6.38	Growth of platinum on opal coated ITO coated glass. 10 cycles. Scan rate: 100 mV s^{-1} .	257

List of Tables

Number	Description	Page
3.1	Soluble fractions of styryl-substituted terthiophene polymer derivatives.	59
3.2	R_f values of monomers and dimers in 20% ethylacetate/hexane on silica TLC plates.	60
3.3	Anodic peaks shown by styryl-substituted terthiophene derivatives.	69
3.4	Oxidation onset potentials of styryl terthiophene derivatives.	71
3.5	Conditions of electrochemical deposition for films prepared on ITO-coated glass for characterisation by UV-VIS-NIR and microscopy.	102
4.1	Polymer oxidation and reduction potentials on the second cycle.	112
4.2	Wavelength maxima shown by NO ₂ STV, CNSTV, STV, OMeSTV and NMe ₂ STV.	116
5.1	Mass percentages of OC ₆ DASTT oligomers separated by different solvents.	136
5.2	Mass percentages of polyC ₇ DASTT separated by different solvents.	145
5.3	Mass percentages of OC ₁₀ DASTT oligomers/polymers separated by different solvents.	156
6.1	Photovoltaic characteristics of a cast film of NMe ₂ STT dimer.	203
6.2	Photovoltaic characteristics of PEC devices constituting nitro-styryl-substituted terthiophene and thienylenevinylene oligomer films.	206
6.3	Photovoltaic characteristics of a cast film of chemically synthesised STV dimer.	207
6.4	Maximum strain rate on oxidation and reduction of films which are oxidised at various potentials. The reduction potential is kept constant at -0.6 V.	227

List of Symbols

A	Ampere
A	Ammeter
A ⁻	Anion
b	Variable number
δI_E	Photovoltaic activity
δI_{SC}	Photovoltaic activity under short circuit
E	Potential
E^0	Standard electrode potential
e ⁻	Electron
EE	Electrochemical efficiency
EE_{ox}	Electrochemical efficiency on oxidation
EE_{red}	Electrochemical efficiency on reduction
E_K	Kinetic energy
E_{ox}	Peak oxidation potential
$E_{oxidation\ onset}$	Oxidation onset potential
E_{red}	Peak reduction potential
F	Faraday's constant
Fc	Ferrocene
H _H	Proton at head position (5-position)
H _T	Proton at tail position (5''-position)
$I_{dark,SC}$	Short circuit current, dark conditions
$I_{light,SC}$	Short circuit current produced under illumination
I_{pp}	Current at peak power
I_{SC}	Short circuit current (Current at zero potential)
λ_{max}	Wavelength at maximum absorbance in spectroscopy
m	Variable number
m	Mass
M	Molecular weight
M_n	Number average molecular weight

M_r	Molar mass
M_w	Weight average molecular weight
n	Oligomer length in terms of monomer units
n	Variable number
n	Number of electrons per monomer unit
N	Number of molecules
n_{av}	Average oligomer length in terms of monomer units
R	Variable functional group
R_f	Retention factor
t	Time
v	Velocity
V	Volt
V	Voltammeter
V_{oc}	Open circuit voltage (Potential at zero current)
V_{pp}	Voltage at peak power.
X^+	Variable cation
z	Charge

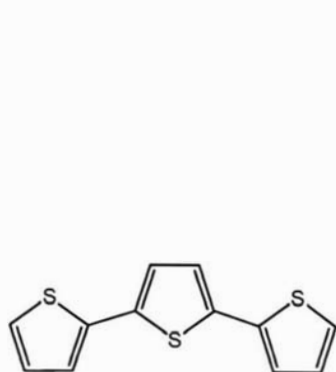
List of Abbreviations

ACTH	Adrenocorticotropic hormone
AFM	Atomic force microscopy
AN	Acetonitrile
Anhyd.	Anhydrous
CE	Counter electrode
CP	Conducting polymer
CV	Cyclic voltammetry
DBTT	3',4'-dibutyl-2,2':5'2"-terthiophene
DBU	1,8-diazabicyclo[5.4.0]undec-7-en
DCM	Dichloromethane
dppp	1,3-diphenylphosphinopropane
ECE	Energy conversion efficiency
EDG	Electron-donating group
EDOT	3,4-ethylenedioxythiophene
<i>EE</i>	Electrochemical efficiency
EI	Electrospray ionisation
EQCM	Electrochemical quartz crystal microbalance
Equiv.	Equivalents
EWG	Electron-withdrawing group
FAB	Fast atom bombardment
Fc	Ferrocene
FF	Fill factor
GPC	Gel permeation chromatography
GPES	General purpose electrochemical system
GRIM	Grignard method
HH	Head-to-head
HOMO	Highest occupied molecular orbital
Hrs	Hours
HT	Head-to-tail

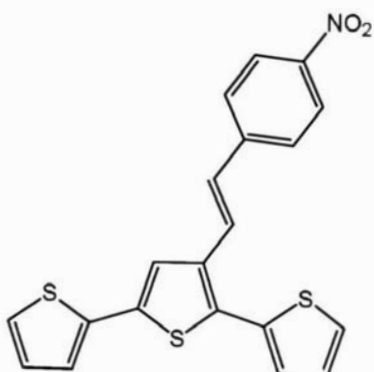
ICP	Inherently conducting polymer
IPRI	Intelligent Polymer Research Institute
ITO	Indium tin oxide
LUMO	Lowest unoccupied molecular orbital
MALDI-TOF MS	Matrix assisted laser desorption/ionisation time-of-flight mass spectrometry
Me	Methyl
MCP	Micro-channel plate
N/A	Not applicable
NMR	Nuclear magnetic resonance
OFET	Organic field effect transistor
OLED	Organic light emitting diode
PCBM	3'-phenyl-3'H-cyclopropa[1,9][5,6]fullerene-C ₆₀ -I _h -3'-butanoic acid methyl ester
PD	Polydispersity
PEC	Photoelectrochemical cell
PEDOT	Poly(3,4-ethylenedioxythiophene)
PEDOT-PSS	Poly(3,4-ethylenedioxythiophene)poly(styrenesulfonate)
PEO	Polyethylene oxide
Ph	Phenyl
PMMA	Polymethylmethacrylate
PPV	Polyphenylenevinylene
PV	Photovoltaic
PVDF	Polyvinylidene fluoride
RE	Reference electrode
RT	Room temperature
SA	Surface area
SCE	Standard calomel electrode
SEM	Scanning electron microscopy
SHE	Standard hydrogen electrode
TBAP	Tetrabutylammonium perchlorate
TBAPF ₆	Tetrabutylammonium hexafluorophosphate
TLC	Thin layer chromatography

THF	Tetrahydrofuran
TOF	Time-of-flight
TPP	Tetraphenyl porphyrin
TT	Tail-to-tail
UV-VIS-NIR	Ultraviolet-visible-near infrared
WE	Working electrode
w.r.t.	With respect to

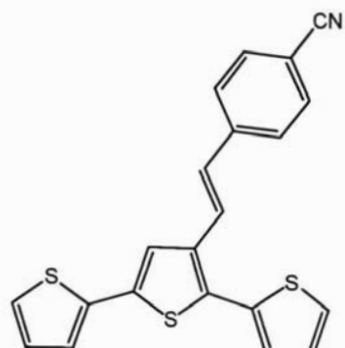
Monomer Abbreviations



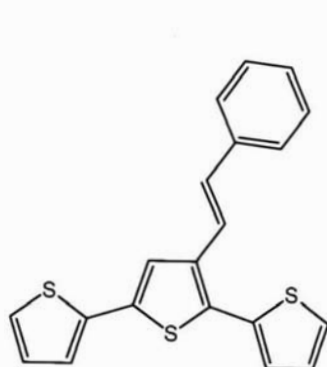
Terthiophene



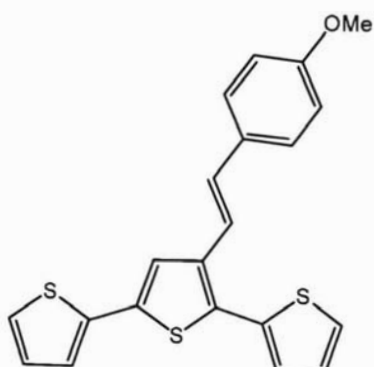
NO₂STT



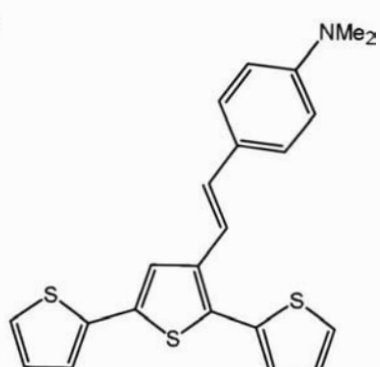
CNSTT



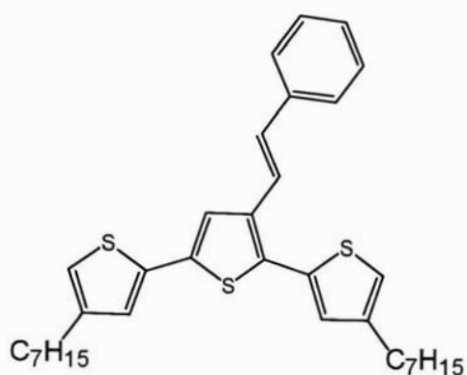
STT



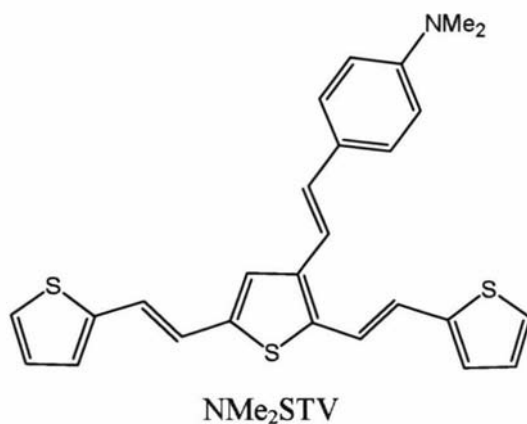
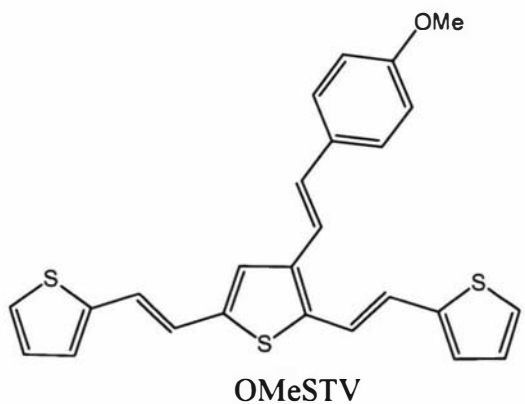
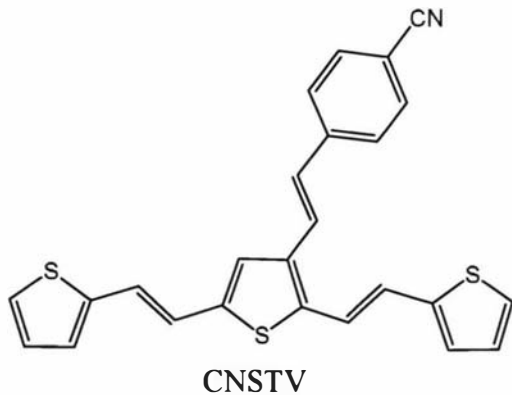
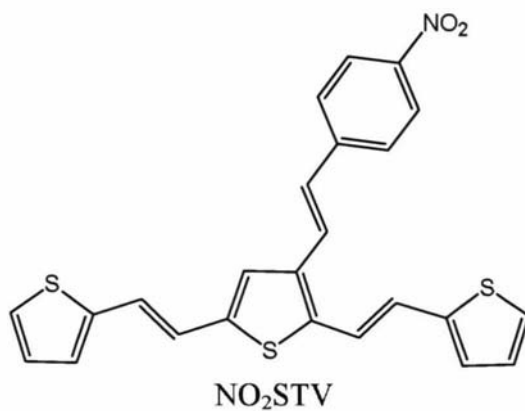
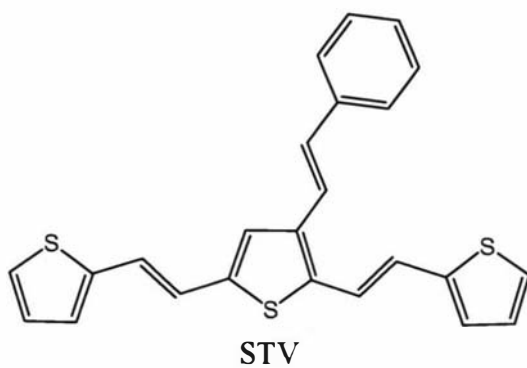
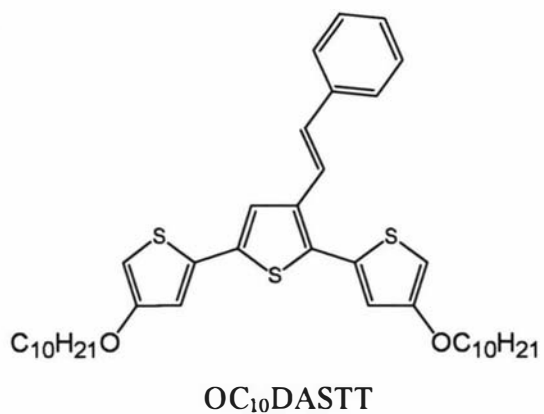
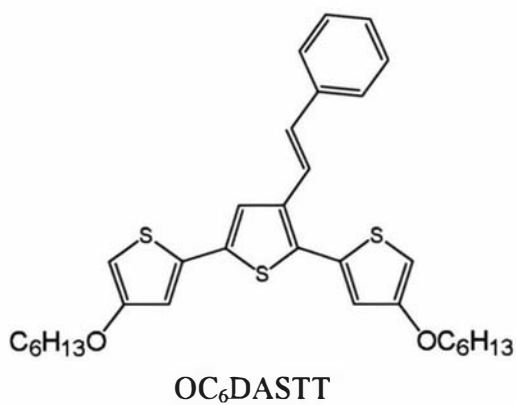
OMeSTT



NMe₂STT



C₇DASTT



STT: Styryl terthiophene

DASTT: Dialkoxy styryl terthiophene or
Dialkyl styryl terthiophene

STV: Styryl terthienylenevinylene

Chapter 1

Introduction

1.1 Introduction

Organic polymers have properties such as flexibility, light weight, strength and resistance to corrosion. In addition, they can be made from readily available and inexpensive starting materials.¹ These properties are valuable for components of clothing, kitchenware, vehicles, and appliances.² Polymers are also renowned and utilised for their high resistance to electricity. However, in 1977, Alan McDiarmid, Alan Heeger and Hideki Shirakawa reported conductivity in polyacetylene (CH)_n. Since then, interest in polymers that intrinsically conduct electricity has been escalating.^{3,4} There were more than 2900 papers published in 2004 relating to conducting polymers. The discovery of conducting polymers merited McDiarmid, Heeger and Shirakawa a joint Nobel prize in 2000.

Conducting polymers combine the many benefits of plastics with the ability to conduct electricity at a level comparable to metals. In addition, conducting polymers possess the ability to act as a switch by reversibly alternating between the conducting state, and a semi-conducting or non-conducting state. This conversion is usually associated with a change in colour.

These properties of conducting polymers provide great potential for their use in a variety of applications. Organic batteries,^{5,6} electrooptical display devices (electrochromic devices, smart windows and organic light emitting diodes (OLEDs)),⁷⁻⁹ sensors,^{10,11} molecular wires,^{12,13} modified electrodes,^{14,15} diodes,¹⁶ capacitors,¹⁷⁻¹⁹ organic field-effect transistors (OFETs),^{4,20} actuators²¹ and solar cells²² are examples of applications employing conducting polymers that are under active research. The broad range of functions demonstrates the versatility of these materials.

1.2 Conducting polymers

There is now a wide variety of conducting polymers and their derivatives. Examples of some that are commonly investigated are given in Fig. 1.1. The fundamental structural feature of all conducting polymers is their extended conjugated π system (alternating single and double bonds), which is delocalised over a number of recurring monomer units along the polymer backbone.^{23,24}

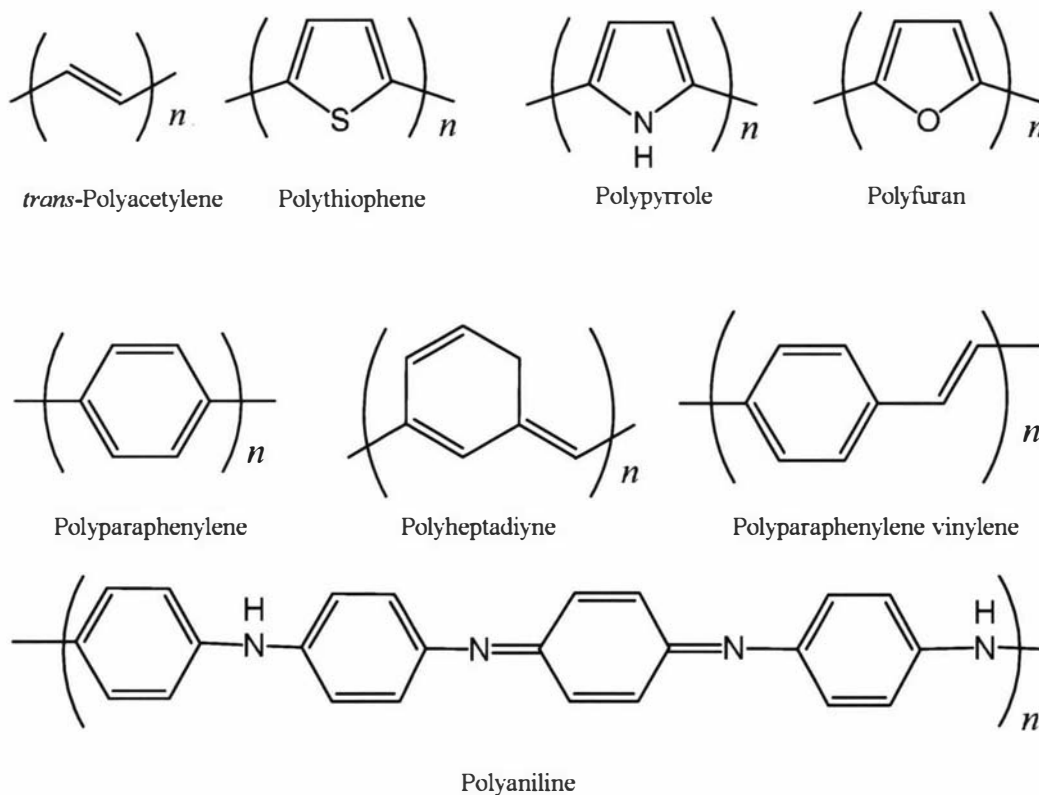


Fig. 1.1. A selection of polymers capable of exhibiting conductivity.

In their neutral state, conjugated polymers are either insulators or semiconductors with conductivity typically ranging from 10^{-10} to $10^{-5} \text{ S cm}^{-1}$, as shown in Fig. 1.2. They are unique, however, in that they can be redox-doped to possess metal-like electronic, magnetic, optical and electrical properties, producing conductivities in the range of $1 - 10^5 \text{ S cm}^{-1}$.⁴

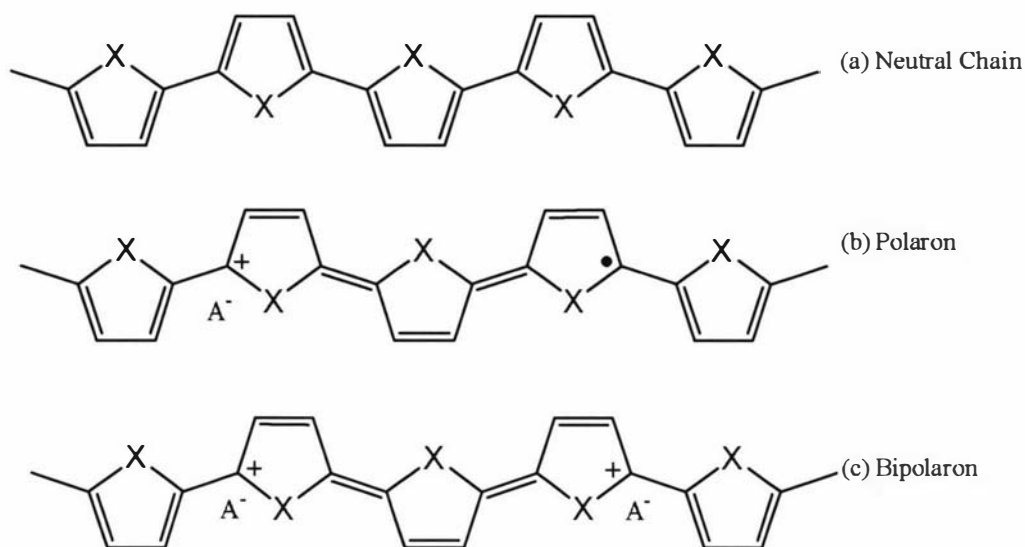


Fig. 1.4. (a) The semi-conducting, aromatic, neutral chain. (b) Formation of a polaron species. (c) The conducting, quinoidal, bipolaron species formed on further oxidation.^{31,33} X = NH or S, A⁻ = anion (e.g. Cl⁻, ClO₄⁻).

An energy level diagram representing the monomer, neutral polymer, and oxidised polymer with formation of polaron/bipolaron species, is shown in Fig. 1.5.³⁴ On polymerisation, the HOMO (highest occupied molecular orbital) and LUMO (lowest unoccupied molecular orbital) of the monomer are broadened.³⁴ The resulting π and π^* molecular orbitals can be described as a fully occupied valence band and an empty conduction band respectively.³⁵ The energy difference between these two orbitals is known as the band gap, and determines important properties of the polymer such as the ability to conduct, and the light energy (wavelength) at which the polymer absorbs or is capable of emitting.

The oxidised species display energy levels that appear between the valence and conduction bands, which effectively narrow the band gap.³⁴ This results in enhanced conductivity and a bathochromic shift in wavelength absorbed by the polymer. In highly doped polymers, these energy levels can overlap with the valence and conduction bands to produce quasi-metallic behaviour.²⁵ Generally, polymers with a longer effective conjugation length have broader conduction and valence bands, resulting in a smaller band gap and consequentially are capable of higher conductivities.^{36,37}

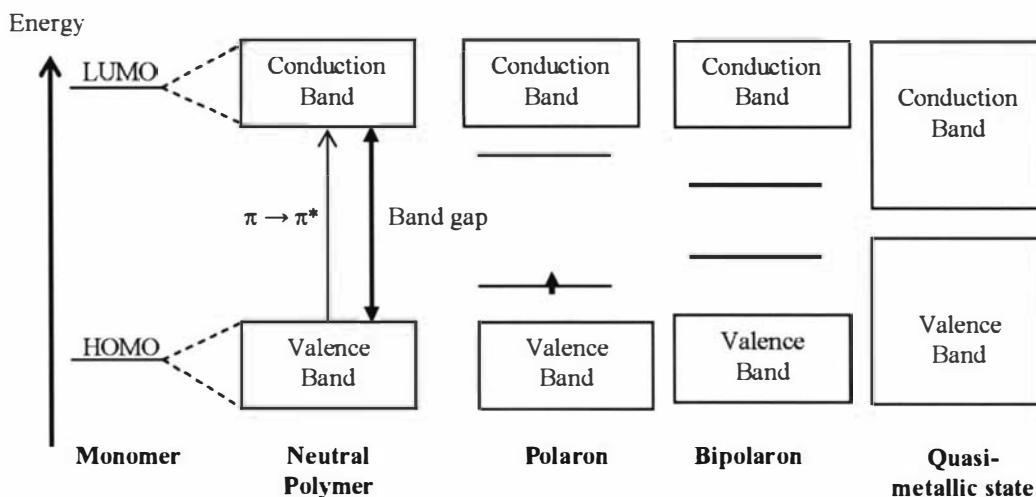


Fig. 1.5. Energy level diagram showing the difference in band structure of a conducting polymer in the neutral state, and oxidised state with formation of polaron and bipolaron species.³⁴

Doping is usually associated with a change in morphology of the polymer matrix, due to incorporation of counterions (and possibly associated solvent molecules) required to balance the charge.²⁹ Oxidative doping usually results in expansion by incorporation of anionic species, and dedoping is associated with the expulsion of anion species causing contraction.²⁹ This ability of the polymer to expand and contract on oxidation and reduction has been utilised for applications in actuator materials.³⁸

A valuable property of some conducting polymers is the ability to be readily modified by the attachment of substituents.^{14,23} Functionalisation by covalent bonding of specific groups to the polymer backbone allows the properties of the polymer to be modified.³⁹ For example, the conductivity and colour absorbed by a polymer can be varied by the attachment of electron withdrawing/donating substituents,⁴⁰ which alter the polymer bandgap,²⁸ and solubility in organic solvents can be increased by attachment of alkyl and/or alkoxy chains.⁴¹ Prosthetic groups, which interact with the environment, can also be attached to give additional functions. For example, porphyrins can be attached to form light harvesting polymers⁴² and polyether groups to create cation sensors.²⁸ The conjugated polymer chains are able to function as paths, or molecular wires, for the reversible transport of electrons between the functional groups and an electrode.¹⁴

Thiophene is one of the most readily functionalised monomers, allowing a wide range of functionalised polythiophenes to be easily prepared.^{8,43} In addition, polythiophenes commonly have relatively high conductivities,⁴⁴ excellent processing possibilities,⁴⁵ and form some of the most chemically stable materials.⁴¹ This makes them one of the most widely investigated linear conjugated systems from both fundamental research and industrial viewpoints.⁴⁶

1.3 Thiophene based polymers

1.3.1 Polymerisation

Polymerisation of thiophene precursors can occur through either the α or β positions (Fig. 1.6) although polymerisation through the more reactive α position (Fig. 1.6b) is usually more favorable.⁴⁴ Polymerisation through the β position (α - β or β - β , Fig. 1.6c & d respectively) produces undesirable defects in the polymer backbone, which may lead to reduced overlap between π orbitals and consequentially lower conductivities.²³

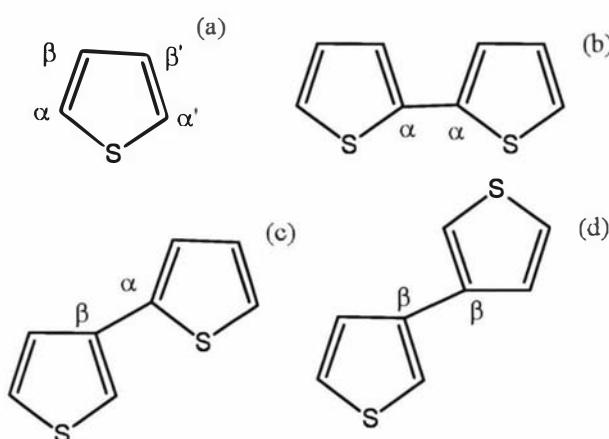


Fig. 1.6. (a) α/β positions on a thiophene ring, (b) α - α coupling, (c) α - β coupling and (d) β - β coupling.

The currently accepted mechanism for the polymerisation of polythiophenes is displayed in Fig. 1.7.^{8,27,47,48} Polymerisation is initiated by the oxidation of two monomer units to produce radical cations, which subsequently couple to form a dimer. Chain propagation occurs by coupling of monomer and/or oligomeric radical cation species.

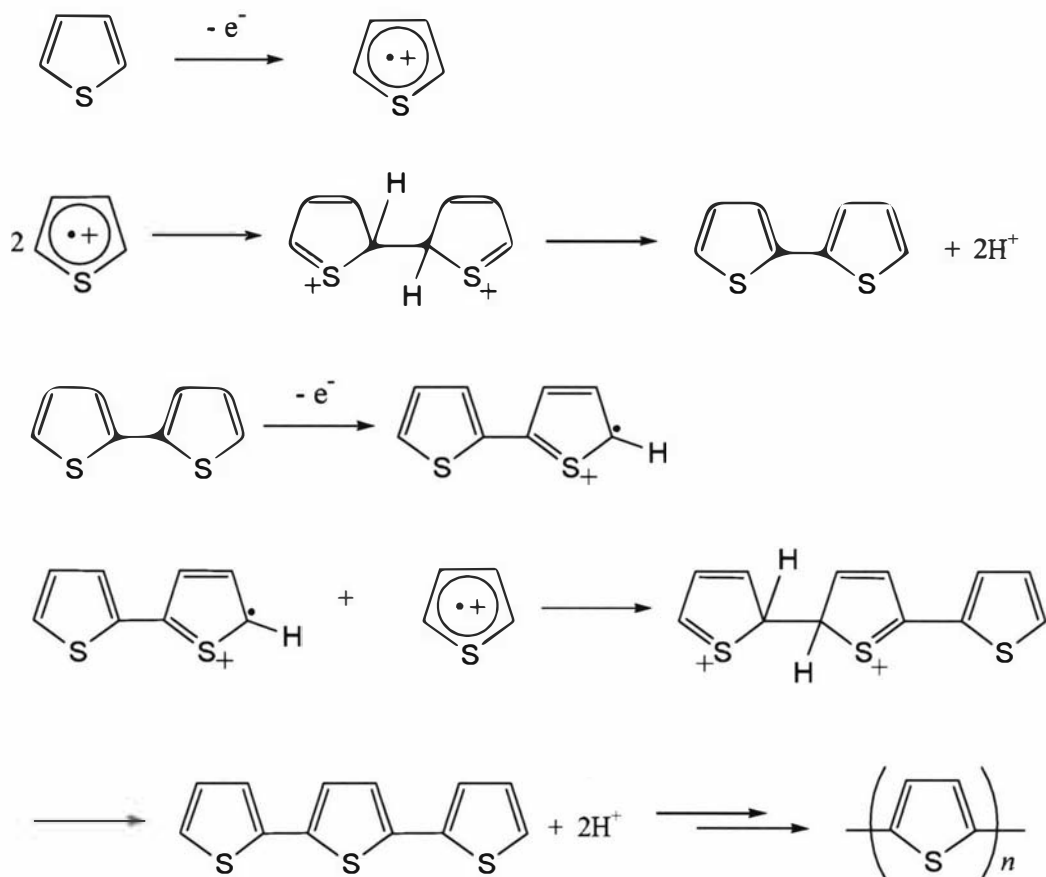


Fig. 1.7. Proposed mechanism for the polymerisation of thiophene.⁸

Functionalisation of thiophene at one or both of the β positions (Fig 1.8) is often used to modify the properties of the resulting polymer. Polymerisation of thiophene monomers, however, often requires oxidation at potentials (thiophene: +1.65 V vs SCE)⁴⁷ that cause over-oxidation (irreversible oxidation) of polymer functional groups, or coupling through the β -position (seen by NMR).⁴⁹⁻⁵¹ This is known as the polythiophene paradox.

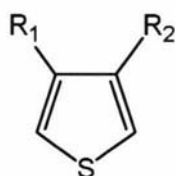


Fig. 1.8. Functionalisation of thiophene through the β positions.

One method of alleviating this problem is by using bithiophene or terthiophene monomers, which require lower oxidation potentials (1.20 V and 1.05 V vs SCE

respectively).^{47,52} However, the resulting polymer length has also been found to decrease with increasing monomer length⁵³ due to a lower reactivity of the longer oligomeric cation radicals.⁵⁴ The attachment of appropriate substituents may also be used to decrease the polymerisation potential by influencing the charge distribution and increasing the reactivity of the monomer and cation intermediate.²⁵ It has been observed, however, that steric effects between bulky substituents can hinder polymerisation by physically obstructing two species from coupling, thus increasing the potential required for polymerisation.⁴³

Several groups^{54,55} have reported that electronic effects induced by substituents strongly affect the reactivity of the monomer and hence the resulting polymer length. Electron-donating substituents have been reported to decrease the oxidation potential of the monomer by increasing the stability of the cation radical formed during the polymerisation process. The decreased reactivity of the resulting radicals leads to a lower degree of polymerisation. Electron-withdrawing substituents appear to exert the opposite effect resulting in more reactive cation radicals and enhanced polymerisation. However, Randriamahazaka *et al.*⁵⁶ found that thiophene monomers substituted with strongly electron-withdrawing substituents (e.g. 3-cyanothiophene and 3-nitrothiophene) that have oxidation potentials approximately 0.5-0.7 V higher than thiophene, do not polymerise at all. This is thought to be due to the highly reactive radical cations initially formed on monomer oxidation undergoing competing reactions with solvent or anion molecules rather than polymerisation.⁵⁶

Monomer units that are not centrosymmetric, such as monosubstituted thiophene, can couple in three orientations: head-to-head (HH), head-to-tail (HT) and tail-to-tail (TT) as shown in Fig. 1.9. Polymerisation can consequentially result in regioregular (repeated sequence of coupling orientations) or regiorandom (arbitrary sequence of coupling orientations) polymers (Fig. 1.10). If there are significant steric interactions between functional groups, these polymers can exhibit significantly different properties.⁵⁷

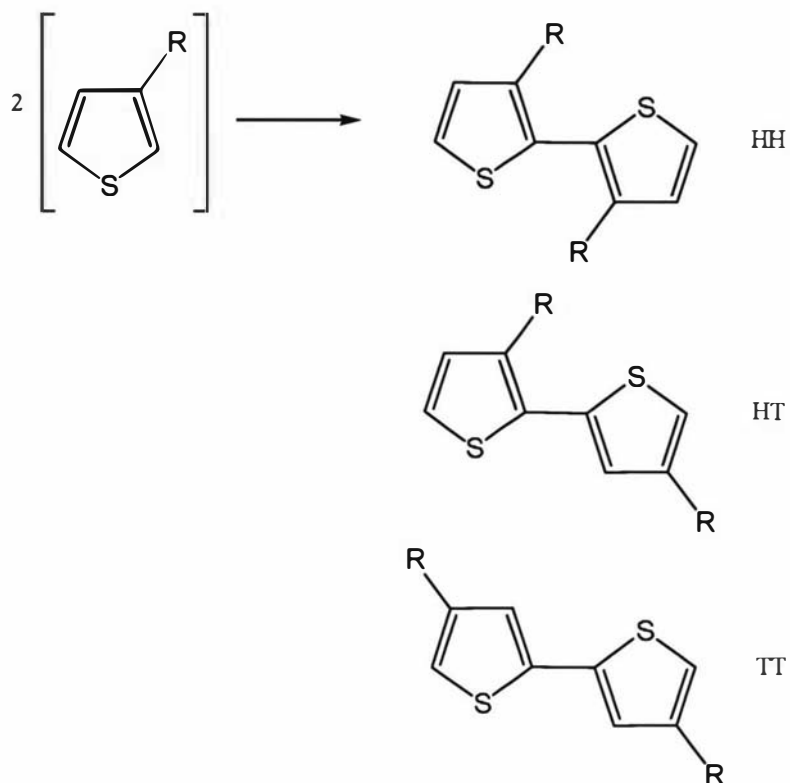


Fig. 1.9. Possible regioisomers formed by coupling of two, non-centrosymmetric monomer units: head-to-head (HH), head-to-tail (HT) and tail-to-tail (TT).

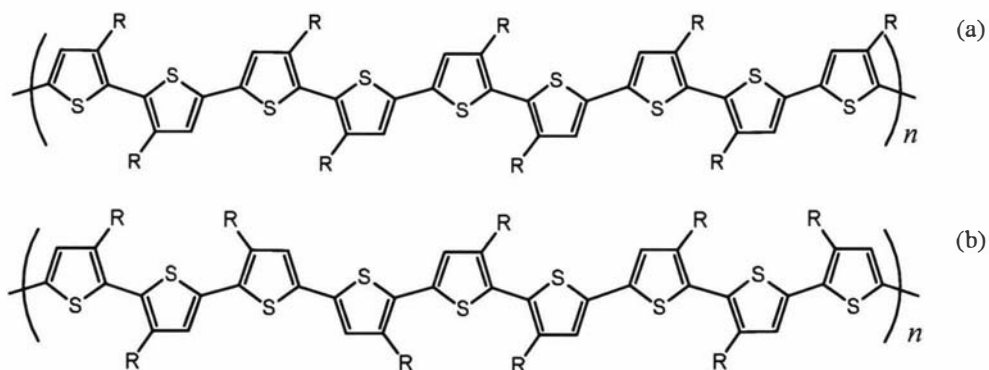


Fig. 1.10. Examples of (a) regioregular and (b) regiorandom functionalised polythiophenes.

The regioregularity of substituted polythiophenes, as well as other critical properties such as polymer length and α - β linkages, may be influenced by the polymerisation method.⁵⁸

1.3.2 Polymerisation methods

Polymerisation of monomers is usually performed using either chemical^{27,58,59} or electrochemical methods.^{8,28,60} Electrochemical synthesis allows deposition of polymer films directly onto a wide range of conductive substrates, including glassy carbon, indium-tin-oxide (ITO) and metals. It provides the opportunity to control film thickness by limiting charge passed, can be used to produce films of insoluble polymers, and allows an *in situ* electrochemical study of the polymerisation process. In addition, electrochemical polymerisation allows a large range of counter-ions to be easily incorporated into the polymer film that can determine its electronic and mechanical properties.

Electrochemical polymerisation can be achieved using potentiodynamic (cyclic voltammetry), potentiostatic (constant potential) or galvanostatic (constant current) methods, although the latter method has been shown to produce films of poorer quality than the former methods.⁶¹ The morphology and properties of polymer films have been found to depend upon many parameters such as the electrode surface, the electrolyte solution, temperature and potential limits applied.⁶¹ Polymerisation of alkylthiophenes using electrochemical techniques has been shown to produce polymers with a regiospecificity of about 70% head-to-tail linkages.⁶²

A cyclic voltammogram for the growth and deposition of polyterthiophene is shown in Fig. 1.11. An increase in current is observed with each cycle. This is typical of conducting polymer growth and is due to an increase in electroactive surface area and/or more facile electrode kinetics. An oxidation onset potential of 0.71 V vs Ag/Ag⁺ is evident.

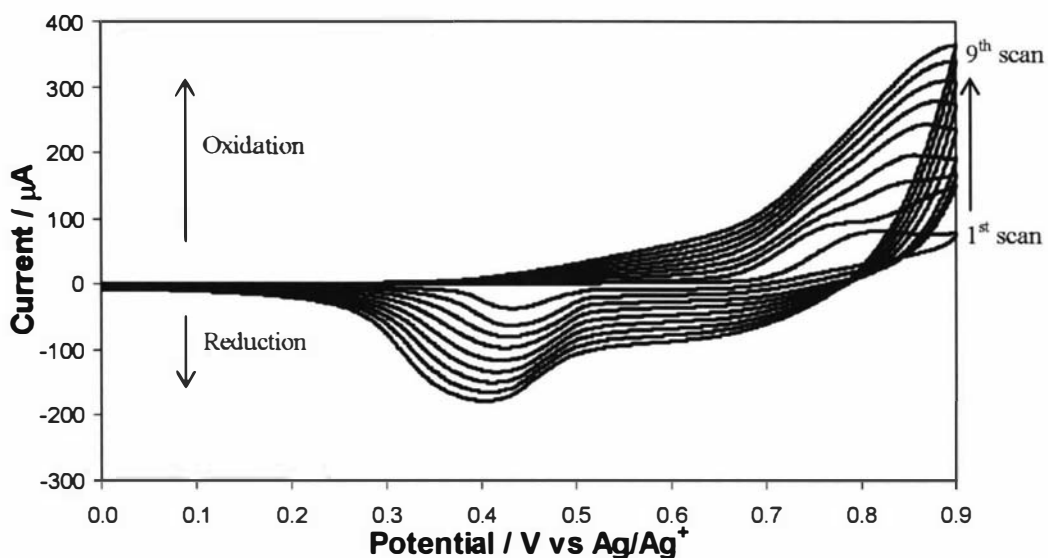


Fig. 1.11. Potentiodynamic growth of terthiophene on a platinum disc electrode (surface area (SA) = 1.8 mm²). Supporting electrolyte: 0.1 M TBAP/AN. Potential limits: 0/+900 mV. 9 cycles. Scan rate: 100 mV s⁻¹.

Chemical synthesis allows the production of large amounts of material and improved control over the assembly of monomer units by certain methods. Reproducibility of chemical polymerisations to produce identical polymer properties, however, is known to be difficult.⁶¹ There are many different chemical polymerisation methods employed.²⁷ One commonly employed method for the synthesis of polythiophenes is the Grignard method (GRIM), which uses a Ni catalyst (Ni⁰ or Ni(dppp)Cl₂) as shown in Fig. 1.12.⁴⁵ This method typically gives regioregularity in poly(alkylthiophenes) of ~90%.^{27,62}

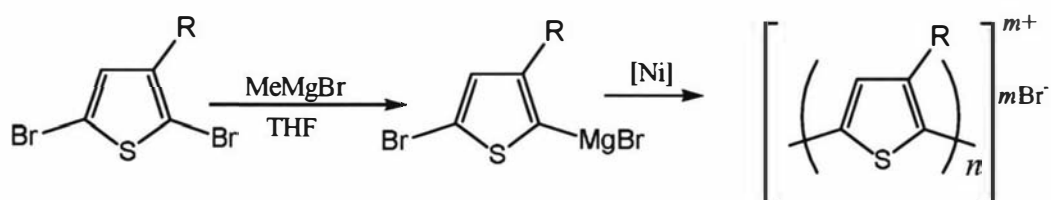


Fig. 1.12. Synthetic polymerisation of functionalised thiophene using the Grignard method.

An alternative to polymerisation by directed chemical synthesis is polymerisation by chemical oxidation. This is a more direct method than chemical synthesis since the monomer does not require modification at the α -positions. The oxidation of thiophene

derivatives using iron(III) chloride is commonly used to prepare polythiophenes from thiophenes,⁶³⁻⁶⁶ bithiophenes^{27,67,68} and terthiophenes.^{44,63,69-71} Iron(III) chloride has been shown to produce polymers of high molecular weight⁷⁰ and regioselectivity of ~80% in alkyl thiophenes.^{62,63,68} The oxidation potential of iron(III) chloride and quality of the resulting polymer, such as conductivity and solubility, has been found to depend strongly upon oxidant concentration,⁶¹ and impurities such as water or ethanol.⁷⁰ A typical reaction using iron(III) chloride is given in Fig. 1.13. The polymer is initially produced in the oxidised state, which is insoluble and difficult to process. The polymers are generally made more processable by reduction to the more soluble, neutral state.⁶²

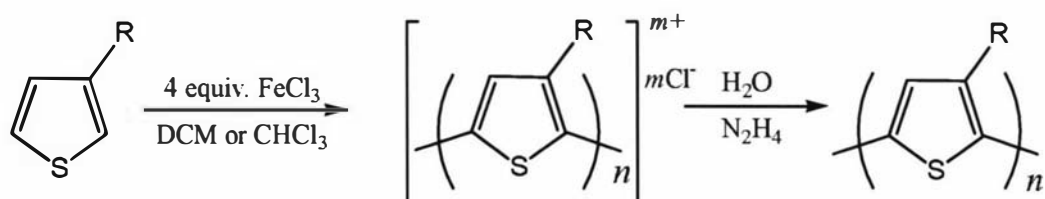


Fig. 1.13. Oxidative polymerisation of functionalised thiophene using iron(III) chloride.

1.3.3 Effect of substituents on polythiophenes properties

Thiophenes can be functionalised by a wide range of substituents (varying in properties such as electron donating/withdrawing effects, size and shape), which may alter the electronic, optical and physical properties of the resulting polymer.³⁶ These properties can be tuned by modification of the substituents to give desired polymer properties. Substituent effects can be categorized into (1) electronic effects⁸ and (2) steric effects.⁷²

In theory, polymers substituted with electron-withdrawing groups (EWGs) should more readily undergo *n*-type doping incorporating a cation into the polymer structure, and polymers substituted with electron-donating groups (EDGs) should more readily undergo *p*-type doping incorporating anions.⁶⁹ EDGs are known to stabilise the oxidised (conducting) state of the polymer, which is useful for many applications.^{8,73} If

the oxidised state is too stable, however, difficulties may arise in reduction to the more soluble and often required neutral state.^{62,74}

Polythiophene derivatives that are stable in a reduced state would be useful for some applications such as charge storage (supercapacitors and organic batteries) and solar cells.⁷⁵ Although many polymers show satisfactory performances in terms of *p*-doping, polymers that show a high level of *n*-doping and are stable in the reduced state are less common. One way to improve *n*-doping is to attach electron-withdrawing substituents to the polymer backbone.²⁸

The HOMO and LUMO energies (and hence bandgap) of polythiophene derivatives can be tuned by adjusting the electron density in the polymer through the use of electron-withdrawing and/or donating substituents. This feature may be utilised for many applications, including OLEDs for display devices, solar cells and OFETs.⁸

The introduction of substituents, however, may lead to steric interactions between the substituents, causing twisting between thiophene rings.⁷⁶ This results in reduced overlap between π orbitals, which increases the band gap and consequently lowers the conductivity of the polymer.^{58,77}

Steric effects can be reduced by two methods. Firstly, unsubstituted thiophene rings can be added to the polymer chain to move bulky substituents apart from each other. This can be achieved by employing substituted thiophene oligomers (bithiophene, terthiophene, tetrathiophene) rather than thiophene,^{54,69,78} or by copolymerising substituted thiophene with unsubstituted bithiophene.^{15,79}

The use of a 'spacer' between the polymer backbone and bulky substituents may also be used to reduce steric hindrance.⁸⁰ Alkyl¹⁵ or alkoxy⁸¹ spacers are commonly used as shown in Fig. 1.14a and b respectively.

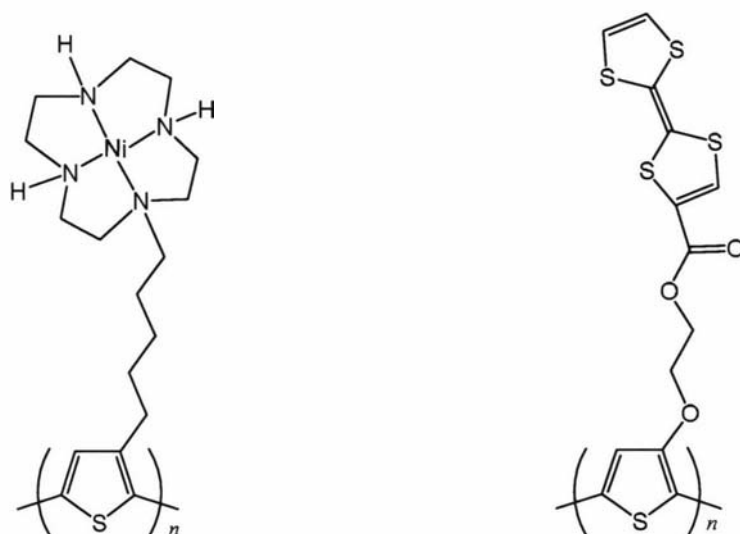


Fig 1.14. Examples of (a) alkyl¹⁵ and (b) alkoxy⁸¹ spacers used to reduce steric hindrance of functional groups between thiophene units.

To allow electronic communication between the polymer backbone and substituent, conjugated linkers, such as phenylene or vinylene, can be employed.²⁵

1.3.4 Styryl-substituted polythiophenes

Functionalisation of thiophene by substituted aromatics (Fig. 1.15) is commonly used to influence the electronic properties of the resulting polymer.^{70,82-84} The ability of aryl-substituents to improve the charge capacity and *n*-doping ability of polythiophenes⁸⁵ has attracted interest in these materials for applications such as rechargeable battery electrodes⁸⁶ and electrochemical capacitors.⁸⁷ However, Visy *et al.* have shown that aryl groups directly bonded to terthiophene force the monomers into a non-planar conformation, thus preventing the extension of the conjugation to the substituents and reducing the conductivity of the resulting polymer.⁵⁴

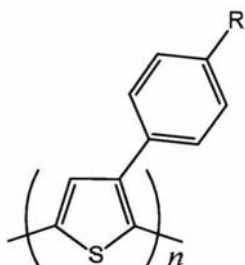


Fig. 1.15. 3-Aryl substituted polythiophene.

In 1994, Smith *et al.*⁸⁸ reported an attempt to improve the planarity and therefore conductivity of aryl-substituted polythiophenes (140 cm^{-1}) by introducing an unsaturated ethylene spacer linkage between the substituted phenyl rings and the polythiophene backbone. The monomer units that were investigated are displayed in Fig. 1.16. It was found, however, that polymerisation of these monomers did not produce electroactive polymers. This was explained by Smith *et al.*,⁴⁸ who revealed by using theoretical calculations, that the 5-position has a very low spin density (reactivity). Although dimerisation through the 2-position was possible, further polymerisation could only be achieved through the more reactive vinylene linker (7-position), causing undesirable defects.

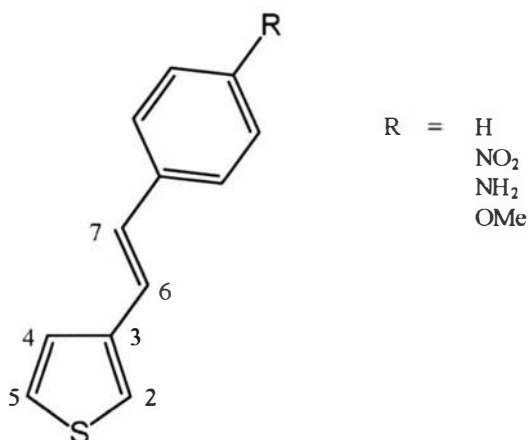


Fig. 1.16. Styryl-substituted thiophene monomers investigated by Cutler.²⁵

It is possible, however, to synthesise electroactive styryl-substituted polythiophenes by copolymerisation: Welzel *et al.*⁸⁹ reported the successful electrochemical copolymerisation of styryl-substituted thiophene with methylthiophene, and Cutler²⁵ with bithiophene. Greenwald *et al.* also achieved chemical co-polymerisation of nitro-substituted styrylthiophene with butylthiophene.⁹⁰

The preparation of an electroactive styryl-substituted polythiophene derivative has also been reported by the electrochemical polymerisation of a substituted styrylterthiophene.⁹¹ The synthesis of styryl-substituted terthiophene (Fig. 1.17) was reported by Collis *et al.* in 2003.⁹² These workers used Wittig chemistry *via* both the terthiophene aldehyde and terthiophene phosphorous species as shown in Fig. 1.18.⁷⁸ This procedure allows a wide variety of substituents to be attached.

Other workers have investigated variants of vinyl-substituted terthiophene-based polymers for photovoltaic applications.^{25,78} Burrell *et al.*⁷⁸ attached a porphyrin dye as shown in Fig. 1.20a in an attempt to further increase the extended conjugated structure and enhance the light harvesting capabilities of the material.⁴² Also using the Wittig reaction, Cutler²⁵ attached an electron-withdrawing nitro-substituent (Fig. 1.20b) to enhance charge separation and increase the photovoltaic performance of polyterthiophene photoelectrochemical (PEC) solar cells. This nitro derivative was electropolymerised and observed to produce a photovoltaic response in these cells.

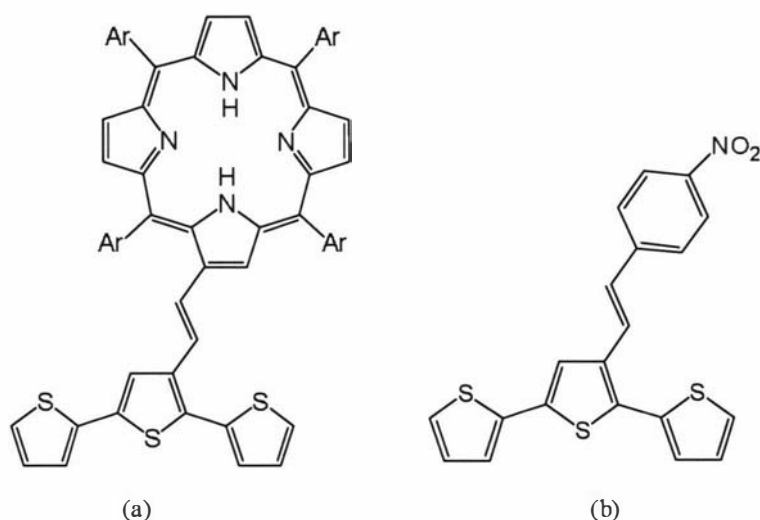


Fig. 1.20. (a) Terthiophene substituted with a tetraphenyl porphyrin (TPP) via a vinyl linker⁷⁸ and (b) nitro-substituted styrylterthiophene synthesised and investigated by Cutler.²⁵

Polymerisation of these materials, however, generally produces insoluble materials that can not be further processed.⁹³ Attachment of alkyl and/or alkoxy chains is one method commonly used to increase the solubility of polythiophenes.^{94,95}

1.3.5 Alkyl and alkoxy substituents

Extensive research has been undertaken into the effect of alkyl substituents on polythiophenes.^{57,73} If sufficiently long, the saturated chains are able to solubilise the polymer in common organic solvents such as DCM, THF and chloroform, which provides considerable advantage for further processing of the polymer.⁹⁶ The chains can also reduce the melting points of alkylthiophenes to allow processing from a melt.⁹⁶ Furthermore, regioregular alkyl chains have been shown by X-ray and light-

scattering studies to improve supramolecular organisation through interdigitation (Fig. 1.21).^{62,97} This can decrease the resulting band-gap and improve conductivity.⁷³

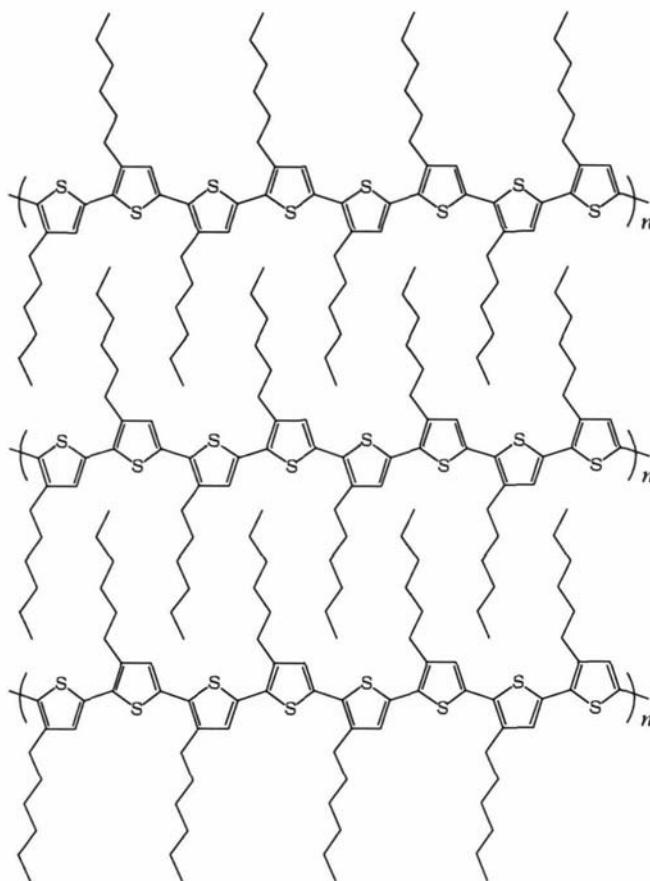


Fig. 1.21. Supramolecular assembly of 3-hexylthiophene by interdigitation of alkyl chains.⁹⁷

Alkoxy chains have also been found to improve polymer solubility.⁶² However, less work has been focused on alkoxy-substituted polythiophenes than alkyl-substituted polythiophenes, presumably due to the high stability of the alkoxy derivatives in the less soluble oxidised state.⁹⁸ Their high stability in the oxidised state means alkoxy derivatives are difficult to reduce, and hence are not very soluble or processable.⁹⁸ The high stability of resulting cationic species in some alkoxythiophene derivatives, has also been found to impede polymerisation and reduce the length of resulting alkoxythiophene polymers.⁸ The use of alkoxybithiophene as a starting material by Zotti *et al.*⁹⁹ was found to moderate this problem.

Alkoxy derivatives do, however, present many advantages over their alkyl counterparts. The stronger electron-donating effect of the alkoxy substituents

decreases the oxidation potential of the monomer,³² although Gallazzi *et al.*⁶² reported that the reactivity of terthiophene monomers depends upon the substitution position of the alkoxy group. Substitution at the 4,4''-position (Fig. 1.22a) was noted to increase monomer reactivity (decrease oxidation potential) more than substitution at the 3,3''-position (Fig. 1.22b).

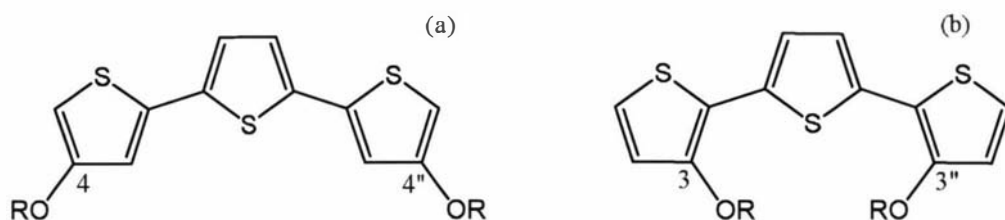


Fig. 1.22. Alkoxy substitution in the (a) 4,4''-positions and (b) 3,3''-positions on terthiophene monomers.

Alkoxy substitution has also been found to generate smaller polymer band-gaps due to increased electron density on the thiophene rings.⁹⁹ This results in lower polymer oxidation potentials and a higher polymer stability in the doped state,³² which is useful for many applications. It has also been suggested by Gallazzi *et al.*⁶² that the higher doping stability may be related to better interactions between alkoxy chains and dopant molecules.

In addition, the presence of an oxygen atom in a 4-position has been shown to allow a more planar polymer chain by reducing steric hindrance between alkoxy substituents,^{59,99} and possibly by producing a favourable interaction with the sulphur atom.¹⁰⁰ This increase in planarity improves π overlap and the effective conjugation length, which in turn leads to enhanced optical and electrical properties.⁹⁹

No detailed study is published on the relationship between the chain length of alkoxy substituents on polythiophenes and polymer solubility, but it has been well established that an increase in chain length of alkyl substituents produces an increase in polymer solubility.⁶¹ Although an increase in alkyl chain length increases the interchain distance,⁶² it has also been found to increase the degree of order and planarity of the

polymer backbone since this is mainly governed by intermolecular interactions of the alkyl side chains.²⁰

1.3.6 Thienylenevinylene based conducting polymers

To date, thienylenevinylene-based polymers (Fig. 1.23) have been found to generate the smallest HOMO-LUMO band gap of all π -conjugated polymers of comparable chain length.⁴⁶ Poly(thienylenevinylene) has been found to produce a band gap that is 0.20 - 0.3 eV lower than that for polythiophene (2.67 eV¹⁰¹).¹⁰² This is caused by an increase in the effective conjugation length due to a suppression of the rotational disorder of the polymer chain created by the rigid ethylene linkages.⁴⁶ The exhibition of low band gaps by thienylenevinylene derivatives has prompted interest in these materials for use in applications such as photovoltaics^{103,104} and field-effect transistors.¹⁰⁵

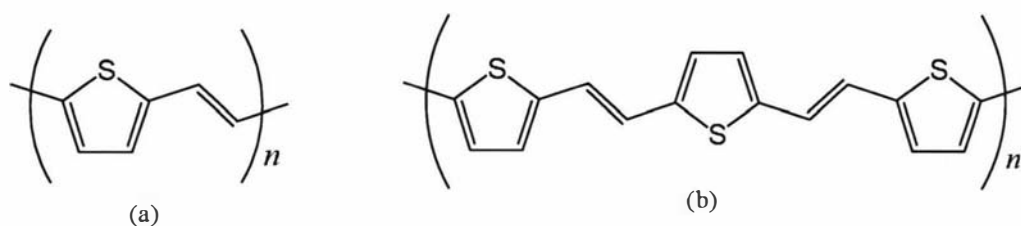


Fig. 1.23. (a) Poly(thienylenevinylene) and (b) poly(terthienylene-vinylene).

As observed for polythiophenes, Ono *et al.* has found that chain extension of thienylenevinylene polymers results in a bathochromic (red) shift of the absorption maximum, and a reduction in oxidation potential.¹⁰⁰ These workers also reported that electron-donating substituents, such as alkoxy groups, reduce the oxidation potential of thienylenevinylene monomers.¹⁰⁰ Other workers have achieved solubilisation of the resulting poly(thienylenevinylene)s by attaching alkyl substituents.^{102,106,107}

1.4 Scope of work

The aim of this study was to investigate the effect of electron-withdrawing and electron-donating substituents on the polymerisation of styryl-substituted terthiophene and terthiylenevinylene derivatives, and the influence of these substituents on the electronic and spectroscopic properties of the resulting polymer. As previously discussed, the use of functionalised terthiophene and terthiylenevinylene oligomers as monomer units reduces the oxidation potential and decreases steric interactions between bulky substituents. The conjugated styryl linker also alleviates steric hindrance between substituents, and allows electronic communication between the functional group and polymer backbone.²⁵

The chemical and electrochemical polymerisation of a series of styryl-substituted terthiophenes (Fig. 1.24, $m = 0$) was investigated in this study, and the resulting materials characterised using mass spectrometry, UV-VIS-NIR and NMR spectroscopy, and microscopy (Chapter 3). For comparison, the electrochemical polymerisation of a corresponding series of styryl-substituted thiylenevinylenes (Fig. 1.2.4, $m = 1$) was also examined (Chapter 4). In order to develop processable polymers for a range of applications, the chemical and electrochemical polymerisation of alkyl and alkoxy-substituted styrylterthiophene was performed (Chapter 5), and preliminary studies of the resulting soluble materials were conducted in applications of solar cells, actuators and batteries (Chapter 6). Attempts were also made to develop high surface area electrode materials using one of these polymers.

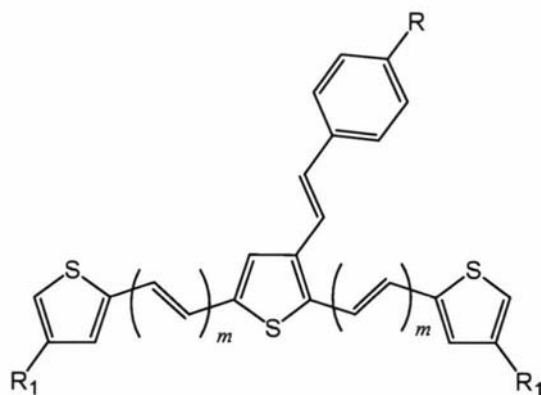


Fig. 1.24. Styryl-substituted terthiophene ($m = 0$) and terthiylenevinylene ($m = 1$) materials investigated in this study.

Chapter 2

Experimental Methods

2.1 Electrochemical techniques

2.1.1 Introduction

Electrochemistry can be used to produce a redox reaction by applying a potential between two electrodes. In the case of conducting polymers, it can be used to oxidise monomeric species in solution to form a polymeric film on an electrode surface. This film can then be repeatedly oxidised and reduced by applying appropriate potentials, as evidenced by the flow of electric current. When compared to other methods used for synthesising conducting polymers such as electrospinning⁷ and chemical methods,²⁷ electropolymerisation presents several distinct advantages. These include absence of a catalyst, direct grafting of the doped conducting polymer onto the electrode surface, and ready control of film thickness by the deposition charge. Electropolymerisation also offers the prospect of an *in-situ* study of the growing process by electrochemical and/or spectroscopic techniques.

2.1.2 Cell design

Electrochemistry was performed in this study using a standard one compartment, three-electrode cell that consisted of a working electrode (WE), counter electrode (CE) and a reference electrode (RE). A schematic of the set-up is shown in Fig. 2.1. In three-electrode circuits, the working electrode is where the electrochemistry of interest occurs. The potential of the WE is monitored by a reference electrode and controlled by the potentiostat. No current flows through this reference electrode; instead, a counter electrode is introduced to complete the circuit. The potentiostat controls the potential difference between the WE and RE by altering the current flowing through the WE – CE circuit.

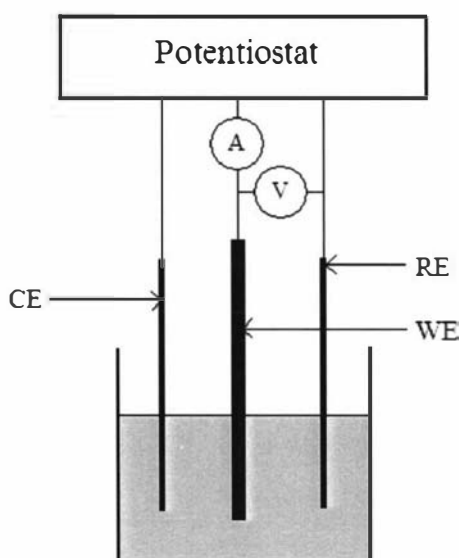


Fig. 2.1. Schematic of a three-electrode one compartment cell.

At the WE, the generation of Faradaic current takes place due to an electron transfer process.⁹¹ A wide variety of types and sizes of substrates may be used for the WE so long as they are conductive. A platinum microelectrode or disc electrode was used in this study for the electrochemical analysis of polymer growth and the resulting polymer.

Microelectrodes have very small surface areas, typically of *ca.* $10 \mu\text{m}^2$. The use of electrodes of micron dimensions provides several advantages over standard electrodes with larger surface areas ($>100 \mu\text{m}^2$). These include a decrease in the ohmic potential (iR) drop at the electrode/solution interface (as very low currents are produced), a decrease in the production of an electrode/solution capacitance, and a change in the diffusion field from the bulk solution to the electrode surface from linear to radial (Fig. 2.2).¹⁰⁸ The formation of a radial diffusion field allows the effects of diffusion of species to the electrode surface, such as monomer and/or electrolyte, to be minimised.¹⁰⁸

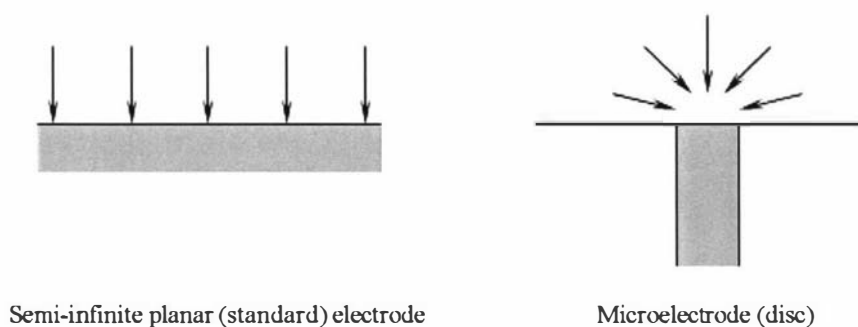


Fig. 2.2. Illustration showing the linear and radial diffusion fields produced at standard electrodes (SA: $>100 \mu\text{m}^2$) and disc microelectrodes.¹⁰⁸

A platinum disc electrode, which has a higher surface area (1.8 mm^2) was employed for the deposition and analysis of more soluble materials. Other working electrodes employed in this study include conductive fabrics, polymer-coated membranes and transparent ITO-coated glass for characterisation of thin polymer films by spectroscopic and microscopic techniques.

The role of the CE is to balance the Faradaic process of the WE with an equal but opposite redox reaction, but has no effect on the Faradaic processes. The processes occurring at the CE are therefore of no interest in this experiment and no attempt is made to monitor this electrodes potential. Platinum or stainless steel mesh was used to ensure the CE provided a larger surface area than the working electrode, so the current flow would not be limited.

A Ag/AgNO_3 reference electrode with a 0.1 M tetrabutylammonium perchlorate (TBAP)/acetonitrile (AN) salt bridge, as shown in Fig. 2.3, was generally used in this study. This electrode has an $E^0 = 0.098 \text{ V}$ vs the Fc^+/Fc (ferrocene) couple and an $E^0 = -0.300 \text{ V}$ vs SHE. In this study, potentials are measured and quoted with respect to this Ag/Ag^+ electrode, except for the spectroelectrochemical experiments in which a silver wire was used as a pseudo reference electrode ($E^0 = +0.380 \text{ V}$ vs Ag/AgNO_3).

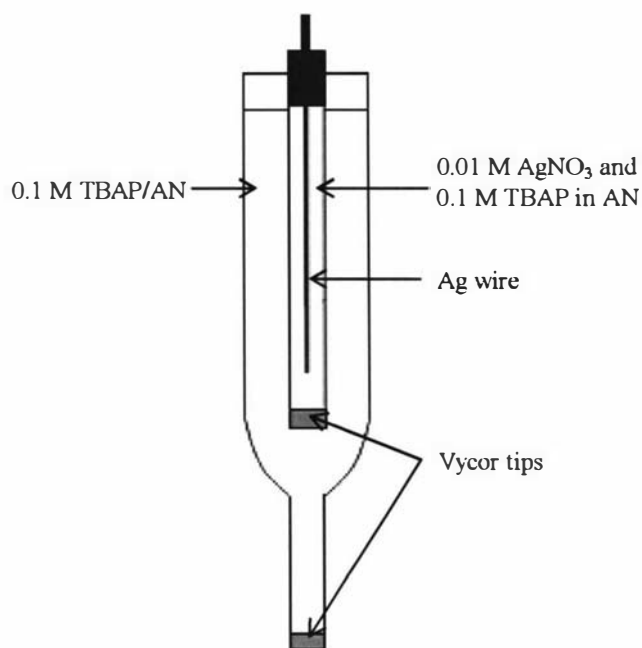


Fig. 2.3. Schematic of the Ag/0.01 M AgNO₃ reference electrode and TBAP/AN salt bridge used in this study.

Monomer concentrations of 5 mM were generally employed for electrochemical analysis. The solvent used for electropolymerisation is an important factor influencing not only the quality of the material obtained, but also its conductivity, morphology and subsequent electrochemical and chemical behaviour.^{61,109} A 1:1 mix of acetonitrile (AN) and dichloromethane (DCM) was most commonly used in this study. Acetonitrile is a versatile and popular polymerisation solvent for several reasons. Firstly, it provides poor solubility or insolubility of most oligomers (materials with chain lengths comprising less than ten monomer units) and conducting polymers, which allows nucleation and growth on an electrode surface.¹¹⁰ It is also slightly basic, assisting proton removal for the polymerisation process.¹⁰⁹ It was found, however, that some monomers investigated in this study have poor solubility in acetonitrile. For this reason, addition of DCM to the solvent mix was sometimes required. A 1:1 AN:DCM mix was found to dissolve all monomers involved in this study at a concentration of at least 5 mM, but provided a sufficiently low solubility of longer oligomers as they were formed so they would adhere to the electrode.

Tetrabutylammonium perchlorate (TBAP) is a commonly employed electrolyte and was used in this study in large excess (100 mM, electrolyte:monomer ratio of minimum 20:1) to ensure the current flow was not limited. All solutions were freshly prepared and degassed by sonication or nitrogen purging immediately prior to experimentation.

2.1.3 Electrochemical techniques

Introduction

Cyclic voltammetry (potentiodynamic growth) and constant potential (potentiostatic growth) have been used to deposit the materials investigated in this study. Although galvanostatic growth (constant current) procedures can be used when control of charge is desired, this method has a propensity to yield polymer of poorer morphology and conductivity.^{109,111}

Cyclic Voltammetry

Voltammetry is an electroanalytical technique in which redox information about the analyte (monomer, oligomers or polymer in this study) can be obtained by measuring the current as a function of applied potential.

In cyclic voltammetry, the potential is applied in a saw tooth mode to the working electrode as demonstrated in Fig. 2.4. The cycle commences at a predetermined potential. The potential is increased or decreased in a linear fashion with a fixed scan rate (usually expressed in mV s^{-1}) to the maximum/minimum limit. The direction of the linear scan is immediately reversed (at the same rate) until the opposite potential limit is attained. The scan direction of the potential scan is again immediately reversed until the starting potential is reached. This cycling may be repeated many times.

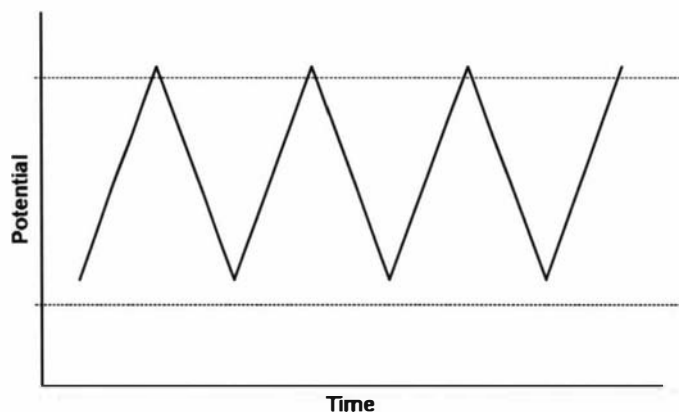


Fig. 2.4. Variation of potential with time for cyclic voltammetry.

A typical cyclic voltammogram (CV), using ferrocene as an example, is shown in Fig. 2.5. Two peaks are displayed due to a single reversible electron transfer process.¹¹² The peak on the positive scan (forward scan) is due to oxidation of ferrocene to a positively charged state, and the peak on the negative scan (reverse scan) is due to reduction back to a neutral state. From cyclic voltammetry, the oxidation potential and reduction potentials of the Fc/Fc^+ couple can be estimated as shown. The total charge passed during the oxidation/reduction process can also be determined by measuring the area under the curve.

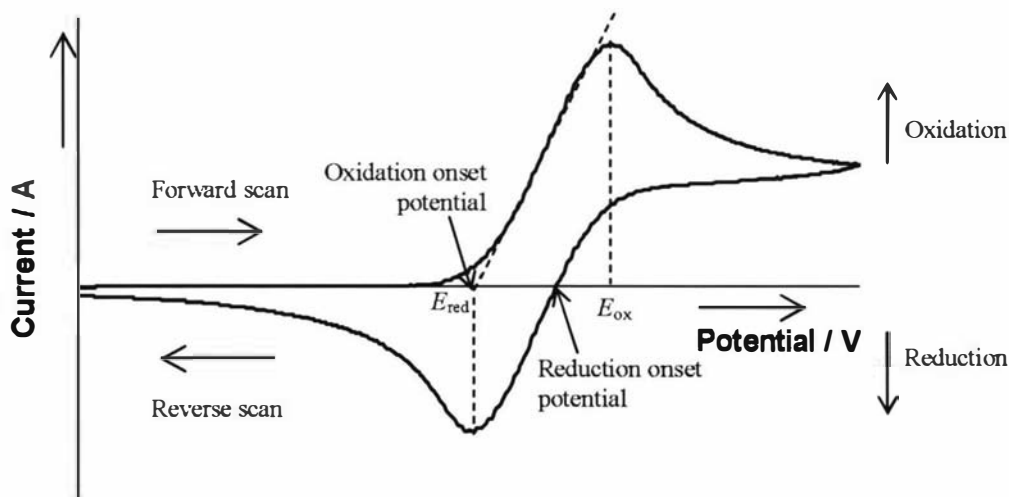


Fig. 2.5. A CV of ferrocene, demonstrating a single reversible electron transfer process on a platinum disc electrode ($\text{SA} = 1.8 \text{ mm}^2$).

Although cyclic voltammetry is often used as a characterisation technique, oxidation of some species may result in insoluble compounds, which are deposited onto the electrode surface. In this way, monomers can be oxidised to form films of oxidised polymer attached to the electrode surface.

The growth CV of terthiophene on a platinum disc electrode is displayed in Fig. 2.6. The initial cycles differ from subsequent scans with respect to charge passed, oxidation threshold potential, and the shape of the current-response curve. As each scan represents further growth of polymer on the electrode, this response is most likely due to deposition onto different substrates with each scan as the platinum surface is modified with the deposited material. The observed increase in current with successive scans is consistent with an increase in electroactive surface area and/or more facile electrode kinetics due to the change in electrode substrate (platinum to polymer) as a polymer film is deposited. A higher electroactive surface area allows more polymer to be deposited and hence more current to flow. In contrast, deposition of a non-conductive polymer film would cause a decrease in current as the electrode becomes insulated from the solution. Also evident is a decrease of the oxidation onset potential after the first cycle. This suggests that polymer growth on the deposited material is more readily achieved than growth on the polished platinum electrode, possibly due to the formation of nucleation sites.

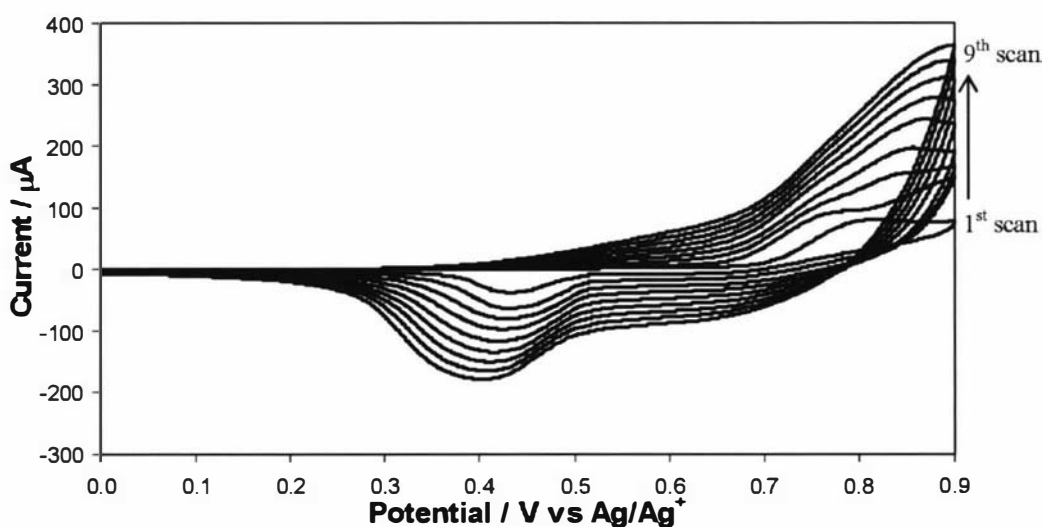


Fig. 2.6. Potentiodynamic growth of terthiophene on a platinum disc electrode ($\text{SA} = 1.8 \text{ mm}^2$). Supporting electrolyte: 0.1 M TBAP/AN. Potential limits: 0/+900 mV. 9 cycles. Scan rate: 100 mV s^{-1} .

One problem with using cyclic voltammetry as a growth method of conducting polymer films, is that over-oxidation can easily occur if scan limits are not set correctly.¹¹² An electrochemical ‘window’ exists for most conducting polymers within which the doping/dedoping process is mostly reproducible (although not necessarily reversible). Anodic potentials which are set too high have been shown to cause irregularly α,β -linked rings¹¹³, oxidation of functional groups,¹¹³ or reactions of the polymer with solvent molecules or impurities (e.g. water or gas).⁷⁰ Each monomer was initially analysed by scanning between potentials of -1 V and $+1.5$ V to determine appropriate scan limits for electrochemical growth. The anodic limit was set at a potential slightly higher than the potential at which material was observed to adhere to the electrode surface.

Films of conducting polymer deposited on an electroactive surface (by methods such as electrochemical growth, or casting or spin-coating of a polymer solution) may be investigated by cyclic voltammetry. This is usually achieved by cycling the film, as the working electrode, in a monomer-free electrolyte solution. The post-polymerisation CV of an electrochemically polymerised dialkoxytyryl-substituted terthiophene (OC₁₀DASTT), deposited on a platinum microelectrode is shown in Fig. 2.7. In comparison to the narrow peaks produced by ferrocene (Fig. 2.4), this CV displays broad oxidation and reduction peaks, typical of redox processes for a number of species and indicating a wide range in polymer lengths. From this CV, the oxidation onset potential, $E_{\text{oxidation onset}}$, of the polymer can be determined, and the total charge passed during the cycle calculated from the area inside the curve.

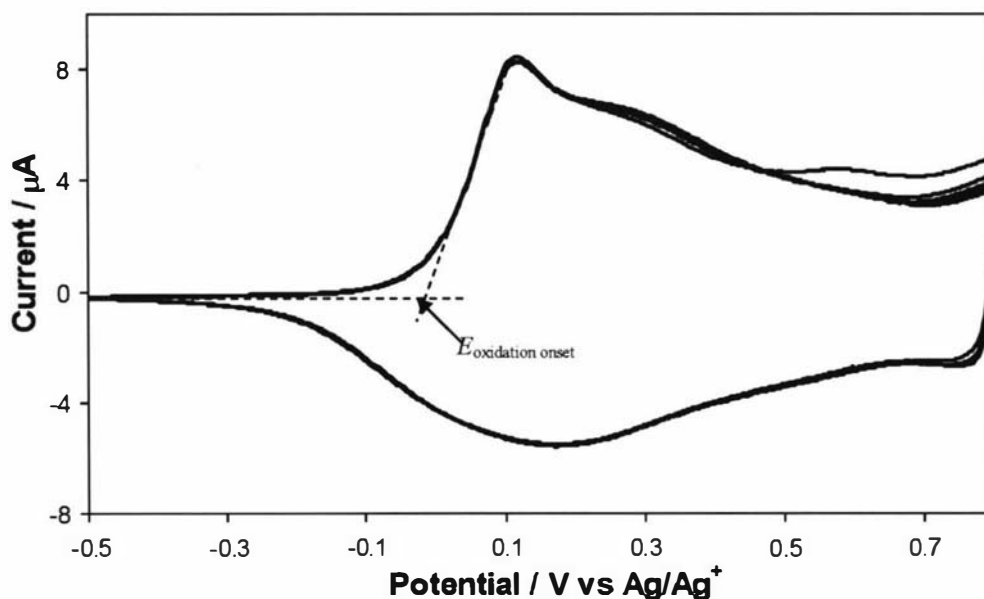


Fig. 2.7. Post-growth CV of OC₁₀DASTT on a platinum micro electrode (SA: 10 μm²). Electrolyte solution: 0.1 M TBAP 1:1 AN:DCM. Potential limits: -500/+800 mV. Scan rate: 100 mV s⁻¹.

Potentiostatic growth

Potentiostatic growth involves ‘stepping’ the potential from a potential that produces no reaction, to one that does. The potential is then held steady as the current produced is measured as a function of time. A typical potential vs time profile and corresponding chronoamperogram are shown in Fig. 2.8. A sharp current transient corresponding to the potential step is observed. This is due to charging of the double layer (layer between the electrode and solution), which produces a non-Faradaic current. Oxidation of the monomer then produces a Faradaic current. If a conducting polymer is formed, the current should increase due to an increase in the electroactive (conducting polymer) surface area.⁶¹ This is observed in the chronoamperogram of the growth of styryl terthiophene (STT) polymer, shown in Fig. 2.9. Polymer growth, as observed by the current produced, may be limited by diffusion of monomer from the bulk solution to the vicinity of the electrode.⁴⁷ Potentiostatic growth is useful as the thickness of the film can be easily estimated and controlled by measuring the charge which has passed.

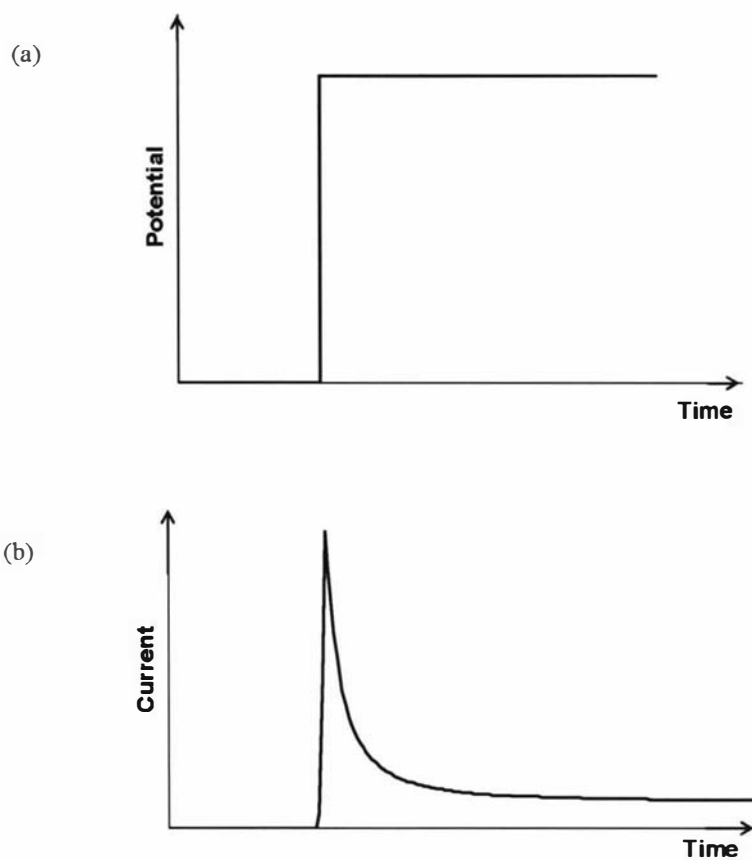


Fig. 2.8. (a) The function of potential versus time with (b) the corresponding chronoamperogram.

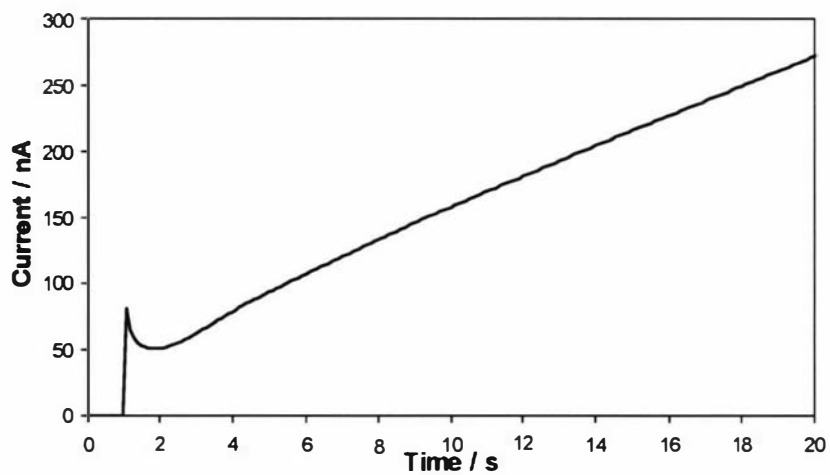


Fig. 2.9. Potentiostatic growth of polySTT on a Pt micro electrode (SA: $10 \mu\text{m}^2$). Solvent: 1:1 AN:DCM. Potential held at -500 mV for 1 s, then stepped to 900 mV for 19 seconds.

2.2 MALDI-TOF mass spectrometry

2.2.1 Introduction

The average molecular weight and polydispersity (range of weights) of conducting polymers determine fundamental properties such as conductivity, colour and solubility.¹¹⁴ Matrix Assisted Laser Desorption/Ionsition Time-Of-Flight Mass Spectrometry (MALDI-TOF MS) is a well established and frequently used technique for studying the chain length of conducting polymers,^{64,73,96,115} and has been used in this study to investigate soluble fractions of chemically and electrochemically synthesised polymers. Compared to other mass spectrometry techniques such as Fast Atom Bombardment (FAB) and Electrospray Ionisation (EI), MALDI-TOF MS is a relatively 'soft' technique in that it results in little molecular fragmentation. This is desired for polymer analysis since a relatively simple spectra displaying the mass of parent ions is produced, and a more accurate distribution of polymer masses can be obtained. MALDI-TOF MS also has a wide mass range of up to 300000 Da.¹¹⁶

Like most mass spectrometry techniques however, MALDI-TOF MS is not quantitative and the intensity of peaks depends on many variables including the type of sample, sample preparation and instrumental parameters.¹¹⁷

2.2.2 Instrumentation

In this study, mass spectrometry was performed using a Micromass MALDI LR mass spectrometer (Micromass Ltd., Manchester, UK), with a 337 nm nitrogen laser with a pulse duration of 2 ns, an acceleration voltage of 15 kV, and MassLynx control and processing software. A fast dual micro-channel plate (MCP) detector was used, with signal gating for the rejection of low mass matrix ions. The instrument was used in linear mode to maximise sensitivity.

A pulsed laser beam is directed at a sample dissolved or suspended in a matrix as shown in Fig. 2.10. The matrix absorbs the laser light energy causing it to vaporise and

carry some of the sample with it. The matrix may subsequently help to ionise the analyte molecules, which are then carried into a mass analyser.

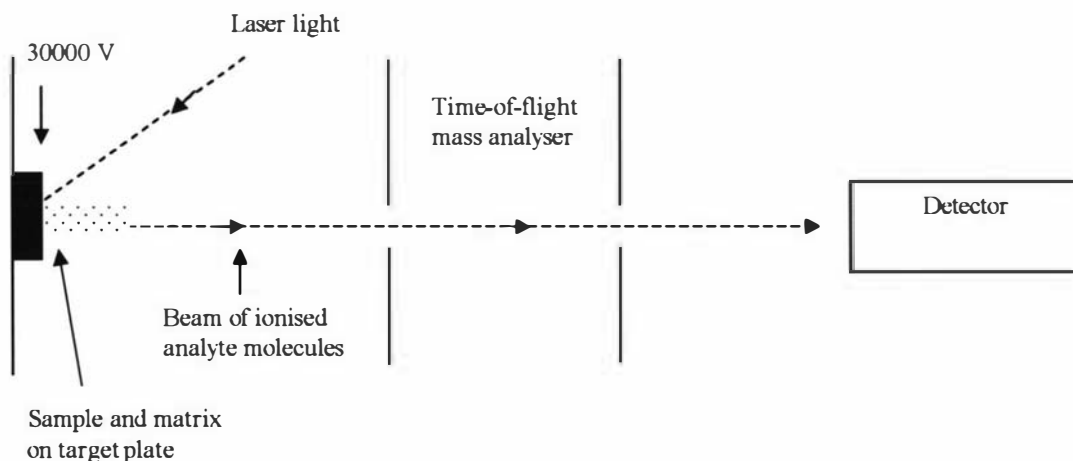


Fig. 2.10. Schematic of MALDI-TOF MS instrumentation.

TOF mass analysers are relatively simple. They are based on accelerating a set of ions to a detector with the same amount of energy. Since the ions have the same amount of kinetic energy (E_K) yet different mass (m), the ions have different velocities (v) and therefore reach the detector at different times. By calibration of the instrument with compounds of known masses, the mass of a sample may be determined from the time of flight.

$$v = \sqrt{\frac{2E_K}{m}}$$

v – Velocity
 E_K – Kinetic energy
 m – mass

The time-of-flight mass analyser can be used in two different modes: linear or reflectron. The fundamental difference between these modes is that the reflectron mode utilises an ion mirror which reflects the ions and creates a longer flight path (Fig. 2.11). By increasing the flight path and slowing down the ions, the ion mirror reduces the ion distribution and effectively increases the resolution. However, it also reduces the sensitivity and lowers the mass limit to below 10000 Da since heavier ions are not able to be reflected.

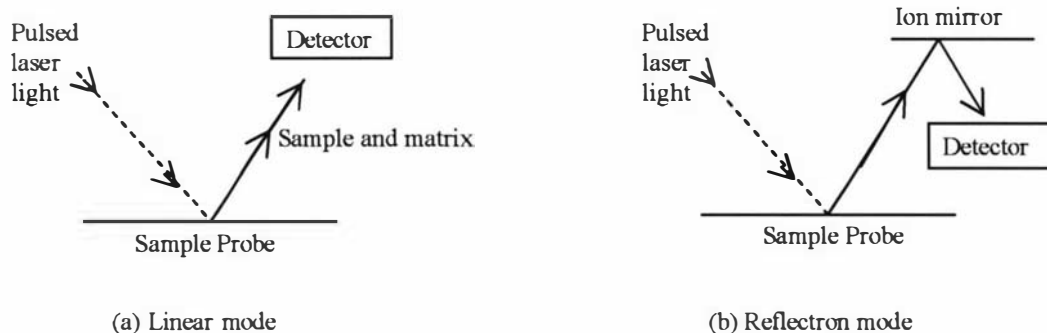


Fig. 2.11. Schematic illustrating the difference between the (a) linear and (b) reflection modes used in MALDI-TOF MS.

The linear method is much more sensitive than the reflectron method and is better suited for mass analysis between 5000 and 300000 Da. However, the linear mode exhibits poor resolution when compared to the reflectron method and other mass analysis techniques. This is because the ions do not travel as far in the mass analyser and are therefore not separated as well before reaching the detector. It was also found in this study that the linear mode can be difficult to calibrate accurately.

Spectra of a terthiophene polymer derivative which has been analysed by the linear and reflectron modes, are shown in Fig. 2.12a and b, respectively, for comparison. Although the longest oligomer detected in the reflectron mode has a mass of ~5300 Da, oligomers with molecular weights of up to ~8300 Da can be detected in the same sample using linear mode. This demonstrates the enhanced sensitivity in detection of oligomers, particularly long oligomers, with the linear method. The reproducibility of spectra obtained from a sample when using the same mode (linear or reflection) is generally very good with peak intensities showing comparable distributions.

Fig. 2.12c is an enlargement of one of the peaks produced by the linear method, most likely corresponding to an oligomer with a mass of 5946.32 Da, and demonstrates the poor resolution of the linear mode. As observed, the band is very broad and ranges over approximately 36 units from approximately 5939 to 5975 Da.

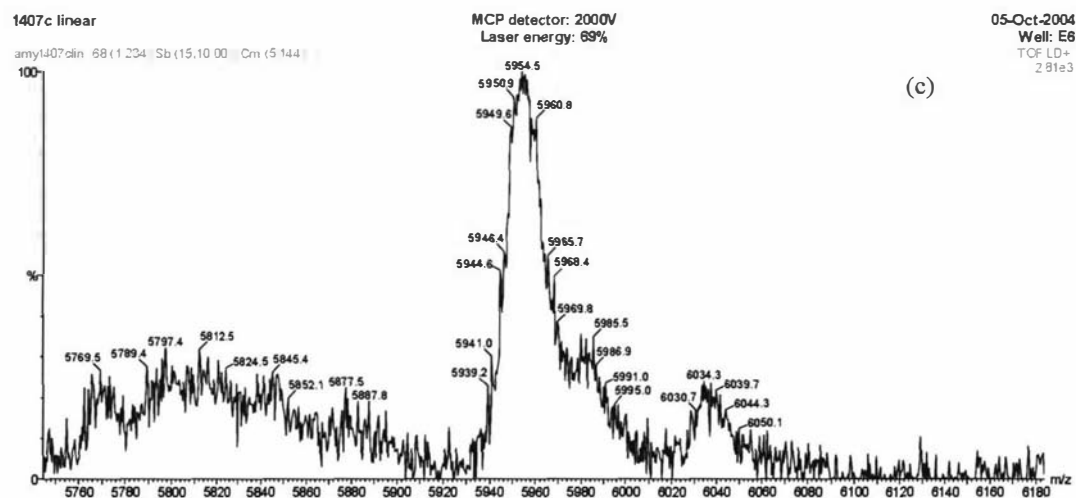
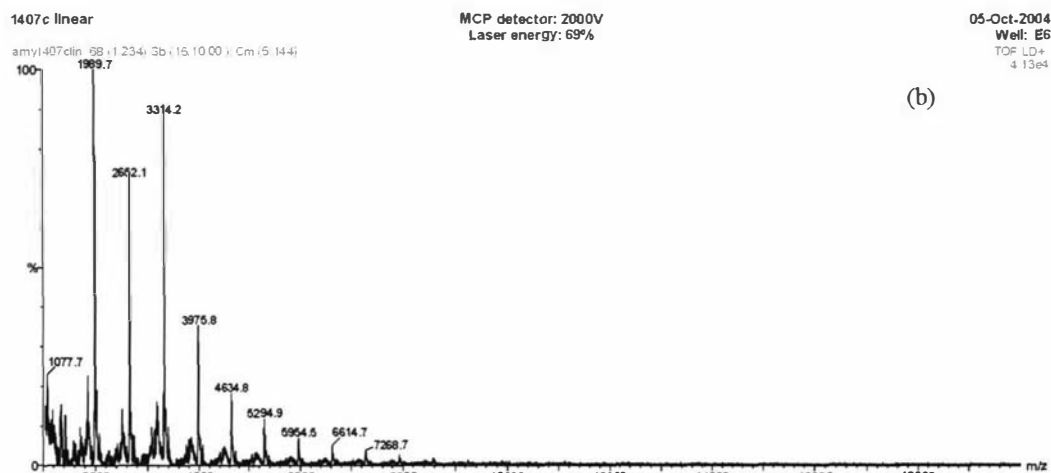
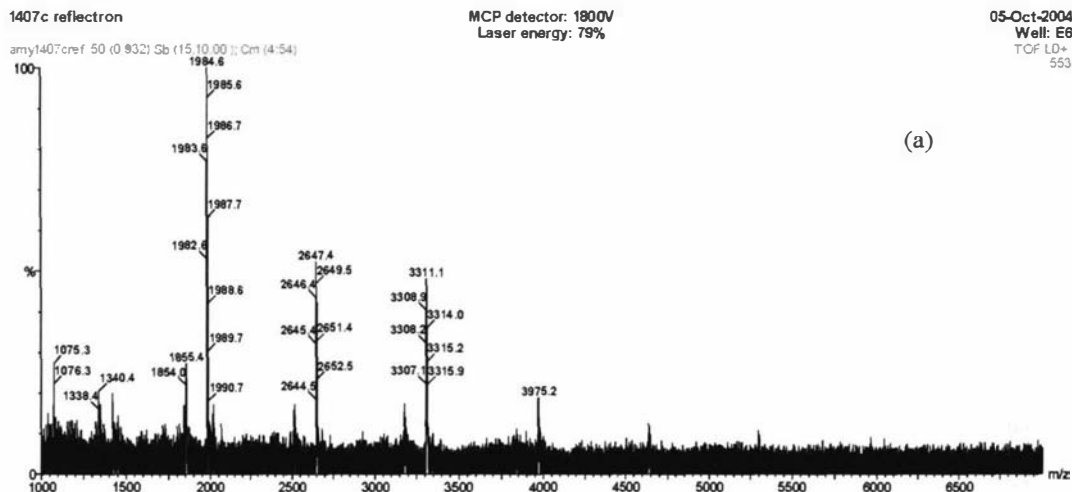


Fig 2.12. MALDI-TOF mass spectra of a polyOC₁₀DASTT sample (monomer $M_r = 662.48 \text{ g mol}^{-1}$). (a) Measured using reflectron mode. (b) Measured using linear mode. (c) Enlargement of a peak generated by the linear mode.

2.2.3 Data acquisition and sample preparation

The MALDI-TOF MS target plate contains wells onto which the sample is loaded. The laser was fired at the sample. After about 5-10 seconds, the sample was exhausted and the laser beam was moved to a spot containing fresh sample. About 5 scans a second were recorded, and at least 100 scans were recorded for each sample in this study. When enough scans were recorded (i.e. the signal:noise ratio was sufficient), the laser was moved to a 'lockmass' well, which contains a calibrant. All scans were then combined.

Sample preparation and instrument settings (acceleration voltage and laser energy) can affect the quality of spectra obtained by affecting the ratio of signal to noise. There are many variables for sample preparation and data acquisition. The effect of the solvent used for sample preparation, the matrix, the sample concentration and spotting methods were investigated by using a sample of chemically polymerised polyOC₁₀DASTT that has a monomer mass of 662.48 Da.

The choice of solvents is limited by the solubility of the sample and matrix. Organic solvents tend to produce a more uniform layer with smaller matrix crystals which gives better reproducibility between samples. Chloroform is a commonly employed solvent and was chosen for the present research as it was found to be the best solvent for the polyterthiophenes investigated in this study. It was necessary, however, to use mixtures of solvents (such as methanol/acetonitrile) to dissolve some of the matrices that were investigated. An aqueous solvent mixture was used for the calibrant.

In order to determine the most appropriate matrix for the analysis of the polymers produced in this work, five different matrices were tested, namely: trans-retinoic acid, 2-(*p*-hydroxyphenylazo)benzoic acid, α -cyano-4-hydroxycinnamic acid, dithranol and terthiophene. Dithranol and terthiophene were found to give the best signal:noise ratio which is consistent with results found in literature on MALDI-TOF MS analysis of polythiophene derivatives.^{64,96} As conducting polymers tend to undergo charge transfer as the predominant cationisation process,⁹⁶ this may be due to the electron-transferring properties of these matrices.⁶⁴

Matrices were prepared at a concentration of 10 mg mL⁻¹. Three sample:matrix ratios (1:5, 1:20 and 1:125) were investigated. These ratios had little effect on the appearance of the spectra. However, it was found that the sample concentration did affect the signal to noise ratio, with the optimal sample concentration typically between 10 mg mL⁻¹ and 0.1 mg mL⁻¹.

Two methods are commonly used for spotting the sample and matrix onto the MALDI-TOF MS target plate: premixing or layering. First the sample and matrix are dissolved in appropriate solvents and at desired concentrations. Premixing involves mixing equal volumes of the matrix and sample solutions and then spotting ~100 µL onto each well. To layer the sample, 50 µL of matrix solution is spotted onto the well and allowed to dry, followed by spotting 50 µL of the sample solution. The sample solution is usually spotted after the matrix solution to allow a more even covering. It was observed that dithranol gave very poor or insignificant signal when layered, but usually resulted in a satisfactory signal when the sample and matrix were premixed. The spotting methods employed while using terthiophene as a matrix did not significantly affect the spectra.

Four calibrants were used to calibrate the MALDI-TOF MS instrument. These were renin (1759 Da), angiotensin (1297 Da), adrenocorticotrophic hormone (ACTH, 2466.7 Da) and bovine insulin (5434.6 Da). ACTH was spotted onto the lockmass well and used as a concurrent calibrant. During acquisition, the laser could be switched to the lockmass well to obtain a peak which represents the calibrant. A separate well was used because often calibrants require a different sample preparation, such as spotting from a different solvent.

The highest laser energy that could be employed without saturating the detector was used for all measurements. It was observed that laser energy affects only the signal:noise ratio and makes no apparent difference to relative peak intensities and or measured oligomer distribution. It was found that an acceleration voltage of 15000 V gave the best signal:noise ratio. In this study, detection has been suppressed below 320, 500 or 1000 Da to prevent saturation of the detector by matrix ions.

2.2.4 Calculation of polydispersity

Polydispersity (PD) is a ratio used to represent the broadness of the molecular weight distribution of a polymer sample. Polydispersity is the ratio of the number average molecular weight (M_n) to the weight average molecular weight (M_w) of a polymer sample. The number average molecular weight is calculated by:

$$M_n = \frac{\sum N_i M_i}{\sum N_i}$$

and the weight average molecular weight is calculated by

$$M_w = \frac{\sum N_i M_i^2}{\sum N_i M_i}$$

where N_i is the number of molecules of molecular weight M_i .⁹⁶

Numerous studies have shown that MALDI-TOF MS provides reasonably accurate molecular weight information for a variety of polymers with a low polydispersity (<1.2).^{64,115,118,119} However, MALDI-TOF MS of samples with a high polydispersity (>1.2) are often reported not to be representative of the molecular weight distribution, with the high-mass component underrepresented with respect to the low-mass component, resulting in significantly lower average molecular weight values.^{96,117,120,121} This mass-discrimination effect is thought to be caused by several factors including mass-dependent desorption/ionisation, sample preparation, ion focussing/transmission and mass-dependent ion detection.^{117,122}

2.3 ^1H NMR Spectroscopy

^1H NMR spectroscopy can be a useful technique for the characterisation of soluble polythiophene derivatives. Defects in polymerisation such as α - β coupling or substitution by nucleophiles derived from the oxidant (such as chloride ions) may be determined.⁶² In addition, if oligomers have equivalent protons at the terminal positions, the chain length of a polymer can sometimes be determined by comparison of the integration of signals due to the terminal protons with signals from protons at other sites.¹¹⁴ For example, polymerisation of terthiophene results in a loss of equivalent protons at the terminal ' α ' positions as seen in Fig. 2.13. This is observed in ^1H NMR spectra as a decrease in integrated area of the signal due to this proton in relation to other signals. The length of the polymer can be determined by the ratio of the terminal protons to protons at the 3' and 4' position.

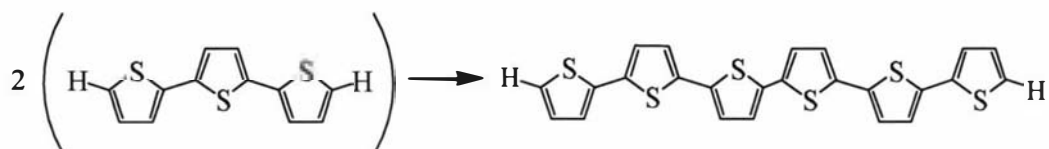


Fig. 2.13. Dimerisation of terthiophene showing the loss in terminal protons.

Terthiophene monomers that are not centrosymmetric, such as the styrylterthiophene derivatives investigated in this study (Fig. 1.24, Chapter 1), show two signals due to inequivalent protons at the terminal positions, H_H (at the 5 position) and H_T (at the 5'' position). These unsymmetric monomers can join in three different orientations: head-to-head (HH), tail-to-tail (TT) and head-to-tail (HT) (Fig. 2.14). ^1H NMR spectra of pure samples of each of these isomers would be expected to show, respectively, a loss in signal due to the H_H protons, equal signals due to the H_T and H_H protons, and a loss in signal due to the H_T protons.

Further polymerisation to produce non-regioregular polymer would be expected to show broad bands due to a range of different protons, but regioregular polymers may show less complicated spectra due to very similar protons.⁵⁸

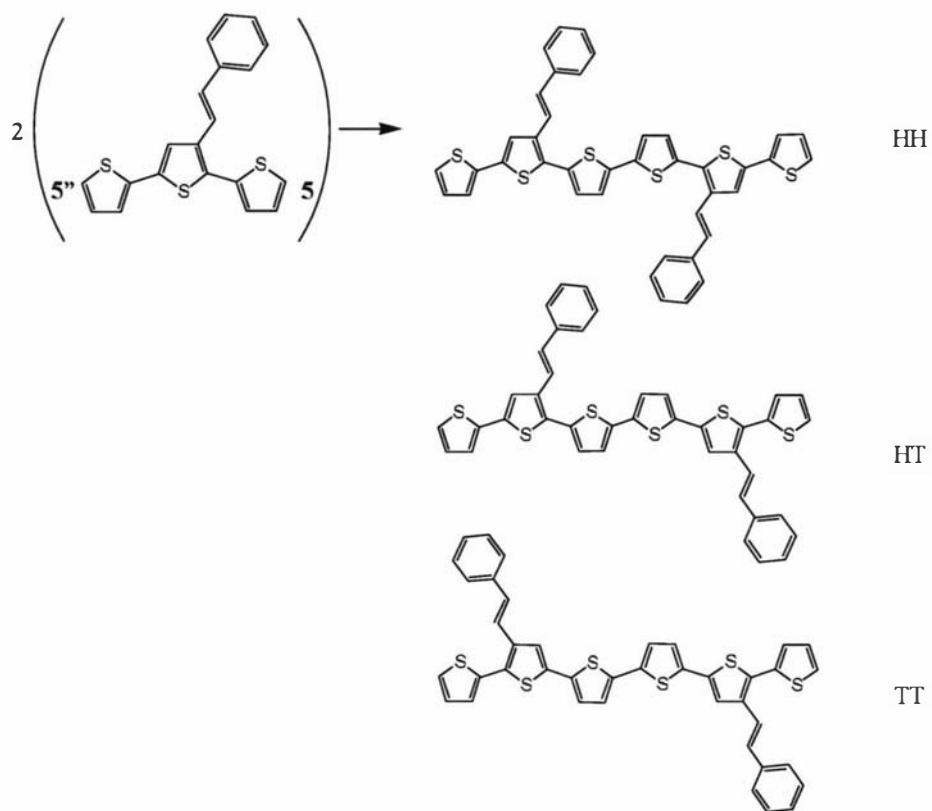


Fig. 2.14. Dimerisation of STT to form three different possible regioisomers: the HH isomer (generated by coupling through the 5 positions), HT isomer (coupling through the 5 and 5' positions) and TT isomer (coupling through the 5' positions).

2.4 UV-VIS-NIR Spectroscopy

Ultraviolet-visible-near infrared (UV-VIS-NIR) spectroscopy is a powerful technique for investigating the electronic properties of conducting polymers. As well as measuring the spectral absorbance of the polymer, properties such as the effective conjugation length, the electronic effect of substituents, the presence of chromophores and the degree to which the polymer is doped can be determined.

All polymers in this study are electrochromic. In the neutral state, thin films usually appear either red or blue, but in the oxidised state they can appear green, or even translucent. This ability of the polymer to reversibly change colour with potential provides promise for applications such as electrochromic display devices and ‘smart windows’.¹²³

Monomeric units possess a HOMO (highest unoccupied molecular orbital) and a LUMO (lowest unoccupied molecular orbital) energy level as shown in Fig. 1.5. Polymerisation of these monomers to give a highly conjugated system results in broadening of these bands to give a corresponding valence band and conduction band. In the neutral state, absorbance bands appear between 200 nm and 900 nm due to $\pi \rightarrow \pi^*$ transitions,¹²⁴ as shown by spectra of 4,4''-bis(decyloxy-3'-nitro-2,2':5',2''-terthiophene) (Fig. 2.15). An increase in the effective conjugation of the polymer leads to broadening of the valence and conduction bands, creating a decrease in the bandgap and a bathochromic shift in this spectroscopic band.¹¹⁴

Oxidation of the polymer may result in the formation of polaron/bipolaron species. These oxidised species show bands which appear between the valence and conduction bands, effectively narrowing the bandgap (Fig. 1.5, Chapter 1), and are typically shown by spectroscopy as an absorbance between about 600 and 1100 nm.¹²⁵ Further oxidation of some conducting polymers may result in a quasi-metallic state being formed. This is shown by UV-VIS-NIR spectroscopy as a broad band extending beyond 1000 nm, known as a ‘free-carrier tail’ (Fig. 2.15).¹²⁵⁻¹²⁷

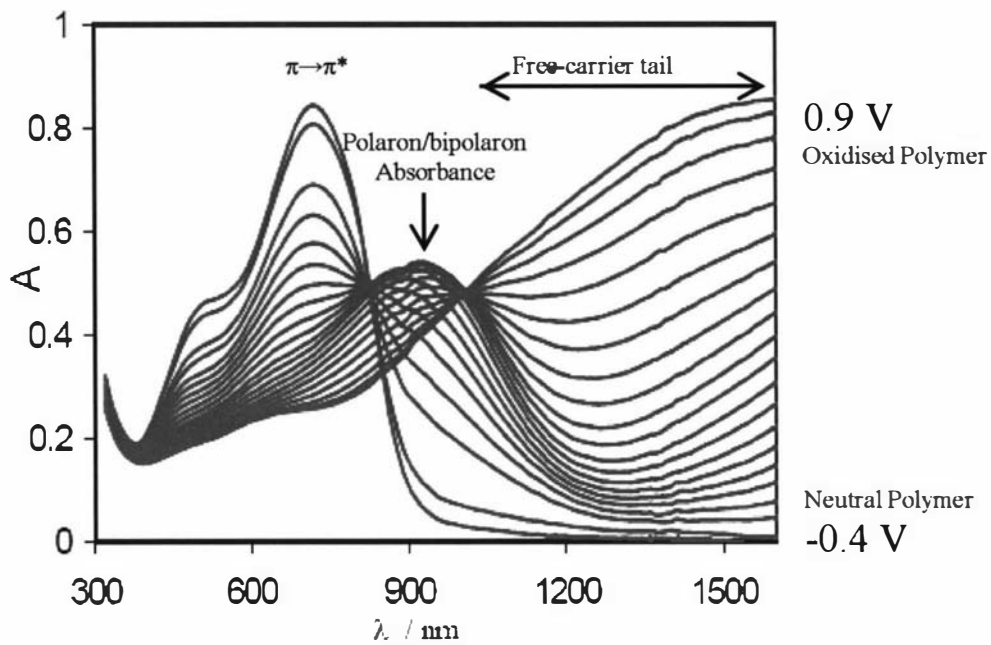


Fig. 2.15. Spectroelectrochemistry of 4,4'-bis(decyloxy-3'-nitro-2,2':5',2''-terthiophene) obtained by Gambhir *et al.*¹²⁸ Reprinted by permission. A free-carrier tail is displayed at wavelengths above 700 nm.¹²⁶

Polymers in this study have been investigated both as films on ITO-coated glass (either cast or electrochemically deposited) and, if soluble, in solution.

2.5 Imaging techniques

The morphology of conducting polymer films may affect their physical properties such as conductivity and tensile strength. Different morphologies are desirable for different applications. For example, a porous film with a high surface area may be advantageous for applications such as photovoltaics, but a more compact, tough and highly conductive film may be required for actuator materials. Surface nanostructures or defects may also affect the properties of a film. Surface morphology can be investigated by several techniques. Scanning electron microscopy (SEM) and atomic force microscopy (AFM) have been employed in this study.

Scanning electron microscopy (SEM) allows visual analysis of surface morphology. SEM operates by scanning the surface with a beam of electrons. Detection of the deflection of the electron beam allows the surface to be imaged. SEM is a useful technique for obtaining a visual image of surfaces. However, the sample must be able to survive being placed under vacuum, and being exposed to a beam of electrons. The resolution of an SEM is limited by lens aberrations to 0.18 nm and magnifications typically range between 2x and 50000x.

Atomic force microscopy (AFM) uses a sharp tip to probe the surface, either by using a dragging motion (contact mode) or tapping motion (tapping mode). Van der Waal interactions between the sample and the tip, which is situated at the end of a cantilever, causes the cantilever to be deflected. Computer generated mapping of these deflections allows production of a 3-dimensional image of the surface. The resolution of the technique is governed by the size of the probe tip, and is typically about 2 nm in the x - y axis and 1 nm in the z axis. The main advantage of AFM is that the surface morphology can be measured and information can be obtained on surface roughness. AFM is carried out in atmospheric conditions and is non-destructive.

2.6 Deposition Techniques

There are several methods to deposit materials on substrates. For device fabrication, a uniform polymer layer is typically preferred. Three techniques which have been employed in this study are casting and spin-coating, (which require soluble materials) and electrochemical deposition (previously discussed). These techniques are effective in different applications because they form films which vary in smoothness, thickness and the state in which the polymer is deposited in (oxidised or reduced).

The simplest method to deposit polymer onto a substrate is to cast it. This involves dissolving the polymer in a solvent, applying the solution to the substrate, and then evaporating the solvent to leave a film. Application of the solution to the substrate can be achieved by drop-casting (dropping solution onto the substrate) or dip-coating (dipping the substrate into the solution). Thickness of the film can be varied by adjusting the concentration of the solution and by applying multiple layers. Evaporation can be achieved simply by exposure to air (which can be slowed by leaving the sample in a closed environment) or by subjecting the sample to a vacuum. Whereas other film deposition techniques (such as electrodeposition and spin-coating) require substrates that are conductive or flat, films can be cast onto a wide range of substrates. Casting also allows a large thickness range to be obtained including films thick enough to be 'free-standing.' However, it is often difficult to control the overall film thickness and homogeneity.

In contrast, spin-coating is a widely used technique to produce very thin and uniform films of soluble materials on flat substrates. It is employed to manufacture films for a variety of applications such as compact disks and flat screen display antireflection coatings. Spin-coating uses simple fluid flow and evaporation processes to form a thin, uniform layer. The substrate is first completely covered with a substantial excess of polymer solution compared to the amount of material required in the final coating. The substrate is then rapidly spun to remove excess solvent and material to leave a thin film. A major advantage of using spin-coating is that it allows the production of films of reproducible thicknesses. The film thickness and morphology can be altered by varying parameters such as solvent, polymer concentration, applying multiple layers,

acceleration rate, spin-rate, time of spinning and solution viscosity. However, the major drawback is that it requires large amounts of material. It was also found in this study that some polymer solutions have a tendency for the polymer to aggregate as it is spun, causing defects.

2.7 Electrospinning

Electrospinning is used to form polymer fibres with a very small diameter (typically <math><500\text{ nm}</math>), which may be useful for applications such as batteries and solar cells where a very high surface area is advantageous. Electrospinning employs an electric field to create a charged jet of polymer solution, while evaporating solvent molecules to form very fine fibres.¹²⁹

A schematic of the experimental setup used in this study is shown in Fig. 2.16. The solution to be electrospun is placed in a hypodermic syringe ~30 cm from a galvanized steel target plate covered with aluminium foil. The positive electrode of a variable high voltage transformer is attached to the metal needle of the syringe, the negative terminal attached to the target plate, and a potential difference (~30 kV) applied across the electrodes. As the solution drips out of the syringe, the positively charged particles overcome surface tension and fly towards the negatively charged target plate.⁴ Electrostatic repulsion of the charged particles assists solvent evaporation to generate fine polymer fibres which collect on the target plate.

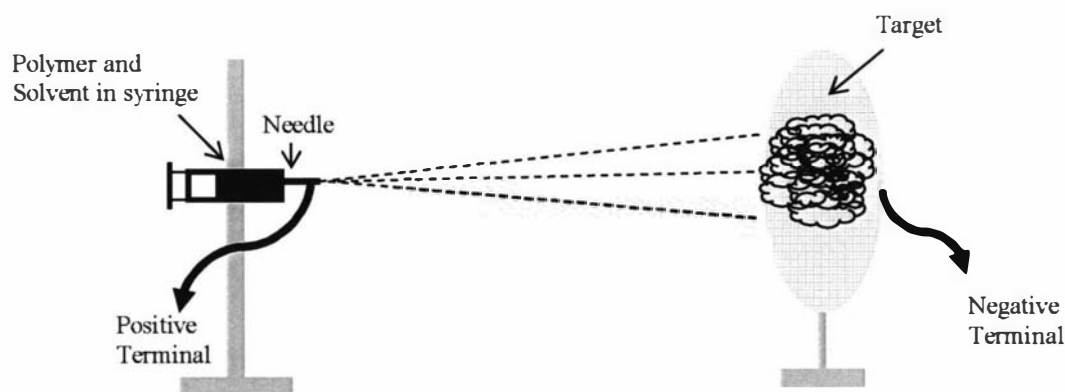


Fig. 2.16. Experimental setup for electrospinning.

The viscoelasticity and surface tension of the solution are known to significantly affect the formation of fibres.¹³⁰ In this study a solution of polymer in chloroform (typically ~40 mg mL⁻¹) was used, with addition of small amounts of polyethylene oxide (PEO) to increase solution viscosity if required.

2.8 Photovoltaic devices

An organic photovoltaic cell consists of a cathode and a polymer coated anode. Irradiation by light of a higher energy than the polymer bandgap results in the formation of an exciton (electron/positive-hole pair, Fig. 2.17). Dissociation of the excitons to produce an excited electron and positive hole (polaron or bipolaron) is most efficient at interfaces between two dissimilar materials, one with a low ionisation potential and good hole-transport properties, and the other with a high electron affinity that can act as an electron-transport material.^{131,132} In polymer-based photoelectrochemical (PEC) cells, the excited electron is passed from the polymer to the electrolyte, where the oxidised component of the electrolyte, e.g. tri-iodide ions, are reduced, e.g. to iodide ions. These effectively transport the electrons to the cathode, where they pass through an external circuit back to the anode.¹³² The photocurrent produced by a cell can be controlled and measured by connecting the cell in parallel with a potentiostat and scanning a range of potentials. A typical $I - V$ curve is given in Fig. 2.18.

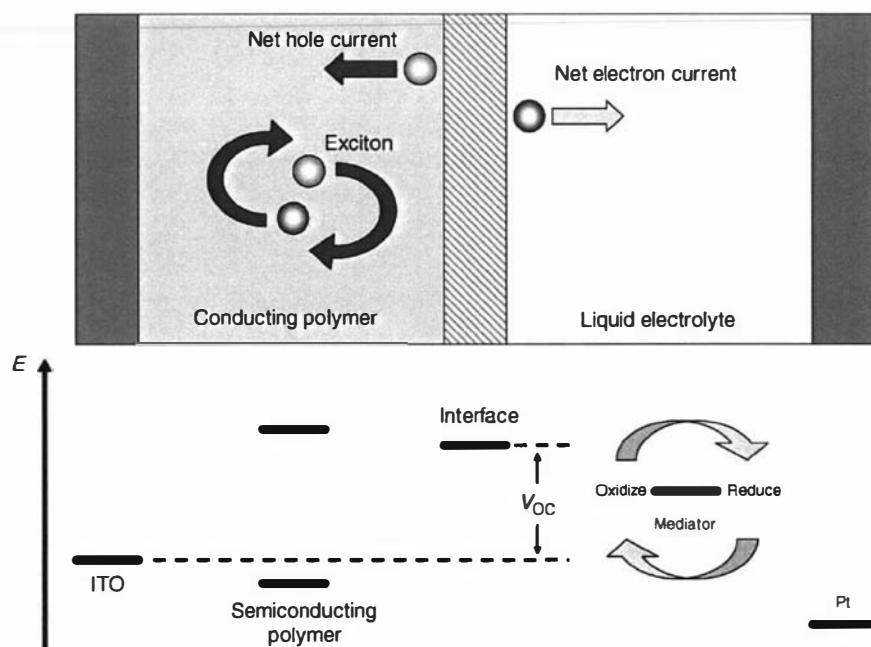


Fig. 2.17. Schematic diagram of a typical polymer photoelectrochemical cell structure consisting of an ITO/polymer/electrolyte/Pt sandwich structure. The interface between the polymer and liquid electrolyte are explicitly included to illustrate that the photovoltage is generated by the difference in standard electrode potential (work function) between the ITO-polymer interface and the polymer-electrolyte interface. Irradiation of the semiconducting polymer results in the formation of an exciton, which is separated at an interface. Redrawn from reference [132].¹³²

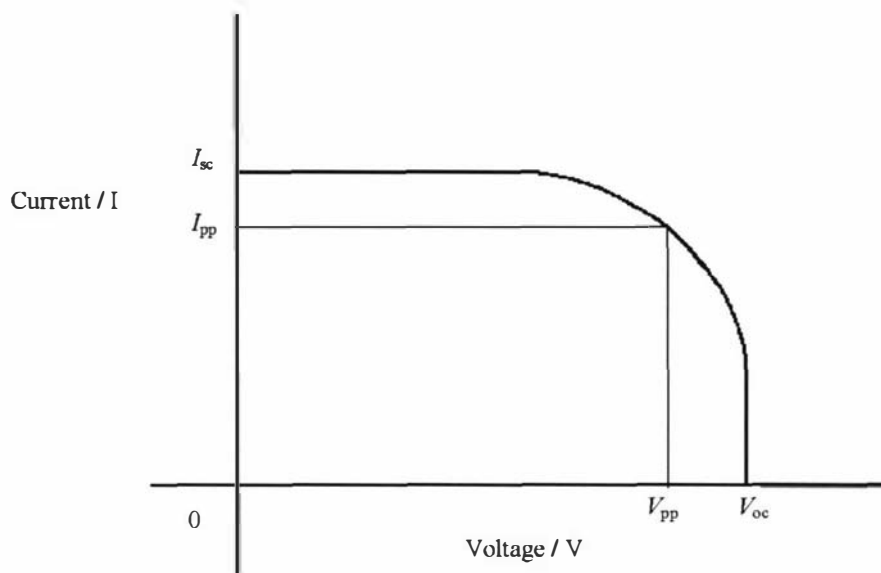


Fig. 2.18. Typical $I - V$ curve of a photovoltaic device. I_{sc} is the short circuit current and V_{oc} is the open circuit voltage. I_{pp} is the current at peak power and V_{pp} is the voltage at peak power.

Data collected from the $I - V$ curve is used to calculate parameters such as the fill factor (FF) and energy conversion efficiency (ECE) to determine the photovoltaic performance. These are defined below:

The open circuit voltage, V_{oc} , is the potential measured at zero current.

The short circuit current, I_{sc} is the current on the $I - V$ curve at zero voltage.

The fill factor (FF) is given by:

$$FF = \frac{\text{Voltage at peak power } (V_{pp}) \times \text{Current at peak power } (I_{pp})}{\text{Open circuit voltage } (V_{oc}) \times \text{Short circuit current } (I_{sc})}$$

The energy conversion efficiency (ECE) is given by:

$$ECE (\%) = \frac{V_{oc} \times I_{sc}}{\text{Total power of light radiating on the cell area}} \times 100$$

Chapter 3

Synthesis and Polymerisation of a Series of Styryl-Substituted Terthiophenes

3.1 Introduction

The objective of the work presented in this chapter was to investigate the effect of electron-withdrawing and electron-donating substituents on the properties of polythiophene. Due to their simple attachment by straightforward chemical synthesis, substituted aryl functionalities have been attached to thiophene monomers (Fig. 3.1a).^{54,133} However, as several workers have demonstrated that the resulting phenylthiophene polymers display low conductivity due to twisting of the rings,^{54,133} a styryl functionality was used in this study to link the substituent to the polythiophene backbone (Fig. 3.1b). The vinylene linker allows conjugation to be preserved while increasing the planarity of the polymer system. Although polymerisation of styryl-substituted thiophene monomers has proven difficult due to susceptibility of the vinylene linker to polymerisation,⁸⁸ copolymerisation of styryl thiophene with bithiophene was achieved by Cutler.²⁵ The separation of the vinyl substituents by bithiophene suggested the possibility of polymerisation of styryl terthiophene derivatives.

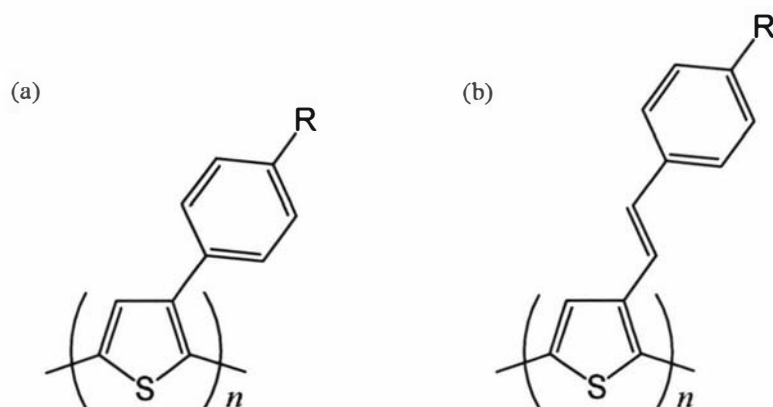


Fig. 3.1. Substituents linked by (a) phenyl and (b) styryl moieties to polythiophene.

In 2003, Collis *et al.* reported the synthesis of a series of terthiophene derivatives consisting of a terthiophene unit linked to a *para*-substituted aryl ring by an alkene moiety, as shown in Fig. 3.2.⁸⁰ In order of increasing electron-withdrawing ability, the five substituents were: dimethylamino (NMe₂), methoxy (OMe), hydrogen (H), cyano (CN), and nitro (NO₂). The facile synthesis of these five styryl monomers presented the opportunity to investigate both their chemical and electrochemical polymerisation, and the properties of the resulting polymers.

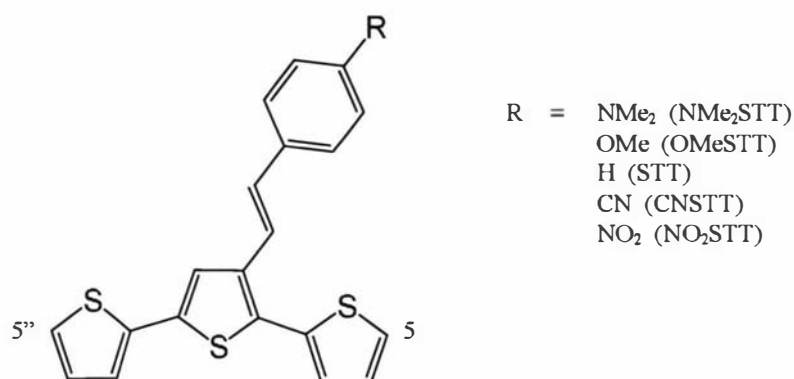


Fig. 3.2. Structures of the five styryl-substituted terthiophene monomer derivatives investigated in this study.

Some initial electrochemical polymerisation studies on NO₂STT has been reported by Cutler *et al.*⁹¹ They showed by post-growth electrochemical analysis and spectroscopic characterisation of the polymer films, that the nitro-styryl substituent has a strong influence on the oxidation potential of the polymer (744 mV), when compared to polyterthiophene (1054 mV). This work confirmed the potential of styryl terthiophenes as precursors to aryl-functionalised polythiophenes.

Therefore, the detailed chemical and electrochemical polymerisation of the five functionalised styryl terthiophenes shown in Fig. 3.2 was undertaken in this study. For convenience, in this study, these monomers will be referred to as NMe₂STT, OMeSTT, STT, CNSTT and NO₂STT.

3.2 Synthesis of monomers

The monomers were prepared according to the method of Collis *et al.*⁸⁰ This procedure employs a Wittig reaction between the terthiophene aldehyde and the appropriate phosphonium salt as shown in Fig. 3.3. The yield obtained depended on the substituent and ranged from 68 to 90%, similar to those reported by Collis *et al.*

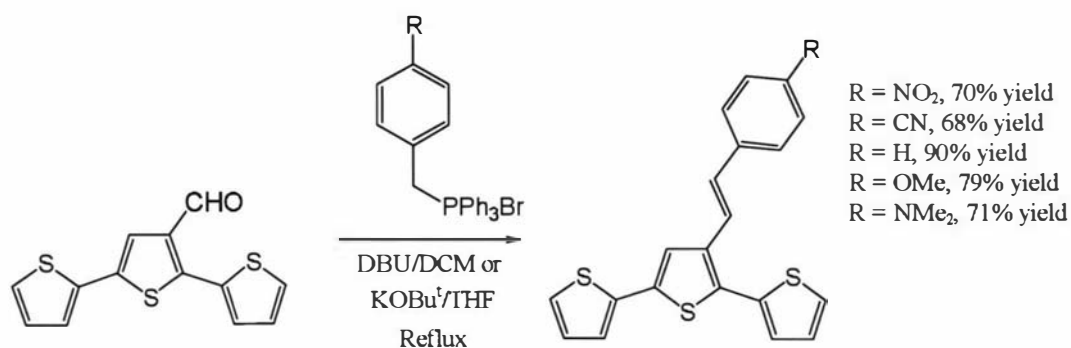


Fig. 3.3. Wittig reaction between a terthiophene aldehyde and phenyl substituted phosphonium salt for the synthesis of the substituted styrylterthiophene monomers used in this study.

3.3 Polymerisation using chemical oxidation

3.3.1 Polymerisation and reduction methods

The general reaction procedure used in this study for the polymerisation of styryl-substituted terthiophenes is given in Fig. 3.4. Four equivalents of iron(III) chloride were added dropwise as a suspension in dichloromethane (DCM) to a solution of monomer in the same solvent. This is a typical process used to polymerise functionalised thiophenes.^{44,63,68,70,98,134,135} The use of iron(III) chloride as an oxidant provides a simple polymerisation method to produce large amounts of high molecular weight polymer.⁷⁰ It was suggested by Laakso *et al.* that the additional equivalents of iron(III) chloride are required as this oxidant is only partially soluble in chloroform, forming an inert solution.¹³⁶ Laakso *et al.* also explained the requirement for extra iron(III) chloride through consumption of this oxidant in the formation of HCl gas.¹³⁶ The slow addition of the oxidant as a slurry was intended to keep the $\text{Fe}^{3+}/\text{Fe}^{2+}$ ratio (and hence oxidation potential) low and more constant throughout the polymerisation procedure to reduce the occurrence of overoxidation.⁷⁰ Several authors have reported that the slow addition of iron chloride as a slurry rather than the rapid addition of solid iron chloride results in a higher yield of soluble polymer.^{70,98} Gallazzi *et al.*⁹⁸ found that adding iron(III) chloride in a single addition to 3,3''-didodecyl-2,2':5'5''-terthiophene resulted in a polymeric yield that was 60% soluble, compared to production of polymeric material, which was 100% soluble, from dropwise addition. It was suggested that this may be related to a sudden accumulation of HCl gas in the reaction mixture, which is produced on polymerisation.⁹⁸

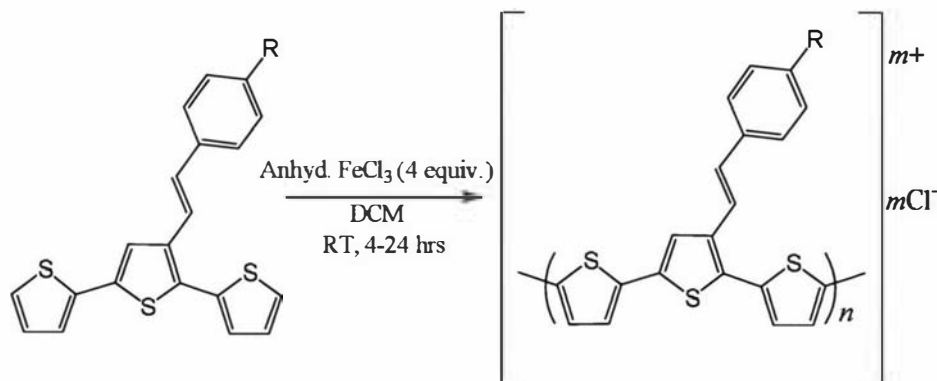


Fig. 3.4. Reaction procedure employed for the chemical polymerisation of styryl-substituted terthiophene derivatives.

After addition of the oxidant, the reaction mixture was stirred for several hours to allow polymerisation. As black congealed precipitates were immediately produced, the mixtures were sonicated at intervals to redisperse the material and allow further reaction to occur. The reactions were stopped by quenching with water when all monomer had reacted as determined by TLC. The crude products were black, insoluble materials, which were assumed to be the oligomeric and/or polymeric material in the oxidised state. This observation is similar to work done by Gallazzi *et al.*⁶² and Wang *et al.*,⁴⁴ on the polymerisation of alkyl- and alkoxy-substituted terthiophenes by iron(III) chloride.

The oxidised polymers were reduced (de-doped) to produce the neutral state (Fig. 3.5), which is generally more soluble in organic solvents than the oxidised form, and more amenable to characterisation.^{62,74} The crude oxidised material was first rinsed with water, and then thoroughly washed with methanol using soxhlet extraction to remove residual oxidant and monomer. A number of substituted polythiophenes appear to readily reduce to the neutral state when the residual oxidant is removed by washing the crude material with water or methanol,^{44,62,98} although Gallazzi has found that a strong reducing agent, such as hydrazine, is required for the reduction of poly(4,4'-dipentoxyterthiophene).

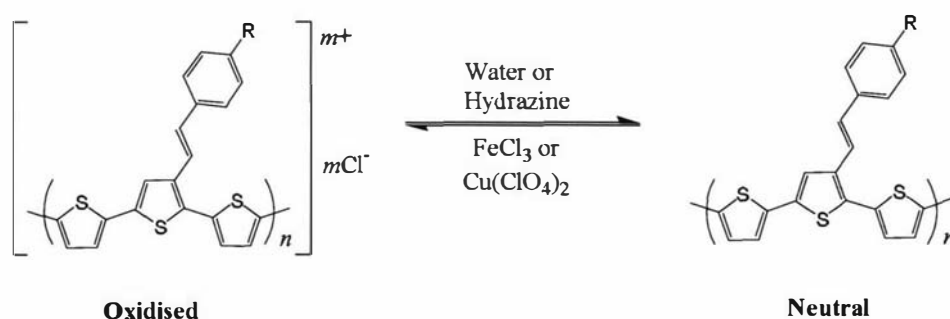


Fig. 3.5. The reversible doping (by iron(III) chloride or copper perchlorate) and dedoping (by washing with water or hydrazine) process of the polymer.

Washing the oxidised polymer with methanol appeared to reduce the material to the neutral state as observed by a change in colour from black to red. Soxhlet extraction of this neutral polymeric material with DCM gave an orange/red powder that is soluble in DCM and chloroform (soluble fraction). A dark red powder remained that was not

soluble in any common solvent (insoluble fraction). The percentage yields of the soluble fractions obtained for each derivative are given in Table 3.1. The mass of the monomer used in the reaction has been used as an approximation of the expected polymer yield since the length of the oligomers can not be accurately measured. At most, this leads to an uncertainty of 0.3% in the calculated polymer yields (due to not taking into account the loss of α -hydrogen on polymerisation).

Table 3.1. Soluble fractions of styryl-substituted terthiophene polymer derivatives.

Polymerised monomer	NO ₂ STT	CNSTT	STT	OMeSTT	NMe ₂ STT
Total soluble yield (%)	<5%	63%	33%	20%	20%

The remaining insoluble material is unlikely to be oxidised oligomer/polymer as attempts to reduce this material with hydrazine did not produce further soluble material. The insoluble component was found to be difficult to characterise and could not be easily further processed, thus further discussion focuses solely on the soluble fraction.

3.3.2 Characterisation of soluble fractions

The soluble fractions were investigated by mass spectrometry and thin layer chromatography (TLC). MALDI-TOF MS (Matrix-Assisted Laser Desorption/Ionisation Time-Of-Flight Mass Spectrometry), described in Chapter 2, is a frequently used method for investigating the chain length of polymer samples.^{118,137,138} MALDI-TOF MS of the neutral, soluble fractions of NMe₂STT, OMeSTT, STT, CNSTT and NO₂STT oligomers are displayed in Fig. 3.6. Dimer is found to be the primary species present in all the samples, with small amounts of trimer and tetramer also detected in NMe₂STT, STT and CNSTT samples. The significant signal at 354 Da observed in the spectrum of NO₂STT may be due to decomposition of the monomer ($M_r = 395.4 \text{ g mol}^{-1}$) or a reaction with the matrix ($M_r = 226.2 \text{ g mol}^{-1}$).

Chromatography was used to investigate the chain length of oligomeric materials. The soluble styryl-substituted terthiophene materials were investigated by thin layer

chromatography (TLC) using silica plates. A significant spot with a polarity less than that of the monomer was observed for all soluble fractions, which may be due to dimer (Table 3.2). Additional spots were observed at even lower retention factor values (R_f) for the NMe₂STT oligomer fraction (one spot) and the STT oligomer fraction (two spots), and these may be due to the presence of longer oligomers, consistent with results from MALDI-TOF mass spectrum. The OMeSTT soluble oligomer fraction also displayed a spot at an R_f value lower than the assumed dimer, which may be due to a regioisomer of the dimer, or an impurity. The CNSTT and NO₂STT oligomer fractions displayed only one spot, consistent with low amounts of oligomeric impurities as indicated by MALDI-TOF mass spectra.

Table 3.2. R_f values of monomers and dimers in 20% ethylacetate/hexane on silica TLC plates.

	NMe ₂ STT	OMeSTT	STT	CNSTT	NO ₂ STT
Monomer R_f	0.60	0.68	0.85	0.54	0.61
Dimer R_f	0.38	0.44	0.7	0.21	0.33

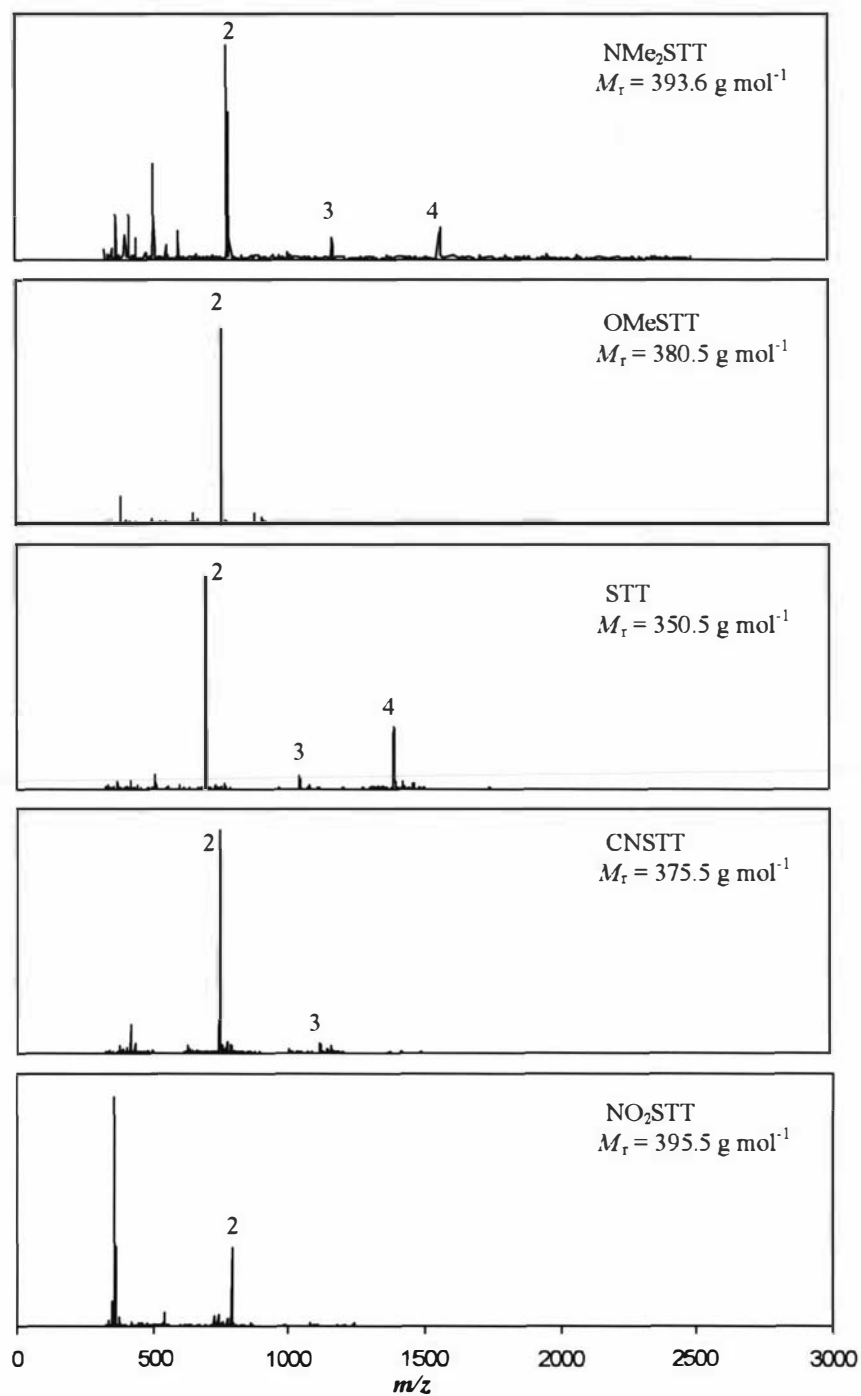


Fig. 3.6. MALDI-TOF MS of crude, soluble fractions of chemically polymerised NMe₂STT, OMeSTT, STT, CNSTT and NO₂STT. Significant signals are labelled with oligomer length in terms of monomer units (n). Detection suppression limit: 320 Da.

3.3.3 Attempted purification of dimer

The results for MALDI-TOF MS indicated that dimers were the major components of the soluble fractions. This is consistent with work by Grant *et al.* who, during the course of this study, reported that attempts at polymerising polyether-substituted styrylterthiophenes, by both iron(III) chloride and electrochemical techniques, resulted in high yields (55-87%) of soluble dimer.¹¹

Attempts were made to isolate and purify the dimers produced in this study. Impurities of trimer and longer oligomers were removed by recrystallisation of the crude soluble materials to provide materials that contained no detectable oligomer impurities as indicated by MALDI-TOF MS and TLC. The purified dimers were reasonably soluble in organic solvents and this provided the opportunity to characterise them by ¹H NMR spectroscopy.

The simple spectra that were obtained by the dimer samples indicate that the samples consist predominantly of a single regioisomer. The monomer and dimer spectra of the dimethylamino derivative are given in Fig. 3.7 as an example, and show the loss of the signal due to H1, and consequential simplification of the H2 quartet to a doublet on dimerisation indicating head-to-head (HH) coupling.

Grant *et al.*¹³⁹ also reported that dimer formation by ether-substituted styrylterthiophenes was regioselective, giving predominantly HH isomers as shown by ¹H NMR spectroscopy. Spectra of the diether-substituted styrylterthiophene monomer and dimer (Fig. 3.8) clearly shows loss of the H1 proton.

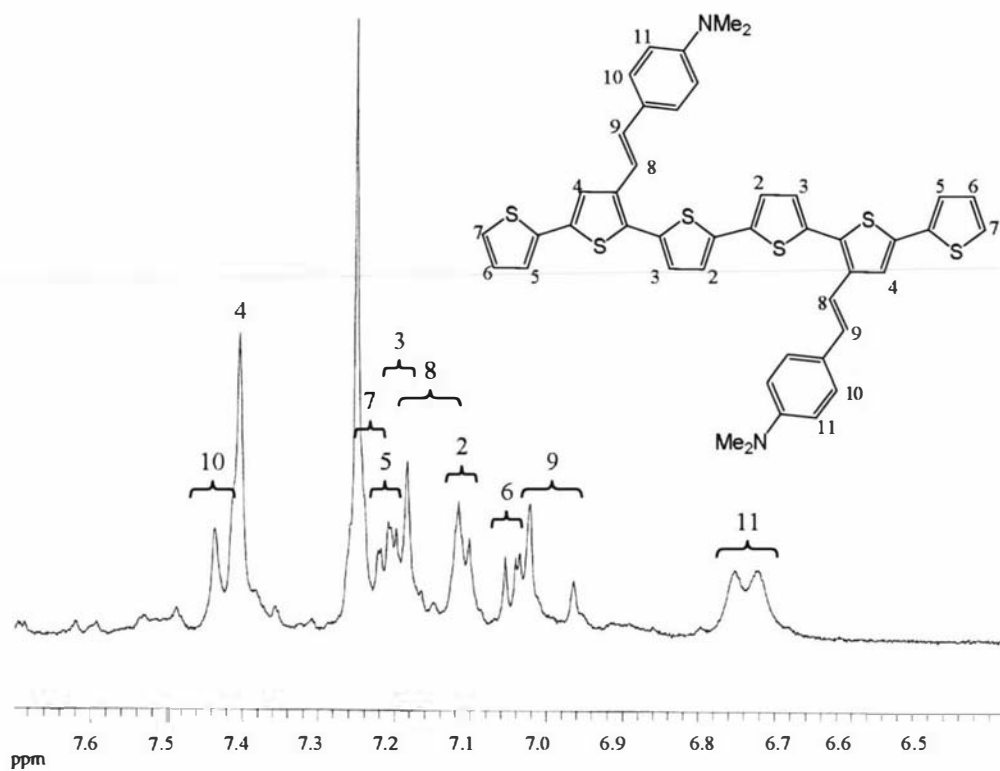
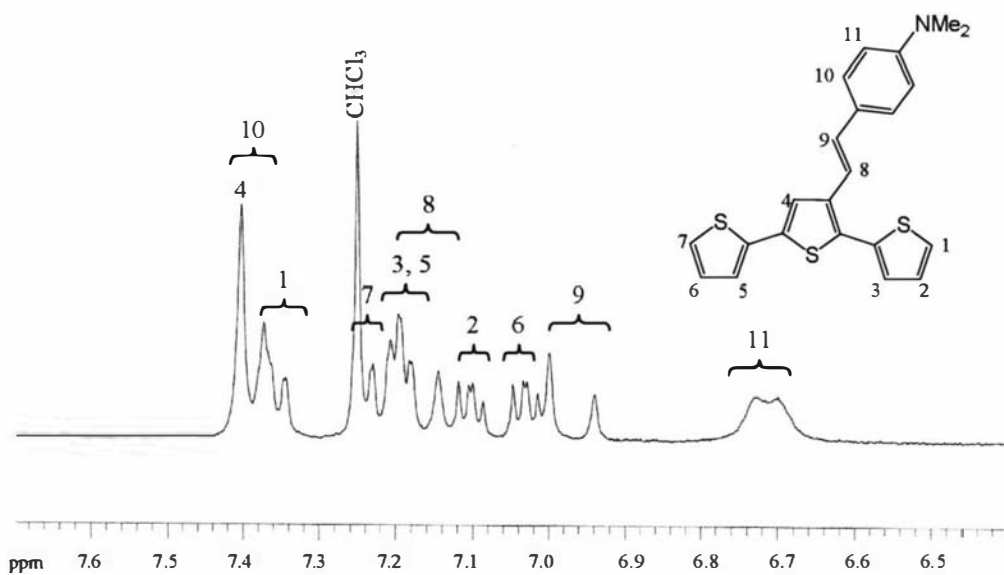


Fig. 3.7. ^1H NMR spectra (aromatic region) of NMe_2STT and the dimeric HH regioisomer produced by chemical oxidation.

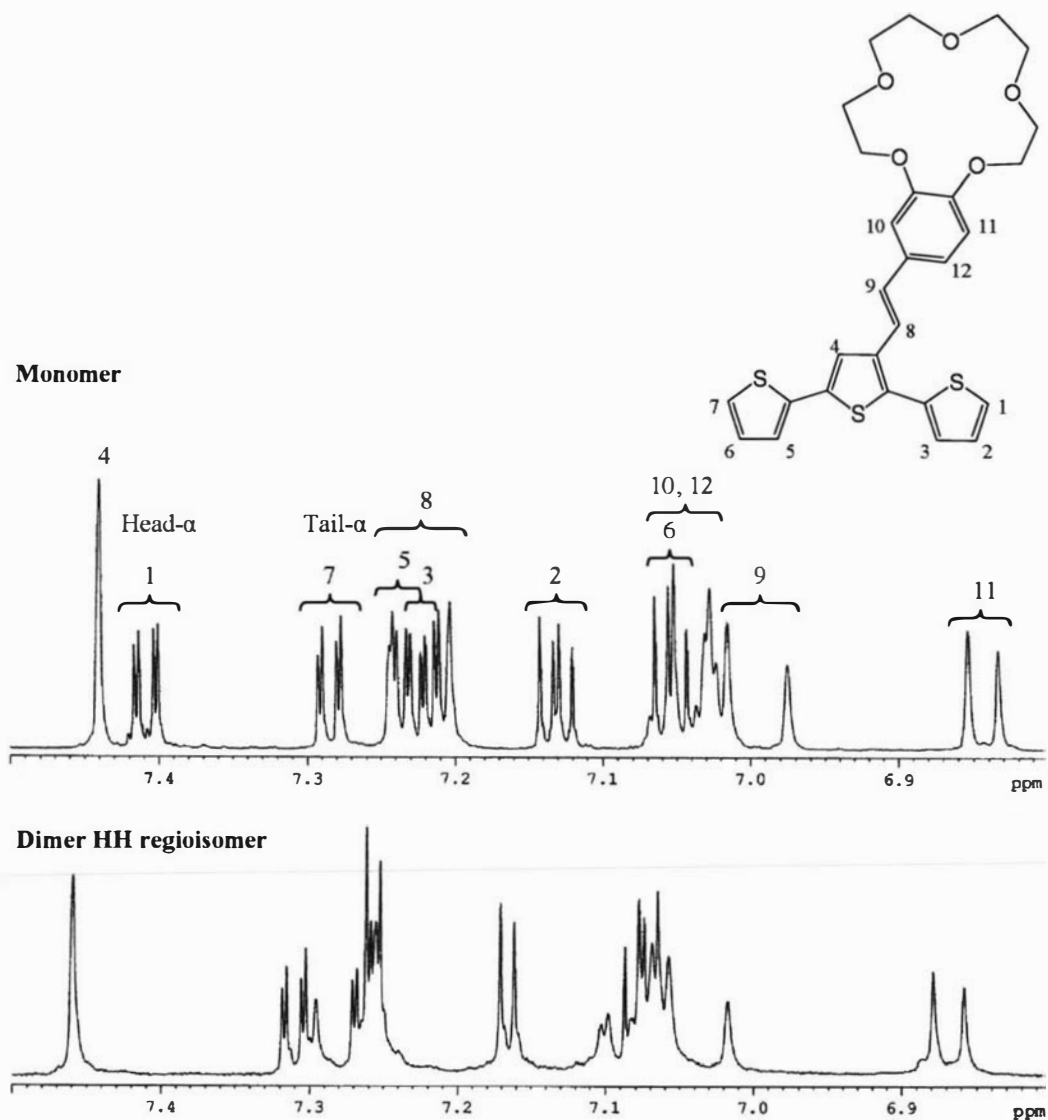


Fig. 3.8. ¹H NMR spectra (aromatic region) of styryl-15-crown-5 terthiophene, and the dimeric HH regioisomer that is produced by oxidation.¹¹ Reproduced by permission.

The high yield of regiospecific dimer produced by these styryl terthiophene derivatives was subsequently supported by theoretical calculations performed by Clarke *et al.*¹⁴⁰ on the reactivity of the terminal ‘ α ’ positions of styryl-substituted terthiophene and sexithiophene. With styryl substitution, the reactivity of these positions appears to decrease as the oligomer length increases, accounting for the low degree of polymerisation and high yield of dimer. It was suggested by Clarke *et al.*¹⁴⁰ that this was due to a ‘trapping’ of the charge required for further polymerisation by the styryl substituent as shown in Fig. 3.9. Clarke *et al.*¹⁴⁰ was also able to account for the regiospecificity and tendency of styryl-substituted terthiophene monomers to produce HH regioisomers by performing theoretical calculations on the STT monomer to show that the 5-position is more reactive than the 5'' position.

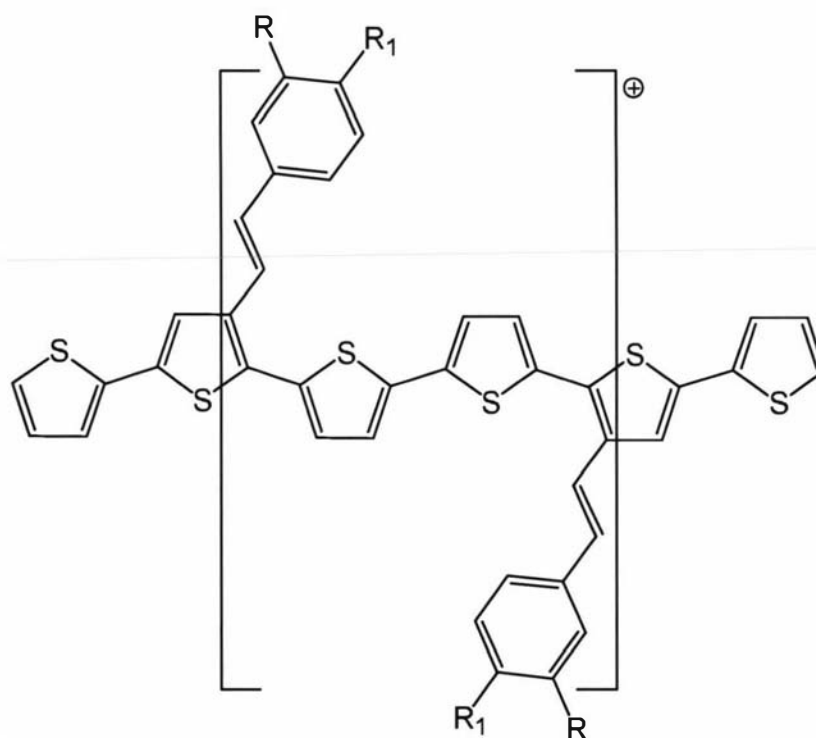


Fig. 3.9. ‘Charge-trapping’ over the two central thiophene rings and styryl substituents as exhibited by theoretical calculations.¹⁴⁰

Although the ¹H NMR spectra confirm results by MALDI-TOF MS and TLC that oligomer impurities have been removed from the dimer samples in this study, additional peaks generated by the dimer samples (the set of low field peaks between 7.46 and 7.70 ppm in the case of NMe₂STT, Fig. 3.7) indicates that impurities are still present. Efforts to further purify the materials, including additional recrystallisations, columns

on silica and alumina, radial chromatography and soxhlet extractions, were not successful.

3.3.4 Conclusions

Chemical oxidation of the styryl-substituted terthiophenes investigated in this study resulted in the production of significant amounts of insoluble material (>36%), which were difficult to characterise. Investigation of the soluble fractions revealed that they consisted primarily of dimer and short chain ($n < 4$) oligomers. The dimer could be further isolated, but not purified, and was shown by ^1H NMR spectroscopy to be regioregular. This regioregularity is consistent with work reported by Grant *et al.*,¹³⁹ and predictions made by Clarke *et al.*¹⁴⁰

3.4 Polymerisation using electrochemical methods

3.4.1 Introduction

Although characterisation of the insoluble fractions of chemically oxidised NMe₂STT, OMeSTT, STT, CNSTT and NO₂STT proved difficult, the soluble yields revealed the production of mostly short oligomers, with chain lengths comprising four monomer units or less. In an attempt to produce longer oligomers, the electrochemical polymerisation of these materials was investigated. Electrochemical polymerisation is a commonly employed method to grow films of conducting polymers^{8,83} and, unlike chemical polymerisation, allows control over the oxidation potential. Electrochemical polymerisation also allows the straightforward growth of insoluble polymer films, which are amenable to characterisation by cyclic voltammetry, spectroscopy and microscopy. Both cyclic voltammetry and potentiostatic methods have been used in this study to grow oligomeric/polymeric films onto platinum and ITO-coated surfaces.

3.4.2 Electrochemical growth

To determine appropriate scan limits and oxidation potentials, each monomer was initially analysed by scanning between potentials of -1 V and +1.5 V. The CV scan of terthiophene (Fig. 3.10) shows several oxidation peaks as is typically observed for short oligothiophenes.^{141,142} The same mechanism is reported to occur for the electrochemical oxidation of thiophene as for thiophene oligomers,^{8,143} and is shown in Fig. 3.11 using thiophene for simplicity. From work reported by Audebert *et al.*¹⁴¹ and Roncali *et al.*¹⁴⁴ on the electrochemical oxidation of terthiophene, the initial anodic peak, $E_{ox,1}$, is assigned to the oxidation of the terthiophene monomer to its radical cation (Fig. 3.11a). As described by Waltman *et al.*,⁷² Audebert *et al.*,¹⁴¹ and Roncali,⁸ the assignment of further anodic peaks depends upon the reactivity of the terthiophene monomer cation. Audebert *et al.* has conclusively shown that terthiophene monomer cations, which are not very reactive, may further oxidise to generate multiply charged cations (Fig. 3.11b).¹⁴¹ On the other hand, very reactive cation species may undergo oxidative degradation reactions with either solvent molecules, electrolyte or impurities (Fig. 3.11c).^{72,145} Between these two stability ranges, which vary depending on

substituents and chain length of the monomer, the radical cations can dimerise by coupling (Fig. 3.11d).^{72,141,143} These resulting oligomers may then oxidise to form cation species (Fig. 3.11e). Further oxidation of these species at higher oxidation potentials may lead to the formation of multiply charged species, polymer or overoxidation (Fig. 3.11f).^{8,145}

No detailed study has been reported on the characterisation and assignment of anodic peaks produced during the growth of terthiophene. However, in a report by Xu *et al.*¹⁴³ on the electropolymerisation of tetrathiophene, after the initial anodic peak due to the oxidation of the monomer to its radical cation, this species was observed to immediately couple to form octathiophene, which deposited on the electrode. The second anodic peak was assigned to oxidation of octathiophene. A similar process is likely to occur in terthiophenes. Audebert *et al.* reports that $E_{ox,1}$ is non-reversible even at very fast scan rates (up to 15000 V s^{-1}) demonstrating that terthiophene cation radicals are highly reactive,¹⁴¹ and suggesting they are likely to polymerise and/or overoxidise. As Cutler *et al.* reported the overoxidation of NO_2STT at potentials above 1.1 V ,⁹¹ the third oxidation peak, $E_{ox,3}$, is most likely due to overoxidation of the terthiophene monomer or oligomer cations. Little can be said about the cathodic peaks in these scans as they may be due to the reduction of cation radicals and/or overoxidised species.

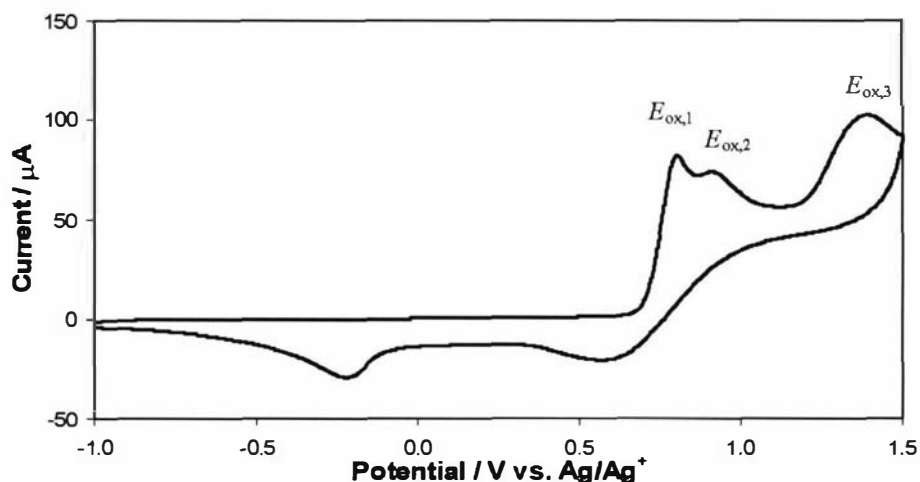


Fig. 3.10. CV of terthiophene monomer on a platinum disc electrode ($\text{SA} = 1.8 \text{ mm}^2$). Supporting electrolyte: 0.1 M TBAP/AN . Potential limits: $-1000/+1500 \text{ mV}$. Scan rate: 100 mV s^{-1} .

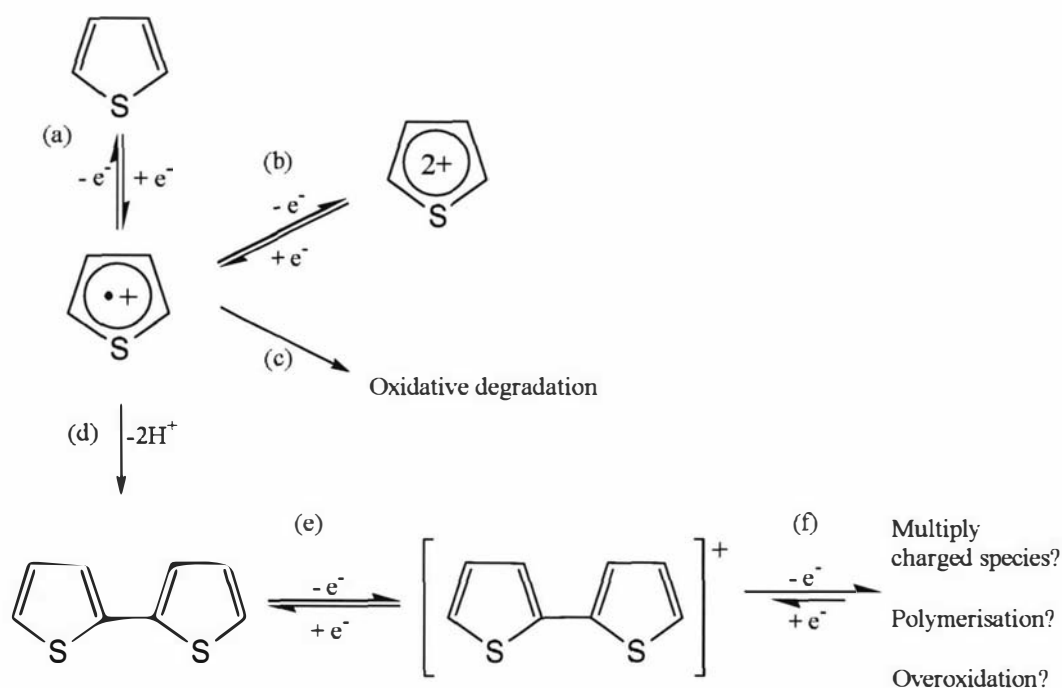


Fig. 3.11. A possible mechanism to explain redox peaks (using thiophene for clarity) observed in the first scan of terthiophene derivatives.

The CV scans of CNSTT, STT, OMeSTT and NMe₂STT are displayed in Fig. 3.12. As for terthiophene, three anodic peaks are observed for each species (listed in Table 3.3). The first peak is assigned to the oxidation of the monomer to the radical cation, and the second to the oxidation of longer oligomers as, for example, in process (f) in Fig. 3.11. Scanning to potentials over the third peak leads to deposition of a black precipitate, most likely due to overoxidised species.

Table 3.3. Anodic peaks shown by styryl-substituted terthiophene derivatives.

Monomer	CNSTT	STT	OMeSTT	NMe ₂ STT
1 st anodic peak	0.75 V	0.72 V	0.66 V	0.28 V
2 nd anodic peak	0.81 V	0.75 V	1.06 V	0.98 V
3 rd anodic peak	1.36 V	1.34 V	1.30 V	1.30 V

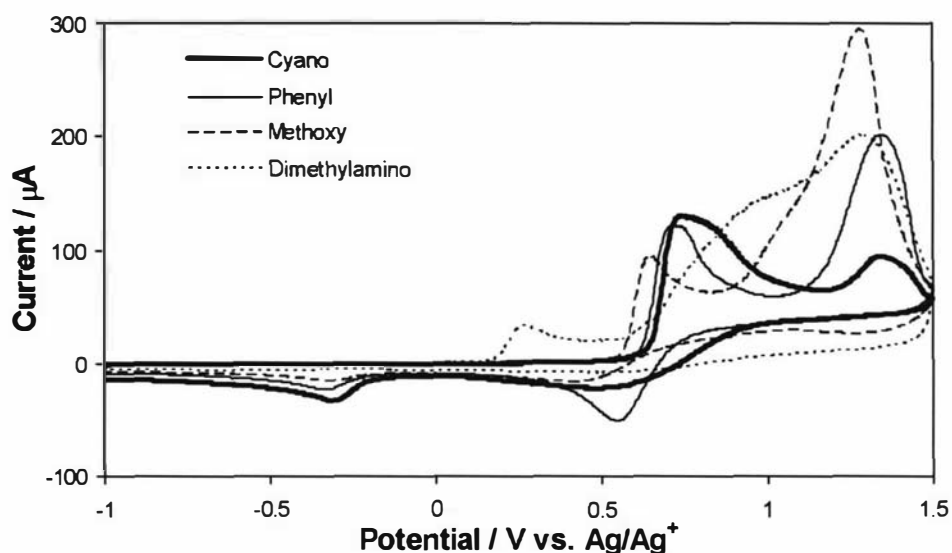


Fig. 3.12. CV scans of CNSTT, STT, OMeSTT and NMe₂STT on platinum disc electrodes (SA = 1.8 mm²). Supporting electrolyte: 0.1 M TBAP/AN. Potential limits: -1000/+1500 mV. Scan rate: 100 mV s⁻¹.

In contrast, a CV of NO₂STT reveals multiple oxidation peaks (Fig. 3.13). As nitro is the most electron-withdrawing substituent of the series, this may be due to a low stability of the corresponding cations.⁷² Instead of polymerising, the cations may be undergoing oxidative degradation by reacting with nucleophiles such as water impurities.^{72,145} This was observed by Waltman *et al.* during the attempted electrochemical polymerisation of 3-cyano- and 3-nitrothiophene.⁷²

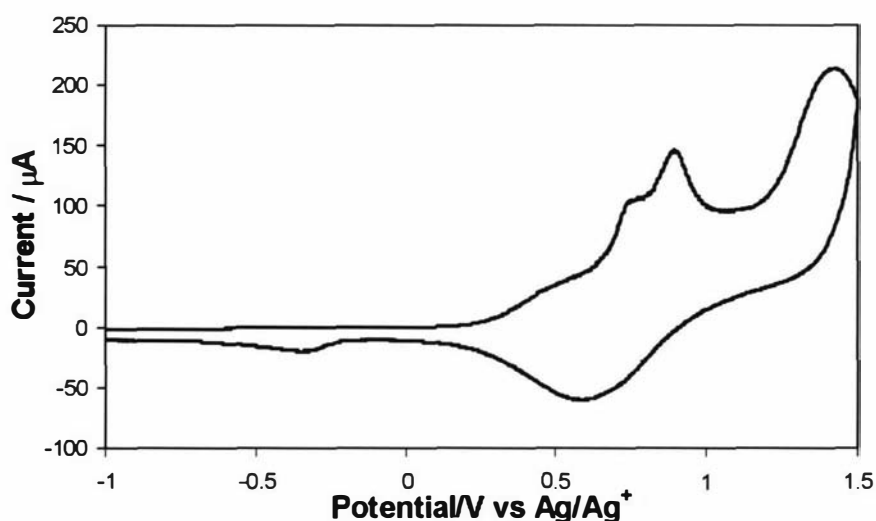


Fig. 3.13 CV of NO₂STT monomer on a platinum disc electrode (SA = 1.8 mm²). Supporting electrolyte: 0.1 M TBAP/AN. Potential limits: -1000/+1500 mV. Scan rate: 100 mV s⁻¹.

The monomer oxidation onset potentials of the terthiophene derivatives were determined from these scans, and are listed in Table 3.4. Oxidation of terthiophene commences at 0.71 V. The higher potential when compared to that for STT (0.62 V) suggests that the styryl group is activating the monomer.

The increasing oxidation potential with increasing electron withdrawing ability of the substituents, except for the nitro derivative, reflects the relative stability of the cation radicals.⁵⁴ Thiophene cation radicals that support electron-donating substituents have been suggested to be stable and therefore readily formed. On the other hand, cation radicals containing electron-withdrawing groups are less stable and therefore harder to form. Similar results have been reported by Michalitsch *et al.*,¹⁰⁹ MacDiarmid *et al.*¹⁴⁶, Collis *et al.*⁸⁰ and Cutler²⁵ for thiophene derivatives. This suggests that cations containing EWGs are more reactive and may form longer polymer chains, whereas cations of short-chain oligomers containing EDGs may not be sufficiently reactive to promote further polymerisation. The nitro derivative does not follow the same relationship, most likely due to facile reactions of the highly reactive cation radical with electrolyte anions and/or impurities.

Table 3.4. Oxidation onset potentials of styryl terthiophene derivatives (vs Ag/Ag⁺).

Monomer	Terthiophen e	NMe ₂ STT	OMeSTT	STT	CNSTT	NO ₂ STT
Oxidation onset potential	0.71 V	0.15	0.52	0.60	0.62	0.21

Growth CVs of NMe₂STT, OMeSTT, STT, CNSTT and NO₂STT on platinum disc electrodes are shown in Figs. 3.14 to 3.18 respectively. Anodic scan limits were set at a potential about 100 mV beyond the potential at which material was observed to deposit. The CVs show an increase in current with successive scans, characteristic of conducting polymer growth as discussed in Chapter 2, Section 2.1.3. Except for the NMe₂STT sample, a decrease in oxidation onset potential is observed after the first scan. This is most likely due to oxidation of deposited oligomers, which are expected to have a lower oxidation potential than the monomer. Long oligothiophenes were shown by Sumi *et al.* to have a lower oxidation potential than short oligomers.¹¹⁴ The

NMe₂STT sample is distinctive, however, in that the oxidation potential increases with scan number. This may be due to a number of reasons such as (1) rapid depletion of the monomer in the vicinity of the electrode,⁶¹ (2) very low conductivity of the film in neutral state, effectively insulating the electrode from the monomer,¹⁴² or (3) hindrance of the interchange of anionic species due to growth of a very compact film.^{72,142}

Multiple oxidation and/or reduction peaks are observed during the growth of CNSTT and NO₂STT. Although multiple peaks are commonly observed during the growth and post-growth cycling of polythiophene derivatives,^{23,99,147} their origin is not well understood. It has been suggested by several authors that the peaks are due to transitions between the neutral, polaron, bipolaron and metallic states of the polymer.¹⁴⁸⁻¹⁵⁰ As discussed by Pringle *et al.*¹⁴⁷ the potential at which these transitions occur may be influenced by factors such as reduction of different areas of the polymer film¹⁴⁷, different length polymer chains,¹¹⁴ the effect of 'charge-trapping',¹⁵¹ and conformational changes of the polymer accompanying radical cation formation.¹⁵²

The growth CV of NO₂STT is consistent with work reported by Cutler *et al.*²⁵

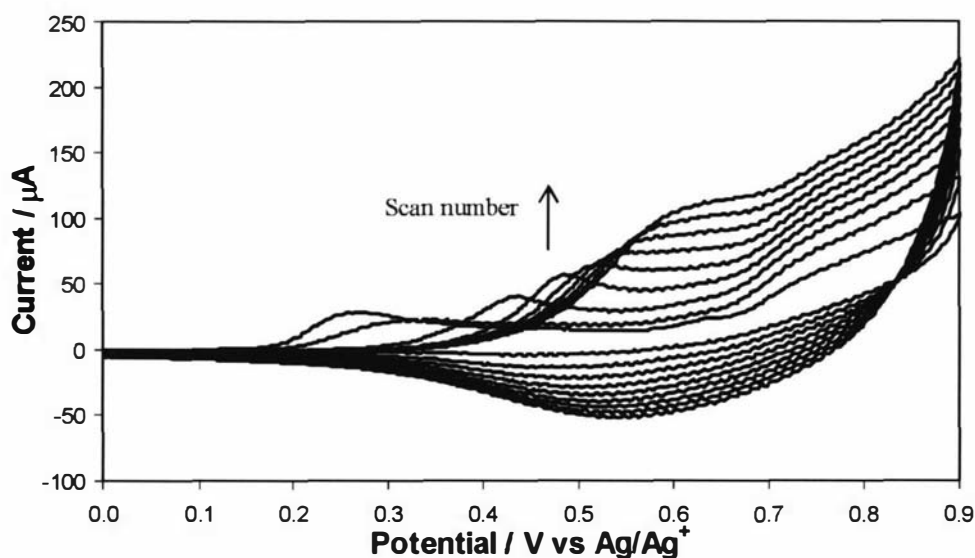


Fig. 3.14. Potentiodynamic growth of NMe₂STT on a platinum disc electrode (SA = 1.8 mm²). Supporting electrolyte: 0.1 M TBAP/AN. Potential limits: 0/+900 mV. 9 cycles. Scan rate: 100 mV s⁻¹.

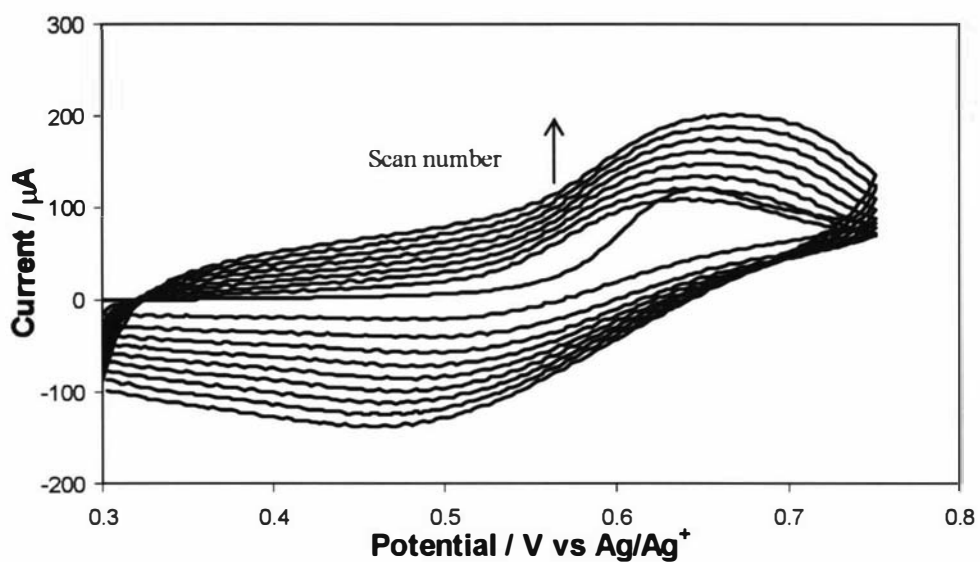


Fig. 3.15. Potentiodynamic growth of OMeSTT on a platinum disc electrode ($SA = 1.8 \text{ mm}^2$). Supporting electrolyte: 0.1 M TBAP /AN. Potential limits: +300/+750 mV. 9 cycles. Scan rate: 100 mV s^{-1} .

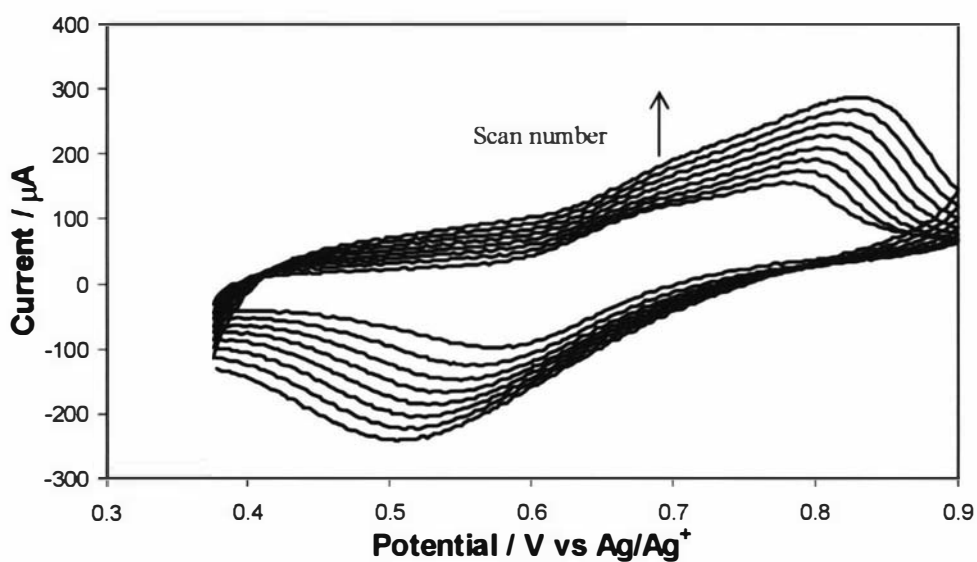


Fig. 3.16. Potentiodynamic growth of STT on a platinum disc electrode ($SA = 1.8 \text{ mm}^2$). Supporting electrolyte: 0.1 M TBAP /AN. Potential limits: +375/+900 mV. 9 cycles. Scan rate: 100 mV s^{-1} .

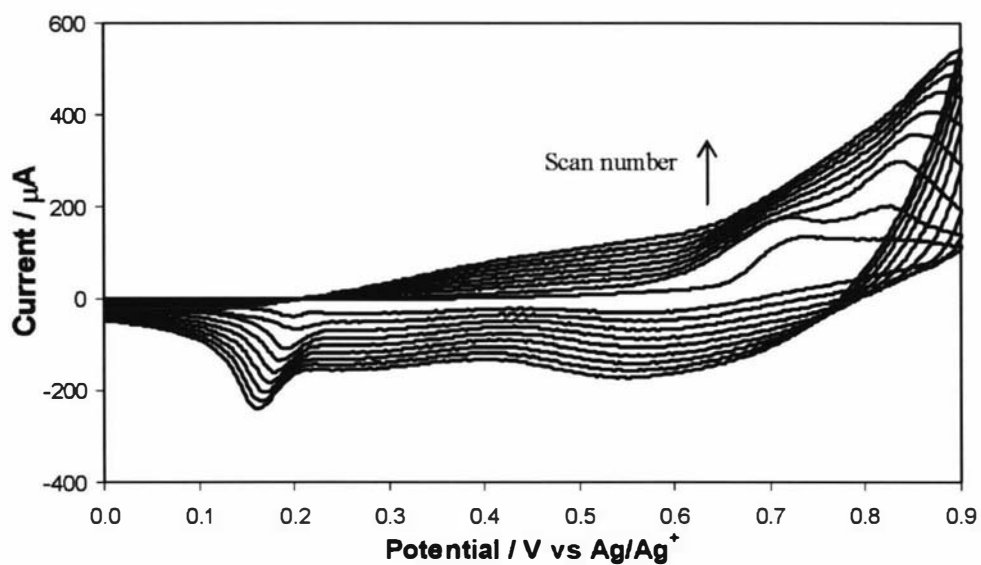


Fig. 3.17. Potentiodynamic growth of CNSTT on a platinum disc electrode (SA = 1.8 mm²). Supporting electrolyte: 0.1 M TBAP/AN. Potential limits: 0/+900 mV. 9 cycles. Scan rate: 100 mV s⁻¹.

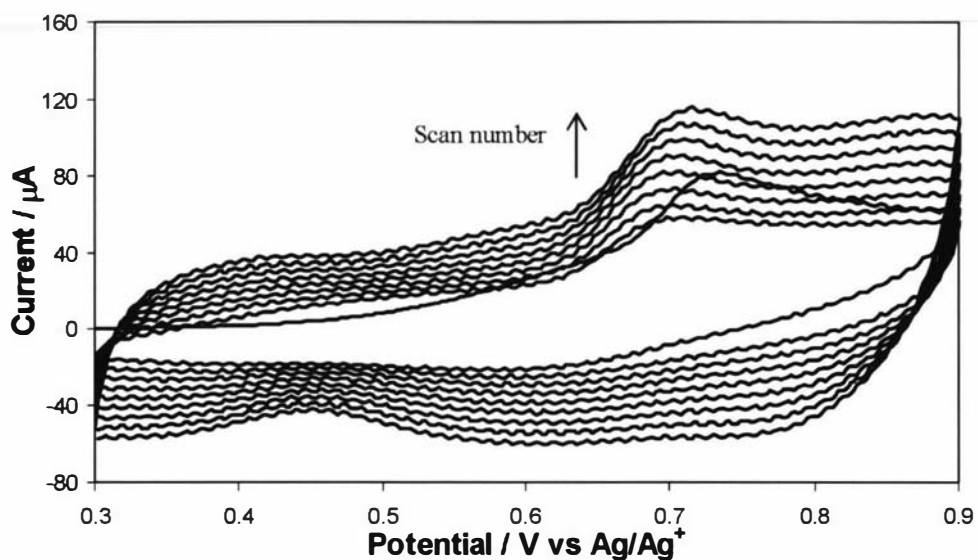


Fig. 3.18. Potentiodynamic growth of NO₂STT on a platinum disc electrode (SA = 1.8 mm²). Supporting electrolyte: 0.1 M TBAP/AN. Potential limits: 0/+900 mV. 9 cycles. Scan rate: 100 mV s⁻¹.

As conducting polymer films are sometimes observed to be different depending on their method of growth,⁶¹ films of styryl terthiophene derivatives were grown using potentiostatic methods for comparison to the potentiodynamically grown films. The

chronoamperograms produced by these materials were observed to be similar. A representative chronoamperogram using that of STT is displayed in Fig. 3.19, and reveals characteristics typical of conducting polymer growth.^{25,47} After the initially high but rapidly tailing current transient ($t < 30$ seconds), the current increases steadily indicating an increase in electroactive surface area (by polymer deposition) and/or more facile electrode kinetics.

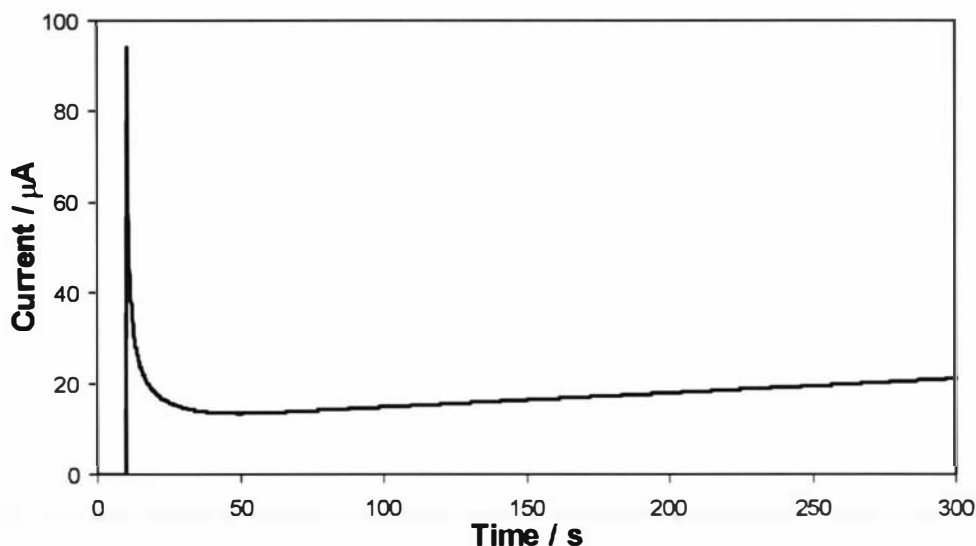


Fig. 3.19. Potentiostatic growth of STT on a platinum disc electrode ($\text{SA} = 1.8 \text{ mm}^2$). Supporting electrolyte: 0.1 M TBAP/AN. Potential held at 0 mV for 10 s, then stepped to 900 mV for 290 s.

Both the potentiostatically and potentiodynamically deposited oligomeric/polymeric films of these styryl terthiophenes were compared using cyclic voltammetry, UV-VIS-NIR spectroscopy and scanning electron microscopy.

3.4.3 Characterisation of electrochemically deposited materials

3.4.3.1 Electrochemical characterisation

The oligomeric/polymeric films of NMe_2STT , OMeSTT , STT , CNSTT and NO_2STT grown using potentiodynamic and potentiostatic methods were compared using cyclic voltammetry. All CVs are completed in monomer-free electrolyte solution.

The post-growth cycles of polyNMe₂STT deposited potentiodynamically and potentiostatically, shown in Fig. 3.20, have different peak potentials, suggesting differences in the films. In both CVs, the peak currents are observed to decrease with increasing cycle number indicating that the films are unstable. In addition, the first scan of the potentiodynamically deposited material shows a current response on the initial anodic scan which is 2.7 times larger than the current response on the cathodic scan. This suggests a modification of the film and may be a result of one of the following processes.

First, short oligomers in the film may further polymerise. Eales *et al.*¹⁴⁵ also observed a difference between the first scan and subsequent scans with poly(terthiophene) films and suggested that the similarity of monomer and polymer oxidation potentials allows deposition of incompletely polymerised species. These incompletely polymerised species (which may even include monomer cations) are thought to become trapped in the film during growth and subsequently polymerised during the initial anodic post-polymerisation scan causing the initial increase in current.

A second possibility is that the film may be undergoing degradation. Loss in electroactivity of thiophene films is often caused by nucleophilic attack of overoxidised cation radicals by nucleophiles such as water contaminants.^{72,145} This is unlikely to occur during polymerisation of NMe₂STT however since cations with electron-donating substituents are likely to be relatively stable. A more likely reaction is the protonation of the dimethylamino substituent by protons produced during growth. Proton production is required by the accepted polymerisation mechanism and has been proved experimentally.¹⁵³

A third prospect is that the morphology of the deposited material may be changing or compacting during the potential scans (i.e. an irreversible electroactuator effect), causing a reduction in the electroactive surface area.

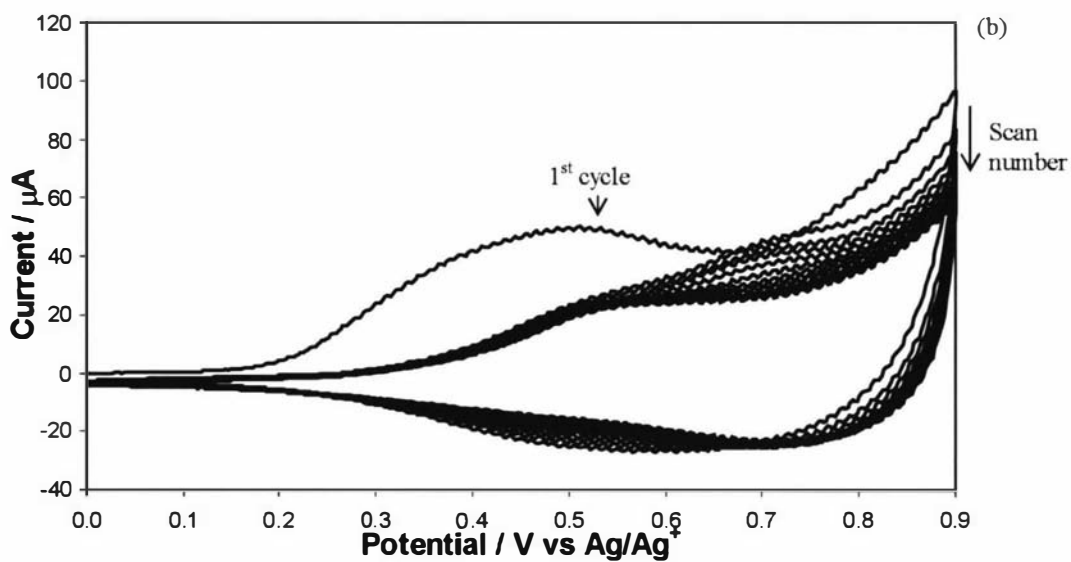
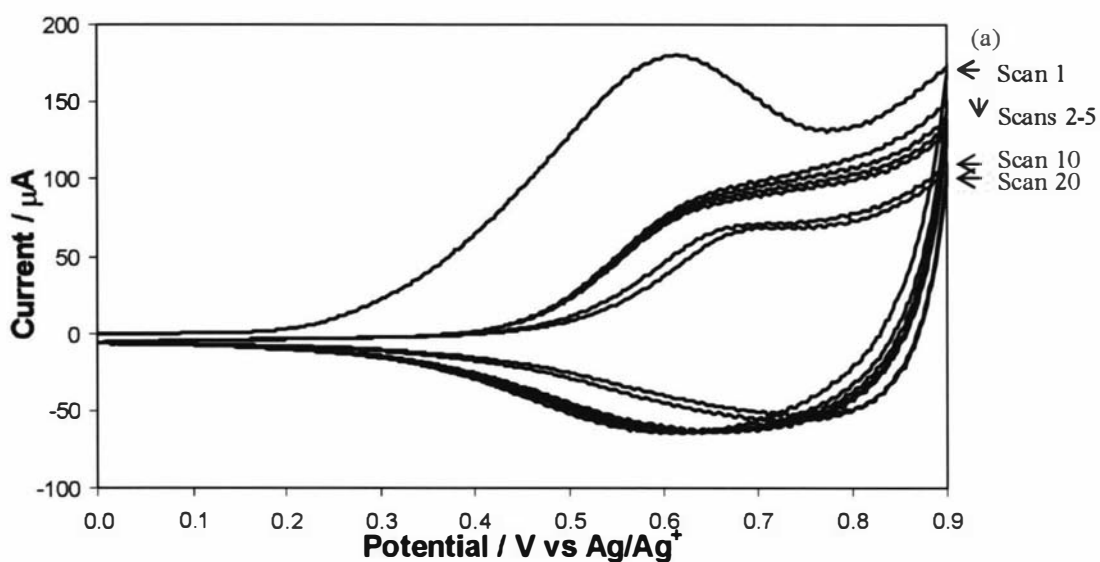


Fig. 3.20. Post-polymerisation CV of NMe_2STT films polymerised (a) potentiodynamically and (b) potentiostatically. Electrode: platinum disc (1.8 mm^2). Electrolyte solution: 0.1 M TBAP/AN . Potential limits: $0/+900 \text{ mV}$. 15 cycles. Scan rate: 100 mV s^{-1} .

Post-growth CVs for potentiodynamically and potentiostatically deposited polyOMeSTT films are shown in Fig. 3.21. The post growth CV of the potentiodynamically deposited material is a simple scan, which shows one broad oxidation peak (0.70 V) and one broad reduction band (0.48 V). The first scan is again distinct from subsequent scans and has a higher oxidation current. Subsequent scans are almost identical and indicate stable, reversible oxidation/reduction properties of the film.

The post-growth CV of the potentiostatically deposited material is very different to that shown by potentiodynamically deposited material and displays a complicated voltammogram with a number of distinct features. The first scan shows two sharp oxidation peaks at 0.32 V and 0.65 V, and two reduction peaks at 0.43 V and 0.32 V. These may be due to the oxidation of short oligomers as the first oxidation peak (0.32 V) completely disappears on the second scan and a large sharp oxidation peak at 0.50 V emerges. This peak and the oxidation peak at 0.65 V are observed to reduce in intensity with increasing scan number to eventually produce a broad band. Interestingly, the reduction peak at 0.42 V remains almost the same in shape and current intensity, but the peak at 0.15 V disappears.

The additional peaks observed by the potentiostatically grown films compared to the potentiodynamically grown film may be due to the different scan limits, and/or the presence of monomer/short oligomers trapped in the potentiostatic film. Multiple oxidation and reduction peaks were reported by Zotti *et al.* during initial post growth cycling of poly(3,3''-dipentoxyterthiophene), and were explained by further polymerisation of deposited oligomers.⁹⁹

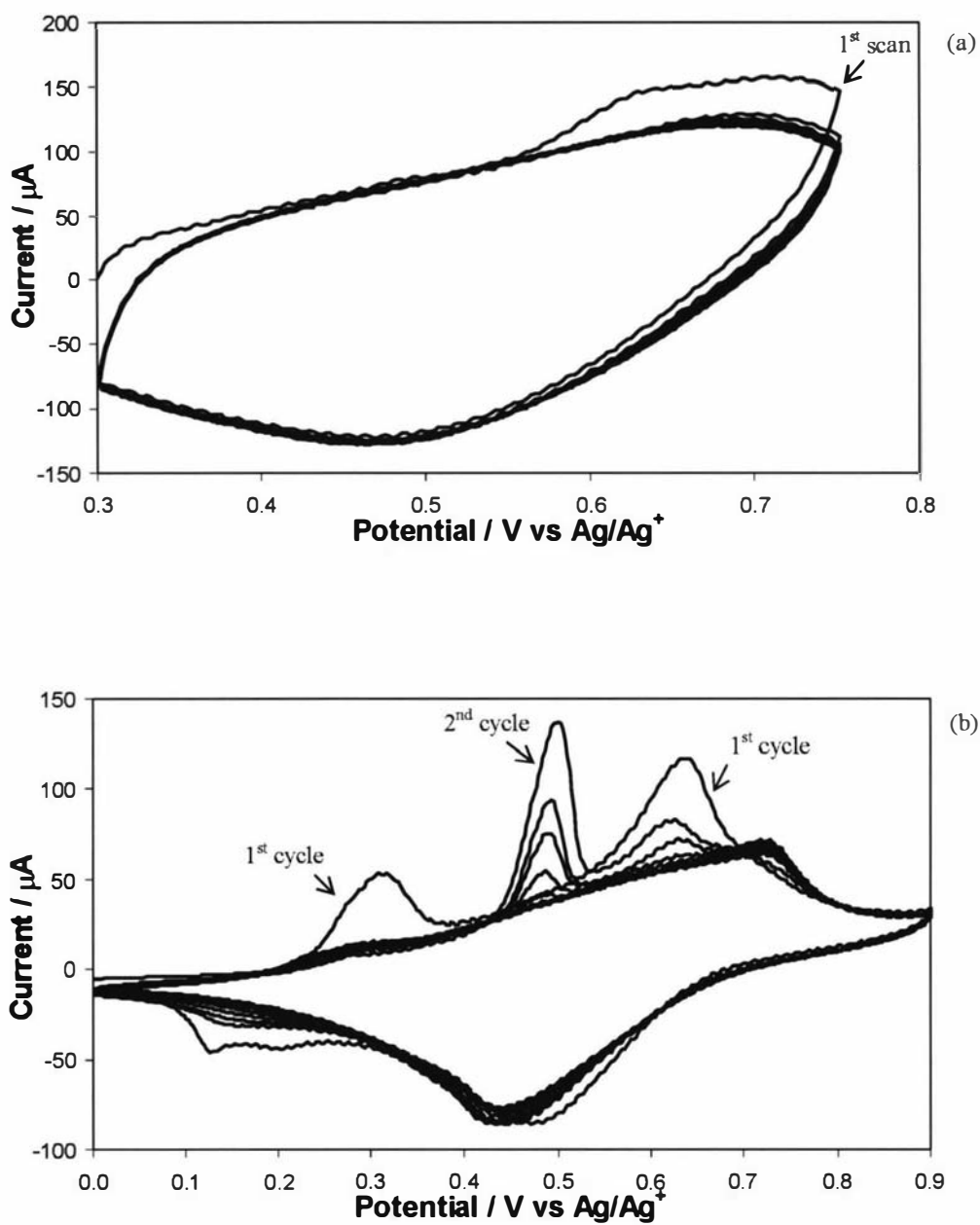


Fig. 3.21. Post-polymerisation CVs of (a) potentiodynamically and (b) potentiostatically deposited oligoOMeSTT films. Electrode: platinum disc (1.8 mm^2). Electrolyte solution: 0.1 M TBAP/AN . Scan rate: 100 mV s^{-1} .

The post-growth CVs of potentiodynamically and potentiostatically grown STT material are shown in Fig. 3.22, and differ significantly. As for the OMeSTT films, the potentiostatic film displays a number of sharp peaks, which may be due to oxidation of trapped monomer/oligomers. The difference in the scans could also be due to the different scan limits. An additional reduction peak at 0.27 V is included during the post growth cycling of the potentiostatically deposited material, which may be partially irreversible.

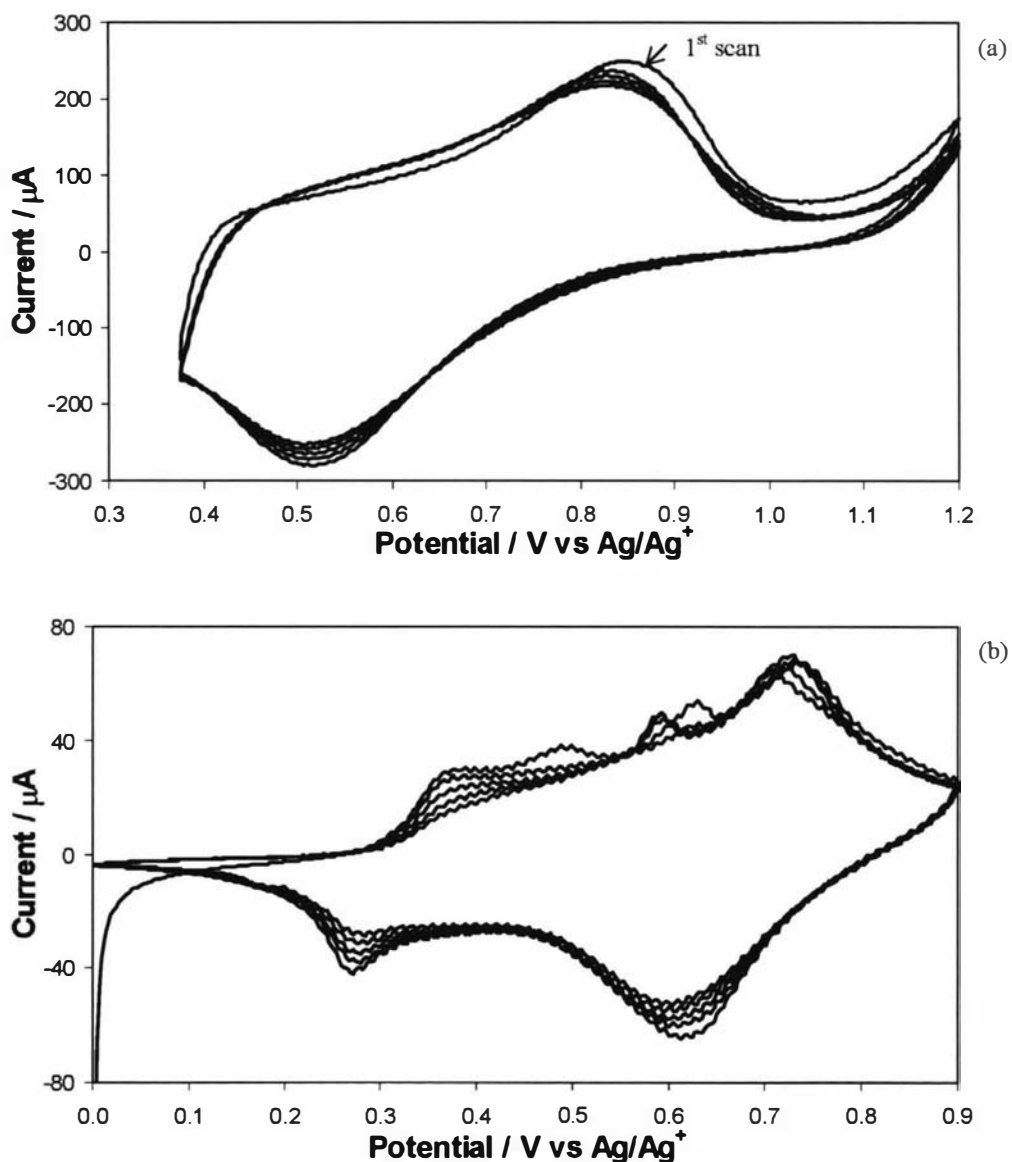


Fig. 3.22. Post-polymerisation CVs of (a) potentiodynamically and (b) potentiostatically deposited oligoSTT films. Electrode: platinum disc (1.8 mm^2). Electrolyte solution: 0.1 M TBAP/AN. Potential limits: +375/+1200 mV. 5 cycles. Scan rate: 100 mV s^{-1} .

The post-polymerisation CVs for potentiodynamically and potentiostatically grown CNSTT films are shown in Fig. 3.23. As previously observed, the first cycle of the potentiodynamically grown material is noticeably different to subsequent scans. The potentiostatically deposited material shows a large decrease in current in the first two scans, which, as mentioned for polymerisation of NMe₂STT, is most likely due to either a change in morphology or further polymerisation of short oligomers.

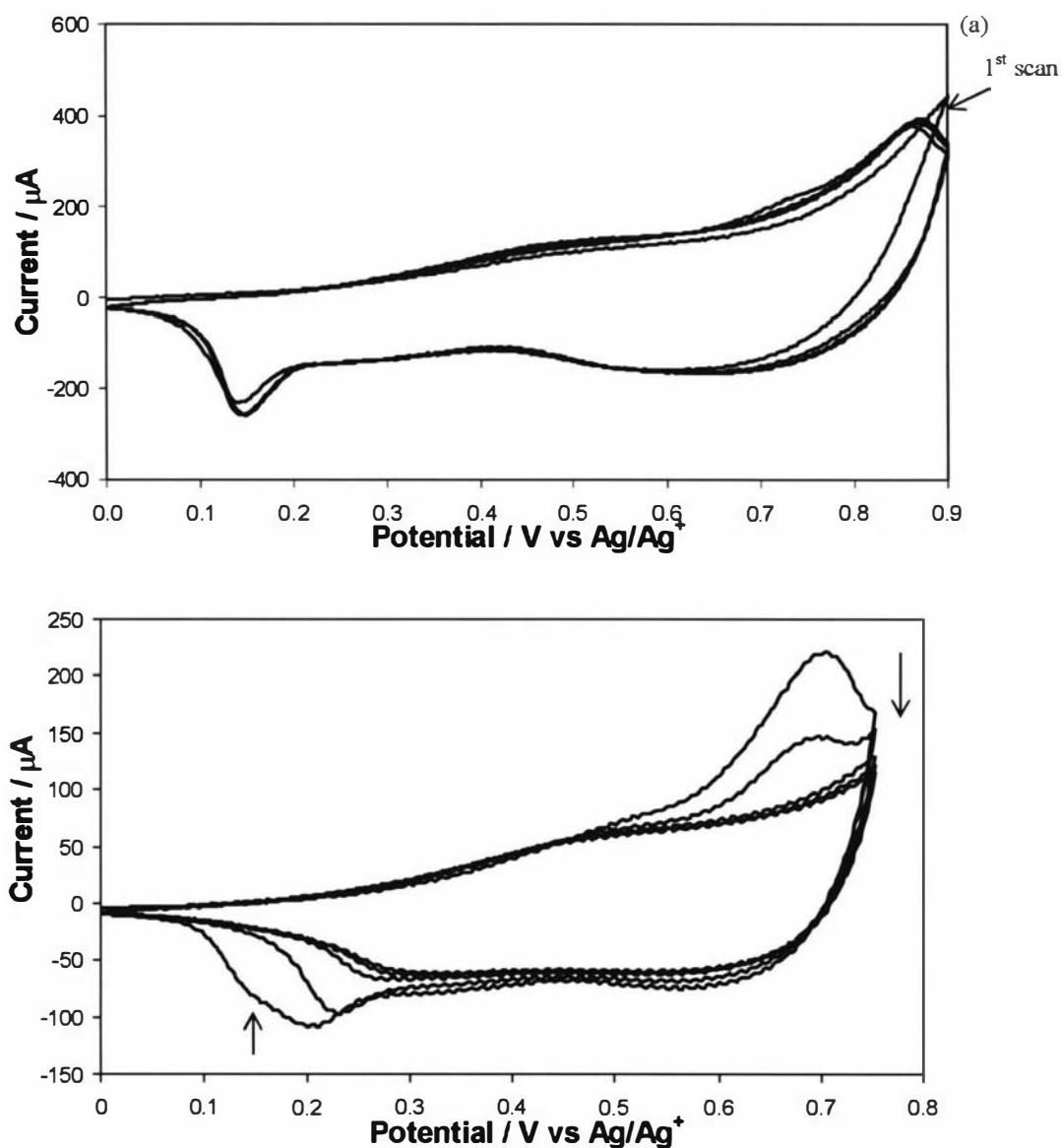


Fig. 3.23. Post-polymerisation CVs of (a) potentiodynamically and (b) potentiostatically deposited oligoCNSTT films. Electrode: platinum disc (1.8 mm²). Electrolyte solution: 0.1 M TBAP/AN. 5 cycles. Scan rate: 100 mV s⁻¹.

Post growth CVs of NO₂STT produced using potentiodynamic and potentiostatic methods are shown in Fig. 3.24. The post-growth CVs displayed by NO₂STT deposited by potentiodynamic and methods are very similar, indicating similar films. A sharp peak is observed on the first scan at 0.56 V, which decreases in current and shifts to 0.49 V on subsequent scans. Further cycling reveals a material that is stable with respect to current produced between the potentials of 0 and 0.9 V, and produces broad oxidation and reduction bands. These CVs are very similar to those measured by Cutler *et al.*⁹¹

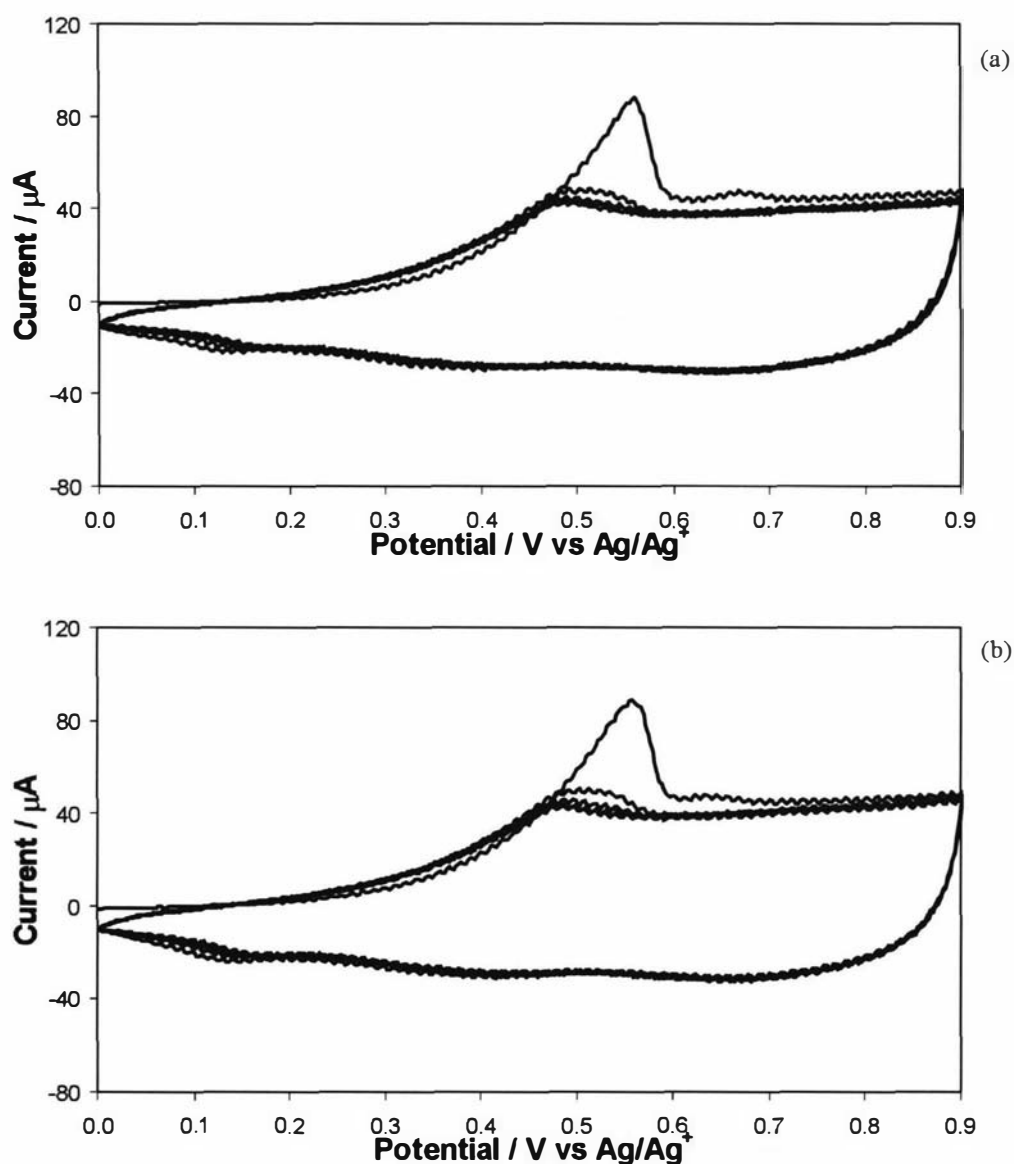


Fig. 3.24 Post-polymerisation CVs of (a) potentiodynamically and (b) potentiostatically deposited oligoNO₂STT films. Electrode: platinum disc (1.8 mm²). Electrolyte solution: 0.1 M TBAP/AN. 5 cycles. Scan rate: 100 mV s⁻¹.

In summary, the post-polymerisation CVs of the deposited materials showed significant changes between the initial scan and subsequent scans. Sharp peaks which are observed in the initial scan may be due to further polymerisation of trapped monomer and/or short oligomers. These are replaced by a broad oxidation band in subsequent cycles, which is consistent with the oxidation of a wider range of oligomer lengths.

Although post-growth CVs of potentiodynamically and potentiostatically deposited NO₂STT and NMe₂STT materials were similar in terms of shape and redox potentials, the OMeSTT, STT and CNSTT showed very different, more complicated post-growth spectra for materials deposited using potentiostatic methods. This may suggest that potentiostatically deposited materials are less stable than potentiodynamically deposited materials and undergo further processes (morphological or chemical) during post-growth potential cycling. Cyclic voltammetry appears to be a better method for the production of stable oligo(styryl terthiophene) films.

3.4.3.2 Analysis by UV-VIS-NIR spectroscopy

The films prepared in this study were observed to be electrochromic, since they changed colour with a change in potential. Red-brown colours were observed for the neutral films of the styrylterthiophene derivatives, and green/blue or purple colours generally observed for the oxidised films.

In order to measure the spectroscopic properties of the materials, films were electrosynthesised on ITO-coated glass by both potentiodynamic and potentiostatic methods. UV-VIS-NIR spectra were obtained for each film in both the oxidised (doped) and neutral (dedoped) state. UV-VIS-NIR spectra for films produced from NO₂STT, CNSTT, STT, OMeSTT and NMe₂STT derivatives are shown in Figs. 3.26 to 3.30 respectively.

Films of NO₂STT, CNSTT, STT, OMeSTT derivatives appeared to be stable with respect to colour in both the oxidised and neutral states. In contrast, films of the NMe₂STT derivative were purple in colour when subjected to an oxidised potential,

but were observed to spontaneously reduce (perceived by a change to an orange/brown colour) when the applied potential was removed.

Spectra of the NO₂STT, CNSTT and STT terthiophene films revealed no variation between potentiodynamic and potentiostatic deposition, although small differences were found in the UV-VIS-NIR spectra of OMeSTT and NMe₂STT films. The spectrum of the NO₂STT film is comparable with results obtained by Cutler *et al.*⁹¹ who also studied electrochemically deposited films of this polymer.

Neutral films of CNSTT, STT and OMeSTT oligomers are observed to generate two absorption maximum (λ_{max}) below 550 nm. The oligoNO₂STT film also shows a λ_{max} at 411 nm, with a shoulder at 496 nm. It is possible that the NMe₂STT film produces a second peak as well, but it is obscured by the peak at 401 nm. It has been postulated by Wagner and Officer,¹⁵⁴ that the two absorptions observed in the spectra for styryl terthiophene monomers can be attributed to a styryl-substituted thiophene chromophore and a terthiophene chromophore (Fig. 3.25). It is anticipated that analogous bands would be observed for styryl-functionalised oligo(terthiophene)s, and indeed Grant confirms this for polyether-substituted styryl-sexithiophenes; the styryl chromophore is observed at *ca.* 340 nm and the sexithiophene chromophore at *ca.* 500 nm.¹¹ On oxidation these bands are observed to diminish while bands at about 800 nm and >1000 nm emerge due to the formation of polaronic and/or dipolaronic species.^{125,127}

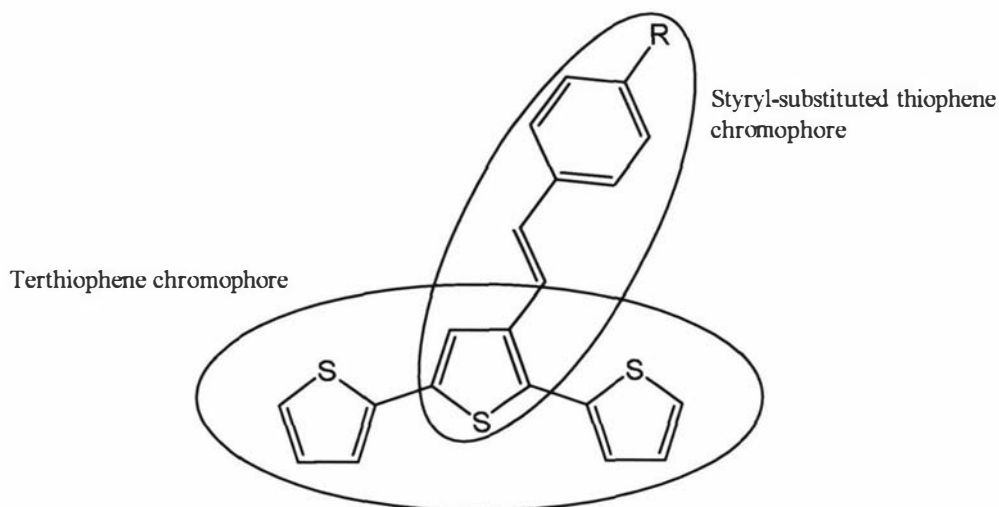


Fig. 3.25. Chromophores produced by styryl-substituted terthiophene derivatives.¹⁵⁴

The absorption maxima measured by UV-VIS-NIR spectroscopy, provide an indication of the band gap of the polymer,²³ and hence the effective conjugation length.¹¹⁴ In the reduced state, the λ_{max} due to the oligothiophene chromophore for the materials in this study are observed to be similar (ranging between 484 and 518 nm), and are comparable to the λ_{max} reported by Grant for a series of styryl-substituted sexithiophene derivatives (ca. 500 nm),¹¹ providing further evidence that these materials are producing predominantly dimer.

When oxidised, the effective conjugation length is increased due to delocalisation of charge. Polaron and bipolaron energy levels are produced, which decrease the band gap between the valence and conduction bands; hence the appearance of bands at higher wavelengths (lower energy). The decline in the $\pi \rightarrow \pi^*$ band and growth in the polaron band (~750 nm) due to the oxidation of the neutral species as the applied potential is increased, is clearly seen by spectroelectrochemistry of oligoSTT (Fig. 3.31).

The spectra of the polyNMe₂STT films (Fig. 3.30) display significantly smaller polaron/bipolaron bands than shown by the other samples. This is most likely due to reduction of the film, which was observed on removal of the oxidising potential. Compared to other styryl-substituted terthiophene derivatives, Clarke *et al.* also

observed the production of very small polaron/bipolaron bands during the chemical oxidation of polyNMe₂STT.¹⁵⁵

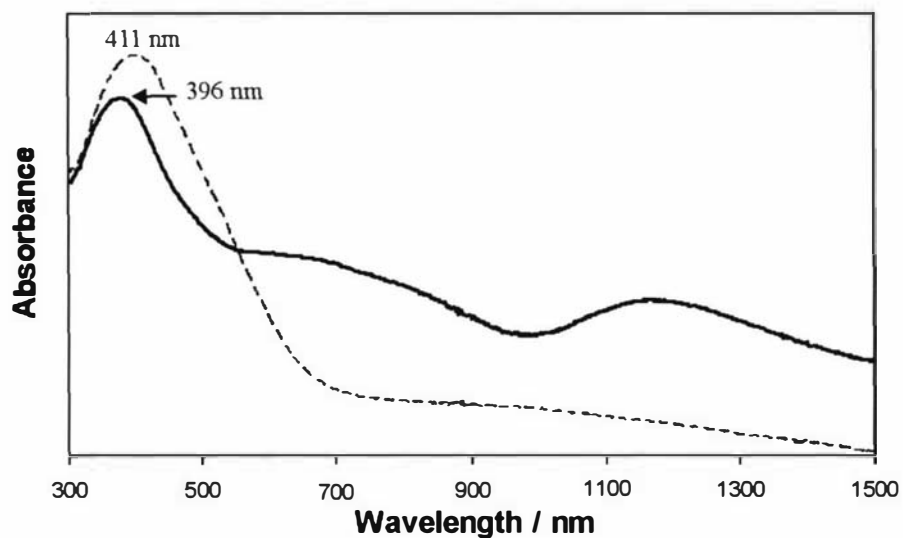


Fig. 3.26. UV-VIS-NIR spectra of a film of electrodeposited oligoNO₂STT in the oxidised (solid line) and neutral (dashed line) states.

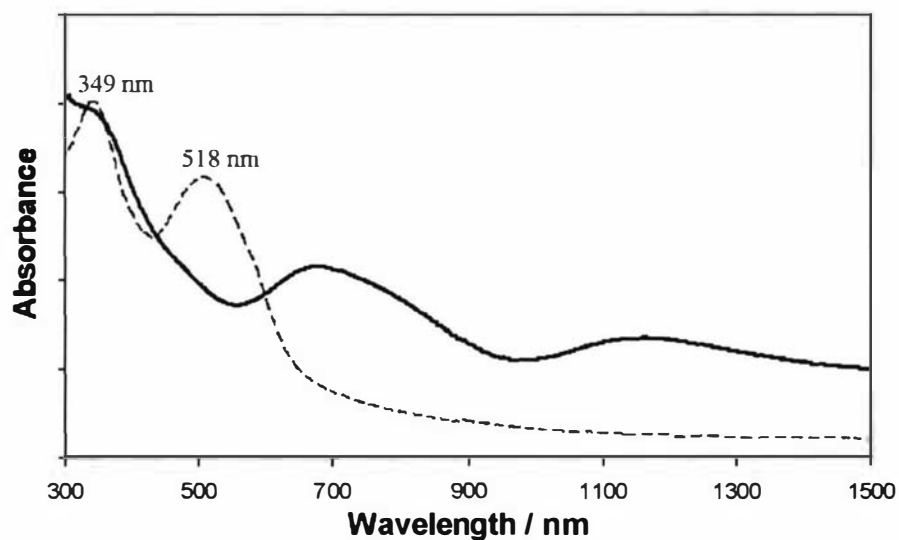


Fig. 3.27. UV-VIS-NIR spectra of a film of electrodeposited oligoCNSTT in the oxidised (solid line) and neutral (dashed line) states.

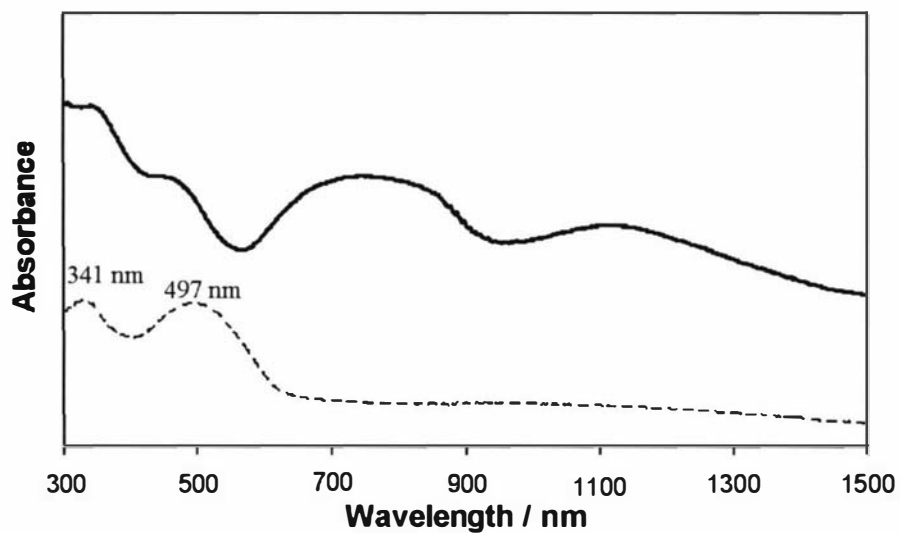


Fig. 3.28. UV-VIS-NIR spectra of a film of electrodeposited oligoSTT in the oxidised (solid line) and neutral (dashed line) states.

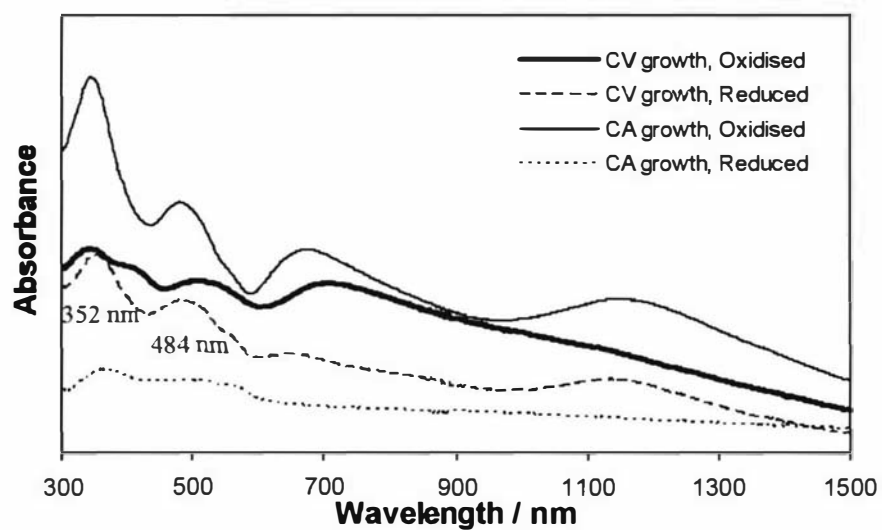


Fig. 3.29. UV-VIS-NIR spectra of oxidised films (solid lines) and neutral films (dashed lines) of OMeSTT deposited using potentiodynamic and potentiostatic methods.

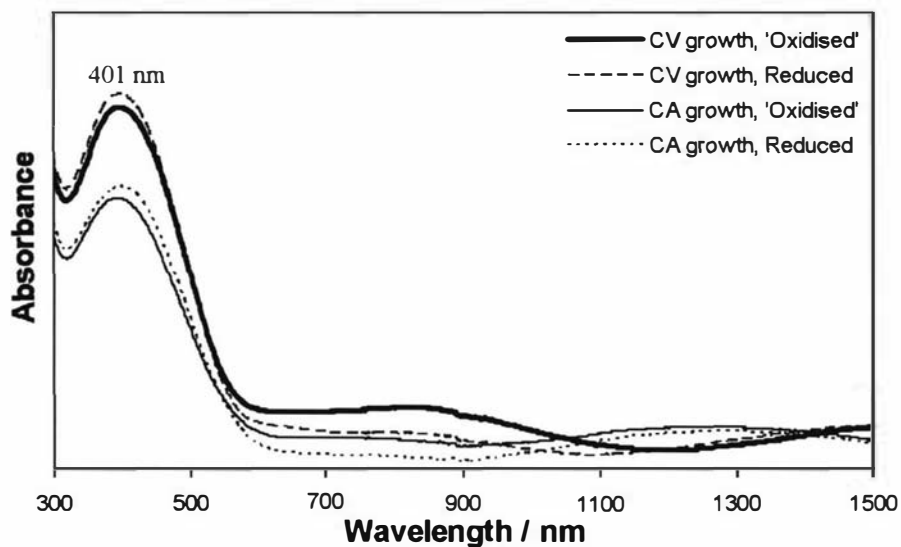


Fig. 3.30. UV-VIS-NIR spectra of films that were previously oxidised (solid lines) and neutral films (dashed lines) of NMe_2STT deposited using potentiodynamic and potentiostatic methods.

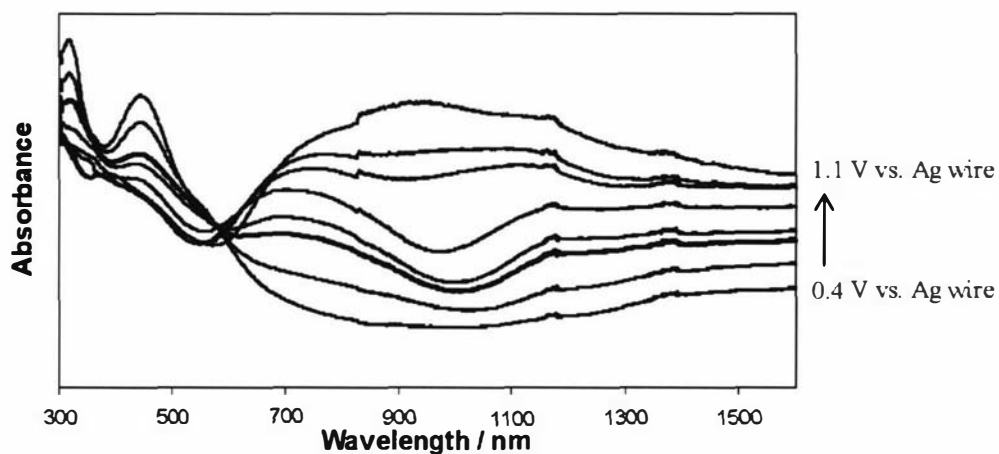


Fig. 3.31. Spectroelectrochemistry of an electrochemically grown film of oligoSTT on ITO-coated glass. Potentials between 0.4 V and 1.1 V were applied in steps of 0.1 V.

In summary, the low λ_{max} due to the $\pi \rightarrow \pi^*$ transition, and the poor free carrier tails displayed by these films when compared to polymeric materials such as polypyrrole,¹²⁶ indicate low conjugation. This in turn, is suggestive of short oligomers rather than polymeric material.

3.4.3.3 Scanning electron microscopy (SEM)

The morphology of films is useful for determining properties such as conductivity and surface area. Generally, more compact films lead to a higher conductivity as polymer molecules have better connections.⁵⁷ On the other hand, porous films or films with rough surfaces can give a higher surface area, which is desirable in many applications to increase reaction efficiencies.

The morphology of the electrochemically deposited films of conducting polymers is dependent on the kinetics of nucleation and growth, which, in turn, generally depends on three parameters:¹⁰⁹

- (I) The structure of the monomer/polymer.
- (II) The nature of the dopant.
- (III) The thickness of the film grafted on the electrode.

SEM images were taken of NMe₂STT, OMeSTT, STT, CNSTT and NO₂STT materials grown on ITO-coated glass. The films were deposited using both potentiostatic and potentiodynamic methods and were compared in the oxidised and neutral state.

SEM images for oligoNMe₂STT films deposited using potentiostatic methods, were found to have an extremely smooth, homogenous morphology with very few features in both the 'oxidised' and neutral forms. The neutral form of the film synthesised using cyclic voltammetry was also very smooth (Fig. 3.32a). The compactness is not inconsistent with the idea that the increase in oxidation potential during potentiodynamic growth of the film, may be due to difficulty in anion exchange during the oxidation process, as discussed in Section 3.4.2. In contrast to the film grown potentiostatically, the 'oxidised' potentiodynamically grown films displayed a 'cauliflower'-like structure (Fig. 3.32b). The significant difference between the neutral and oxidised films is surprising since the UV-VIS-NIR spectra showed little difference between the films. However, as they are two different films (although deposited under

identical conditions), it cannot be ruled out that the cauliflower structure shown by the 'oxidised' film is due to a slightly faster nucleation and growth process.

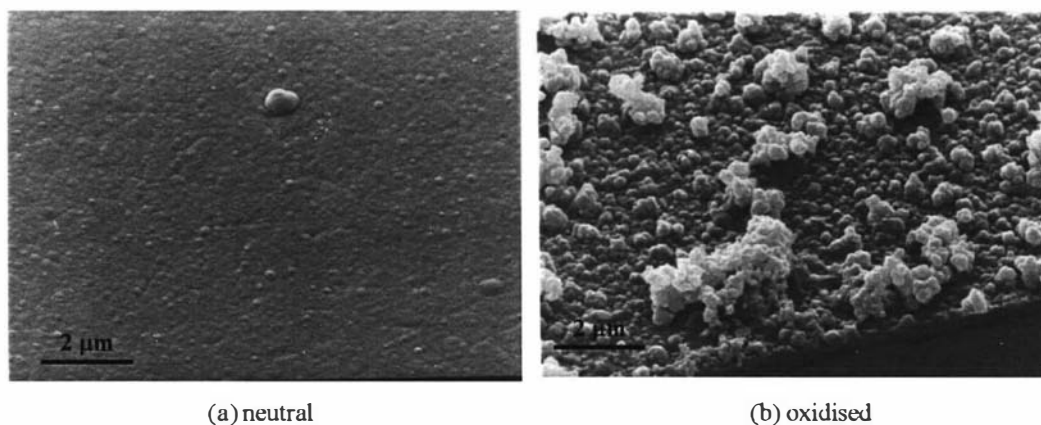


Fig. 3.32. SEM images of neutral and oxidised films of oligoNMe₂STT deposited onto ITO-coated glass using potentiodynamic methods. Magnification: x10000.

Oxidised oligoOMeSTT films deposited by potentiostatic (Fig. 3.33) methods and potentiodynamic methods appear almost identical in structure. Neutral films were observed to poorly adhere to the ITO-coated glass.

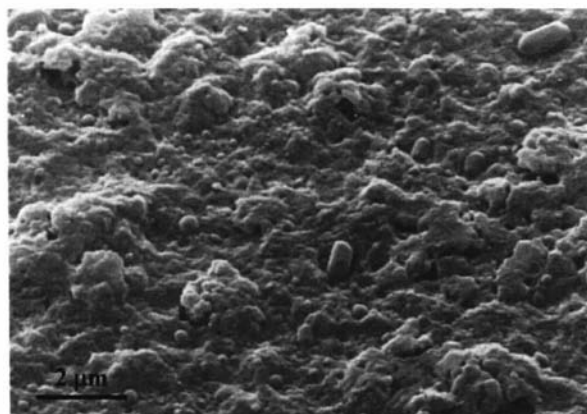


Fig. 3.33. SEM image of an oxidised film of OMeSTT deposited using potentiodynamic methods. Magnification: x10000.

Potentiostatically and potentiodynamically deposited oligoSTT films display common features as shown in Fig. 3.34 and Fig. 3.35. The neutral films reveal crystalline-looking structures; very similar structures were also observed by Grant *et al.* of electrochemically deposited dimeric STT derivatives.¹¹ On oxidation, these structures disappear to leave a porous film. The cracks observed in the oxidised

potentiodynamically deposited film (Fig. 3.35a) may be due to evaporation of the solvent causing a contraction of the film and suggest a brittle texture when dry.

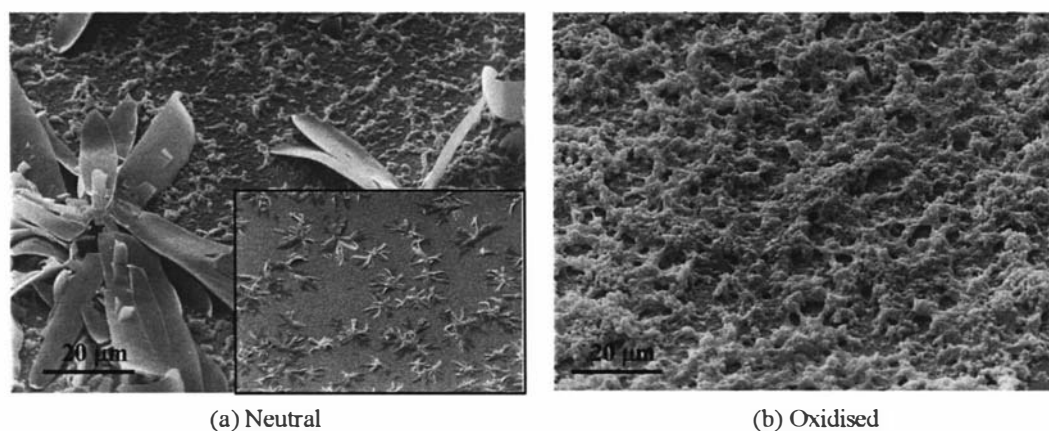


Fig. 3.34. Potentiostatically deposited films of STT oligomers. (a) Neutral film: x1400, inset: x70. (b) Oxidised film: x1400.

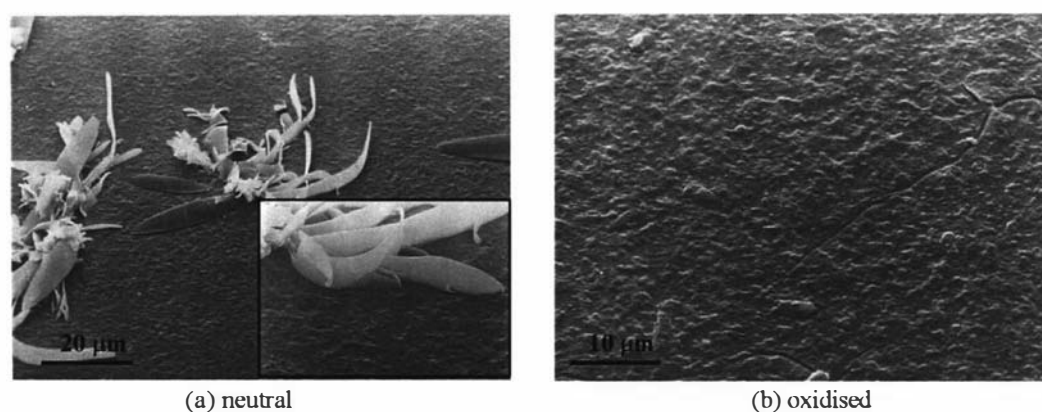


Fig. 3.35. SEM images of oligoSTT films deposited using cyclic voltammetry. (a) Neutral film: x1000, inset: x5000. (b) Oxidised state: x2000 magnification.

The oxidised and neutral oligoCNSTT films deposited using constant potential and cyclic voltammetry are shown in Figs. 3.36 and 3.37 respectively. The films show distinct fibre growth, with particularly prominent fibres in both the oxidised and neutral films deposited using potentiodynamic methods. Fibres are an interesting feature because they increase the surface area of the polymer.

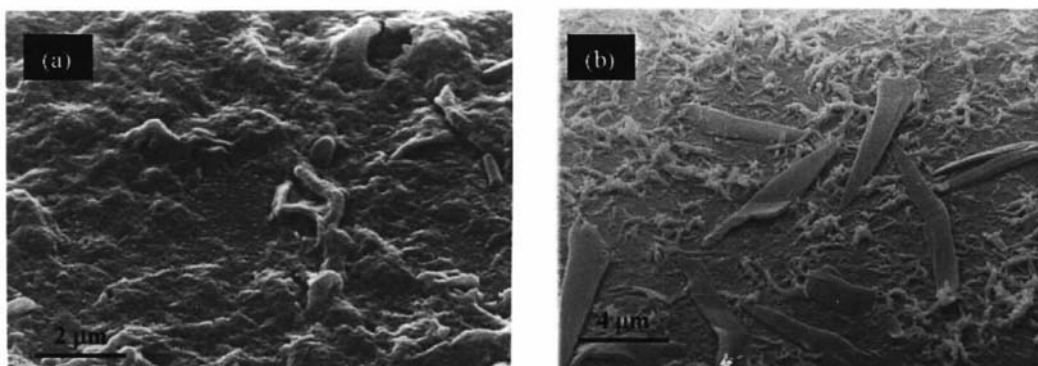


Fig. 3.36. SEM images of oligoCNSTT films deposited using a constant potential. (a) oxidised state, x10000 magnification, (b) neutral state, x5 000 magnification.

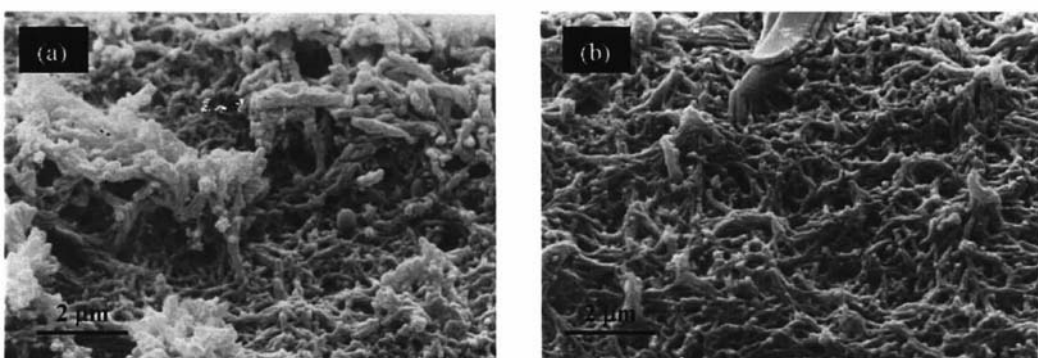


Fig. 3.37. SEM images of oligoCNSTT films deposited using cyclic voltammetry. (a) oxidised state, x10000 magnification, (b) neutral state, x10000 magnification.

Films of NO₂STT deposited by potentiostatic and potentiodynamic methods were observed to be very similar in the neutral state. The film deposited using a constant potential is shown in Fig. 3.38 and reveals a surface consisting of short, fibre-like structures. Oxidised films vary slightly depending on whether they have been deposited using potentiostatic or potentiodynamic methods as shown in Fig. 3.39.

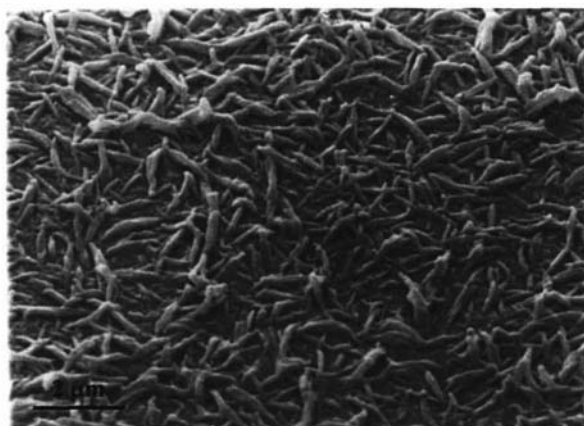


Fig. 3.38. SEM image of a neutral oligoNO₂STT film deposited using a constant potential, x 10000 magnification.

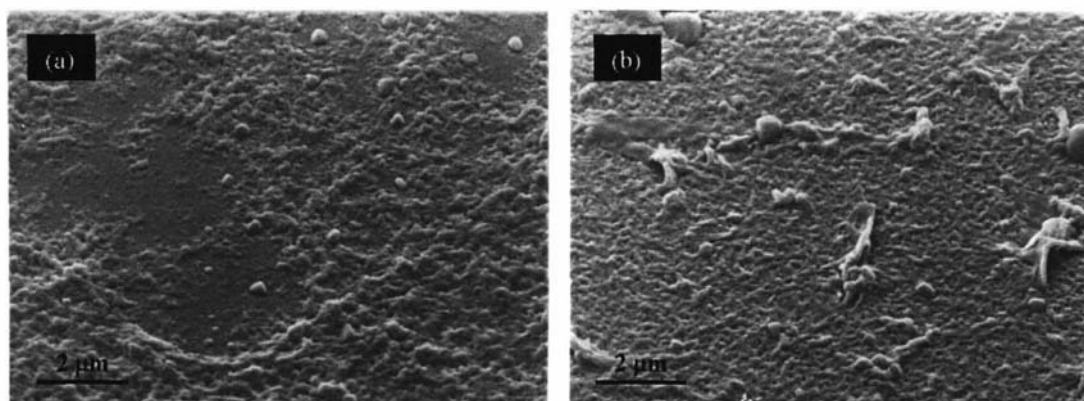


Fig. 3.39. SEM images of oxidised oligoNO₂STT films deposited by (a) potentiostatic and (b) potentiodynamic methods, x10000 magnification.

In summary, SEM images of electrodeposited styryl-substituted terthiophene derivatives show crystalline structures. Similar structures observed by Grant *et al.* in dimeric films of styryl-substituted terthiophene derivatives, suggest these materials also consist primarily of short oligomers.¹¹

3.5 Conclusions

A series of styryl-functionalised terthiophene derivatives that supported substituents of varying electron withdrawing/donating ability were synthesised. These materials were oxidised using both chemical and electrochemical techniques and the resulting materials investigated using MALDI-TOF MS, ¹H NMR spectroscopy, cyclic voltammetry, UV-VIS-NIR spectroscopy and microscopy. The materials comprise significant amounts of insoluble material (37-95%), which was difficult to further characterise and process. The soluble fractions were found to consist predominantly of dimer and short oligomers rather than polymer. It was also shown by ¹H NMR spectroscopy that dimerisation was regioselective, to form primarily the head-to-head isomer. The high yields of head-to-head dimer is consistent with previous work accomplished by Grant¹¹ on ether-substituted styrylterthiophene compounds and with predictions made from theoretical calculations of the polymerisation of these materials.

3.6 Experimental

3.6.1 Reagents and materials

All reagents were used as received from suppliers unless specified otherwise. Chloroform obtained from BDH Laboratory Supplies (London) was used in all reactions unless specified otherwise and contains 0.5 to 1.0% ethanol as a stabiliser. TBAP (Fluka, Purum) was partially dried under vacuum at 70°C for 48 hours, followed by further drying under vacuum with potassium hydroxide.

Note: as the length of the oligomers yielded can not be accurately measured, the theoretical yield has been calculated without taking into account the loss of hydrogen on polymerisation. At most, this leads to an uncertainty of 0.3% in the calculated polymer yields.

3.6.2 Synthesis of styryl-substituted terthiophene monomers

The following monomers were synthesised according to the procedure reported by Collis *et al.*⁸⁰ The NMR spectra obtained matched those previously reported.

Synthesis of NO₂STT

trans-1-((2',2'':5',2'''-terthiophen)-3''-yl)-2-(4''''-nitrophenyl)ethane

A mixture of 3'-formyl-2,2':5'2''-terthiophene (3.31 g, 12 mmol), 4-nitrobenzyl triphenylphosphonium bromide (6.67 g, 13.87 mmol) and DBU (2.07 mL, 13.86 mmol, 2.11 g) in dry DCM (165 mL) was heated under reflux. After 8 hrs, the reaction mixture was diluted with dichloromethane (300 mL) and washed with 1 M solution of HCl (2 x 100 mL), 10% sodium bicarbonate solution (100 mL) and water (100 mL). The organic layer was dried and concentrated to give a crude orange solid. The solid was dissolved in a small quantity of DCM/hexane (1:1) and passed through a column of silica with continued elution using this solvent system until all the yellow/orange material had been collected. Analysis of the material by ¹H NMR spectroscopy indicated it consisted of a mixture of the *cis* and *trans* isomers in a ratio of 3:2. This material was dissolved in dry chloroform (500 mL) and irradiated for 3 hours using a

250 W flood lamp. After removal of the solvent, analysis of the sample by ^1H NMR spectroscopy indicated it consisted of essentially the *trans* product. The material was recrystallised from dichloromethane/ether to give the product as orange crystals (3.30 g, 70%).

^1H NMR (270.2 MHz, CDCl_3) δ 8.22-8.17 (2H, AA' part of AA'XX'); 7.60-7.55 (2H, XX' part of AA'XX'); 7.49 (d, 1H, $J = 16.2$ Hz), H 1), 7.44 (dd, 1H, $J = 5.1, 1.2$ Hz, H5'), 7.41 (s, 1H, H 4''); 7.28 (dd, 1H, $J = 5.1, 1.1$ Hz, H 5'''); 7.22 (dd, 1H, $J = 3.6, 1.1$ Hz, H3'''); 7.20 (dd, 1H, $J = 3.6, 1.2$ Hz, H 3'); 7.15 (dd, 1H, $J = 5.1, 3.6$ Hz, H 4'); 7.05 (dd, 1H, $J = 5.1, 3.6$ Hz, H 4'''); 7.05 (d, 1H, $J = 16.2$ Hz, H 2).

Synthesis of CNSTT

trans-1-((2',2'':5'',2'''-terthiophen)-3''-yl)-2-(4''''-cyanophenyl)ethane

A mixture of 3'-formyl-2,2':5'2''-terthiophene (3.3 g, 11.7 mmol), 4-(cyanobenzyl) triphenylphosphonium bromide (6.45 g, 14.1 mmol) and DBU (2.11 ml, 14.13 mmol, 2.15 g) in dry DCM (200 mL) was heated under reflux. After 3 hrs the reaction mixture was diluted with DCM (300 mL) and washed with 1 M solution of HCl (100 mL), 10% sodium bicarbonate solution (100 mL) and water (100 mL). The organic layer was dried and concentrated to give a crude yellow solid. Analysis of this crude material by ^1H NMR spectroscopy indicated it contained the triphenylphosphine oxide byproduct and only the *trans* product. A silica column was used to separate the yellow solid product. This was recrystallised from ether/pentane to give yellow crystals (3.006 g, 68%).

^1H NMR (270.2 MHz, CDCl_3) δ 7.64-7.61 (2H, AA' part of AA'XX'); 7.55-7.52 (2H, XX' part of AA'XX'), 7.45 (d, 1H, $J = 16.2$ Hz, H 1), 7.43 (dd, 1H, $J = 5.1, 1.2$ Hz, H 5'), 7.41 (s, 1H, H 4''), 7.27 (dd, 1H, $J = 5.1, 1.1$ Hz, H 5'''); 7.2 (dd, 1H, $J = 3.6, 1.1$ Hz, H3'''); 7.19 (dd, 1H, $J = 3.6, 1.2$ Hz, H3'). 7.14 (dd, 1H, $J = 5.1, 3.6$ Hz, H 4'); 7.05 (dd, $J = 5.1, 3.6$ Hz, H 4'''); 7.00 (d, 1H, $J = 16.2$, Hz, H 2).

Synthesis of STT

trans-1-((2',2'':5'',2''''-terthiophen)-3''-yl)-2-(phenyl)ethane

A mixture of 3'-formyl-2,2':5'2''-terthiophene (3.3 g, 11.9 mmol), benzyl triphenylphosphonium bromide (6.2 g, 14 mmol), DBU (2.2 ml, 14 mmol, 2.15 g) in dry DCM (330 mL) was heated under reflux. After 3 hrs the reaction mixture was diluted with DCM (300 mL) and washed with 1 M solution of HCl (2 x 100 mL), 10% sodium bicarbonate solution (100 mL) and water (100 mL). The organic layer was dried and concentrated to give a crude yellow solid. Analysis of this crude material by ¹H NMR spectroscopy indicated it consisted primarily of the desired *trans* product. A silica column (1:5 ethylacetate/hexane) was used to separate the product as a yellow oil, which crystallized on standing. Recrystallisation from ether/pentane gave the product as yellow crystals (3.778 g, 90%).

¹H NMR (270.2 MHz, CDCl₃) δ 7.51-7.46 (m, 2H, aryl H); 7.43 (s, 1H, H 4''); 7.39 (dd, 1H, *J* = 5.2, 1.2 Hz, H5''); 7.37 (d, 1H, *J* = 16.1 Hz, H 1); 7.40-7.34 (m, 2H, aryl H); 7.27 (dd, 1H, *J* = 5.1, 1.1 Hz, H 5'''); 7.30-7.24 (m, 1H, aryl H); 7.22 (dd, 1H, *J* = 3.6, 1.1 Hz, H 3'''); 7.21 (dd, 1H, *J* = 3.6, 1.2 Hz, H3'); 7.12 (dd, 1H, *J* = 5.2, 3.6 Hz, H 4'); 7.04 (dd, 1 H, *J* = 5.1, 3.6 Hz, H 4'''); 7.04 (d, 1H, *J* = 16.1 Hz, H 2).

Synthesis of OMeSTT

trans-1-((2',2'':5'',2''''-terthiophen)-3''-yl)-2-(4''''-methoxyphenyl)ethane

A mixture of (4-methoxybenzyl) triphenylphosphonium chloride (9.97 g, 24 mmol, 2 equiv.) and KOBu¹ (2.68 g, 24 mmol) in dry THF (100 mL) was heated under reflux for 15 min. To this was added a solution of 3'-formyl-2,2':5'2''-terthiophene (3.3 g, 12 mmol) in dry THF (100 mL). After 8 hrs the reaction was halted, diluted with dichloromethane (200 mL) and washed with 1 M solution of HCl (2 x 100 mL), 10% sodium bicarbonate solution (100 mL) and water (100 mL). The organic layer was dried (MgSO₄) and concentrated to give a crude yellow solid. This material was adsorbed onto silica before being passed through a column of silica with 10% ethylacetate/hexane as solvent. The yellow solid was recrystallised from ether/pentane to afford the product as yellow crystals. (3.61 g, 79%).

¹H NMR (270.2 MHz, CDCl₃) δ7.45-7.41 (2H, AA' part of AA'XX'); 7.40 (s 1H, H4''); 7.37 (dd, 1H, J = 5.1, 1.2 Hz, H 5'); 7.25(dd, 1H, J = 5.1, 1.2 Hz, H 5'''); 7.22 (d, 1H, J = 16.2 Hz, H 1); 7.21, (dd, 1H, J = 3.6, 1.2 Hz, H 3'''); 7.19 (dd, 1H, J = 3.6, 1.2 Hz, H 3'); 7.12 (dd, 1H, J = 5.1, 3.6 Hz, H 4'); 7.04 (dd, 1H, J = 5.1, 3.6 Hz, H 4'''); 6.99 (d, 1H, J = 16.2 Hz, H2); 6.92-6.86 (2H, XX' part of AA'XX'); 3.83 (s, 3H, OMe).

Synthesis of NMe₂STT

trans-1-((2',2'':5'',2'''-terthiophen)-3''-yl)-2-(4''''-N,N-dimethylaminophenyl)ethane

A mixture of (4-*N,N*-dimethylaminobenzyl) triphenylphosphonium iodide (13.1 g, 25.1 mmol, 2.1 equiv.) and KOBu^t (2.82 g, 25.1 mmol) in dry THF (100 mL) was heated under reflux for 15 min then cooled. To this was added a solution of 3'-formyl-2,2':5'2''-terthiophene (3.3 g, 11.9 mmol) in dry THF (100 mL) and heated under reflux. After 8 hrs the reaction was diluted with dichloromethane (200 mL) and washed with 1 M solution of HCl (100 mL), 10% sodium bicarbonate solution (100 mL) and water (100 mL). The organic layer was dried (MgSO₄) and concentrated to give a crude yellow solid. The solid was dissolved in a small quantity of dichloromethane/hexane (1:1) and passed through a column of silica with continued elution with the same solvent system until the yellow material had been collected. This was recrystallised from ether to afford the product as yellow crystals. (3.33 g, 71%).

¹H NMR (270.2 MHz, CDCl₃) δ7.42 (s, 1H, H 4''); 7.43-7.49 (2H, AA' part of AA'XX'); 7.36 (dd, 1H, J = 5.2, 1.2 Hz, H 5'); 7.23 (dd, 1H, J = 5.1, 1.2 Hz, H 5'''), 7.20 (d, 1H, J = 16.1 Hz, H 1); 7.19 (dd, 1H, J = 3.6, 1.2 Hz, H 3'''); 7.15 (dd, 1H, J = 3.6, 1.2 Hz, H3'); 7.11 (dd, 1H, J = 5.2, 3.6 Hz, H 4')7.04 (dd, 1H, J = 5.1, 3.6 Hz, H 4'''); 6.99 (d, 1H, J = 16.1 Hz, H 2); 6.76-6.70 (2H, XX' part of AA'XX'); 3.00 (s, 6H, NMe₂).

3.6.3 Polymerisation of styryl-substituted terthiophene monomers

Polymerisation NMe₂STT

A suspension of anhydrous FeCl_3 (180 mg, 1.078 mmol, 4.23 equiv.) in dry DCM (15 mL) was added dropwise over 1 hr to a stirred solution of NMe_2STT (100 mg, 2.55×10^{-4} mol, 1 equiv.) dissolved in dry DCM (4 mL). The mixture was stirred at room temperature for 4 hrs and sonicated every 30 min. The reaction mixture was then filtered to give a black powder, which was washed with H_2O (300 ml), and then washed with methanol for 24 hrs using a soxhlet extractor. The resulting red powder (0.776 g) was dried in vacuo for 24 hrs and then exhaustively extracted with DCM for 24 hrs in a soxhlet extractor. The eluent gave a red powder which was precipitated in chloroform/hexane to concentrate the most soluble dimers, giving a yield of 20 mg (20%). NMR, MALDI and TLC showed that it consisted mostly of HH isomers of dimer (~80%), but also a little trimer, tetramer and/or HT/TT isomers of dimer (~20%).

Polymerisation of OMeSTT

A suspension of anhydrous FeCl_3 (180 mg, 1.078 mmol, 4.10 equiv.) suspended in dry DCM (15 mL) was added dropwise over 1 hr to a stirred solution of OMeSTT (of 100 mg, 2.63×10^{-4} mol, 1 equiv.) dissolved in dry DCM (4 mL). The mixture was stirred at room temperature for 4 hrs, sonicating briefly every 30 min. The reaction mixture was then filtered to give a black powder, which was rinsed with H_2O (300 ml) and then washed in methanol using a soxhlet extractor for 24 hrs. The resulting red powder was dried in vacuo for 24 hrs and then exhaustively extracted in DCM using a soxhlet extractor for 24 hrs. The orange eluent gave a red powder, which was precipitated in chloroform/hexane, the eluent giving a yield of 19.5 mg (19.5%). NMR, MALDI and TLC showed that it consisted mostly of HH isomers of dimer (~80%), but also a little trimer, tetramer and/or HT/TT isomers of dimer (~20%).

Polymerisation of STT

A suspension of anhydrous FeCl_3 (180 mg, 1.078 mmol, 3.77 equiv.) in dry DCM (15 mL) was added dropwise (over 1 hr) to a stirred solution of STT (100 mg, 2.86×10^{-4} mol, 1 equiv.) dissolved in dry DCM (4 mL). The mixture was stirred at room temperature for 4 hrs and sonicated briefly every 30 min. The reaction mixture was then filtered to give a black powder, which was rinsed with H_2O (300 ml), and then washed with methanol using a soxhlet extractor. The resulting red powder was

dried in vacuo for 24 hrs before being exhaustively extracted in DCM using a soxhlet extractor to give a bright orange eluent (33 mg, 33%). The eluent was dried to give a red/black powder. It was then precipitated in chloroform/hexane, the eluent giving a yield of 4 mg (4%). NMR, MALDI and TLC showed that this fraction consisted mostly of HH isomers of dimer (~70%), but also a little trimer, tetramer and/or HT/TT isomers of dimer (~30%).

Polymerisation of CNSTT

A suspension of anhydrous FeCl_3 (180 mg, 1.078 mmol, 4.04 equiv.) in dry DCM (15 mL) was added dropwise over 1 hr to a stirred solution of CNSTT (100 mg, 2.67×10^{-4} mol, 1 equiv.) dissolved in dry DCM (4 mL). The mixture was stirred at room temperature for 24 hrs, sonicating briefly every 30 min for the first 4 hrs. The reaction mixture was then filtered to give a black powder, which was rinsed with H_2O (300 mL), and then washed for 24 hrs with methanol using a soxhlet extractor. The resulting red powder was dried in vacuo for 24 hrs and then soxhletted for 24 hrs with DCM. The orange eluent gave a red powder, which was then precipitated in chloroform/hexane, the eluent giving a yield of 63 mg (63%). NMR, MALDI and TLC showed that it consisted mostly of HH isomers of dimer (~70%), but also a little monomer, trimer, tetramer and/or HT/TT isomers of dimer (~30%).

Polymerisation of NO_2STT

A suspension of anhydrous FeCl_3 (180 mg, 1.078 mmol, 4.26 equiv.) in dry DCM (15 mL) was added dropwise (over 10 min.) to a stirred solution of NO_2STT (100 mg, 2.532×10^{-4} mol, 1 equiv) in dry DCM (4 mL). The mixture was stirred for 1 hr under reflux. The reaction mixture was then filtered to give a black powder which was washed with methanol using a soxhlet extractor for 24 hrs. The resulting black, clumpy material (92 mg) was dried in vacuo for 24 hrs and then soxhletted for 24 hrs with DCM. The red eluent (<5 mg) was adsorbed onto silica and passed through a column of silica with continued elution using DCM/hexane (1:1) as a solvent until the orange material had been collected (<1 mg).

3.6.4 Electrochemical synthesis

The electrochemical synthesis of the polymers and their electrochemical analysis were performed with an Ecochemie Autolab system PGSTAT30 potentiostat/galvanostat service, with the associated General Purpose Electrochemical System (GPES) software.

If possible, polymers were electrochemically deposited using both potentiostatic and potentiodynamic methods. However, good solubility of some films in the neutral state prevented their potentiodynamic growth. Anodic and cathodic limits were chosen based on oxidation and reduction potentials of the monomer. A scan rate of 100 mV s^{-1} was used for all growth cyclic voltammetry. Fifteen cyclic voltammograms were used to grow the polymer. The cathodic limit was also used for potentiostatic growth where the chosen potential was held for 20 seconds. All electrochemical experimentation was performed at a controlled temperature of 22°C .

Films were grown onto either a platinum microelectrode or disc electrode (surface area = 1.8 mm^2). The platinum microelectrode reduces the effects of diffusion and allows the monomer to be recovered as an electrolyte is not required. As not all polymers grew well on the microelectrode, a platinum disc electrode was occasionally employed. Films were also grown onto ITO-coated glass for characterisation of the film by spectroscopic and microscopic techniques as well as analysis by mass spectrometry. Platinum mesh (1 cm^2) was used as a counter electrode and Ag/AgNO₃ electrode with a 0.1 M TBAP/AN salt bridge used as the reference electrode.

The concentration of monomer for all solutions was 5 mM and an electrolyte concentration (if required) of 100 mM. A solvent that allows solubility of the monomer without solvation of the deposited polymerised material is needed to deposit polymer on the electrode surface. The styryl terthiophene monomer derivatives were dissolved in acetonitrile, and a 1:1 mixture of AN:DCM was found to have the required intermediate relative permittivity for the alkyl and alkoxy derivatives. All solutions were degassed by sonication prior to measurements. After deposition, the modified

electrode was rinsed in acetonitrile and transferred to monomer-free electrolyte solution to be electrochemically analysed.

Films prepared for UV-VIS-NIR analysis were electrodeposited on ITO-coated glass using potentiodynamic and potentiostatic growth conditions given in Table 3.5. The films were held at an oxidising potential (using the upper limit) in monomer-free 0.1 M TBAP/AN for 180 seconds to polymerise any trapped oligomers and to fully oxidise the films. The UV-VIS-NIR of the oxidised films was measured. The films were then reduced at 0 V for 180 seconds (using the lower limit) and the UV-VIS-NIR of the neutral film measured. SEM images were taken of this film, and another film prepared under identical conditions but left in the oxidised state.

Table 3.5. Conditions of electrochemical deposition for films prepared on ITO-coated glass for characterisation by UV-VIS-NIR and microscopy.

	Potentiodynamic Growth		Potentiostatic Growth	
	Potential limits	Cycles	Potential	Time
NMe₂STT	0 - 0.9	5	0.9	20
OMeSTT	0.3 - 0.75	3	0.75	10
STT	0.375 - 0.9	5	0.9	10
CNSTT	0 - 0.9	5	0.9	5
NO₂STT	0.3 - 0.9	5	0.9	15

3.6.5 MALDI-TOF MS

Spectra were recorded in the linear mode in this study due the higher sensitivity of this technique. Dithranol was used as the matrix. Chloroform was used as the solvent for both the sample and the matrix. The sample was prepared by mixing a sample solution (~500 µg mL⁻¹) monomer solution with an equal volume of a 10 mg mL⁻¹ matrix solution. 100 µL of this mixture was spotted onto a target plate. Detection has been suppressed below 320 *m/z* units to prevent overload of the detector by matrix ions.

3.6.6 UV-VIS-NIR spectroscopy

UV-VIS-NIR spectra were obtained using a Shimadzu UV1601 spectrometer, scanning over the range 300-1500 nm. Samples that were measured in solution were dissolved in chloroform, and were oxidised with $\text{Cu}(\text{ClO}_4)_2 \cdot \text{H}_2\text{O}$ and reduced with hydrazine. H_2O .

Electrochemically deposited films were doped or dedoped by being held at either an oxidising or reducing potential respectively, in monomer-free solution.

3.6.7 ^1H NMR spectroscopy

^1H NMR spectra were obtained at 270.19 MHz using a JMN-GX270 FT NMR Spectrometer with Tecmag Libra upgrade. The chemical shifts are relative to the residual proton signal in deuterated solvents (CDCl_3 δ 7.27). Chemical shifts are reported as position (δ), multiplicity (s = singlet, d = doublet, t = triplet, q = quartet, dd = doublet of doublets, m = multiplet), coupling constant (J Hz), relative integral and assignment.

3.6.8 SEM imaging

SEM analysis was performed by Mr. Doug Hopcroft at HortResearch, Palmerston North, New Zealand. Samples were mounted on an aluminium specimen stub, sputter coated with approximately 100-150 nm of gold and studied using a Cambridge 250 Mk3 Scanning Electron Microscope in the secondary electron mode. Images were recorded on Ilford FP4 black and white film at the chosen magnifications and printed on Kodak multigrade paper

Chapter 4

Electrochemical Polymerisation of a Series of Styryl-Substituted Terthiénylenevinylenes

4.1 Introduction

The last 10 years has seen a growing interest in poly(thienylenevinylene) and its derivatives (Fig. 4.1), which have been found to produce the largest effective conjugation and hence the lowest HOMO-LUMO bandgap of all conducting polymers of comparable lengths.⁴⁶ These materials differ from polythiophenes by having ethylene linkers between the thiophene rings. The rigid ethylene linkers suppress rotational disorder of the polymer chain to allow enhanced π -orbital overlap,⁴⁶ and reduce the overall aromatic structure of the polymer, resulting in an increase in π -electron delocalisation. The ensuing low bandgaps give poly(thienylenevinylene) and its derivatives great potential for use in applications such as solar cells¹⁰³ and field-effect transistors.^{105,106}

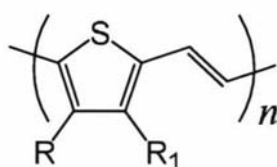


Fig. 4.1. A polythienylenevinylene derivative

A series of styryl-substituted terthiénylenevinylene (STV) derivatives (Fig. 4.2) have been synthesised by Wagner *et al.*¹⁵⁶ Their chemical polymerisation, also investigated by Wagner *et al.*, was found to produce predominantly dimer. This absence of polymerisation was not unexpected as it was previously shown by Levillain *et al.* that tetrathienylenevinylene oligomers readily dimerise,¹⁰⁷ which may be due to the low reactivity of the terminal 'α' positions of the monomers as a result of their extended π -

conjugation.²³ NMR spectroscopic studies revealed that the dimers produced by Wagner *et al.* were not regiospecific and likely consisted of mixtures of HH, HT and TT isomers.¹⁵⁷ This is in contrast to the dimerisation of styryl-substituted terthiophenes where these materials were found to exhibit regioselectivity giving the HH isomer (as discussed in Chapter 3), and may be caused by loss of the polaron trap due to an increased planarity of the molecule produced by the addition of the vinyl linkers.

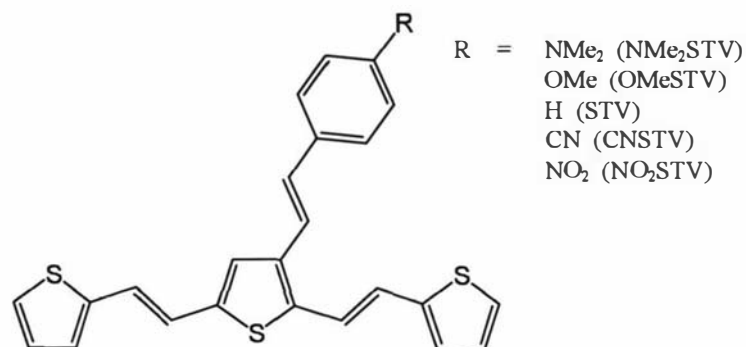


Fig. 4.2. Terthiylenevinylene monomer derivatives.

In this study, the electrochemical polymerisation of these materials was investigated and compared to the styryl-substituted terthiophenes discussed in Chapter 3.

4.2 Electrochemical deposition

Electrochemical analysis of polymer growth and polymer characteristics was performed on platinum microelectrodes. As described in Chapter 2, the small electroactive surface area of the microelectrode minimises distortion of experimental data by ohmic potential drop and capacitance effects, and eliminates diffusion effects of the monomer species to the electrode. The NMe₂STV monomer, however, was observed to grow very poorly on the platinum microelectrode (<0.5 nA after 15 cycles) so a platinum disc electrode (SA – 1.8 mm²) was used for the electrochemical growth and analysis of this material. An anodic limit 200 – 300 mV more positive than the potential at which polymerisation was observed to commence was chosen for polymer growth to reduce the possibility of oxidation of the vinyl groups.

The electrochemical growth cyclic voltammograms of NO₂STV, CNSTV, STV and OMeSTV are given in Figs. 4.3 to 4.6 respectively, with the initial cycles given as insets for clarity. The NO₂STV, CNSTV and STV voltammograms are similar and show an oxidation onset potential of 0.56 V, indicating that the reactivity of the 5 and 5' positions are not significantly affected by electron-withdrawing substituents at the *para*-position on the phenyl ring. This is in contrast with the observations made of analogous terthiophene derivatives where the substituents were found to strongly affect the oxidation potential. The OMeSTV derivative oxidises at a lower potential (0.44 V), possibly due to stabilisation of the resulting radical cation by the electron-donating substituent as described in Chapter 3.

The oxidation onset potential of STV (0.56 V) is much lower than that measured for STT (0.74 V on a microelectrode), indicating that the vinyl linkers between the thiophene rings have a significant effect on the oxidation potential of the styryl derivatives. The lower oxidation potential may be caused by improved stabilisation of the more conjugated terthiophenevinylene radical cation.

Subsequent cycles show two oxidation peaks. The oxidation peak at potentials above 0.6 V commences at potentials similar to the oxidation potential of monomer (0.56 V) on the first few cycles, indicating that this peak may be due to further oxidation of

monomeric species. The oxidation peak at lower oxidation potentials (<0.5 V) is due to the oxidation of the deposited electroactive film. The cathodic peak is most likely due to reduction of the oxidised film back to neutral material. A positive shift of the anodic peaks, and negative shift of the cathodic peaks is observed during the growth of the NO_2STV and CNSTV films as these films thicken. Similar shifts were observed by Pringle *et al.* during the growth of thiophene, and were suggested to be caused by heterogeneous electron-transfer kinetics, and a decrease in film conductivity, counterion mobility and possibly conjugation length.¹⁴⁷

The growth cyclic voltammogram of NMe_2STV (Fig. 4.7) appears different to growth of the other samples. A much lower oxidation onset potential of 0.22 V is observed, and four oxidation and four reduction peaks are produced on the first scan. Subsequent scans show an increase in oxidation onset potential, and a decreasing growth in current with each cycle, indicating the deposition of poorly conducting material. These observations suggest that processes other than polymerisation through the 5 and 5'' positions are occurring, possibly involving the dimethylamino substituent. Polymerisation through the dimethylamino substituent has been suggested by Kitani *et al.* in the electrochemical oxidation of *N,N*-dimethylaniline.¹⁵⁸

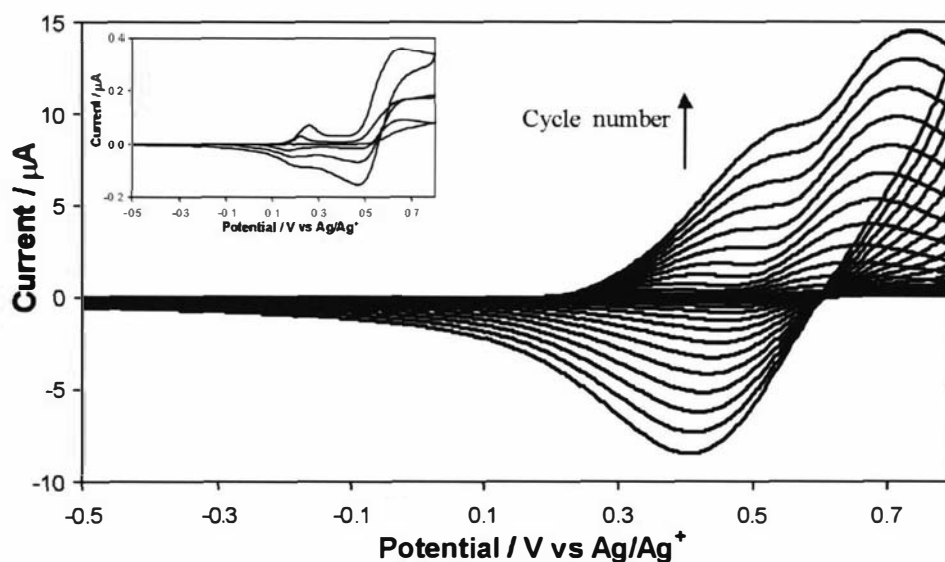


Fig. 4.3. Potentiodynamic growth of NO_2STV on a platinum micro electrode ($\text{SA} = 10 \mu\text{m}^2$). Monomer concentration: 5 mM. Supporting electrolyte: 0.1 TBAP/1:1 AN:DCM. Potential limits: -500/+800 mV. 15 cycles. Scan rate: 100 mV s^{-1} . Inset: first three cycles.

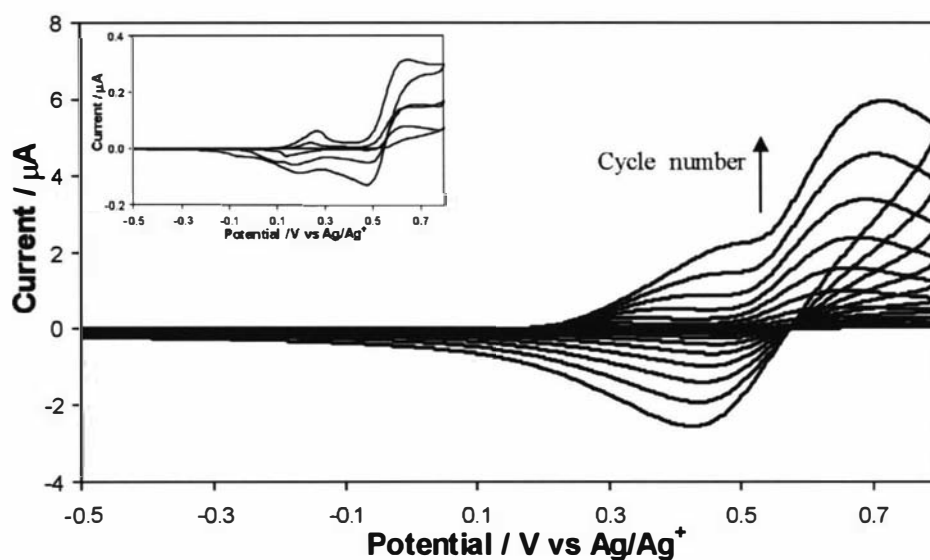


Fig. 4.4. Potentiodynamic growth of CNSTV on a platinum micro electrode ($SA = 10 \mu\text{m}^2$). Monomer concentration: 5 mM. Supporting electrolyte: 0.1 TBAP/1:1 AN:DCM. Potential limits: -500/+800 mV. 15 cycles. Scan rate: 100 mV s^{-1} . Inset: first three cycles.

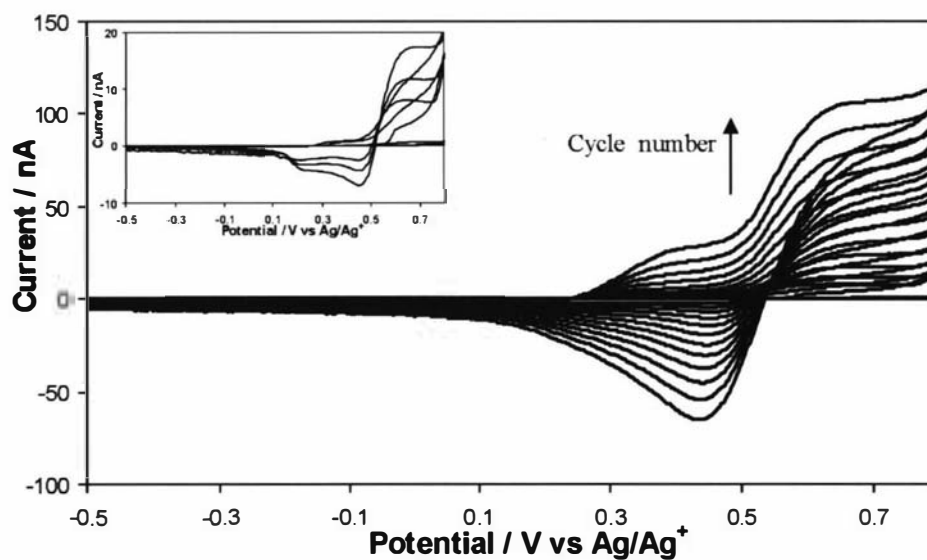


Fig. 4.5. Potentiodynamic growth of STV on a platinum micro electrode ($SA = 10 \mu\text{m}^2$). Monomer concentration: 5 mM. Supporting electrolyte: 0.1 TBAP/1:1 AN:DCM. Potential limits: -500/+800 mV. 15 cycles. Scan rate: 100 mV s^{-1} . Inset: first six cycles.

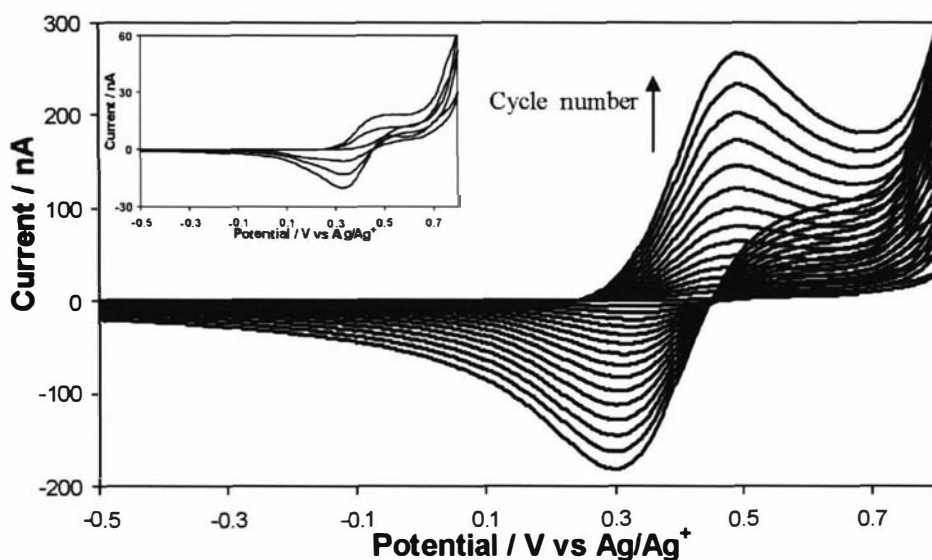


Fig. 4.6. Potentiodynamic growth of OMeSTV on a platinum micro electrode ($SA = 10 \mu\text{m}^2$). Monomer concentration: 5 mM. Supporting electrolyte: 0.1 TBAP /1:1 AN:DCM. Potential limits: -500/+800 mV. 15 cycles. Scan rate: 100 mV s^{-1} . Inset: first three cycles.

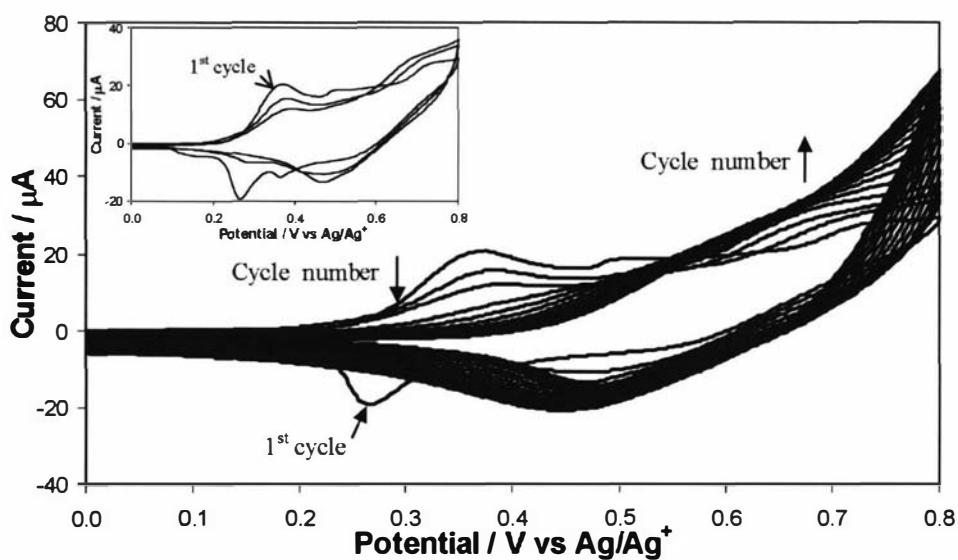


Fig. 4.7. Potentiodynamic growth of NMe₂STV on a platinum disc electrode ($SA = 1.8 \text{ mm}^2$). Monomer concentration: 5 mM. Supporting electrolyte: 0.1 TBAP /1:1 AN:DCM. Potential limits: 0/+800 mV. 15 cycles. Scan rate: 100 mV s^{-1} . Inset: first three cycles.

4.3 Characterisation of films

4.3.1 MALDI-TOF MS characterisation

Except for the NMe₂STV derivative, the neutral terthienylenevinylene films grown on ITO-coated glass were found to be soluble in chloroform to give solutions of various shades of purple. Analysis of the dissolved materials using MALDI-TOF MS revealed that the films comprised mostly dimer, with traces of trimer and tetramer. This is consistent with MALDI-TOF MS of the chemically oxidised materials.¹⁵⁶

In contrast, the NMe₂STV derivative was found to be only partially soluble in chloroform to give a brown solution. MALDI-TOF MS analysis of this material gave a major peak at 888 Da, which corresponds to the dimer, but also major peaks at 773 and 1200 Da. Although these peaks do not correspond to any obvious product, it appears that NMe₂STV is undergoing secondary reactions, consistent with the observations from the electrochemical growth data.

4.3.2 Cyclic voltammetry

Post-growth CVs of electrochemically deposited NO₂STV, CNSTV, STV, OMeSTV and NMe₂STV materials in monomer-free electrolyte are shown in Fig. 4.8 to Fig. 4.12, and reveal a considerable variation in the stability of the depositions. The deposited NO₂STV derivative appears to be very stable, the deposited CNSTV derivative slightly degrades, and a substantial reduction in current on post growth cycling of the deposited STV derivative indicates a very unstable material was produced. The OMeSTV appears stable after the first cycle, and the NMe₂STV deposition is very unstable and completely degrades after 10 cycles. The variation in stability of the films may be due to further polymerisation of short oligomers or film degradation, as discussed for films of terthiophene oligomers (Chapter 3, Section 3.4.3.1).

The peak oxidation and reduction potentials of the deposited materials after ten cycles in monomer-free electrolyte are listed in Table 4.1. The NO₂STV and OMeSTV depositions each show one oxidation and reduction peak, which are assigned to oxidation and reduction of oligomeric material. The peaks are narrow, which is consistent with a low polydispersity¹⁵⁹ and the presence of predominantly dimer as indicated by MALDI-TOF MS results. The CNSTV and STV depositions generate two distinct oxidation peaks. As discussed in Chapter 3, Section 3.4.2, the presence of multiple peaks may be due to a number of reasons, including the presence of different length oligomers.¹¹⁴ The two anodic peaks may be due to the oxidation of dimeric and trimeric material. The low oxidation onset potentials (0.14 and 0.21 V respectively) of these derivatives support the presence of oligomers longer than dimer.¹⁰⁰ Another possible explanation for two oxidation peaks is the formation of multiple oxidation states. Elandalousi *et al.* reported the formation of multiple oxidation and reduction peaks during the electrochemical cycling of butyl-substituted octathienylenevinylene due to the formation of cation, dication and trication states.³⁷ Electron-spin resonance (ESR) spectroscopic characterisation could provide clarification of these hypotheses. No obvious trend is shown between the oxidation potential of the peaks and the electron withdrawing or donating properties of the substituents.

Table 4.1. Oligomer oxidation and reduction potentials on the second cycle.

	NO ₂ STV	CNSTV	STV	OMeSTV
$E_{\text{oxidation onset}} / \text{V}$	0.27	0.14	0.21	0.30
E_{ox} / V	0.59	0.39	0.32	0.52
		0.63	0.54	
$E_{\text{red}} / \text{V}$	0.43	0.54	0.32	0.29

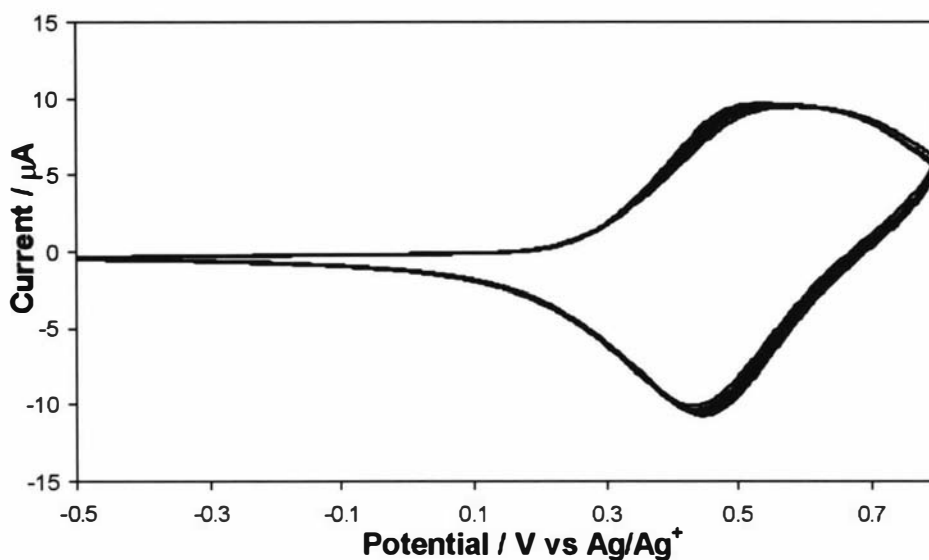


Fig. 4.8. Post growth cycling of oligoNO₂STV deposited on a platinum micro electrode (SA = 10 μm^2). Supporting electrolyte: 0.1 TBAP/AN. Potential limits: -500/+800 mV. 10 cycles. Scan rate: 100 mV s^{-1} .

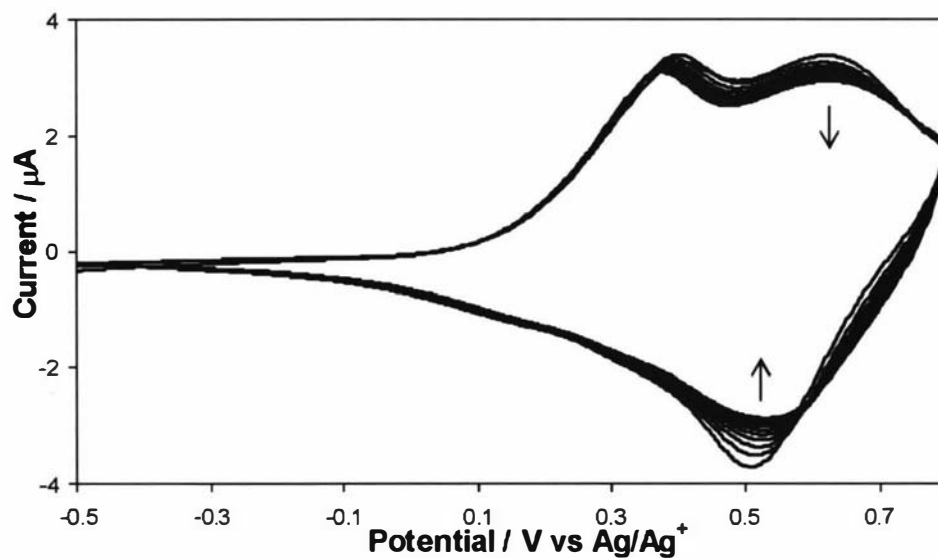


Fig. 4.9. Post growth cycling of oligoCNSTV deposited on a platinum micro electrode (SA = 10 μm^2). Supporting electrolyte: 0.1 TBAP/AN. Potential limits: -500/+800 mV. 10 cycles. Scan rate: 100 mV s^{-1} .

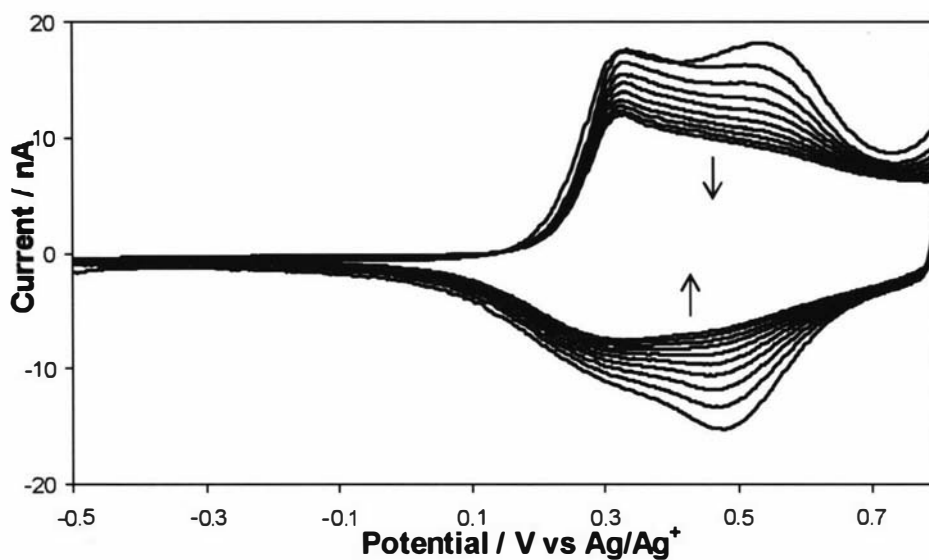


Fig. 4.10. Post growth cycling of oligoSTV deposited on a platinum micro electrode ($SA = 10 \mu\text{m}^2$). Supporting electrolyte: 0.1 TBAP/AN. Potential limits: -500/+800 mV. 10 cycles. Scan rate: 100 mV s^{-1} .

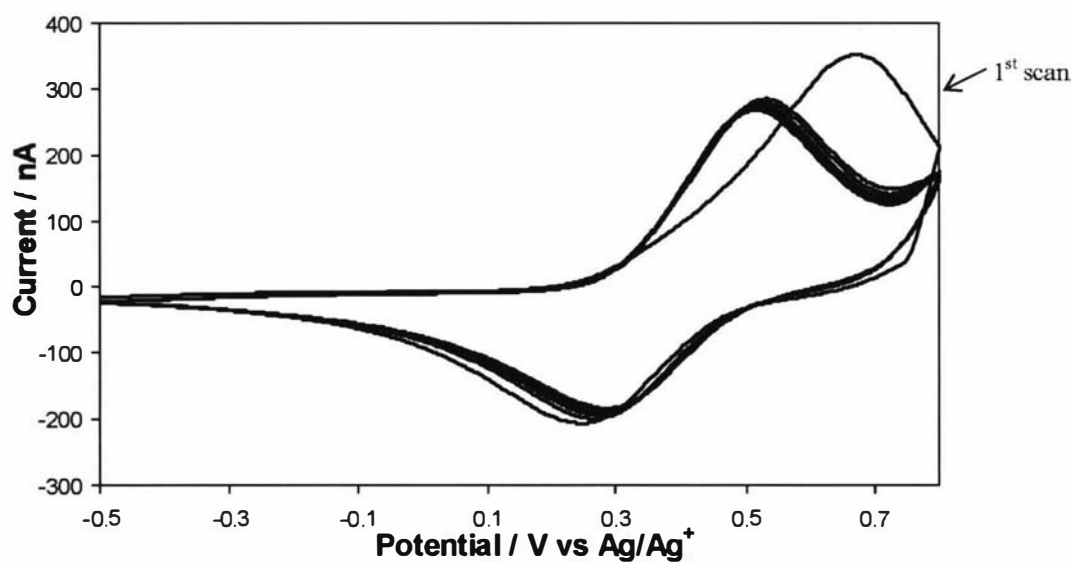


Fig. 4.11. Post growth cycling of oligoOMeSTV deposited on a platinum micro electrode ($SA = 10 \mu\text{m}^2$). Supporting electrolyte: 0.1 TBAP/AN. Potential limits: -500/+800 mV. 10 cycles. Scan rate: 100 mV s^{-1} .

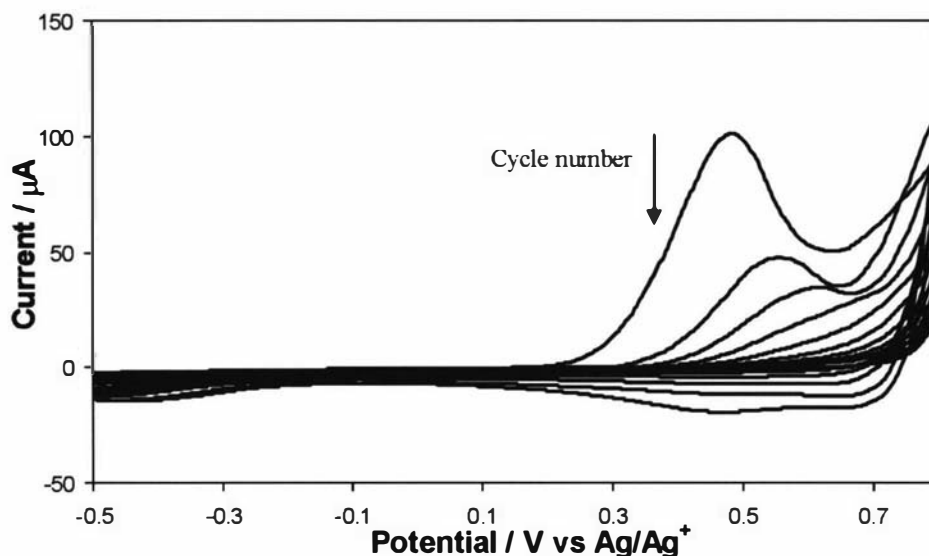


Fig. 4.12. Postgrowth cycling of oligoNMe₂STV deposited on a platinum disc electrode (SA = 1.8 mm²). Supporting electrolyte: 0.1 TBAP/AN. Potential limits: -500/+800 mV. 10 cycles. Scan rate: 100 mV s⁻¹.

4.3.3 UV-VIS-NIR spectroscopy

Electrochemically deposited films of NO₂STV, CNSTV, STV, OMeSTV and NMe₂STV oligomers on ITO-coated glass were investigated using UV-VIS-NIR spectroscopy (Figs. 4.13 to 4.17 respectively). The films were first oxidised by applying a potential of 800 mV for 3 minutes. They were then removed from the electrochemical apparatus and immediately scanned. The films were then reduced (to a neutral state) by applying a potential of -500 mV, and were again spectroscopically scanned. The films were generally observed to be green/grey in both states, except for the NMe₂STT film, which appeared brown in both the oxidised and reduced states. The CNSTV film was the only material to show significant electrochromic properties by turning purple when reduced.

The spectra of the NO₂STV, CNSTV, STV and OMeSTV deposits have several features in common. In the reduced state, two peaks are observed below 800 nm most likely due to $\pi \rightarrow \pi^*$ transitions.¹²⁴ The band at lower wavelengths (350 - 385 nm) is present in the monomers, but is absent in thienylenevinylene oligomers without styryl

substituents, indicating that it is due to the styryl substituents.¹⁵⁶ The band at higher wavelengths (520 – 660 nm) is likely due to the oligo(terthiylenevinylene) chromophore, as observed and discussed for the terthiophene materials in Chapter 3 (Section 3.4.3.2). On oxidation, these peaks greatly reduce in intensity (although are still present) and broad bands at about 900 nm and 1400 nm appear due to the formation of radical cation species. Levillian *et al.*,¹⁰⁷ reported similar peaks at 860 nm and 1400 nm in the spectra of oxidised hexyl-substituted tetrathienylenevinylene due to formation of the radical cation, and Casado *et al.*,¹⁶⁰ reported bands at 858 nm and 1555 nm in the spectra of an oxidised vinylene-bridged sexithiophene co-oligomer, which were also assigned to radical cation species. The NMe₂STV film is different from the other spectra in that it displays two broad bands at approximately 450 nm and 860 nm rather than prominent peaks. This film does not appear to be electrochromic.

A summary of peak positions for the thienylenevinylene derivative films in the oxidised and reduced states are given in Table 4.2.

Table 4.2. Wavelength maxima shown by NO₂STV, CNSTV, STV, OMeSTV and NMe₂STV oligomer films.

	Assignment	NO ₂ STV	CNSTV	STV	OMeSTV
Reduced film	$\pi \rightarrow \pi^*$	375 nm	385 nm	350 nm	375 nm
		520 nm	660 nm	600 nm	545 nm
Oxidised film	$\pi \rightarrow \pi^*$	385 nm	400 nm	350 nm	345 nm
		535 nm	585 nm	530 nm	530 nm
	Polaron/bipolaron peaks	825 nm	855 nm	890 nm	910 nm
		1380 nm	1440 nm	1345 nm	1380 nm

As found for the oligo(terthiophene)s, the λ_{\max} generated by the oligo(terthiylenevinylene) derivatives gives an indication of the effective conjugation length, and hence the oligomer length.¹⁰⁰ The relationship between the electron withdrawing/donating effect of the substituent and the λ_{\max} due to the $\pi \rightarrow \pi^*$ transition (in the neutral state) for both terthiophene and thienylenevinylene derivatives is given

in Fig. 4.18. The λ_{max} of the oligo(terthienylenevinylene)s are consistently higher than for the corresponding oligo(terthiophene) derivatives, due to an increase in the conjugation length caused by the addition of the ethylene linker between the thiophene rings. For example, dimers have chains consisting of 16 double bonds, compared to sexithiophenes that have 12 double bonds. The increased effective conjugation of the terthienylenevinylene materials may also be due to an increase in π -orbital overlap created by a more planar oligomer chain due to the ethylene linkages or reduced intermolecular steric interactions as discussed previously (Section 4.1).

A correlation of the λ_{max} with the substituent for both the oligo(terthienylenevinylene) and the oligo(terthiophene)s is also evident. The cyano derivatives produce the highest λ_{max} suggesting these derivatives produce materials with the longest mean effective conjugation length. The higher λ_{max} may also be due to a lower HOMO-LUMO bandgap caused by a lowering of the LUMO level, which is known to occur with the attachment of electron-withdrawing substituents.²³

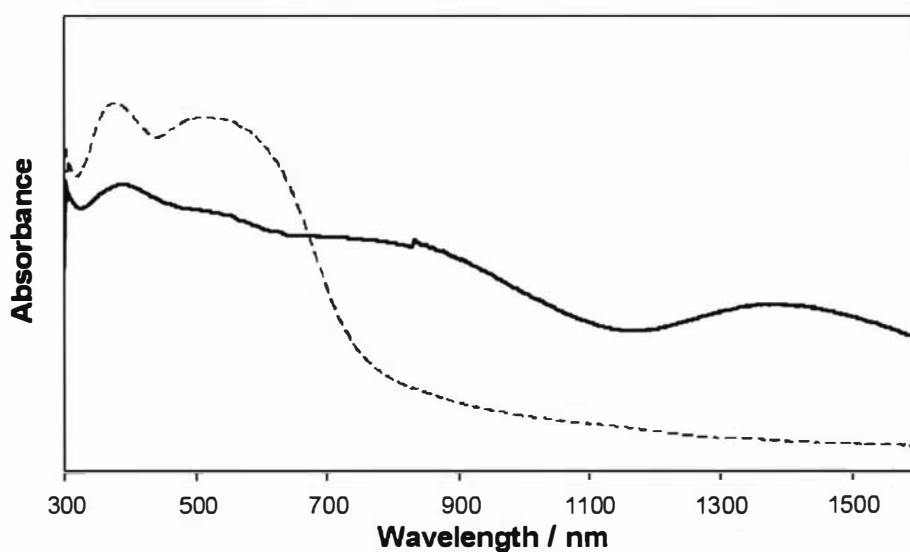


Fig 4.13. UV-VIS-NIR spectrum of oligoNO₂STV electrodeposited onto ITO-coated glass and electrochemically oxidised (solid line) and reduced (dashed line).

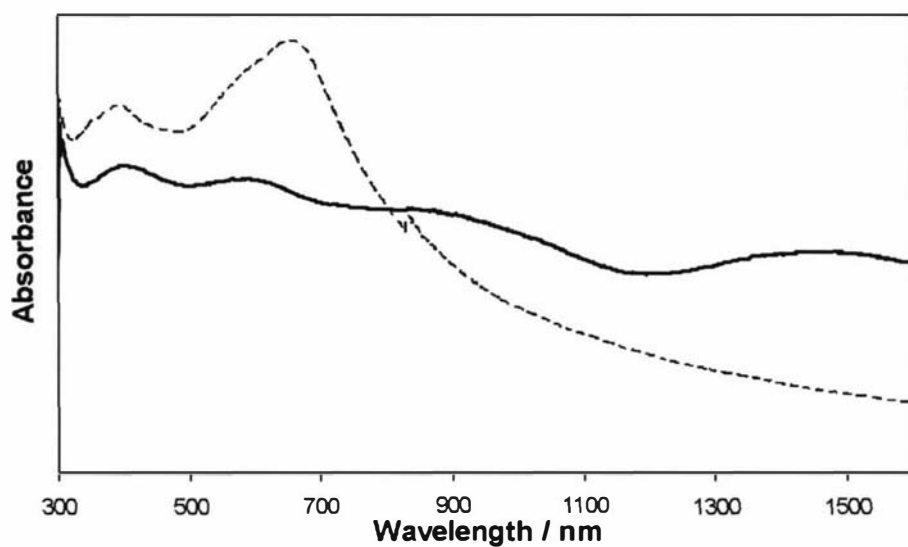


Fig. 4.14. UV-VIS-NIR spectrum of oligoCNSTV electrodeposited onto ITO-coated glass and electrochemically oxidised (solid line) and reduced (dashed line).

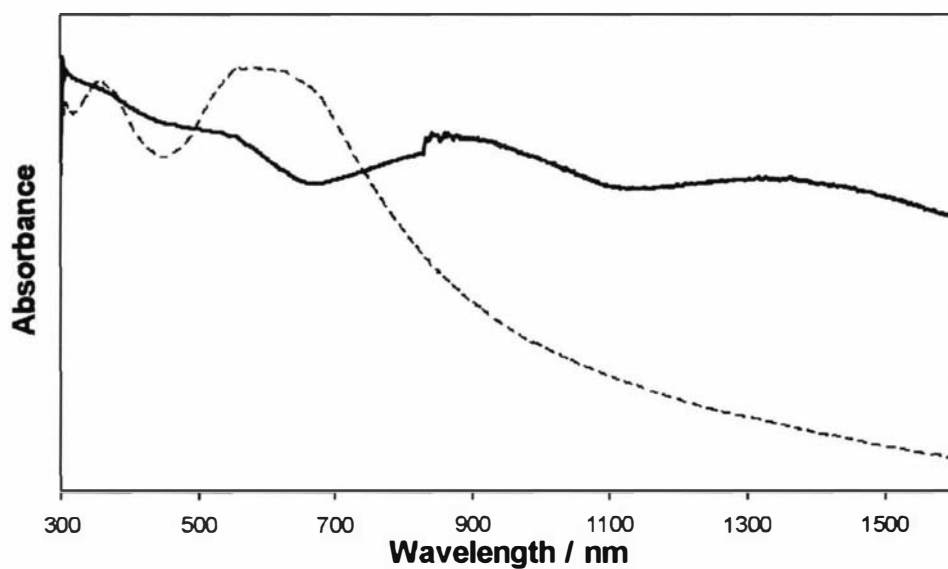


Fig. 4.15. UV-VIS-NIR spectrum of oligoSTV electrodeposited onto ITO-coated glass and electrochemically oxidised (solid line) and reduced (dashed line).

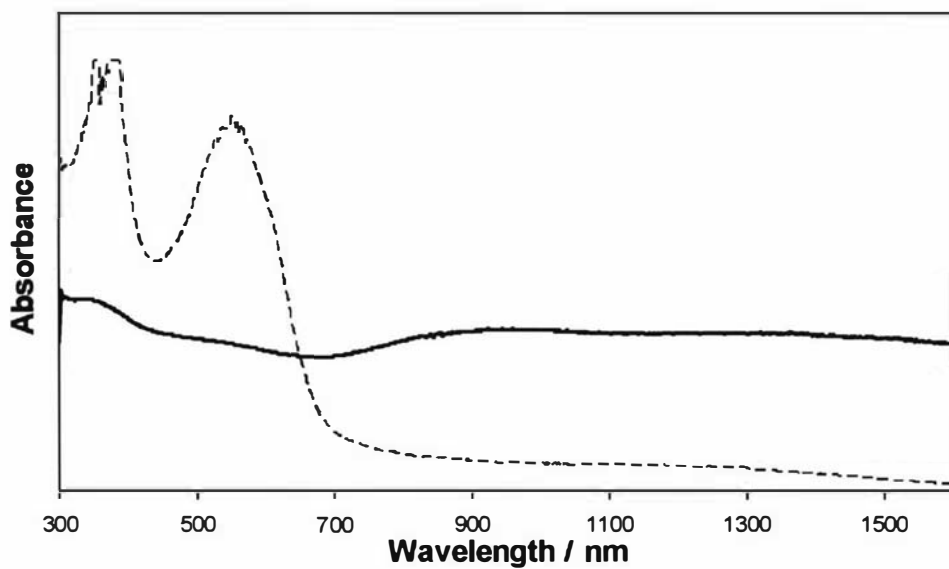


Fig. 4.16. UV-VIS-NIR spectrum of oligoOMeSTV electrodeposited onto ITO-coated glass and electrochemically oxidised (solid line) and reduced (dashed line).

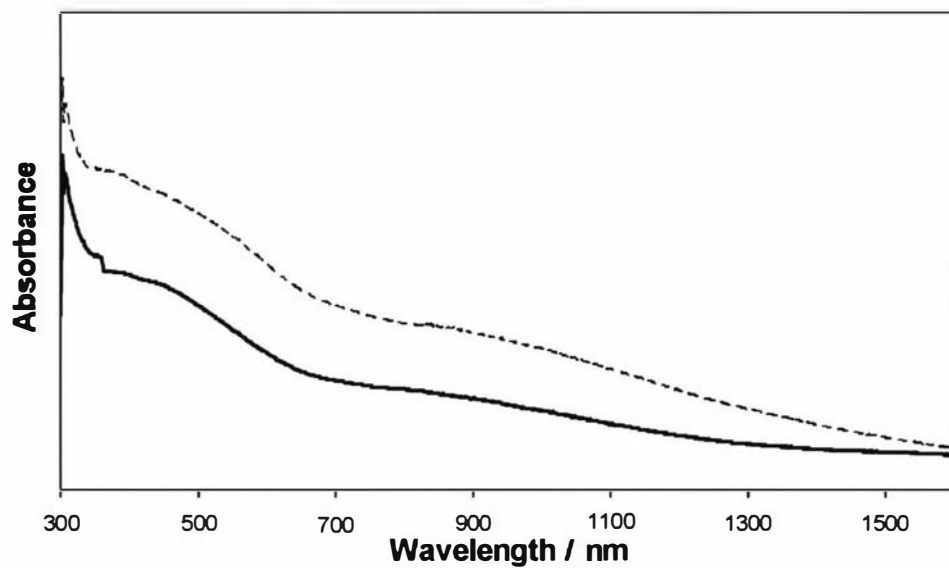


Fig. 4.17. UV-VIS-NIR spectrum of NMe₂STV electrodeposited onto ITO-coated glass and electrochemically oxidised (solid line) and reduced (dashed line).

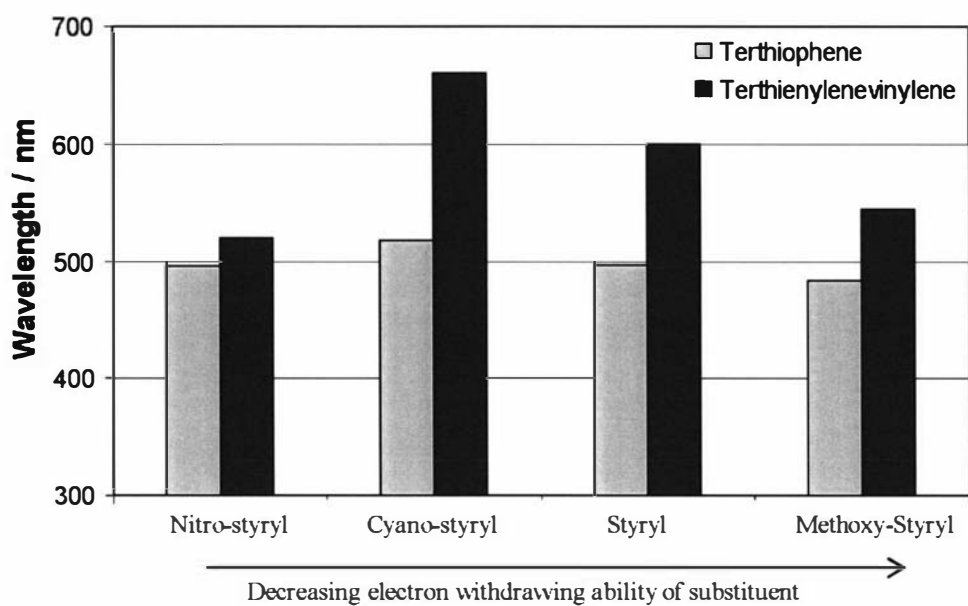


Fig. 4.18. Relationship between electron withdrawing/donating effect of the substituent and the wavelength maxima due to the $\pi \rightarrow \pi^*$ transition of the oligomer-chain chromophore for both terthiophene and thienylenevinylene derivatives.

As for the terthiophene derivatives discussed in Chapter 3, films of these terthienylenevinylene derivatives do not display free-carrier tails in the oxidised state, indicating a quasi-metallic state is not obtained by these materials.

4.4 Conclusions

Electrochemical deposition of styryl-functionalised terthiylenevinylenes was found (by MALDI-TOF MS) to produce predominantly dimer with traces of short oligomers, rather than polymer. Cyclic voltammetry and spectroscopic analysis supported the presence of oligomers with short conjugation lengths in these films, consistent with analysis of chemically oxidised materials¹⁵⁶ and with analogous styryl-substituted terthiophene derivatives. The low degree of polymerisation may be due to low reactivity of the terminal ‘ α ’ positions of the monomers due to their extended π -conjugation.²³

Bathochromic shifts of the $\pi \rightarrow \pi^*$ absorbance band, suggesting smaller band gaps, were consistently observed for electrochemically deposited styryl-substituted terthiylenevinylene derivatives compared to the analogous terthiophene derivatives discussed in Chapter 3. This is consistent with reports in the literature of smaller band gaps produced by poly(thiylenevinylene)s than polythiophenes,¹⁰² and is most likely due to an increase in the effective conjugation length. This may be a result of (1) an increase in the number of conjugated double bonds along the polymer chain and/or (2) a more rigid polythiophene backbone caused by the inflexible ethylene linkers and/or (3) enhanced orbital overlap due to less twisting caused by interactions between the vinyl linker of the styryl functionality and the thiophene rings.

Electrochemical oxidation of the cyano-substituted monomer derivative appears to produce a film with the lowest λ_{max} suggesting that this derivative produces the material with the lowest bandgap.²³ This premise was supported by this film producing the lowest oxidation onset potential of the terthiylenevinylene series. Electrochemical polymerisation of NMe₂STV gave unusual results including unexpected MALDI-TOF MS signals, multiple oxidation and reduction peaks by cyclic voltammetry and broad peaks by UV-VIS-NIR spectroscopy, suggesting that secondary reactions involving the dimethylamino substituents may be occurring.

As for the terthiophene derivatives discussed in Chapter 3, these terthiylenevinylene materials produce small free-carrier tails, indicating poorly conducting materials. An

attempt was therefore made to enhance polymerisation, and increase the solubility of these materials by attachment of alkyl or alkoxy chains to the terthiophene monomers.

4.5 Experimental

4.5.1 Reagents and materials

All reagents were used as received from suppliers unless specified otherwise. Chloroform obtained from BDH Laboratory Supplies (London) was used in all reactions and contains 0.5 to 1.0% ethanol as a stabiliser. TBAP (Fluka, Purum) was dried under vacuum at 70°C for 48 hours and then under vacuum with potassium hydroxide.

4.5.2 Synthesis of materials

Monomer synthesis was completed by Dr. Pawel Wagner at Massey University and are reported by Wagner *et al.*¹⁵⁶

The electrochemical synthesis of the polymers and their electrochemical analysis were performed with an Ecochemie Autolab system PGSTAT30 potentiostat/galvanostat service, with the associated General Purpose Electrochemical System (GPES) software. Films were electrochemically deposited onto a platinum microelectrode (SA = 10 μm^2) or disc electrode (SA = 1.8 mm^2) for growth and post-growth analysis, and onto ITO-coated glass (*ca.* 1 cm^2) for characterisation of the film by spectroscopy and mass spectrometry. Platinum mesh (1 cm^2) was used as a counter electrode and a Ag/AgNO₃ electrode with a 0.1 M TBAP/AN salt bridge used as the reference electrode. The concentration of monomer for all solutions was 5 mM in an electrolyte solution consisting of 0.1 M TBAP in AN. All solutions were degassed by sonication prior to measurements. Polymers were grown using both potentiostatic and potentiodynamic methods. An anodic limit 200 – 300 mV beyond the potential at which polymerisation was observed to commence was chosen for polymer growth. Fifteen cycles were used to deposit onto the microelectrode or disc electrode, and 2 to 5 cycles used to deposit onto ITO-coated glass to obtain a film thickness suitable for UV-VIS-NIR spectroscopy. A scan rate of 100 mV s^{-1} was used for all growth cyclic voltammetry and post-growth analysis. The anodic limit was also used for potentiostatic growth where the chosen potential was held for 20 seconds. All

electrochemical experimentation was performed at a controlled temperature of 22°C. After deposition, the modified electrode was rinsed in acetonitrile and transferred to monomer-free electrolyte solution to be electrochemically analysed.

Films prepared for UV-VIS-NIR analysis on ITO-coated glass were held at an oxidising potential (anodic limit) in monomer-free 0.1 M TBAP/AN for 180 seconds to polymerise any trapped oligomers and to fully oxidise the films. The UV-VIS-NIR spectra of the oxidised films were measured. The films were then reduced at -0.5 V for 180 seconds (using the cathodic limit used for cyclic voltammetry) and the spectra again measured. The reduced films were dissolved in chloroform for MALDI-TOF MS.

4.5.3 UV-VIS-NIR spectroscopy

UV-VIS-NIR spectra were obtained using a Shimadzu UV1601 spectrometer, scanning over the range 300-1500 nm.

4.5.4 MALDI-TOF MS

Spectra have been recorded in the linear mode in this study due the higher sensitivity of this technique. Dithranol was used as the matrix. Chloroform was used as the solvent for both the sample and the matrix. The sample was prepared by mixing a sample solution ($\sim 500 \mu\text{g mL}^{-1}$) monomer solution with an equal volume of a 10 mg mL^{-1} matrix solution. $100 \mu\text{L}$ of this mixture was spotted onto a target plate. Detection has been suppressed below $320 m/z$ units to prevent overload of the detector by matrix ions.

Chapter 5

Polymerisation of Alkyl and Alkoxy Substituted Styrylterthiophenes

5.1 Introduction

In Chapters 3 and 4 it was shown that oxidation of styryl-substituted terthiophenes and terthienylenevinylenes produced predominantly short oligomers ($n < 4$) with limited conjugation. The styryl-substituted terthiophenes also produced large amounts of insoluble material (37 – 95% of total yield), making them unsuitable for device fabrication. The most common method for increasing polythiophene processability is by solubilisation through the attachment of long alkyl or alkoxy chains.⁶² Alkoxy chain lengths of between 4 and 7 carbons, and alkyl chains of between 6 and 12 carbons have been typically attached.^{17,59,73,111} It has been shown that alkyl chains with a length less than 12 carbons do not significantly affect the electrical properties of polythiophenes.^{59,65} Chains are often attached directly to thiophene, bithiophene or terthiophene, or to a phenyl ring that is attached to the thiophene ring.^{32,161} In addition to improving polymer solubility, alkoxy chains have been shown to decrease the oxidation potential of the polymer, and, if located at a position α to where polymerisation occurs, may promote electropolymerisation kinetics.¹¹¹

The chemical and electrochemical polymerisation of alkyl- and alkoxy-substituted styryl terthiophenes is discussed in this chapter. Two styryl terthiophene derivatives, C₇DASTT and OC₆DASTT (Fig. 5.1), were initially considered as their chains are approximately the same length. The unsubstituted styryl functionality was chosen for an initial investigation of the effect of alkyl and alkoxy substituents on the resulting styryl-substituted polyterthiophene. The alkyl and alkoxy chains were substituted at the 4 and 4'' positions, as Gallazzi *et al.* reported that terthiophenes substituted by alkyl or alkoxy substituents at the 4 and 4'' positions are much more reactive and form

polymers of higher molecular weight than terthiophenes substituted at the 3 and 3'' positions.^{62,162}

Both the OC₆DASTT and C₇DASTT monomers were available in our laboratories, having been previously made by Dr. Pawel Wagner, Dr. Sanjeev Gambhir or Ms. Amy Watson.

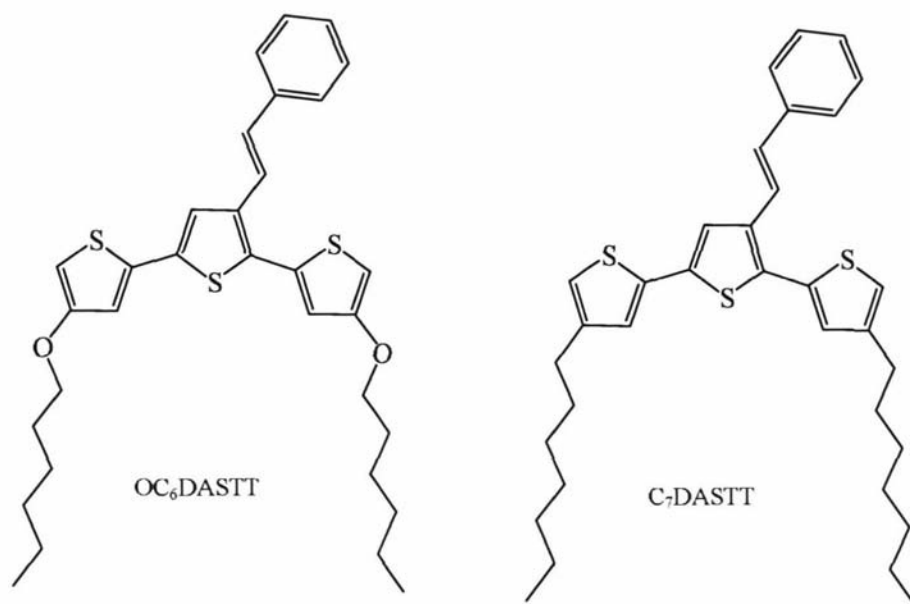


Fig. 5.1. Alkyl- and alkoxy-substituted styrylterthiophene monomers that were polymerised and investigated in this study.

5.2 Chemical polymerisation of OC₆DASTT

5.2.1 Polymerisation and reduction procedure

For reasons previously discussed in Chapter 1, Section 1.3.2, the iron(III) chloride oxidation method was investigated for the polymerisation of OC₆DASTT. A similar method to that used in Chapter 3 was employed, slowly adding 4 equivalents of oxidant as a slurry in chloroform to a solution of the monomer. However, since chloroform was observed to be a better solvent than DCM for the styrylterthiophene derivatives discussed previously (dissolving a larger portion of the oligomeric material), chloroform was used as a solvent for the polymerisation reaction. It was hypothesised that a better solvent may lead to the production of longer polymer due to oligomers staying in solution and allowing further polymerisation to occur. The reaction procedure is outlined in Fig. 5.2.

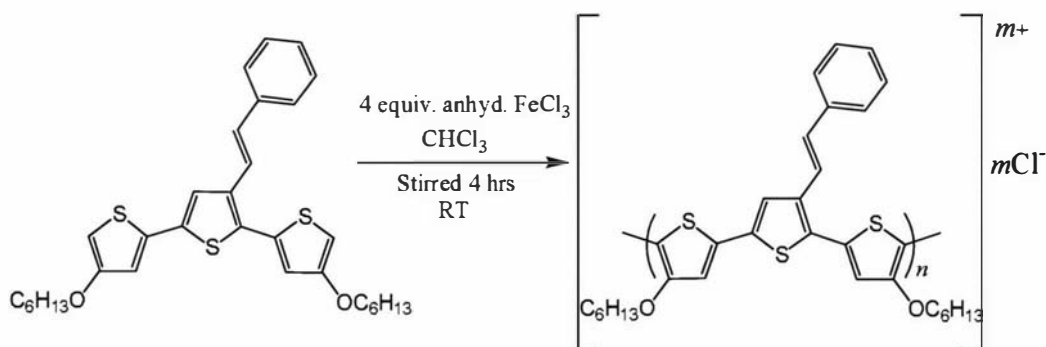


Fig. 5.2. Polymerisation of OC₆DASTT.

Initial addition of small amounts of iron(III) chloride (as a slurry in chloroform) to the OC₆DASTT monomer solution resulted in a change in the colour of the reaction mixture from yellow to red/purple. This is possibly due to the formation of short oligomers in the neutral state. Further addition of oxidant led to the formation of a black precipitate, similar to that observed by chemical oxidation of the styryl-substituted terthiophene derivatives in Chapter 3. This was assumed to be the oligomers/polymers in the oxidised state.

Many substituted polythiophenes are reported to easily reduce to the neutral state by washing the oxidant from the crude material with water or methanol.^{44,62,70,98} This process is not well understood. However, several workers have reported that alkoxy-substituted polythiophenes are difficult to reduce to the neutral state, and require washing with strong reducing agents, usually hydrazine or aqueous ammonia.^{62,99,163} An attempt was made in this study to reduce the resulting black, insoluble polymer by stirring with an aqueous hydrazine solution.

PolyOC₆DASTT was found to be very difficult to reduce. Stirring with hydrazine for 24 hours resulted in the production of only 26% soluble material, which was later confirmed to be in the neutral state by UV-VIS-NIR spectroscopy. Further reduction of the insoluble material by stirring for several days with hydrazine provided an additional 43% of soluble material, to give a total of 67% soluble, neutral material. The soluble fraction was observed to be an intense purple colour in chloroform solution, and, when dried, appeared as a shiny, flexible, bronze-coloured film. The insoluble fraction appeared as a black, clumpy material.

The difficulty in reducing the polyOC₆DASTT material was partially attributed to the poor ability of the aqueous hydrazine solution to wet and penetrate the polymer particles. It was later found that the reduction process could be improved by grinding the polymer into a powder to increase the surface area available to the hydrazine. In addition, it was found that the aqueous hydrazine solution would better wet the hydrophobic polymer if the organic solvent was first completely removed.

After such treatment and then stirring for several hours with hydrazine, chloroform was added to the mixture to dissolve the reduced surface layer of the particles so that the underlying oxidised polymer could be exposed, and reduced by the hydrazine. The organic layer containing the reduced polymer was then washed and dried, while the insoluble polymer was separated, dried, and the reduction process repeated until no increase in soluble material was obtained. An attempt was also made to improve the wettability of the polymeric material by adding the hydrazine in methanol, but this did not aid the reduction process.

This difficulty in reducing alkoxy substituted polythiophenes was also observed by Gallazzi *et al.*,⁶² who found they could only reduce very low molecular weight fractions of poly(4,4''-dipentoxyterthiophene). Gallazzi *et al.* proposed that the less soluble character of the alkoxy-substituted terthiophenes when compared to analogous alkylthiophenes, may be due to a mesomeric effect of the oxygen creating a partial double bond character between the thiophene units (Fig. 5.3). This would increase the rigidity of the polymer backbone that would, in turn, likely decrease the solubility of the polymer.

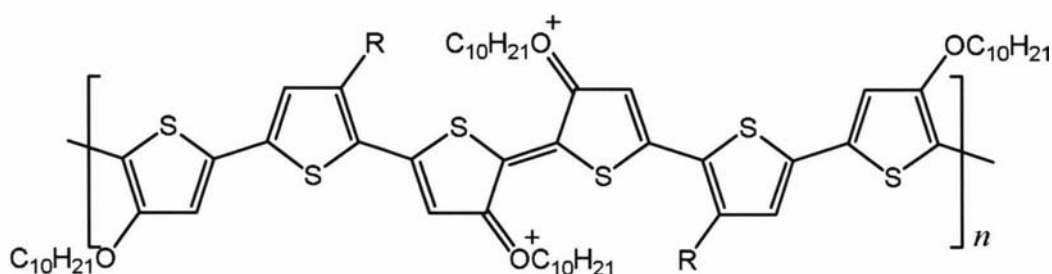


Fig. 5.3. Possible structure created by the mesomeric effect of the oxygen on alkoxy substituted thiophene polymers.⁶²

It is also likely that the higher electron-donating ability of the alkoxy substituents than alkyl substituents stabilises the positive charge and increases the stability of alkoxy-substituted polythiophenes in the oxidised state.^{62,162}

5.2.2 Characterisation of the soluble fraction of polyOC₆DASTT

The MALDI-TOF mass spectrum of the soluble fraction of polyOC₆DASTT is shown in Fig. 5.4, with peaks labelled according to the number of monomer units (n) in the oligomer. Although MALDI-TOF MS is a well established and frequently used technique for studying the chain length of conducting polymers,^{64,73,96,115} spectra of polymer samples with a high polydispersity (>1.2) are often observed to be skewed slightly towards a lower molecular weight, as described in Chapter 2, Section 2.2.^{96,117,120} The polydispersity of the crude polyOC₆DASTT sample was estimated as *ca.* 1.39 by calculating approximate values of M_n and M_w using the ion-count measured for each oligomer/polymer of molecular weight, M_i , as the number of molecules, N_i , of

that particular molecular weight. Due to the high polydispersity, it was thought possible (and later confirmed in Section 5.2.4) that significant skewing of the data towards shorter oligomers was occurring.

Although the spectrum of polyOC₆DASTT may not be representative of the actual oligomer distribution, and peak intensities have been reported to vary for different materials,¹¹⁷ the presence of signals at higher *m/z* may indicate a higher molecular weight for polyOC₆DASTT when compared to the chemically oxidised materials in Chapter 3.

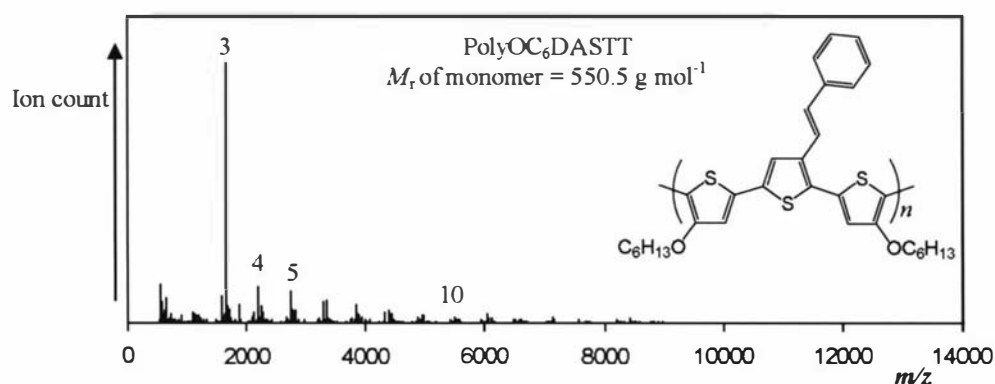


Fig. 5.4. MALDI-TOF mass spectrum of polyOC₆DASTT. Signals are labelled with the assigned oligomer length in terms of monomer units (*n*).

An increase in oligomer length of polyOC₆DASTT, when compared to the chemically oxidised materials studied in Chapter 3, is also evident from spectroscopic analysis. The absorption spectra of this soluble polyOC₆DASTT fraction was recorded, and then the polymer oxidised using an excess of Cu(ClO₄)₂·H₂O and the spectra again recorded (Fig. 5.5). Three bands appear in the neutral state. The major peak at 532 nm is assigned to the $\pi \rightarrow \pi^*$ transition of the oligo(terthiophene) chromophore as described in Chapter 3, Section 3.4.3.2. The broad band at about 950 nm is due to small amounts of oxidised material. The shift in the $\pi \rightarrow \pi^*$ transition (from 497 nm in oligoSTT to 532 nm in polyOC₆DASTT) is evidence of an increase in the mean conjugation length of these materials compared to the materials investigated in Chapter 3.^{114,127}

The oxidised state displays a broad band between 500 and 900 nm, which, by comparison to UV-VIS-NIR spectra of poly(3-hexylthiophene) reported by

Skompska *et al.*¹²⁵ is attributed to polaron/bipolaron species. The significant free-carrier tail generated by polyOC₆DASTT in the oxidised state at a wavelength greater than 900 nm shows quasi-metallic behaviour, and is further evidence of extended conjugation.¹²⁷

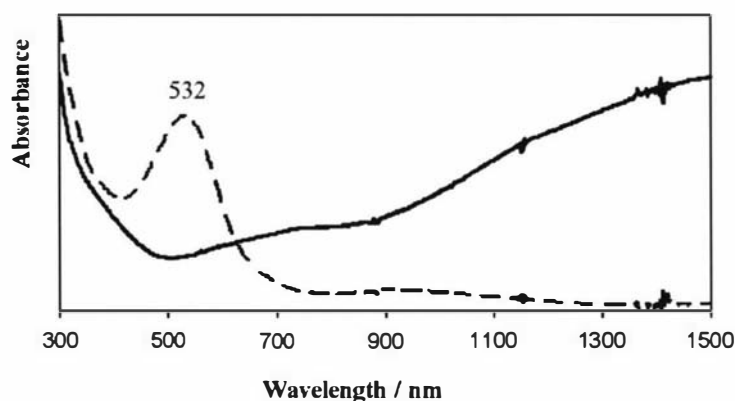


Fig. 5.5. UV-VIS-NIR spectrum of the soluble fraction of polyOC₆DASTT in solution in the oxidised state (excess Cu(ClO₄)₂, solid line) and neutral state (dashed line). The π-π* band in the neutral state is labelled with its wavelength maximum.

A cyclic voltammogram of a cast film of polyOC₆DASTT on an ITO-coated glass electrode (Fig. 5.6) displays very broad oxidation and reduction peaks. Broad oxidation and reduction peaks may be due to a number of factors. Yasser *et al.* suggested that the broadness of the anodic peak observed while cycling polythiophenes is indicative of the length of conjugated segments, with broad peaks consistent with a wide distribution of the various lengths of conjugated segments, each with a particular E_{ox} .¹⁵⁹ Alternatively, Pringle *et al.*¹⁴⁷ proposed that the broad bands observed while cycling thiophene in an ionic liquid may be related to the reorganisation of the polymer chain that occurs with ion movement into/out of the film matrix, or due to a range of oxidation potentials due to defects in the polymer chain.

The very low oxidation onset potential shown by polyOC₆DASTT (-0.34 V) implies the presence of highly conjugated oligomers. It is well established theoretically¹⁶⁴ and experimentally^{114,127,165,166} that an increase in conjugation length of conducting polymers results in a reduction of oxidation potential.

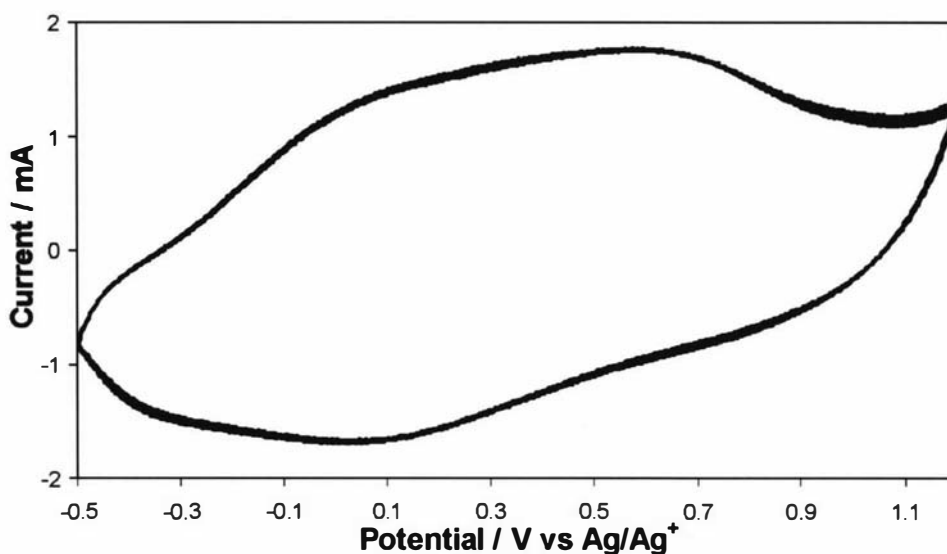


Fig. 5.6. CV of chemically polymerised OC₆DASTT, which has been cast as a film onto an ITO-coated glass electrode (*ca.* 1 cm²). Supporting electrolyte: 0.1 M TBAP/AN. Potential limits: -500/+1200 mV. 16th to 20th cycles. Scan rate: 100 mV s⁻¹.

The remaining insoluble material (33%) is likely to be made up of longer polymer chains, which are either in the reduced or oxidised state, since long oligomers are less soluble than short oligomers.^{96,127} It has been also been shown by Bredas *et al.*¹⁶⁴ and Sumi *et al.*¹¹⁴ that long oligomers are more difficult to reduce, and therefore solubilise, than short oligomers. The difficulty of reducing long oligomers compared to short oligomers was also observed in this study, as oligomers from later reductions were found to be longer than oligomers that were obtained by previous reductions. It is also possible that the insoluble material is a result of cross linking between oligomers, or oligomer defects. However, this is unlikely since Gallazzi *et al.*⁶² reported that the NMR spectrum of remaining insoluble chemically polymerised poly(4,4'-dipentoxyterthiophene) confirmed that the insolubility was not due to polymerisation structural defects such as branching or β -coupling.

5.2.3 Improvement of the polyOC₆DASTT soluble fraction

As the insoluble material was believed to consist of polymers too long to be soluble or reduced, it was thought the soluble fraction could be increased by reducing the

polymer length. The degree of polymerisation can be moderated either by reducing the rate of reaction or by reducing the reaction time. In these investigations, the reaction time was kept constant while the rate of reaction was reduced by either decreasing the oxidant:monomer ratio or lowering the temperature.

Effect of the oxidant concentration.

An iron(III) chloride oxidant-to-monomer ratio of about 4:1 was used for initial reactions in this study since this ratio is commonly reported in the literature for the polymerisation of thiophene derivatives.^{44,63,70,98,134,135} An attempt was made to decrease the resulting oligomer length by employing a lower oxidant:monomer ratio. Kumar *et al.*¹⁶⁷ found that decreasing the oxidant:monomer ratio during polymerisation of a C₁₄ alkyl derivative of EDOT produced a higher yield of soluble polymer. GPC characterisation of the soluble product revealed this was most likely caused by a significant decrease in the average molecular weight of the resulting polymer.

The polymerisation of OC₆DASTT using a 1:1 oxidant to monomer ratio was investigated. Since investigation of the reaction mixture by TLC showed the presence of large amounts of monomer after 4 hours, the reaction mixture was stirred for a further 92 hours to allow time for the polymerisation to complete. Other conditions were not changed from the initial polymerisation (Fig. 5.2). A black precipitate was produced, which was reduced with hydrazine to give a chloroform-soluble fraction of 55%. A soxhlet extraction of this soluble material with methanol resulted in a yellow product, which was shown by MALDI-TOF MS to consist of unreacted monomer that was 31% of the total expected yield. It appears that using only one equivalent of oxidant results in the production of mostly long, insoluble polymeric material (45%), and unreacted monomer (31%).

Effect of temperature.

An attempt was made to increase the soluble fraction of polyOC₆DASTT by reducing the reaction temperature to slow the rate of polymerisation and reduce the average oligomer length. Gallazzi *et al.*⁶² investigated the effect of temperature during

polymerisation of 3,3''-dihexylterthiophene and reported that polymerisation at 30°C produces shorter oligomers than polymerisation at 50°C.

By keeping the conditions the same as for the first polymerisation of polyOC₆DASTT (Fig. 5.2), but reducing the temperature during the reaction from room temperature to -10°C (difference of *ca.* 30°C), the total soluble material obtained was increased from 67% to 78% of the expected yield. The increase in the soluble fraction with decrease in temperature, is most likely due to a reduction in rate of the polymerisation reaction and hence the production of shorter (more soluble) oligomers, as observed by Gallazzi *et al.*⁶²

5.2.4 Polymer separation according to chain length

An attempt was made to separate the soluble polyOC₆DASTT product (in the neutral state) into fractions according to chain length. This was expected to provide materials with lower polydispersities (range of oligomer lengths), and different properties than the crude material. It has been established that an increase in chain length of polythiophenes results in a bathochromic shift of the $\pi \rightarrow \pi^*$ transition, and an increase in the doped conductivity of the material.^{114,127}

Separation of the crude neutral polyOC₆DASTT product mixture was accomplished by subjecting the total amount of neutral polymeric material to sequential soxhlet extractions using a series of solvents. As reported by other researchers,^{96,127} different length oligomers were found to have different solubilities, with longer oligomers being less soluble. Methanol and hexane were used first to remove any residual monomer and very short oligomers such as dimer and trimer. Acetone followed by dichloromethane and chloroform were then used to extract increasingly longer oligomers. Each solvent was found to be able to dissolve the oligomers extracted by the preceding solvents. For example, acetone dissolved all material extracted from the methanol and hexane fractions, and DCM dissolved all material extracted from the methanol, hexane and acetone fractions. Chloroform was found to dissolve all soluble material. A photograph of chloroform solutions of the monomer and these oligomer fractions is displayed in

Fig. 5.7. The more intense colour of the latter fractions suggests these contain polymers with longer conjugation lengths.

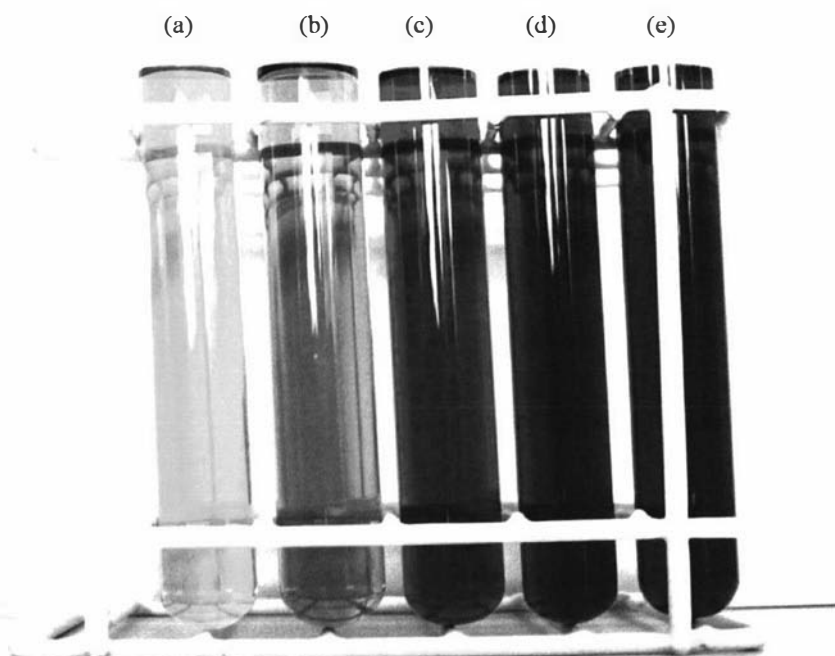


Fig. 5.7. Photograph of the monomer and solvent fractions as solutions in chloroform. (a) Monomer, (b) hexane, (c) acetone, (d) dichloromethane and (e) chloroform.

The amount of polyOC₆DASTT (polymerised using 4 equivalents of iron chloride at -10°C) that was extracted by each solvent, and the total soluble fraction obtained, are listed in Table 5.1 as mass percentages of the total expected polymer yield. The expected yield is based on the mass of the monomer given that the length of the polymer products is not accurately known. At most, this leads to an uncertainty of 0.3% in the calculated polymer yields due to not taking into account the loss of α -hydrogen on polymerisation.

No material was extracted by methanol. As both the oxidant and monomer dissolve in methanol, this confirmed that all of the oxidant had been removed, and that no unreacted monomer remained. The majority of the soluble material (66%) was extracted into dichloromethane and chloroform.

Table 5.1. Mass percentages of OC₆DASTT oligomers separated by different solvents.

Methanol (%)	Hexane (%)	Acetone (%)	DCM (%)	CHCl ₃ (%)	Total soluble material
0	7	5	24	42	78%

MALDI-TOF mass spectra of the polyOC₆DASTT oligomer fractions are given in Fig. 5.8. Signals have been labelled with the assigned oligomer length in terms of monomer units (n). As expected, the average oligomer length increases with each successive solvent extraction. Short oligomers ($n = 1 - 4$) have been for the most part extracted by hexane and acetone. The DCM fraction is shown to consist of oligomers of length $n = 4 - 13$, with an average oligomer length of $n = 7$. The chloroform fraction consists of even longer oligomers with an average length of approximately $n = 14$ and displaying signals corresponding to oligomers of length up to $n = 35$. The initial cluster of peaks observed in this spectrum (less than *ca.* 3000 Da) is likely due to multiple charging of oxidised polymer or fragmentation of longer polymer chains, given that all of the polymeric material of mass < 4000 Da should have been extracted into one of the other solvents.

In Section 5.2.2 it was noted that it was difficult to determine the number average molecular weight (M_n) of the crude polyOC₁₀DASTT soluble fraction from the MALDI-TOF MS data due to the high sample polydispersity (Section 2.2.4). By estimating the number average molecular weight (M_n) of each solvent fraction and considering the yields of the solvent fractions, an average length of about $n = 11$ was estimated for the total polymer sample. This estimate of the average polymer length of polyOC₆DASTT ($n \sim 11$) is much higher than what appears to be the case from the spectrum of the crude material ($n \sim 3$, Fig. 5.4), and supports the notion of significant skewing of the crude MALDI-TOF MS data to smaller oligomer lengths. As indicated previously, Byrd *et al.* showed that degree of skew is more likely to occur for wide polydisperse polymer samples ($PD > 1.2$) than for narrow polydisperse polymer samples ($PD < 1.2$).¹¹⁷

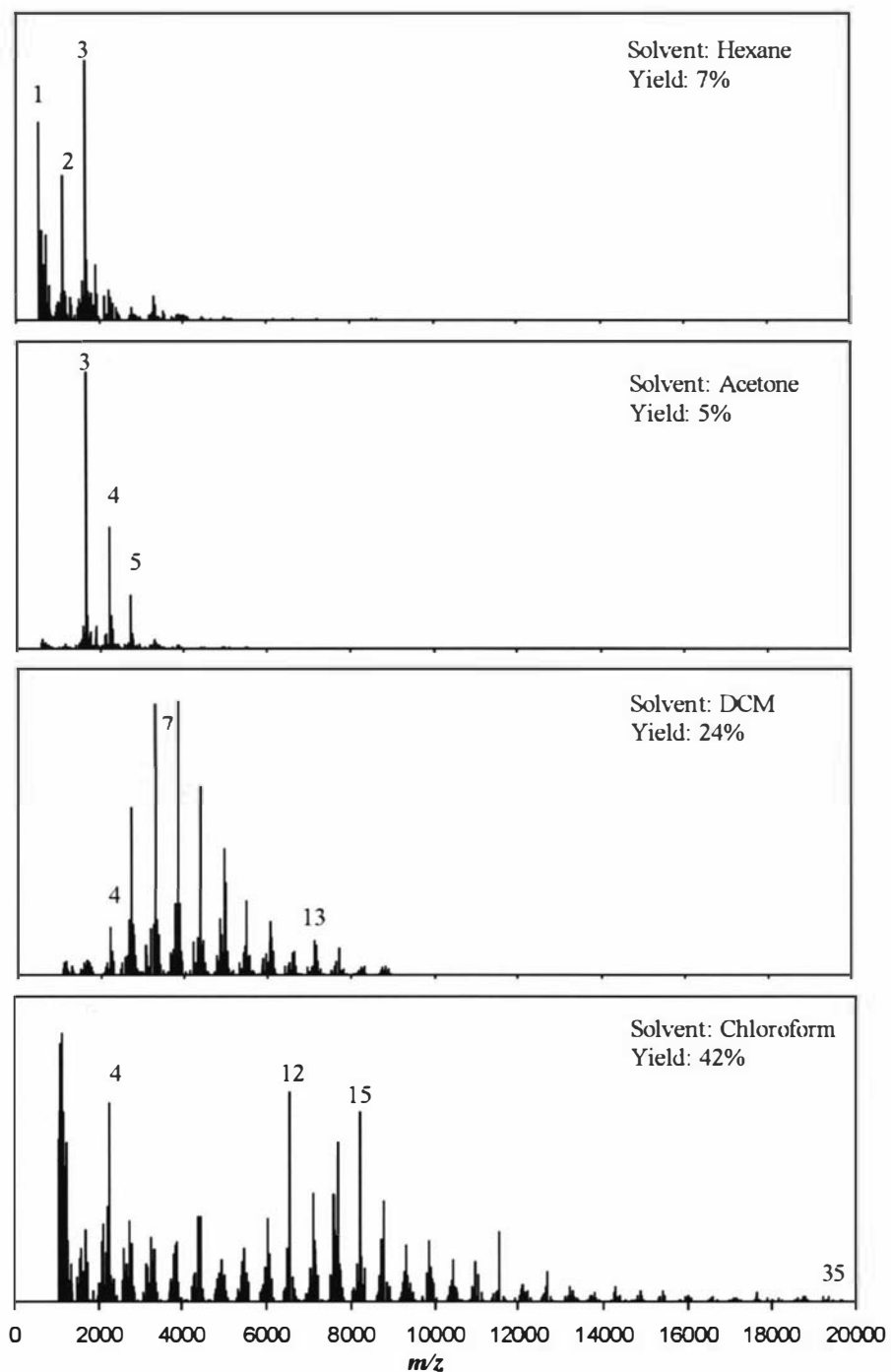


Fig. 5.8. MALDI-TOF mass spectra of OC₆DASTT oligomer fractions extracted using hexane followed by acetone, dichloromethane and chloroform. Signals are labelled with the assigned oligomer length in terms of monomer units (n). M_r of monomer: 550.5 g mol⁻¹.

The absorption spectra of the OC₆DASTT oligomer fractions, in both the neutral and oxidised states are shown in Fig. 5.9. A considerable increase in the intensity and λ_{max}

of the free-carrier tail produced by the materials in the oxidised state is observed with subsequent solvent extractions, (assuming a λ_{max} higher than 1500 nm for the chloroform fraction as estimated by extrapolation). In addition, an overlay of the spectra of the materials in the neutral state (Fig. 5.10) clearly shows a significant bathochromic shift of the λ_{max} due to the $\pi \rightarrow \pi^*$ transition with each extraction, in accordance with the range of colours displayed by these fractions (Fig. 5.7). The bathochromic shift of both the free-carrier tail and the $\lambda_{\text{max}}(\pi \rightarrow \pi^*)$ indicate an increase in the mean conjugation length of the materials with subsequent Soxhlet extractions.¹¹⁴ This is consistent with an increase in the mean oligomer length as indicated by the MALDI-TOF MS results (Fig. 5.8).

It is interesting to note the increase in two absorbances at *ca.* 660 and 900 nm with increasing oligomer length (Fig. 5.10). While the shoulder at 660 nm may be indicative of longer oligomers, the broad absorbance at 900 nm suggests that the “neutral” oligomer fraction is partially oxidised. This may be due to polymer that was not fully reduced by hydrazine. As mentioned previously, it has been shown by Bredas *et al.*¹⁶⁴ and Sumi *et al.*¹¹⁴ that long thiophene polymers are more difficult to reduce than short oligomers. Partially oxidised material may also result from an increasing tendency for the longer polymers to oxidise on standing. This could be attributed to an increased polaron stability in these styryl-substituted polymers as a result of the “defect confinement” postulated for styryl-substituted sexithiophenes.¹⁴⁰

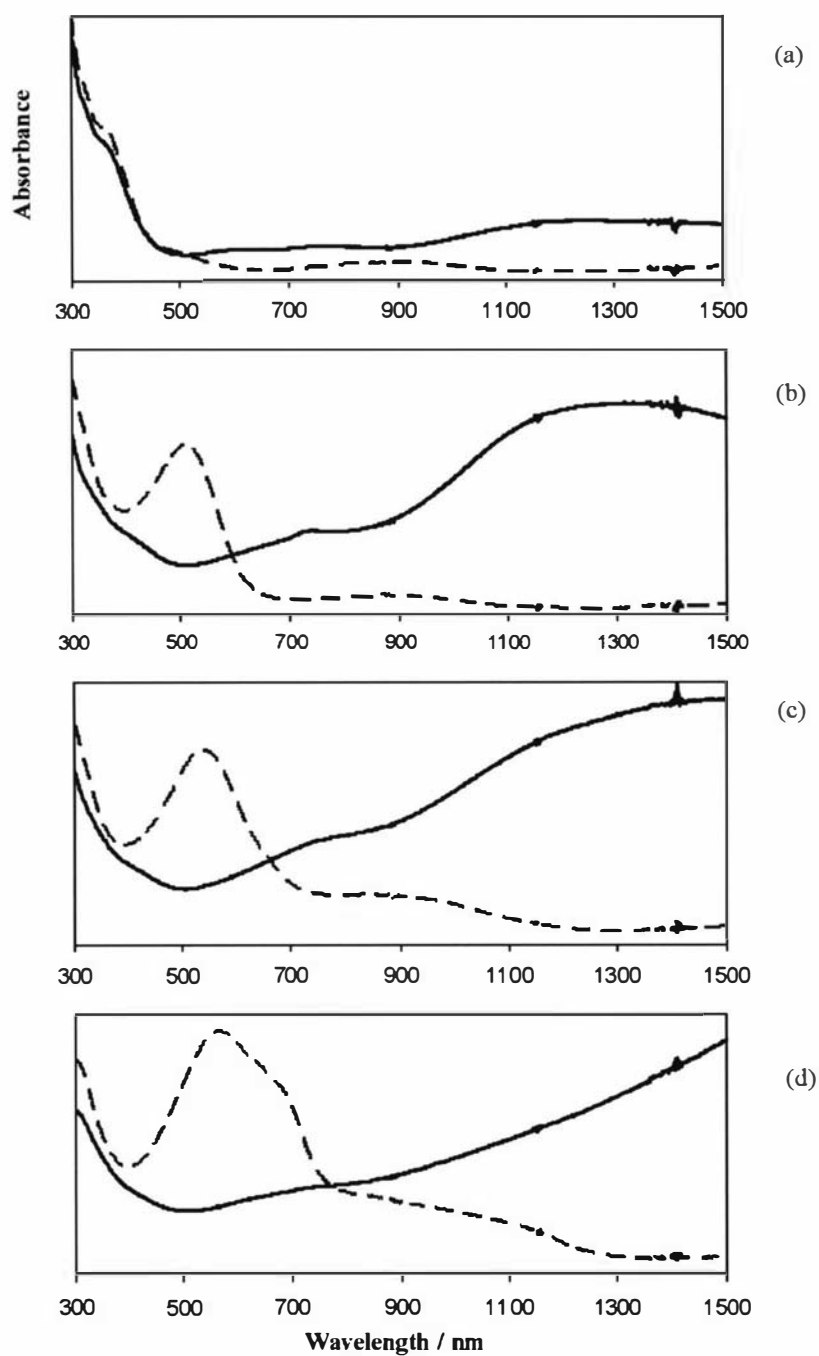


Fig. 5.9. UV-VIS-NIR spectra of OC₆DASTT oligomer fractions separated by (a) hexane, (b) acetone, (c) DCM and (d) chloroform. Samples were measured in the oxidised state (excess Cu(ClO₄)₂, solid line) and neutral state (dashed line) from solutions in chloroform.

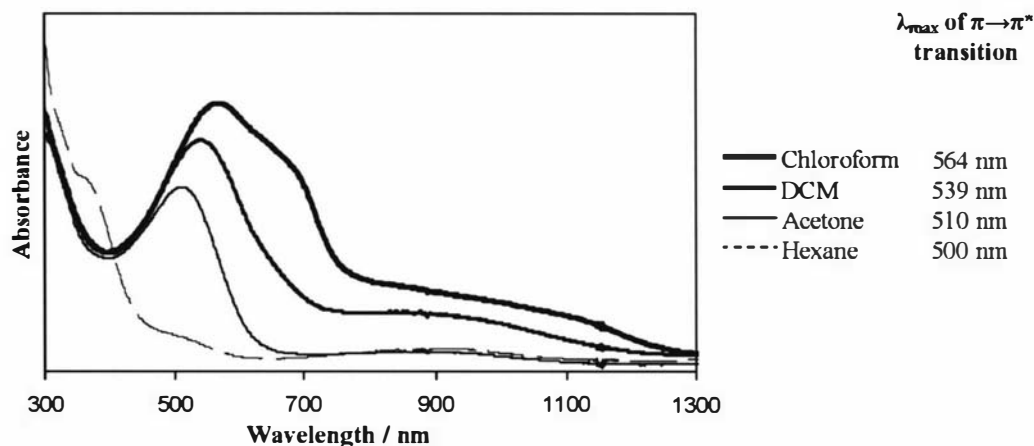


Fig. 5.10. UV-VIS-NIR spectra of neutral samples of OC_6DASTT oligomer fractions which have been separated using hexane, acetone, DCM and chloroform. The λ_{max} of the major $\pi \rightarrow \pi^*$ transition for each fraction is shown.

^1H NMR spectra of these fractions showed very broad peaks, indicating that polymerisation is not regioselective.

5.2.5 Conclusions

OC_6DASTT was successfully polymerised by iron(III) chloride. As anticipated from previous work by others,⁶² the attachment of alkoxy chains to the polymer backbone was found to greatly increase the solubility of the polymeric product in organic solvents, compared to oligoSTT investigated in Chapter 3. Poly OC_6DASTT was found to be very stable (w.r.t. charge) in the oxidised state, and hence difficult to reduce. A soluble fraction of 67% was initially obtained by reduction with hydrazine, but was increased to 78% by decreasing the polymerisation temperature from room temperature to -10°C , probably due to a decrease in the average oligomer length. The insoluble material most likely consists of oligomers that are too long to be soluble and/or too long to be reduced (and therefore solubilised).

UV-VIS-NIR spectroscopy of the soluble fraction revealed a significant free-carrier tail generated by this material in the oxidised state, consistent with the production of highly conductive materials. The soluble material was successfully separated into fractions of different length oligomers/polymers by soxhlet extractions in a series of solvents.

MALDI-TOF MS of these fractions showed that the total soluble product consists of polymers with an average length of *ca. n* = 11. The effective conjugation length of the polymer fractions was observed (by UV-VIS-NIR spectra) to increase with an increase in polymer length (determined by MALDI-TOF MS).

5.3 Chemical polymerisation of C₇DASTT

5.3.1 Introduction

The polymerisation of C₇DASTT (Fig. 5.1) was investigated. Gallazzi *et al.* have shown that alkyl-substituted polythiophenes are more easily reduced than alkoxy derivatives, and are consequently easier to solubilise.⁶² C₇-alkyl chains, which are approximately the same length as the OC₆-alkoxy chains, were chosen to allow a more direct comparison to OC₆DASTT.

5.3.2 Polymerisation and reduction

C₇DASTT was polymerised using a similar method to that used for the polymerisation of OC₆DASTT (Fig. 5.2). As for OC₆DASTT, chloroform was found to be a good solvent for the C₇DASTT polymerisation. The reaction was completed at room temperature, rather than at -10°C, to allow the formation of longer polymer chains.

After four hours, the reaction mixture manifested a black precipitate, similar to that observed for the polymerisation of OC₆DASTT, and the styryl-substituted terthiophenes discussed in Chapter 3. As for those materials, the insoluble material was assumed to be oxidised polymer. Removal of the unreacted oxidant from the chloroform reaction mixture by washing with water resulted in an immediate change to a bright orange solution, most likely due to reduction of polyC₇DASTT to the neutral state. Andersson *et al.* suggested that the high stability of alkyl substituted polythiophene derivatives (including 4,4''-alkyl-substituted poly(terthiophene)) in the neutral state may be due to low accessibility of the counter ion to the polymer backbone due to steric hindrance by the alkyl side chains.¹⁶⁸

Upon removal of the chloroform solvent, a red gum was obtained that was 100% soluble in chloroform. The MALDI-TOF mass spectrum of this crude material (Fig. 5.11) showed a peak distribution similar to that observed by polyOC₆DASTT (Fig. 5.4).

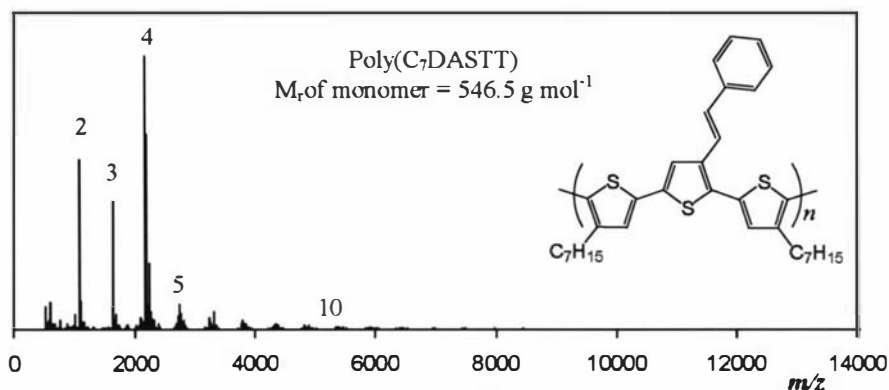


Fig. 5.11. MALDI-TOF mass spectrum of poly(C₇DASTT). Signals are labelled with the assigned oligomer length in terms of monomer units (n).

The UV-VIS-NIR spectra of polyC₇DASTT, measured in both the neutral and oxidised states are given in Fig. 5.12. Neutral C₇DASTT oligomer/polymer affords two peaks at 323 nm and 407 nm due to the styrylthiophene and oligoterthiophene chromophores respectively, as described for the materials in Chapter 3. The much lower $\lambda_{\text{max}}(\pi \rightarrow \pi^*)$ of the polyC₇DASTT oligoterthiophene chromophore (407 nm) than that observed for the polyOC₆DASTT oligoterthiophene chromophore (532 nm) may be indicative of a shorter mean effective conjugation length.^{114,127} The hypsochromic shift may also be partially attributed to the alkyl substituents. While non-bonding pair substituents, such as alkoxy groups, are reported to shift absorptions substantially to longer wavelengths, alkyl substituents are known to shift absorptions less significantly to longer wavelengths.¹⁶⁹

As is typical for polythiophenes,¹⁷⁰ two bands are observed in the oxidised state, assigned to the polaron/bipolaron species (788 nm) and polymeric chains displaying quasi-metallic behaviour (free-carrier tail, 1363 nm). However, the low λ_{max} of the free-carrier tail in comparison to that of polyOC₆DASTT (Fig. 5.5, peak > 1500 nm) also suggests that the polyC₇DASTT sample may consist of shorter oligomers.

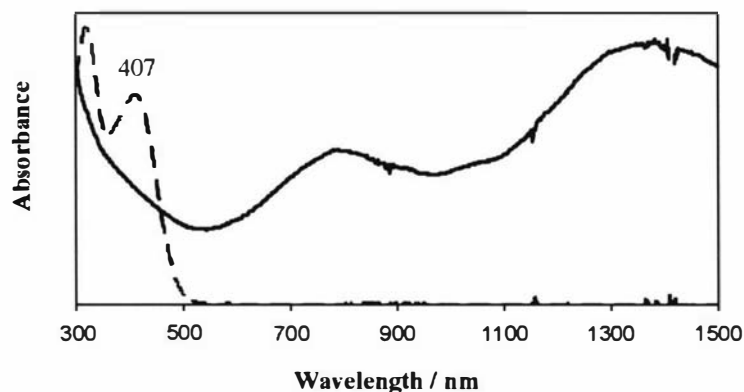


Fig. 5.12. UV-VIS-NIR spectra of polyC₇DASTT in the oxidised state (excess Cu(ClO₄)₂, solid line) and neutral state (dashed line).

The CV of a polyC₇DASTT film cast on ITO-coated glass (Fig. 5.13) displays an oxidation peak at 0.98 V and a reduction peak at 0.32 V, consistent with a one-electron reversible redox process. In comparison to polyOC₆DASTT (Fig. 5.6), which generated very broad oxidation and reduction bands suggesting a wide distribution of oligomer lengths, the polyC₇DASTT peaks are well-defined, not inconsistent with a narrow distribution of oligomer lengths.¹⁵⁹

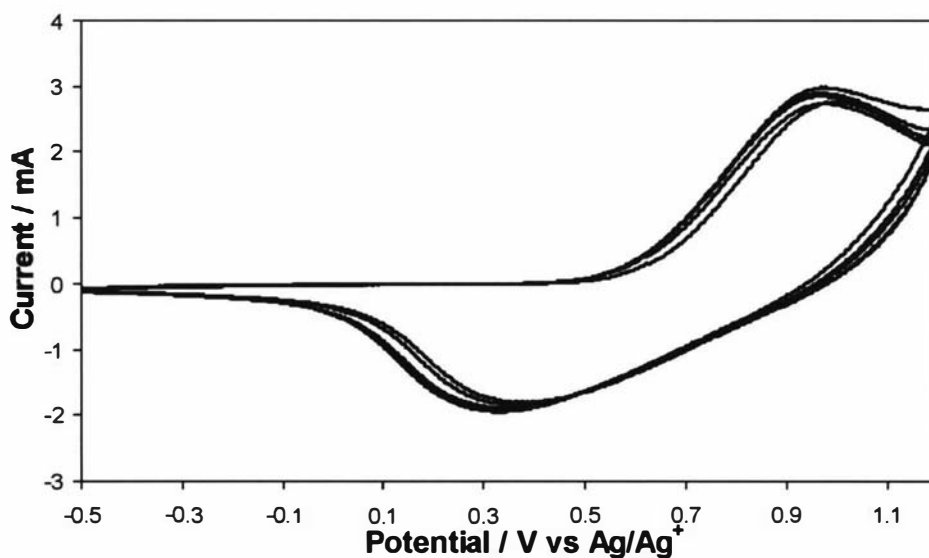


Fig. 5.13. CV of a chemically polymerised C₇DASTT film, which has been cast onto an ITO-coated glass electrode (SA: ~1 cm²). Supporting electrolyte: 0.1 M TBAP/AN. Potential limits: -500/+1200 mV. 5 cycles. Scan rate: 100 mV s⁻¹.

5.3.3 Polymer separation according to oligomer length

PolyC₇DASTT was separated into fractions of different length polymers using sequential Soxhlet extractions in a series of solvents as for polyOC₆DASTT. Unlike the neutral polyOC₆DASTT fractions, which were observed to be a range of colours in chloroform solution, the neutral polyC₇DASTT polymer fractions were all orange. The mass percentages obtained in each solvent are listed in Table 5.2, and the MALDI-TOF mass spectra of each fraction given in Fig. 5.14. As 63% of the crude product is extracted by methanol and hexane, which is shown to consist of mostly short polymers ($n = 1 - 8$), the overall molecular weight appears to be low with an average polymer length of about $n = 6$ (estimated as for polyOC₆DASTT, Section 5.2.4). Inspection of the DCM fraction reveals the presence of polymers up to $n = 12$. It appears that polyC₇DASTT consists of oligomers/polymers that are significantly shorter than those measured for polyOC₆DASTT, where an average polymer length of $n = 11$ was estimated, and polymer with a length of up to $n = 35$ was detected (Fig. 5.8).

Table 5.2. Mass percentages of polyC₇DASTT separated by different solvents.

Methanol (%)	Hexane (%)	Acetone (%)	DCM (%)	CHCl ₃ (%)	Total soluble material
6	57	13	23	1	100%

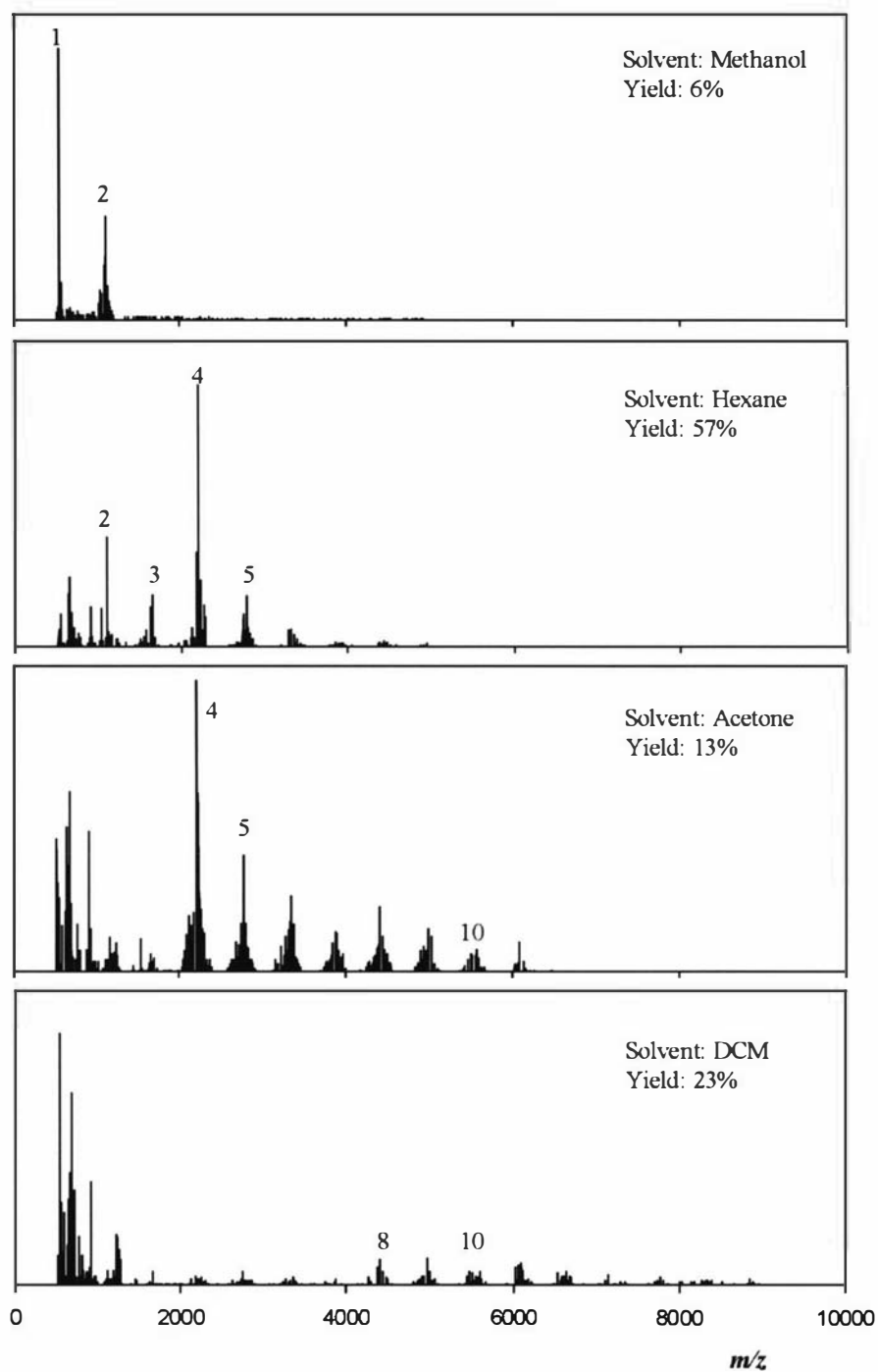


Fig. 5.14. MALDI-TOF MS of C_7 DASTT oligomer fractions extracted using methanol followed by hexane, acetone and dichloromethane. Signals are labelled with the assigned oligomer length in terms of monomer units (n). M_r of monomer: 546.5 g mol^{-1} .

Absorption spectra of C₇DASTT polymer fractions, in both the neutral and oxidised states, are displayed in Fig. 5.15, with an overlay of the spectra of the neutral fractions in Fig. 5.16. The λ_{max} due to the $\pi \rightarrow \pi^*$ transition of the oligo(terthiophene) chromophore (*ca.* 410 nm) is observed to slightly increase with subsequent extractions, indicating an increase in effective conjugation length.¹¹⁴ There is also a significant bathochromic shift in the free-carrier tail (>1000 nm) with subsequent extractions, which also indicates the presence of oligomers with a longer conjugation length in later fractions.¹¹⁴ The increase in polymer length with subsequent extractions is consistent with conclusions from MALDI-TOF MS data for these fractions.

Comparison of the positions of the $\lambda_{\text{max}}(\pi \rightarrow \pi^*)$ and the free carrier tail of the C₇DASTT polymer fractions to those of the OC₆DASTT polymer fractions (Fig. 5.8) suggests that the C₇DASTT solvent fractions contain oligomers/polymers with much shorter effective conjugation lengths. This is consistent with the shorter C₇DASTT oligomer/polymer lengths detected by MALDI-TOF MS. In addition, it is clear that the reduced (neutral) form of polyC₇DASTT is not as prone to partial oxidation as polyOC₆DASTT is, as all the C₇DASTT oligomer fractions appear fully reduced. This supports the proposal that the long chain soluble fractions of polyOC₆DASTT are partially oxidised as a result of polaron stabilisation by the alkoxy groups.

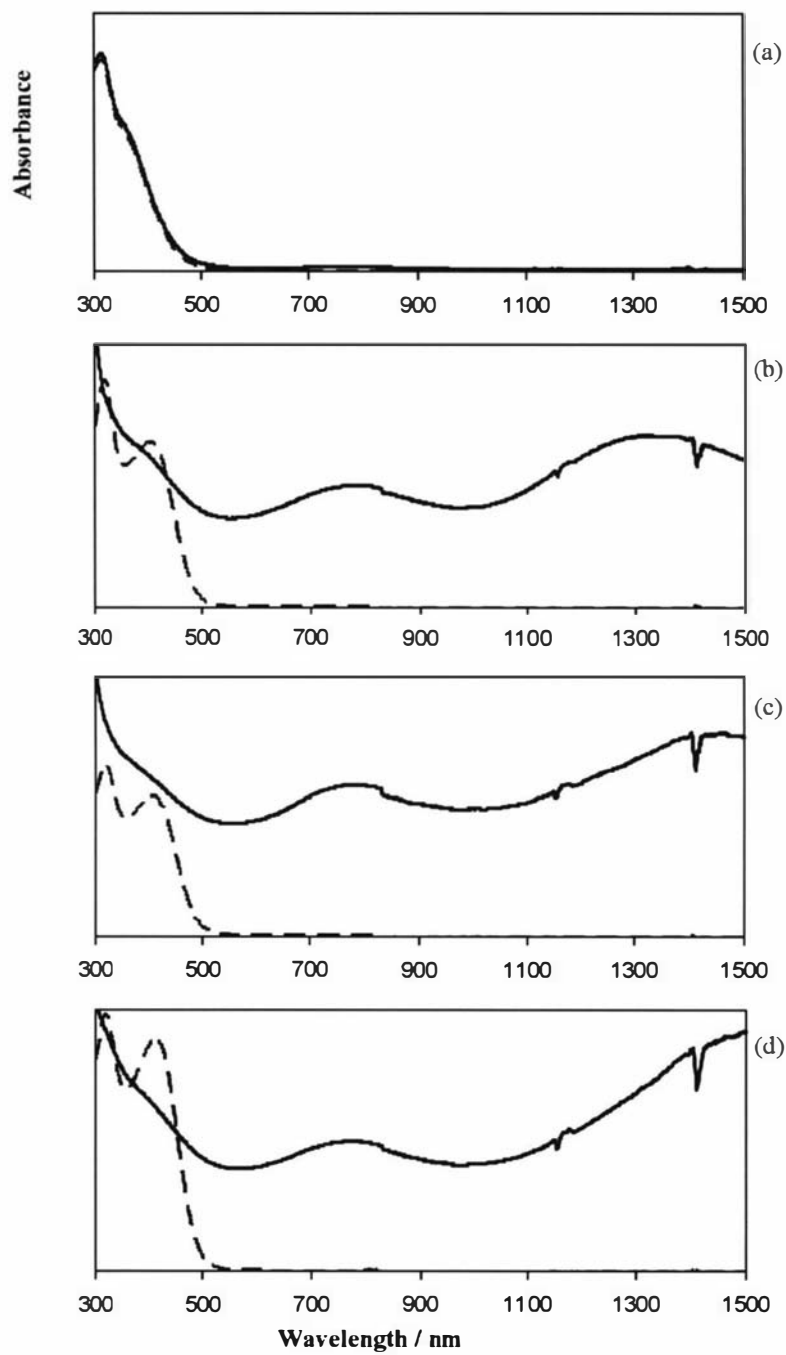


Fig. 5.15. UV-VIS-NIR spectra of C₇DASTT oligomer fractions separated by (a) methanol, (b) hexane, (c) acetone and (d) DCM. Samples were measured in the oxidised state (excess Cu(ClO₄)₂, solid line) and neutral state (dashed line) from solutions in chloroform.

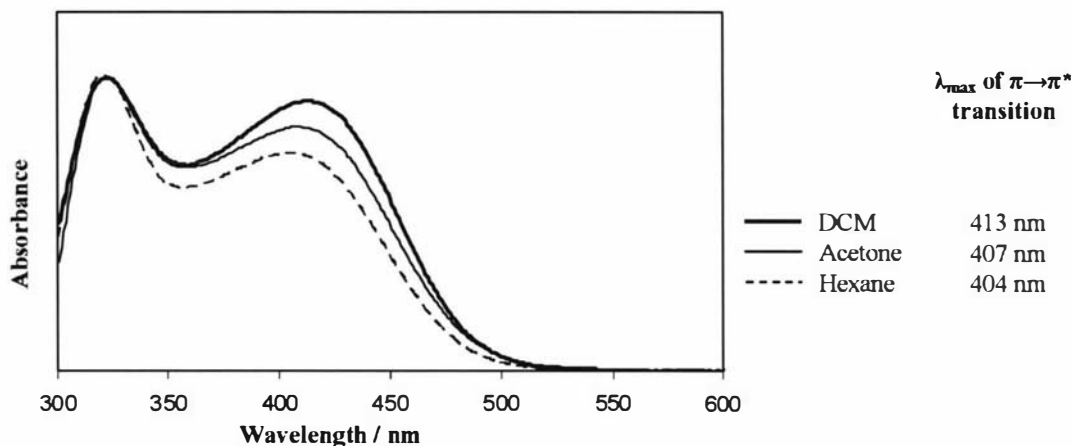


Fig. 5.16. UV-VIS-NIR spectra of neutral samples of C_7 DASTT oligomer fractions which have been separated using hexane, acetone and DCM. The λ_{max} of the $\pi \rightarrow \pi^*$ transition for each fraction is shown.

5.3.4 Conclusions

C_7 DASTT was successfully polymerised with iron(III) chloride to give a polymeric product that was 100% soluble in chloroform. The increase in the soluble fraction of poly C_7 DASTT (100%) compared to that obtained for poly OC_6 DASTT (78%) may be due to two reasons. First, an average polymer length of $n = 6$ was estimated for this product (from MALDI-TOF MS of oligomer fractions), which is much shorter than the average length of poly OC_6 DASTT, which was estimated as *ca.* $n = 11$. It has been shown by several workers that shorter oligothiophenes are more soluble than long oligothiophenes.^{44,114,127} Secondly, poly C_7 DASTT was found to be very easy to reduce to the neutral, more soluble state than poly OC_6 DASTT.

UV-VIS-NIR spectra of poly C_7 DASTT showed a substantial polaron band and less significant free-carrier tail than poly OC_6 DASTT, indicative of a shorter effective conjugation length. This could be due to the presence of shorter oligomers as revealed by MALDI-TOF MS. The oxygen atom of alkoxy substituents appears to be activating polymerisation in some way. This is consistent with observations by

Giroto *et al.*¹¹¹ and Gallazzi *et al.*⁶² on the polymerisation of 4,4''-pentoxy-substituted terthiophene derivatives.

Since C₇DASTT gave shorter oligomers than OC₆DASTT, further attention was focussed on alkoxy derivatives, and increasing the soluble fraction. A terthiophene substituted with longer alkoxy chains was investigated.

5.4 Chemical polymerisation of OC₁₀DASTT

5.4.1 Introduction

OC₆DASTT gave longer oligomers than C₇DASTT, but only 78% of the oligomeric/polymeric product was soluble. An attempt was made to further increase the soluble fraction by investigating styrylterthiophene with longer, C₁₀-alkoxy chains attached (Fig. 5.17). This compound is referred to as OC₁₀DASTT.

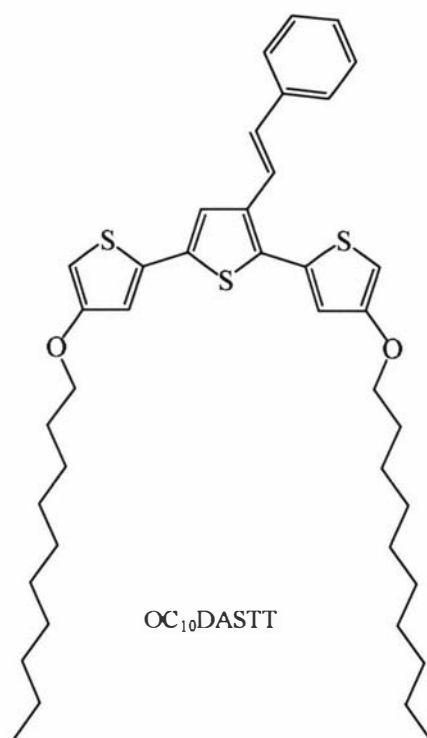


Fig. 5.17. C₁₀-dialkoxy styrylterthiophene (OC₁₀DASTT).

5.4.2 Polymerisation

The reaction conditions used to polymerise OC₁₀DASTT (Fig. 5.18) were similar to those used for the polymerisation of OC₆DASTT. Since a higher soluble yield of polyOC₆DASTT was obtained when polymerising at temperatures of -10°C rather than RT, this temperature was used for the polymerisation of OC₁₀DASTT.

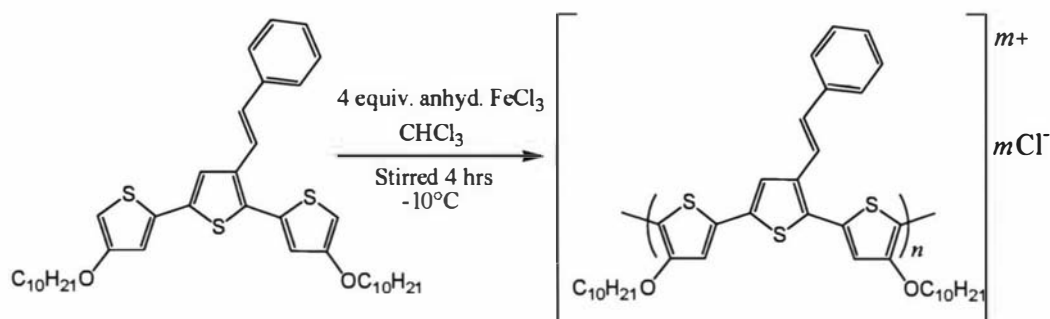


Fig. 5.18. Reaction procedure employed for the polymerisation of OC₁₀DASTT.

Polymerisation using these conditions gave a soluble fraction of 97%, considerably higher than that obtained for OC₆DASTT (78%), and the MALDI-TOF MS of the soluble product (Fig. 5.19) shows peaks due to oligomers of lengths up to $n = 15$.

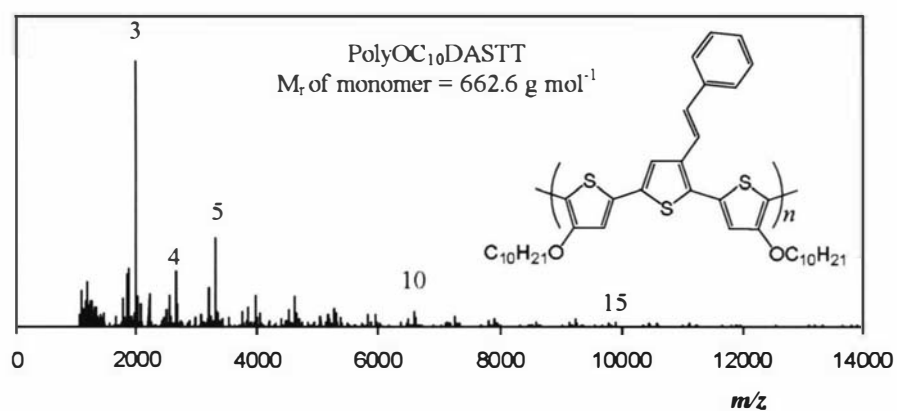


Fig. 5.19. MALDI-TOF MS of polyOC₁₀DASTT. Signals are labelled with the assigned oligomer length in terms of monomer units (n).

The UV-VIS-NIR spectra of polyOC₁₀DASTT (Fig. 5.20) in the neutral and oxidised states offers further evidence of long polymer chains. The λ_{max} for the $\pi \rightarrow \pi^*$ transition of the material in the neutral state is 537 nm, which is slightly higher than that observed for polyOC₆DASTT (532 nm). This is consistent with reports by Casalbore-Miceli *et al.*¹⁶² of a bathochromic shift in absorbance maxima with an increase in alkyl chain length on poly(terthiophene)s. It was suggested by Casalbore-Miceli *et al.* that this shift may be due to an increasing planarity of the polythiophene chains.¹⁶² As seen for polyOC₆DASTT, a 'shoulder' has appeared at about 700 nm and a second absorbance at about 900 nm indicative of partial oxidation.

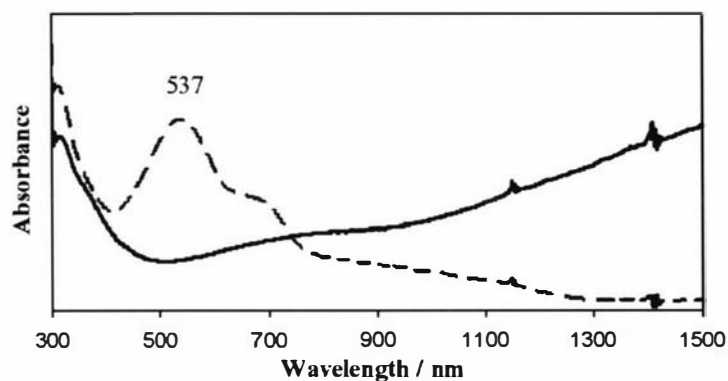


Fig. 5.20. UV-VIS-NIR spectra of polyOC₁₀DASTT in chloroform in the oxidised state (excess Cu(ClO₄)₂, solid line) and neutral state (dashed line). The major λ_{max} for the $\pi \rightarrow \pi^*$ absorbance is labelled.

A cyclic voltammogram of a cast film of polyOC₁₀DASTT on an ITO-coated glass electrode (Fig. 5.21) displays very broad oxidation and reduction peaks, as for the cast film of polyOC₆DASTT (Fig. 5.6, Section 5.2.2). The first cycle is significantly different to subsequent cycles as is commonly observed in post-growth CVs of polythiophenes.¹⁴⁷ Although the origin of this is not well understood, possible causes may include degradation of the polymer film,^{72,145} a change in the organisation of the polymer chains and morphology of the film affecting ion movement into/out of the film, and further polymerisation of shorter oligomers,¹⁷¹. A higher oxidation onset potential is observed (-0.23 V) than for the polyOC₆DASTT film (-0.34 V). This may indicate that the polyOC₁₀DASTT film consists of polymer with a lower mean conjugation length.^{114,164}

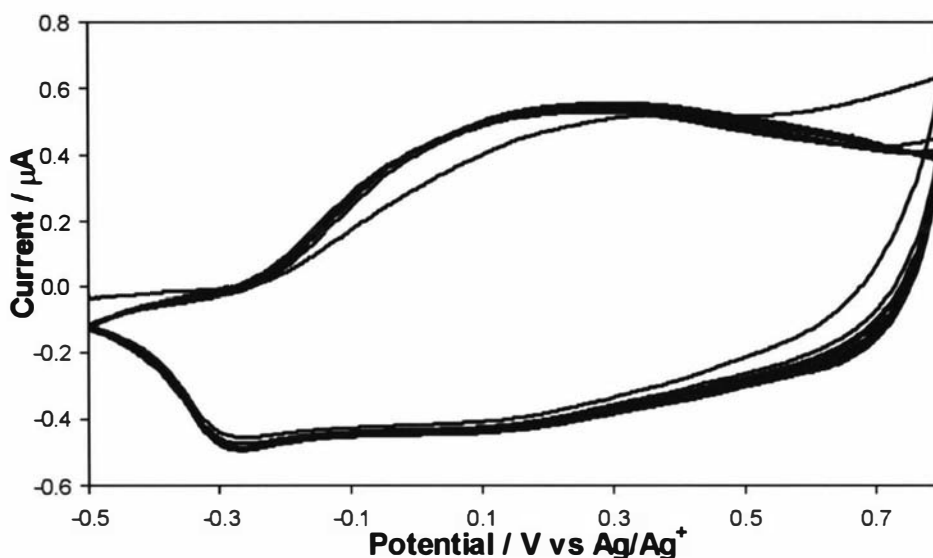


Fig. 5.21. CV of chemically polymerised OC₁₀DASTT, which has been cast as a film onto an ITO-coated glass electrode (SA: ca.1 cm²). Supporting electrolyte: 0.1 M TBAP/AN. Potential limits: -500/+1200 mV. 10 cycles. Scan rate: 100 mV s⁻¹.

Attempts were made to further increase the average polymer length of polyOC₁₀DASTT without decreasing the soluble fraction. The effect of the order of addition of reagents on the soluble fraction of polyOC₁₀DASTT was investigated. While polymerising 3,3''-didodecyl-2,2':5'5''-terthiophene with iron(III) chloride, Gallazzi *et al.*⁹⁸ found that the molecular weight was strongly dependent on the addition sequence of the reagents, which affected the initial oxidant concentration. They compared the difference between adding iron(III) chloride to a solution of monomer, and adding a solution of the monomer to the iron(III) chloride. Although they observed 100% solubility for both resulting polymers, a product consisting of longer oligomers was obtained when the monomer was added to the iron(III) chloride.

In all previous reactions mentioned in this study, the iron(III) chloride oxidant was added dropwise (as a suspension in chloroform) to the monomer over about thirty minutes. Polymerisation of OC₁₀DASTT by addition of the oxidant to the monomer resulted in a soluble fraction of 97%, but it was found that by adding the monomer to the oxidant, a soluble fraction of only 44% was obtained. Assuming the insoluble polymer is due to oligomers too long to be soluble, this result is consistent with

Gallazzi's result of longer oligomer formation by removing impurities. This increase in oligomer length when the monomer is added to the oxidant is most likely due to the initial high ratio of oxidant to monomer, as a similar increase in polyOC₆DASTT oligomer length was previously observed when the oxidant:monomer ratio was increased from 1 to 4 equivalents (Section 5.2.4).

The effect of ethanol on the soluble fraction polymer length was also investigated. While polymerising a C₁₂ alkyl-substituted terthiophene with iron(III) chloride, Gallazzi *et al.*⁹⁸ found that the molecular weight and yield of soluble product was strongly dependent on the quality of the reagents. They found that washing and drying the reagents produced a higher soluble yield, presumably as a result of a shorter oligomer length. It was unclear, however, which impurity was causing the decrease in solubility and no explanation was offered. Although polythiophene reactions are reported to be generally less sensitive to water than other conducting polymers such as polypyrrole and polyaniline,^{47,172} both ethanol and water have been shown to influence the oxidation potential of iron(III) chloride.⁷⁰

The chloroform solvent used in the reactions to this point contained 0.5 – 1.0% ethanol. The effect of this ethanol was investigated by comparing the product of an ethanol-free reaction with one containing 0.75% ethanol. It was found that with ethanol present, a soluble fraction of 100% was achieved, but when the ethanol was removed, a soluble fraction of only 61% was obtained. Since iron(III) has its greatest affinity for ligands that coordinate via oxygen,¹⁷³ it is likely that iron-ethanol complexes form, impairing the iron(III) oxidation potential and slowing polymerisation to produce shorter oligomers. These results for the polymerisation of an alkoxy terthiophene contradict the findings of Gallazzi *et al.*⁹⁸ This suggests that either the effect of ethanol is different for the polymerisation of alkyl-substituted terthiophenes or Gallazzi *et al.* had removed another impurity which was causing the production of insoluble polymer.

Since both altering the addition sequence of the reagents, and removing water and/or ethanol impurities resulted in a much lower soluble fraction, the products from these reactions were not further investigated, and the initial product mixture (Section 5.4.2) was fractionated.

5.4.3 Polymer separation according to length

As for polyOC₆DASTT and polyC₇DASTT, the crude polyOC₁₀DASTT was separated into fractions of different length oligomers/polymers. The amount extracted in each solvent is given as mass percentages of the total expected polymer yield in Table 5.3. The corresponding MALDI-TOF mass spectra for each solvent fraction are displayed in Fig. 5.22. MALDI-TOF mass spectra of the polyOC₁₀DASTT solvent extractions display very similar oligomer/polymer distributions to that obtained for polyOC₆DASTT. The major difference in the two polymerisations is the higher amount of polyOC₁₀DASTT extracted into chloroform (54% compared to 42%). As found for polyOC₆DASTT, an average estimated length of about $n = 11$ is obtained for the crude sample of polyOC₁₀DASTT. Although addition of a longer alkoxy chain increases the total yield of soluble polymer, it does not appear to significantly affect the degree of polymerisation.

Table 5.3. Mass percentages of OC₁₀DASTT oligomers/polymers separated by different solvents.

Methanol (%)	Hexane (%)	Acetone (%)	DCM (%)	CHCl ₃ (%)	Total soluble material
0	13	4	26	54	97%

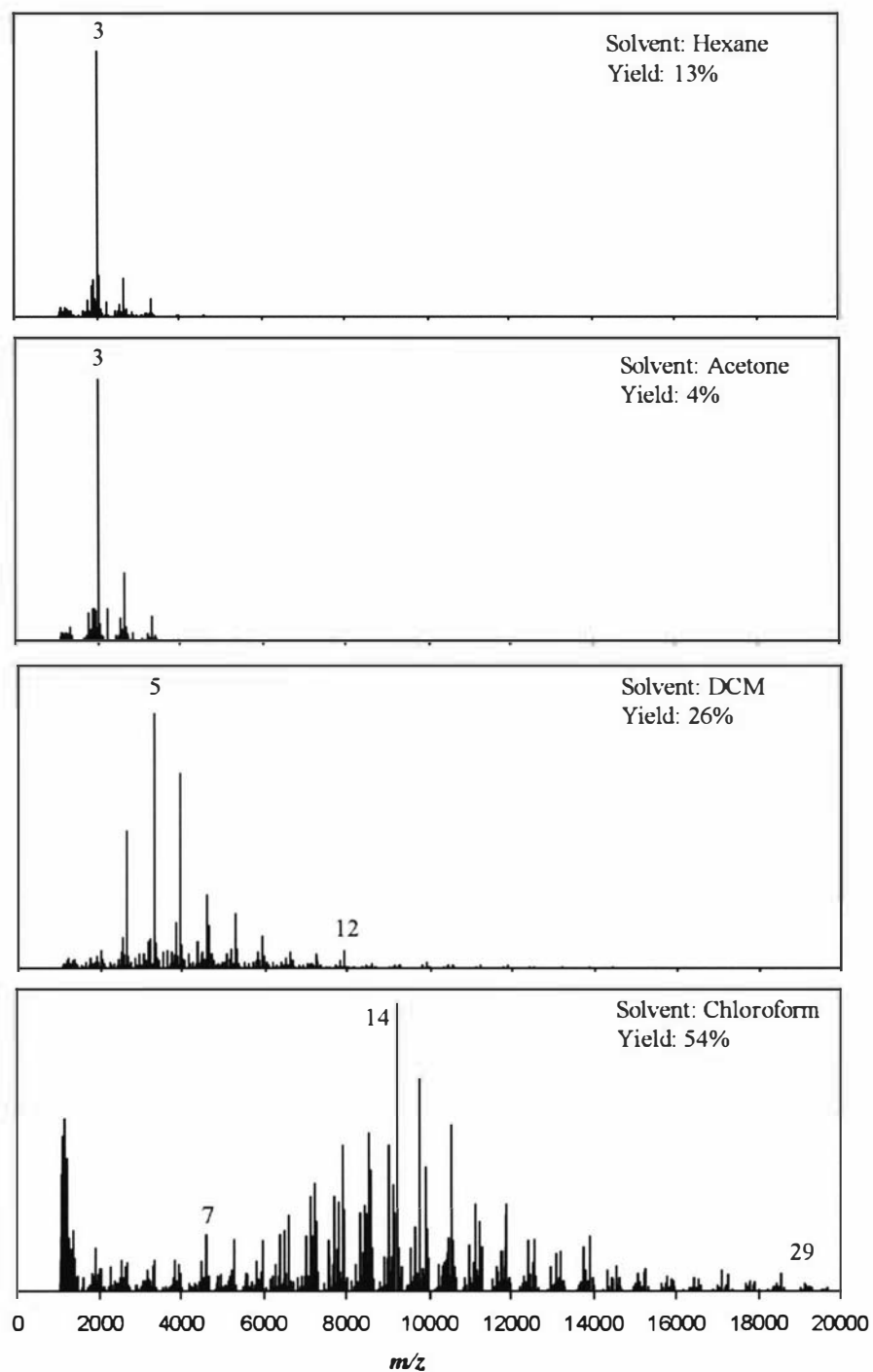


Fig. 5.22. MALDI-TOF mass spectra of OC₁₀DASTT polymer fractions extracted using hexane followed by acetone, dichloromethane and chloroform. Signals are labeled with the assigned oligomer length in terms of monomer units (*n*). M_r of monomer: 662.4 g mol⁻¹.

The UV-VIS-NIR spectra of the OC₁₀DASTT oligomer/polymer fractions are displayed in Fig. 5.23, and an overlay of the spectra of the neutral materials in Fig. 5.24. As for the OC₆DASTT polymer fractions (Fig. 5.8), a considerable increase in the intensity of the free carrier tail, and a significant bathochromic shift of the λ_{max} ($\pi \rightarrow \pi^*$) is observed with subsequent extractions. It is interesting to note that each of the fractions of polyOC₁₀DASTT consistently display a λ_{max} ($\pi \rightarrow \pi^*$) at higher wavelengths than those measured for polyOC₆DASTT (Fig. 5.8). This is consistent with observations by Casalbore-Miceli *et al.*¹⁶² on the effect of increasing alkyl chain lengths, and may be due to better supramolecular ordering of polymer chains.

Significantly, the major absorbance of the chloroform fraction of polyOC₁₀DASTT now appears to be due to the partially oxidised polymer (651 nm) rather than the neutral polymer (*ca.* 560 nm). This suggests an increasing ease of oxidation of polyOC₁₀DASTT due to increased charge stabilisation by the longer alkoxy substituents compared to polyOC₆DASTT.

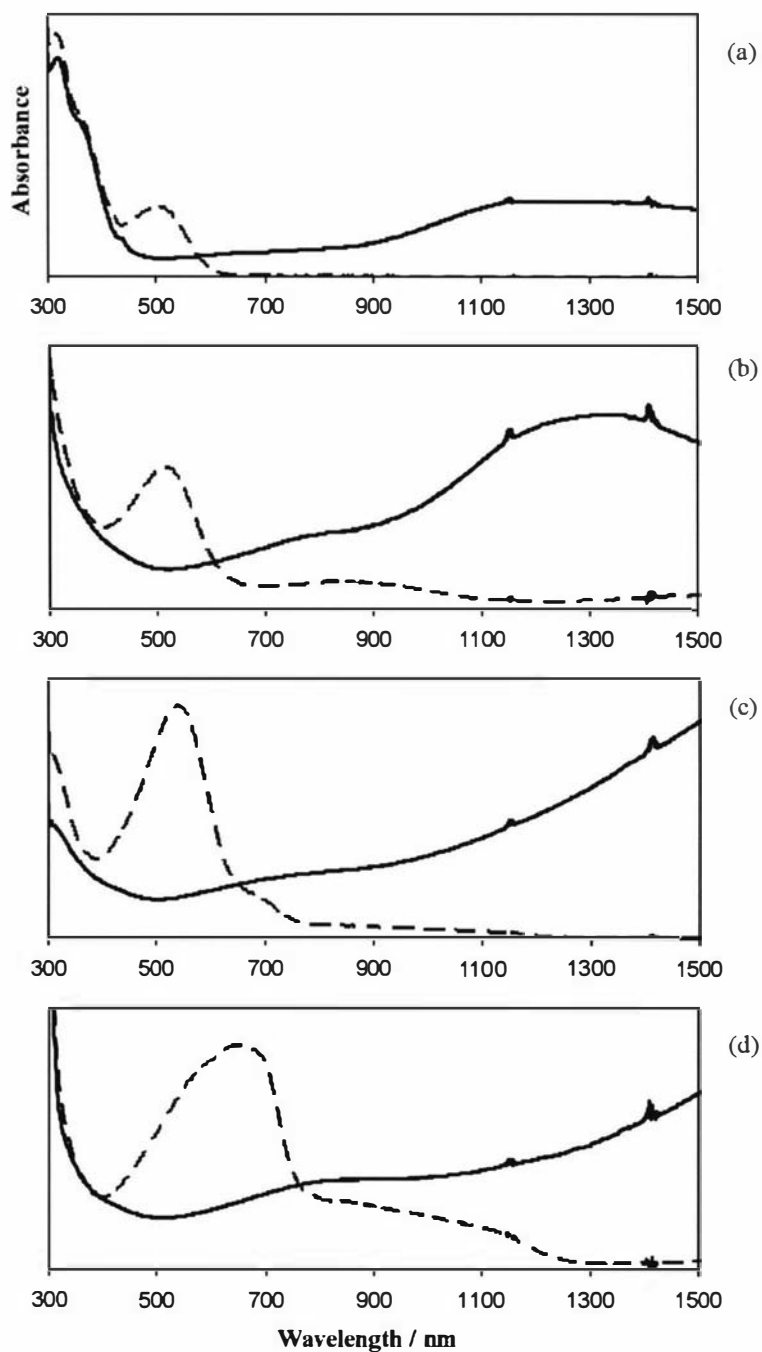


Fig. 5.23. UV-VIS-NIR spectra of OC₁₀DASTT oligomer fractions separated by (a) hexane, (b) acetone, (c) DCM and (d) chloroform. Samples were measured in the oxidised state (solid line, oxidised using excess Cu(ClO₄)₂) and neutral state (dashed line) from solutions in chloroform.

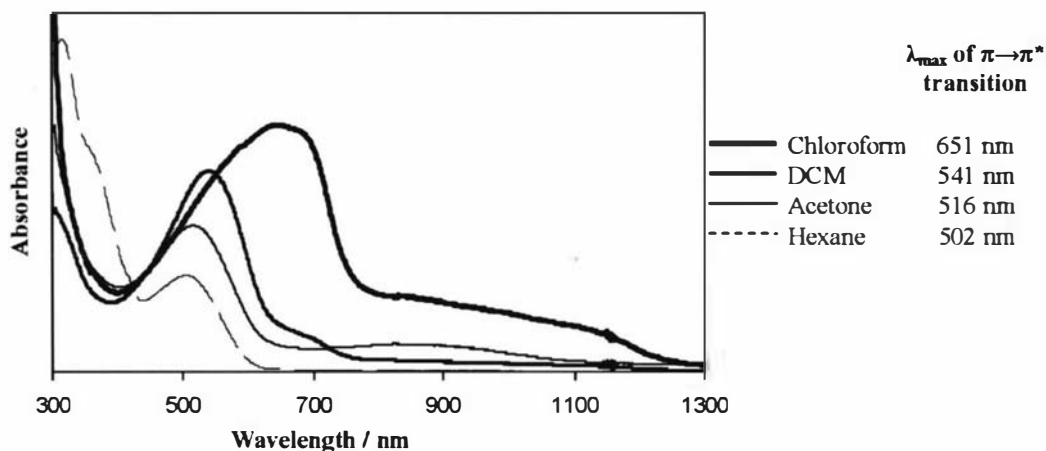


Fig. 5.24. UV-VIS-NIR spectra of OC₁₀DASTT oligomer fractions which have been separated using hexane, acetone, DCM and chloroform. The λ_{max} of the $\pi \rightarrow \pi^*$ transition for each fraction is listed.

Cyclic voltammetry of fractions of different length OC₁₀DASTT oligomers, which were drop-cast onto a GC electrode, are displayed in Fig. 5.25. The oxidation onset potential is observed to decrease with each oligomer extraction (the acetone, DCM and chloroform fractions commence oxidation at 0.28 V, 0.19 V and 0.09 V respectively), consistent with an increasing oligomer length¹¹⁴ as indicated by MALDI-TOF MS and UV-VIS-NIR spectroscopy. The reduction peak also shows a decrease in potential with increasing oligomer length: the acetone, DCM and chloroform fractions show peaks at 0.49 V, 0.20 V and -0.16 V respectively. The lower oxidation and reduction potentials suggest that longer oligomers are more stable in the oxidised state.

As each of the films consist of the same amount of material (15 $\mu\text{g mm}^{-2}$) and covered the same area of electrode (7 mm^2), the significant increase in current produced by the films as the polymer length increases may be caused by increasing conductivity of the films.

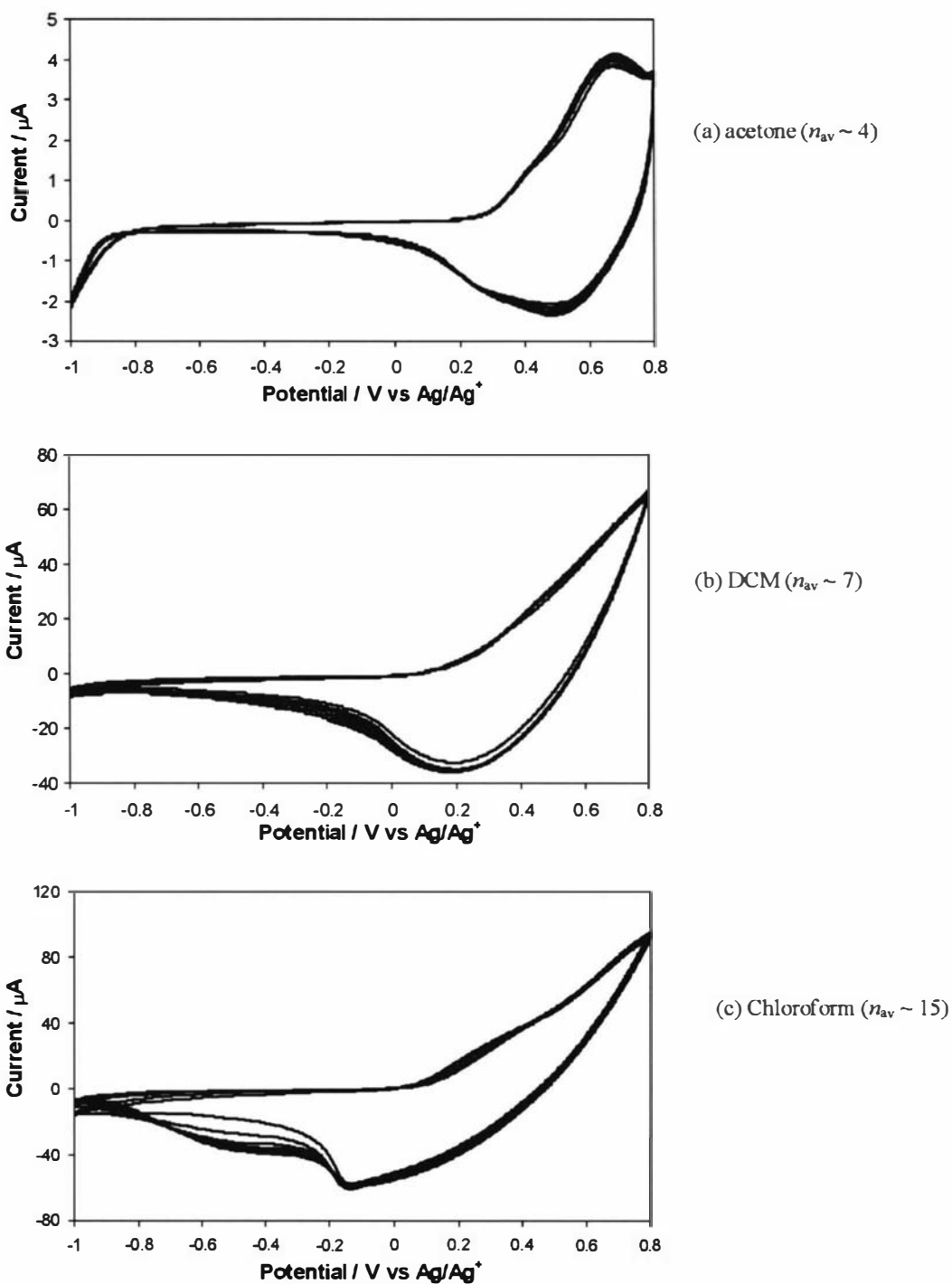


Fig. 5.25. Cyclic voltammetry of OC₁₀DASTT oligomer fractions that have been cast onto a glassy carbon electrode (SA: 7 mm²). Supporting electrolyte: 0.1 M TBAP/AN. Potential limits: -1000/+800 mV. 10 cycles. Scan rate: 100 mV s⁻¹. The average oligomer length as estimated from MADLI-TOF MS data is displayed in terms of monomer units (n_{av}).

The reaction conditions shown in Fig. 5.18 were successfully used to polymerise OC₁₀DASTT to produce soluble polyOC₁₀DASTT in gram quantities. This allowed the material to be tested for use in devices such as actuators, solar cells and batteries as described in Chapter 6.

5.4.4 Conclusions

OC₁₀DASTT was successfully polymerised using iron(III) chloride to give a soluble fraction of 97% with an average polymer length of about $n = 11$. Although no enhancement in polymerisation was achieved by the attachment of longer alkoxy chains to the terthiophene monomer (polyOC₁₀DASTT and polyOC₆DASTT show a similar range of oligomer/polymer lengths), the amount of soluble polymer was significantly increased by the attachment of longer alkoxy chains.

5.5 Electrochemical polymerisation

5.5.1 Introduction

Polymerisation by cyclic voltammetry allows an *in-situ* investigation into the growth process of polythiophenes. Films of the alkyl and alkoxy styrylterthiophene derivatives were prepared by cyclic voltammetry, as well as deposited by potentiostatic (constant potential) methods to determine the difference in film growth by these techniques.

Post-growth cyclic voltammetry of the resulting polymer films (in monomer-free solution) was performed to investigate the redox processes. However, an extensive mechanistic study of the electrochemical growth and redox processes of the polymer films was beyond the scope of this study.

A platinum microelectrode (surface area: $10 \mu\text{m}^2$) was used for the electrochemical growth and analysis of the alkyl and alkoxy substituted derivatives. The small electroactive surface area of the microelectrode eliminates diffusion effects of the monomer species to the electrode, and minimises distortion of experimental data by ohmic potential drop and capacitance effects as described in Chapter 2. In addition, films were electrochemically deposited onto ITO-coated glass (surface area: $\sim 1 \text{ cm}^2$). Post-growth cyclic voltammetry of these films allowed comparison to the cyclic voltammetry of the cast films of the chemically oxidised materials (Sections 5.2.2, 5.3.2 and 5.4.2). The morphology of these films, in both the neutral and oxidised states, was investigated by scanning electron microscopy (SEM).

For direct comparison between the polymerisation of STT and the alkyl and alkoxy (DASTT) derivatives, a growth CV of oligoSTT on a platinum microelectrode was first determined, and is shown in Fig. 5.26. The lower current compared to that for the polymerisation of STT on the platinum disc electrode (Fig. 3.16, Chapter 3, Section 3.4.2) is due to the much smaller surface area of the microelectrode ($10 \mu\text{m}^2$ compared to 1.8 mm^2). A higher oxidation onset potential of 0.74 V is also observed on the platinum microelectrode, compared to the platinum disc electrode (0.60 V). This indicates that nucleation and growth on the smaller surface area microelectrode is

more difficult, likely due to ready diffusion of insoluble oligomers away from the electrode surface by hemispherical diffusion, rather than their deposition. The increase in current with successive cycles indicates the growth of an electroactive film. The positive shift of the anodic peak as the film thickens during polymerisation may indicate that the film is not very conductive or that counter-ion mobility is hindered.

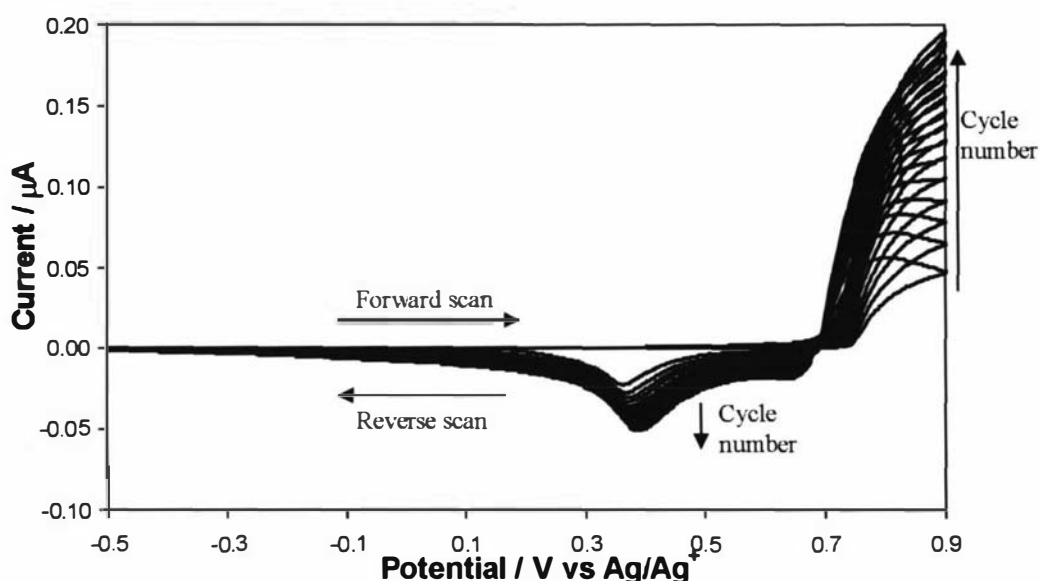


Fig. 5.26. Growth CV of oligoSTT (5 mM) on a platinum microelectrode (SA: $10 \mu\text{m}^2$). Electrolyte solution: 0.1 M TBAP/1:1 AN:DCM. Potential limits: -500/+900 mV. 15 cycles. Scan rate: 100 mV s^{-1} .

5.5.2 Electrochemical growth and post-growth analysis of polyC₇DASTT

The potentiodynamic growth of C₇DASTT on a platinum microelectrode (Fig. 5.27) shows an increase in current with scan number, indicating growth of an electroactive film. A plot of the current produced at the upper vertex (0.8 V) for each cycle (Fig. 5.28) displays an exponential increase. This indicates a very conductive film, and fast growth kinetics.

Oxidation commences at 0.64 V. The lower oxidation onset potential when compared to that of STT (0.74 V) may be due to stabilisation of the resulting radical cation species by the electron-donating effect of the alkyl substituents.⁸ This lower oxidation potential may be contributing to faster growth kinetics by the alkyl derivative, as

indicated by double the amount of current produced after fifteen cycles ($0.4 \mu\text{A}$) compared to that generated by the growth of STT after the same number of cycles ($0.2 \mu\text{A}$).

On further cycling, the onset of this anodic peak, which is possibly due to monomer oxidation, shifts towards lower oxidation potentials (0.60 V on the 15th scan) suggesting that oxidation onto the polymer film is more readily achieved than onto the platinum surface. In addition, a small peak at 0.41 V emerges on subsequent scans, possibly due to the oxidation of the resulting polymer.

Two reduction peaks are shown: a sharp peak at 0.59 V and broader peak at 0.43 V . As discussed in Chapter 3, Section 3.4.2, it has been suggested that the presence of multiple peaks during the growth and post-growth cyclic voltammetry of polythiophene derivatives may be due to transitions between the neutral, polaron, bipolaron and metallic states, which are affected by factors such as reduction of different areas of the polymer film¹⁴⁷, different length polymer chains,¹¹⁴ the effect of 'charge-trapping'¹⁵¹ and conformational changes accompanying radical cation formation.¹⁵²

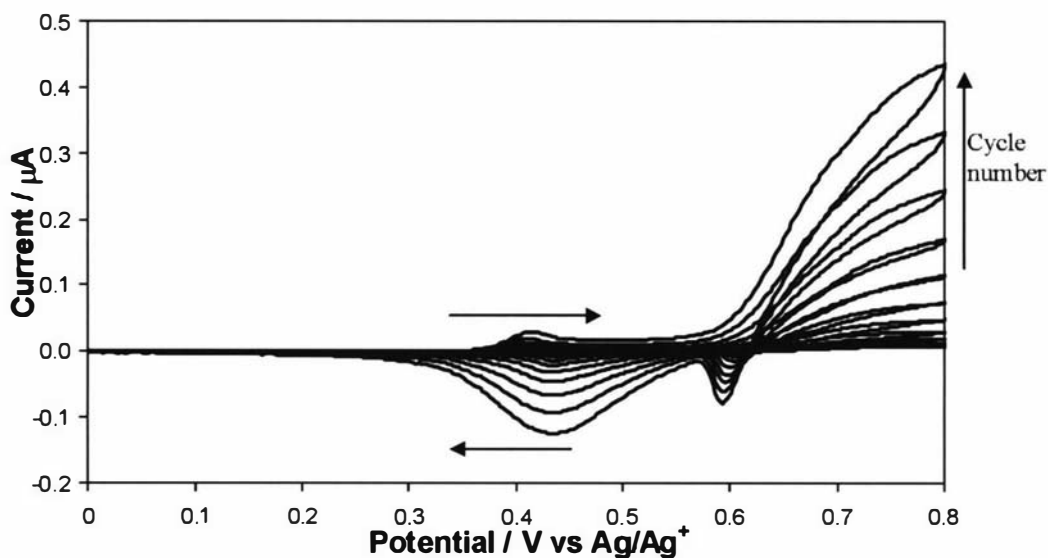


Fig. 5.27. Growth CV of C₇DASTT (5 mM) on a platinum microelectrode ($10 \mu\text{m}^2$). Electrolyte solution: 0.1 M TBAP/1:1 AN:DCM. Potential limits: 0/+800 mV. 15 cycles. Scan rate: 100 mV s^{-1} .

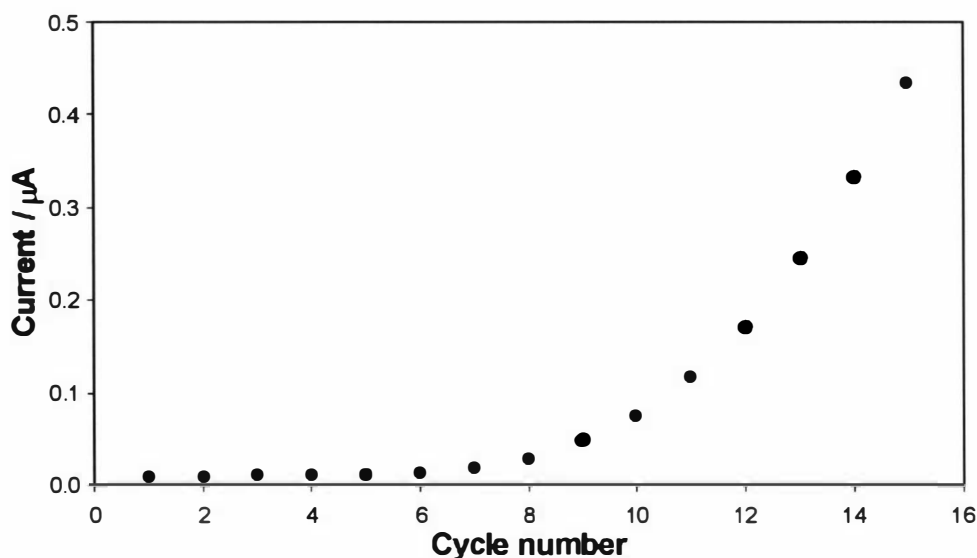


Fig. 5.28. Relationship between the current produced during the growth of C₇DASTT (measured at 0.8 V) and the cycle number.

The post-growth cycling of the resulting polyC₇DASTT film in monomer-free solution is displayed in Fig. 5.29. One anodic peak and one broad cathodic peak are observed. The anodic scan of the first cycle is significantly different from subsequent scans, displaying a much larger peak current. As mentioned previously, possible causes of the different first cycle may include degradation of the polymer film,^{72,145} a change in the organisation of the polymer chains and/or morphology of the film affecting ion movement into/out of the film, and further polymerisation of short oligomers.^{111,171} The higher anodic current when compared to cathodic current further supports the inclusion of monomer or short oligomers in the film.¹¹¹ Solvation of short oligomers resulting in their removal from the film is also possible.⁹⁹ Subsequent scans show a much smaller decrease in current of the anodic peak (indicating lesser changes to the film), and a shift of this peak to higher potentials. This may be due to a decrease in conductivity of the film, or to a change in morphology resulting in a decrease in counter-ion mobility.¹⁴⁷

A high oxidation onset potential for polyC₇DASTT (0.48 V) is observed. This is consistent with a high stability in the neutral state and correlates with the observation in Section 5.3.2 of the ease of reduction of the chemically polymerised C₇DASTT.

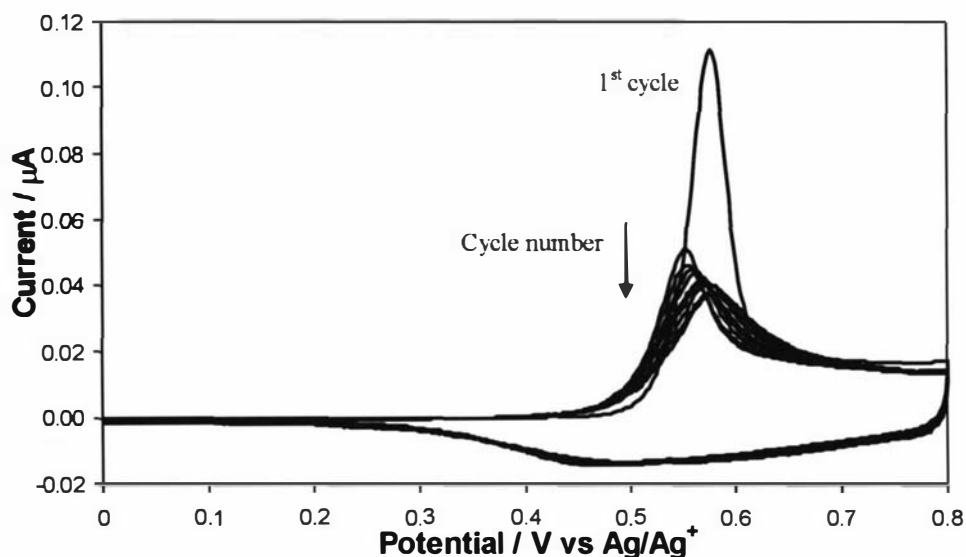


Fig. 5.29. Post growth cycling of polyC₇DASTT which has been deposited using cyclic voltammetry on a platinum micro electrode (SA: 10 μm²). Supporting electrolyte: 0.1 M TBAP/AN. Potential limits: -500/+800 mV. 10 cycles. Scan rate: 100 mV s⁻¹.

The chronoamperogram of the growth of C₇DASTT onto a platinum microelectrode is shown in Fig. 5.30. The potential used for the potentiostatic growth was chosen as 700 mV. Use of this potential resulted in polymerisation and film deposition. When the potential is stepped from 0 mV to 700 mV, a small, sharp transient is produced due to non-Faradaic charging of the electrode/solution interface. The current then increases steadily indicating an increase in electroactive surface area (by polymer deposition) and/or more facile electrode kinetics. The change in the current-time transient after approximately 10 seconds of growth of C₇DASTT may be due to a change in the deposition morphology. It has been shown by Pringle *et al.* that the growth of some polythiophenes initially results in a smooth compact film, but further growth may result in the deposition of material of porous morphology.¹⁴⁷ The increased surface area of the polymer-modified electrode caused by porous material (compared to the smooth film) may affect the rate at which more material is deposited and consequently the current produced.

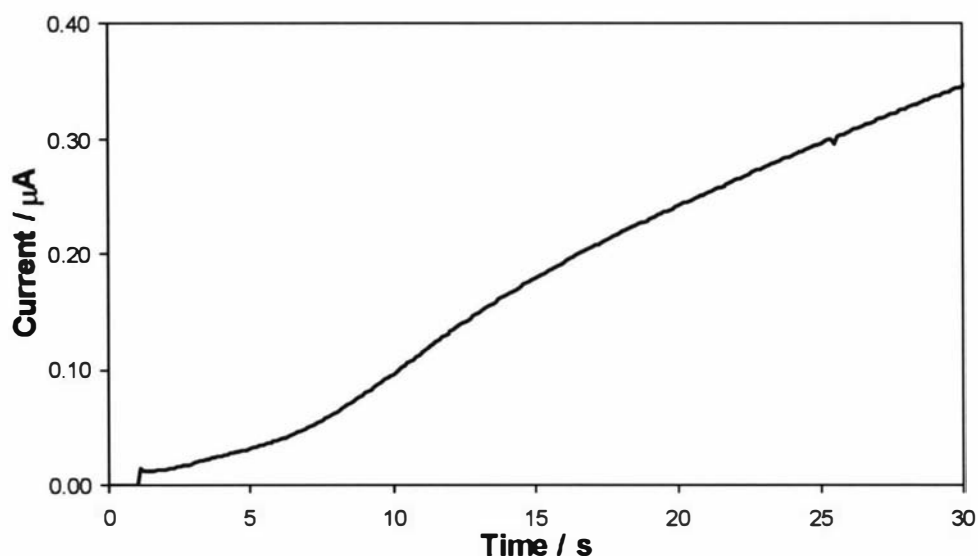


Fig. 5.30. Potentiostatic growth of C₇DASTT (5 mM) on a platinum micro electrode (SA: 10 μm²). Solvent: 1:1 AN:DCM. Potential held at 0 mV for 1 s, then stepped to 700 mV for 29 seconds.

The post-growth CV (in monomer-free solution) of this film is displayed in Fig. 5.31. As observed for the potentiodynamically grown polyC₇DASTT film (Fig. 5.29), the first scan is distinct to subsequent scans. These subsequent scans are significantly different to the post-growth CV of the potentiodynamically grown polyC₇DASTT film in terms of the number, position and shape of the oxidation and reduction peaks. Subsequent scans show two oxidation peaks (0.58 and 0.76 V) and two reduction peaks (0.58 and 0.41 V). As previously discussed (Chapter 3, Section 3.4.2), the presence of multiple oxidation peaks may be due to transitions between the neutral, polaron, bipolaron and metallic states.

An attempt was made to polymerise C₇DASTT onto an ITO-coated glass slide (~1 cm²) using both cyclic voltammetry and potentiostatic methods. Although small amounts of black material were produced (assumed to be oxidised polyC₇DASTT), the material did not adhere to the electrode. Consequentially, no further studies were performed on this material.

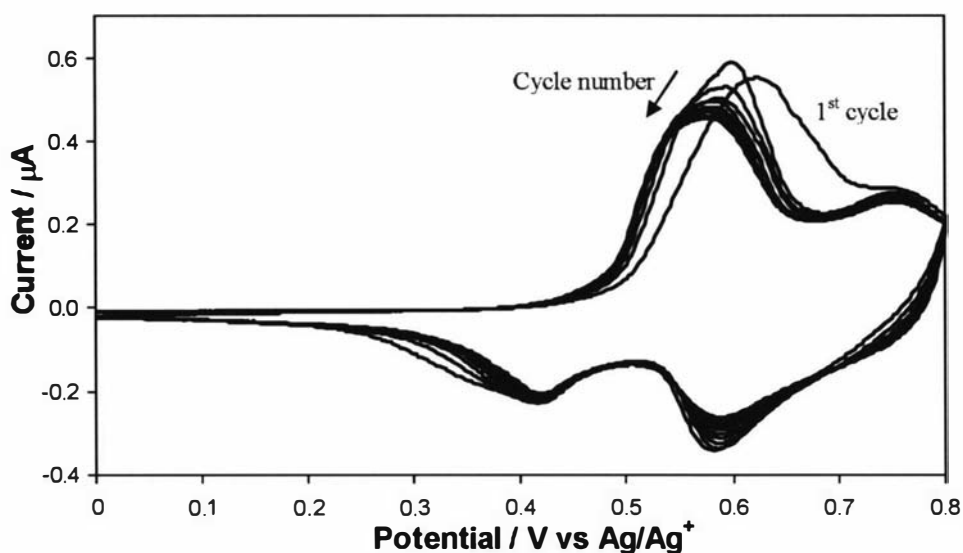


Fig. 5.31. Post growth cycling of polyC₇DASTT, which has been deposited potentiostatically on a platinum microelectrode (SA: 10 μm²). Supporting electrolyte: 0.1 M TBAP/AN. Potential limits: 0/+800 mV. 10 cycles. Scan rate: 100 mV s⁻¹.

5.5.3 Electrochemical growth and post-growth analysis of polyOC₆DASTT

The growth CV of OC₆DASTT is in Fig. 5.32. The decrease in oxidation onset potential (0.61 V) compared to both STT and C₇DASTT (0.74 and 0.64 V respectively) may be due to enhanced stabilisation of the resulting monomer cation radicals caused by the strong electron-donating effect of the alkoxy substituents.

This CV shows a significant increase in current with each scan indicating rapid growth of an electroactive polymer film. A maximum current of 2.3 μA is generated after 15 cycles, which is more than 5 times higher than produced during the growth of C₇DASTT (0.4 μA) and 10 times higher than that produced during the growth of STT (0.2 μA) after the same number of cycles. This indicates very fast growth kinetics, and may be a result, in part, of the reduced oxidation onset potential.

After the first cycle, an oxidation peak is produced at *ca.* -0.06 V ($E_{ox,1}$), which increases to 0.05 V after 15 cycles. This is followed by a broad oxidation peak at

ca. 0.2 V ($E_{\text{ox},2}$), and another peak at 0.65 V ($E_{\text{ox},3}$). A broad reduction band is generated with peaks at 0.44 V ($E_{\text{red},1}$) and 0.14 V ($E_{\text{red},2}$). The post-growth CV of this film in monomer-free solution (Fig. 5.33) displays similar peaks to the growth CV in terms of shape and position, but with the loss of the oxidation peak, $E_{\text{ox},3}$, which is probably due to oxidation of the monomer species. The other redox peaks, including small peaks appearing at about 0.55 V on oxidation ($E_{\text{ox},4}$) and -0.5 V on reduction ($E_{\text{red},3}$), are most likely due to transitions between the neutral, polaron, bipolaron and metallic states of the deposited polymeric material. The oxidation onset potential of the polymeric material (0.11 V), is much lower than that of both the potentiodynamically deposited STT and C₇DASTT derivatives (0.30 and 0.44 V respectively). A decrease in oxidation potential of polythiophenes by attachment of alkoxy substituents has been reported by Girrotto *et al.*¹¹¹ and may be due to a stabilisation of the oxidised species and/or a result of an increase in oligomer length.¹¹⁴ The low oxidation potential of electropolymerised polyOC₆DASTT is also consistent with the apparent stability of this material in the oxidised state, as observed by the chemically polymerised materials (Section 5.4.2).

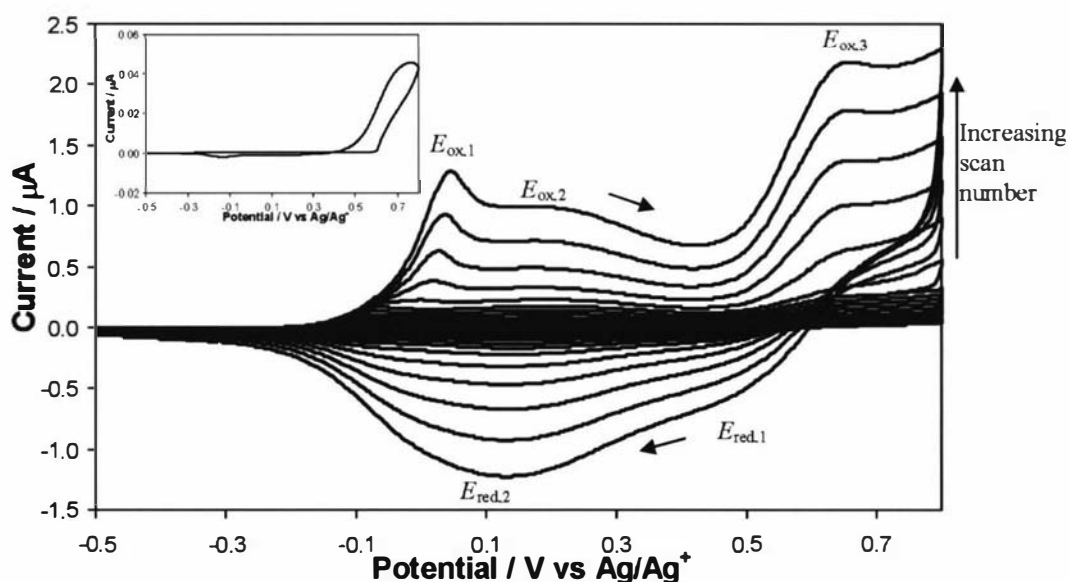


Fig. 5.32. Growth CV of OC₆DASTT (5 mM) of a platinum micro electrode (SA: 10 µm²). Electrolyte solution: 0.1 M TBAP/1:1 AN:DCM. Potential limits: -500/+800 mV. Scan rate: 100 mV s⁻¹. The first scan is shown as an inset.

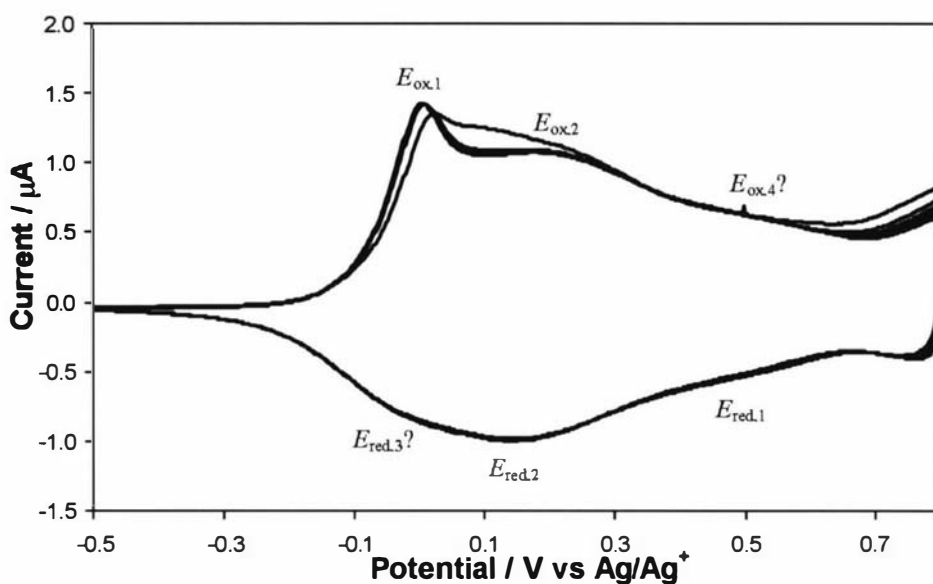


Fig. 5.33. Post growth cycling of polyOC₆DASTT which has been deposited using cyclic voltammetry on a platinum microelectrode (SA: 10 μm²). Supporting electrolyte: 0.1 M TBAP/AN. Potential limits: -500/+800 mV. 10 cycles. Scan rate: 100 mV s⁻¹. Small peaks may be present at about 0.55 V on oxidation ($E_{ox,4}$) and -0.5 V on reduction ($E_{red,3}$),

The chronoamperogram of the potentiostatic growth of polyOC₆DASTT is displayed in Fig. 5.34. A potential of 0.8 V was chosen for polymerisation, as this potential generates polymerisation, and does not appear to cause overoxidation. As for the potentiostatic growth of polyC₇DASTT, a small, sharp current transient is initially observed due to non-Faradaic charging of the electrode/solution interface, and is followed by a steadily increasing current with time. The change in the current/time transient at *ca.* 16 seconds may be due to deposition of polymer with a different (possibly more porous) morphology, as discussed for the growth of polyC₇DASTT.

The post-growth CV of this potentiostatically grown film is displayed in Fig. 5.35, and is very similar to the post-growth CV of the potentiodynamically deposited material (Fig. 5.33), in terms of shape and position of the peaks. The major difference is a smaller $E_{ox,2}$ shoulder, and a more prominent $E_{red,4}$ peak.

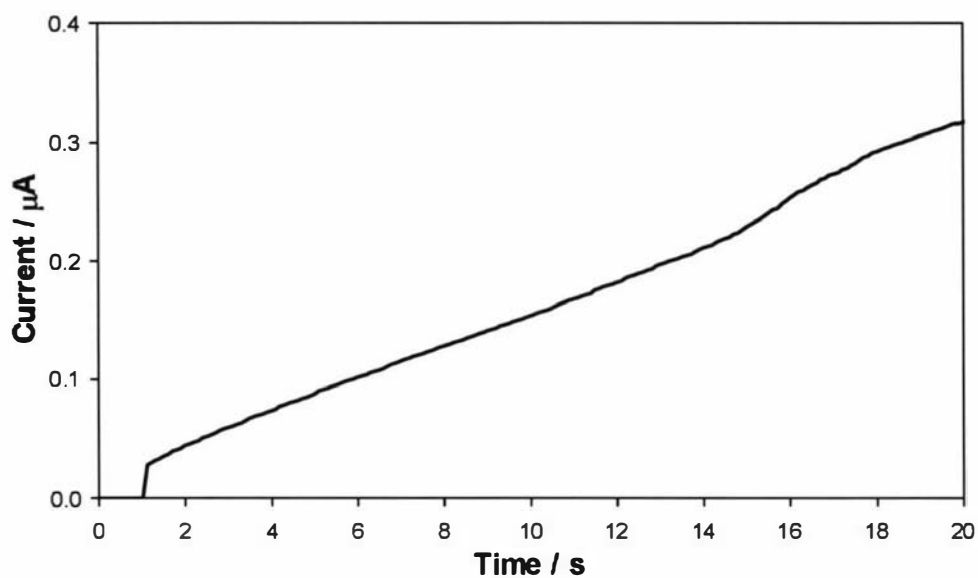


Fig. 5.34. Potentiostatic growth of OC₆DASTT (5 mM) on a platinum microelectrode (SA: 10 μm²). Electrolyte solution: 0.1 M TBAP/1:1 AN:DCM. Potential held at -500 mV for 1 s, then stepped to 800 mV for 19 s.

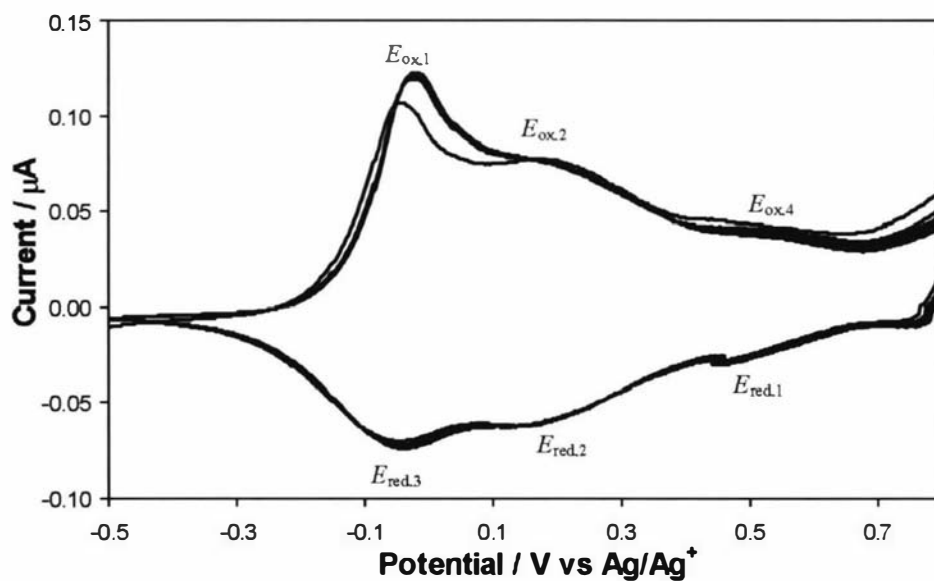


Fig. 5.35. Post growth cycling of polyOC₆DASTT which has been deposited potentiostatically on a platinum microelectrode (SA: 10 μm²). Supporting electrolyte: 0.1 M TBAP/AN. Potential limits: -500/+800 mV. 10 cycles. Scan rate: 100 mV s⁻¹.

Films of polyOC₆DASTT were also grown onto ITO-coated glass for SEM analysis and to obtain enough material for MALDI-TOF mass spectrometry. The growth CV is shown in Fig. 5.36, with an oxidation onset potential of 0.67 V. This higher oxidation

onset potential when compared to the film grown on the platinum microelectrode (0.61 V) suggests that nucleation onto the ITO surface is more difficult. In addition, the shape of the CV is significantly different to that generated by growth on the platinum microelectrode, possibly due to inhibition of the growth by formation of a monomer-depleted area around the large electrode.

The post-growth CV this film (Fig. 5.37) displays one broad oxidation peak at 0.30 V and one broad reduction peak at 0.04 V. The peaks are not quite as broad as observed in the CV generated by the cast film of chemically oxidised polyOC₁₀DASTT (Fig. 5.6), possibly due to a narrower polymer polydispersity,¹⁵⁹ or a more regular film morphology.

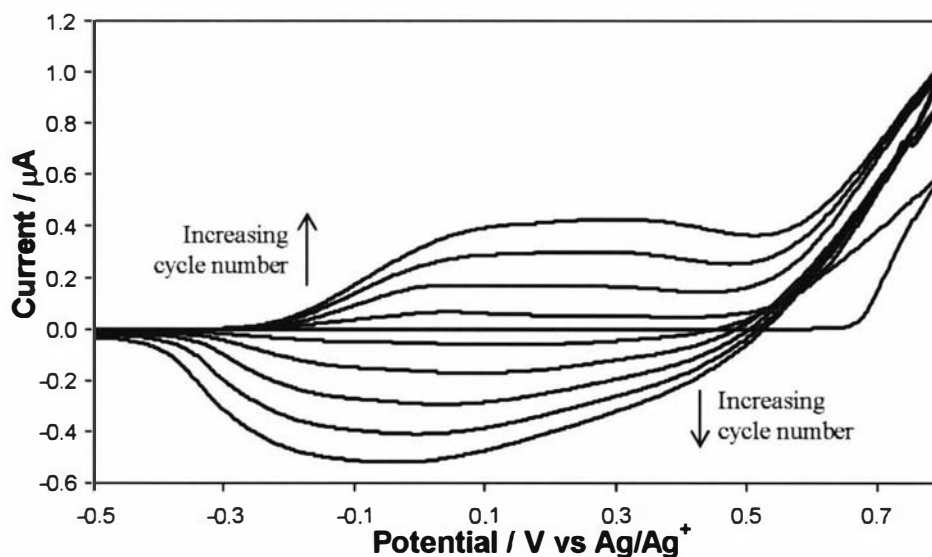


Fig. 5.36. Growth CV of OC₆DASTT (5 mM) on an ITO-coated glass electrode (SA: $\sim 1 \text{ cm}^2$). Electrolyte solution: 0.1 M TBAP/1:1 AN:DCM. Potential limits: -500/+800 mV. 5 cycles. Scan rate: 100 mVs^{-1} .

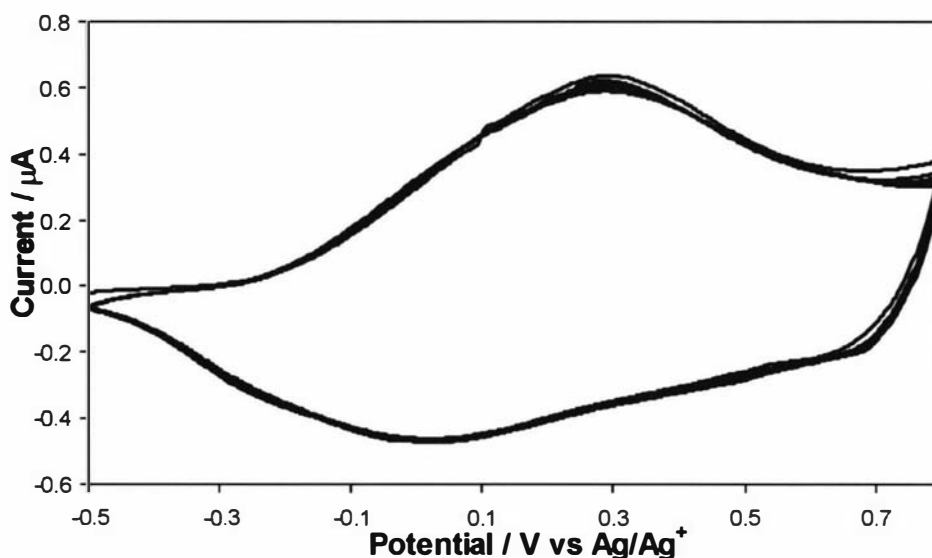


Fig. 5.37. Post growth cycling of polyOC₆DASTT that has been deposited potentiodynamically on an ITO-coated glass electrode (SA: ~1 cm²). Supporting electrolyte: 0.1 M TBAP/AN. Potential limits: -500/+800 mV. 10 cycles. Scan rate: 100 mV s⁻¹.

SEM images of this film in both the neutral and oxidised states are displayed in Fig. 5.38. In contrast to films of electrodeposited oligoSTT that showed both deposition of precipitous material and the formation of crystalline structures (Chapter 3, Section 3.4.3.3), the films are very smooth in both states. An electro-actuation effect is observed with significant folding produced on oxidation of the film. Expansion/contraction of conducting polymer films on oxidation/reduction is commonly observed.^{29,38,174} As discussed by Fuchiwaki *et al.*, this property has been found to originate from (1) insertion/extraction of bulky anions (and possibly associated solvent molecules), (2) conformational change of the polymer film due to delocalisation of the π -electrons, and/or (3) electrostatic repulsion between like-charges.²⁹ The consequence of the folding can be seen in the neutral film with areas which appear raised and detached from the electrode.

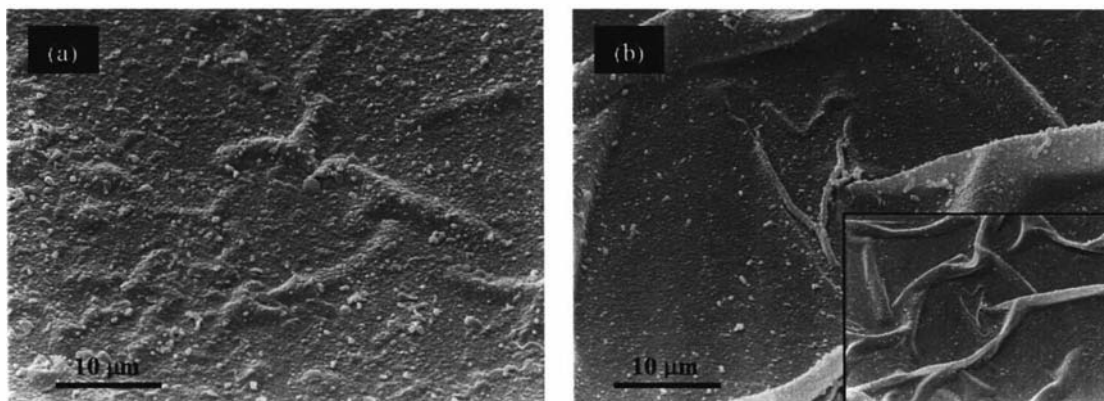


Fig. 5.38. Potentiodynamically deposited films of OC₆DASTT oligomers on ITO-coated glass. (a) Neutral film: x1400, (b) Oxidised film: x1400, inset: x350.

The film on the ITO-coated glass was found to be soluble in chloroform (in the neutral state) and was analysed by MALDI-TOF MS. The spectrum (Fig. 5.39) indicates the presence of oligomers up to $n = 14$, consistent with the MALDI-TOF MS data from the chemically polymerised OC₆DASTT polymer.

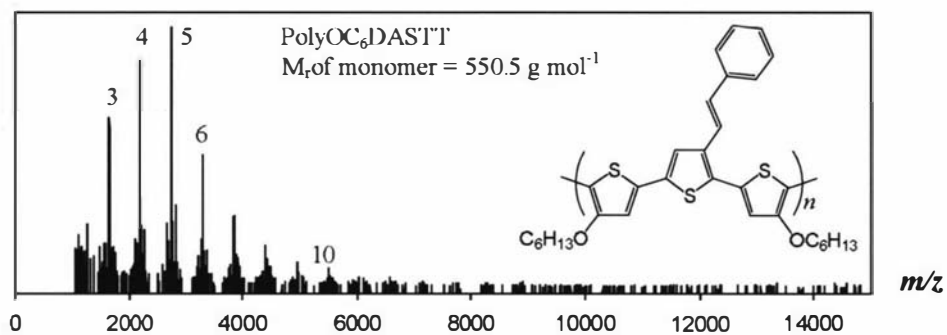


Fig. 5.39. MALDI-TOF MS of polyOC₆DASTT, which was polymerised by potentiodynamic deposition onto an ITO-coated glass electrode. Significant signals are labelled with oligomer length in terms of monomer units (n). Detection suppression limit: 1000 Da.

5.5.4 Electrochemical growth and post-growth analysis of polyOC₁₀DASTT

The CV generated by the growth of polyOC₁₀DASTT is displayed in Fig. 5.40, and reveals an oxidation onset potential of 0.56 V. The lower potential compared to that of OC₆DASTT (0.61 V) under identical experimental conditions, may be caused by the stronger electron-donating properties of the longer alkoxy chains. Further cycles appear similar to those produced by the growth of polyOC₆DASTT (Fig. 5.32), generating a narrow oxidation peak between 0 and 0.1 V, followed by a broad peak at *ca.* 0.3 V, and a peak at *ca.* 0.65 V due to further oxidation of monomer species. Reduction also produces a similarly shaped broad peak to that produced during the growth of PolyOC₆DASTT. A notable difference between the growth of the two alkoxy derivatives is the much larger current generated during the growth of polyOC₁₀DASTT, which shows a maximum current of 9.5 μA after 15 cycles, compared to 2.2 μA produced by polyOC₆DASTT after the same number of cycles. This indicates much faster growth of OC₁₀DASTT and may be a result of the lower oxidation potential of this material.

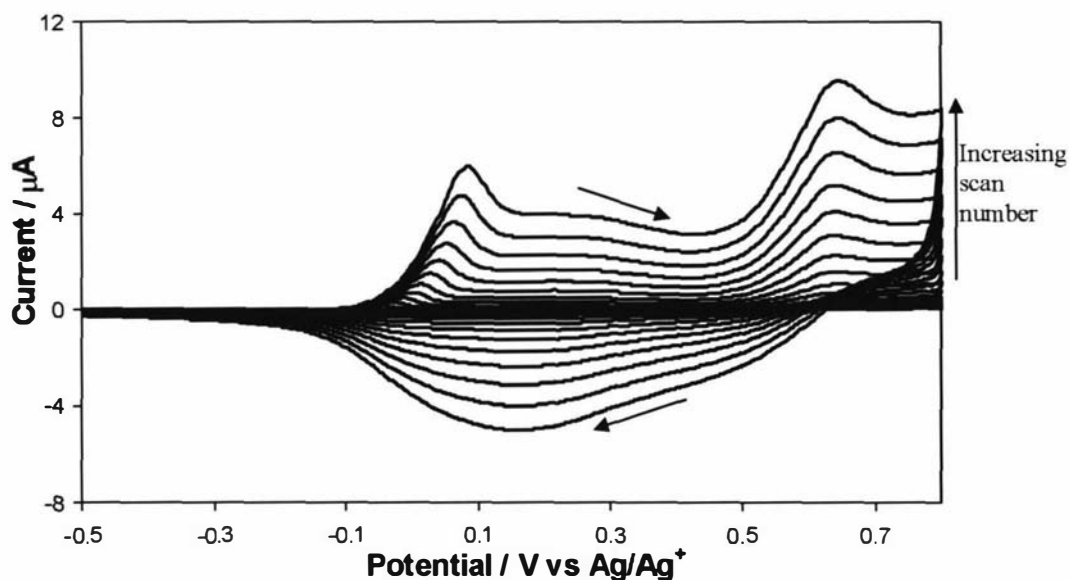


Fig. 5.40. Growth CV of OC₁₀DASTT (5 mM) on a platinum microelectrode (SA: 10 μm^2). Electrolyte solution: 0.1 M TBAP 1:1 AN:DCM. Potential limits: -500/+800 mV. Scan rate: 100 mV s^{-1} .

The post-growth CV of the resulting film in monomer-free solution (Fig. 5.41) displays an oxidation onset potential of -0.02 V and $E_{ox,1}$ peak potential of 0.12 V. These potentials are significantly higher than those observed by potentiodynamically deposited polyOC₆DASTT, which displayed oxidation onset and $E_{ox,1}$ peak potentials of -0.11 and 0.01 V respectively. This indicates a decrease in the mean conjugation length of deposited polyOC₁₀DASTT compared to the polyOC₆DASTT film^{114,127} The remaining oxidation and reduction peaks are very similar, in terms of position and shape, to those produced by potentiodynamically deposited polyOC₆DASTT.

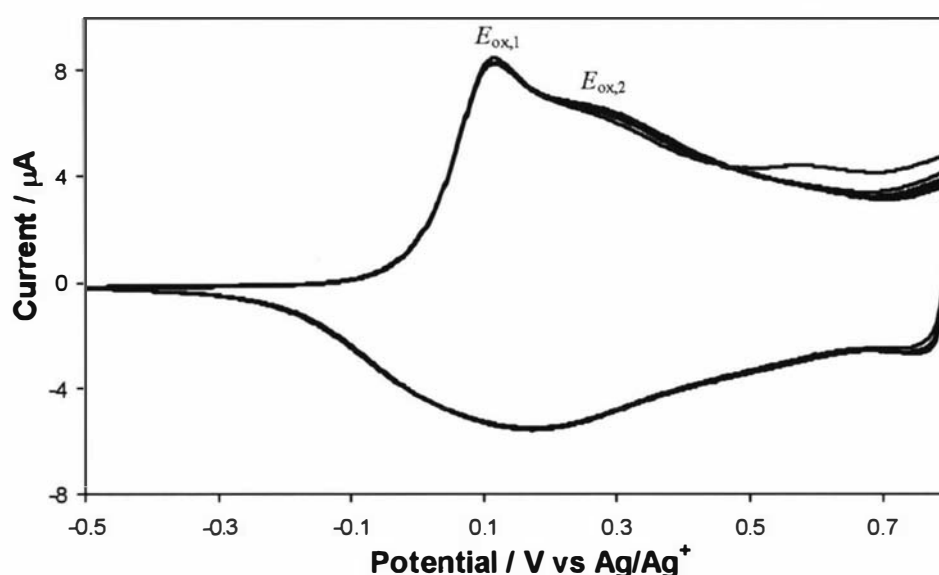


Fig. 5.41. Post growth cycling of polyOC₁₀DASTT which has been deposited potentiodynamically on a platinum microelectrode (SA: 10 μm^2). Supporting electrolyte: 0.1 M TBAP/AN. Potential limits: -500/+800 mV. 10 cycles. Scan rate: 100 mV s^{-1} .

The chronoamperogram for the growth of polyOC₁₀DASTT (Fig. 5.42) shows a steady increase in current with time (after the initial sharp transient due to non-Faradaic current), indicating growth of an electroactive film. The current-time transient is very similar to that shown in the first 14 seconds by the growth of polyOC₆DASTT, indicating a similar rate of deposition, and possibly deposition with a similar morphology.

The post-growth CV of this film is shown in Fig. 5.43. As for the CVs of the polyOC₆DASTT films (Figs. 5.33 and 5.35), this CV of potentiostatically deposited

polyOC₁₀DASTT is similar to the CV of potentiodynamically deposited material (Fig. 5.41), but displays a smaller $E_{ox,2}$ shoulder and a more prominent $E_{red,3}$ peak.

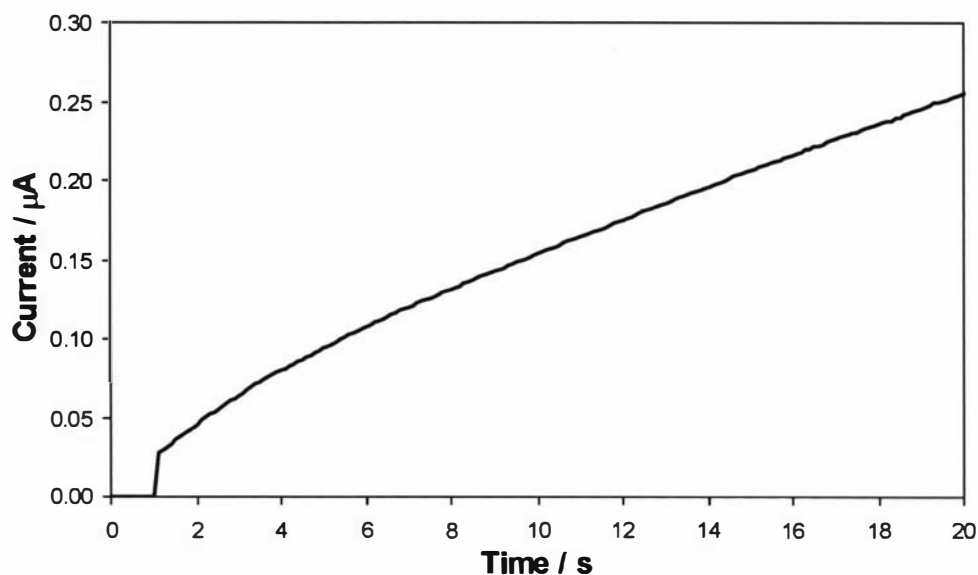


Fig. 5.42. Potentiostatic growth of polyOC₁₀DASTT (5 mM) on a platinum microelectrode (SA: 10 μm^2). Electrolyte solution: 0.1 M TBAP/1:1 AN:DCM. Potential held at -500 mV for 1 s, then stepped to 800 mV for 19 s.

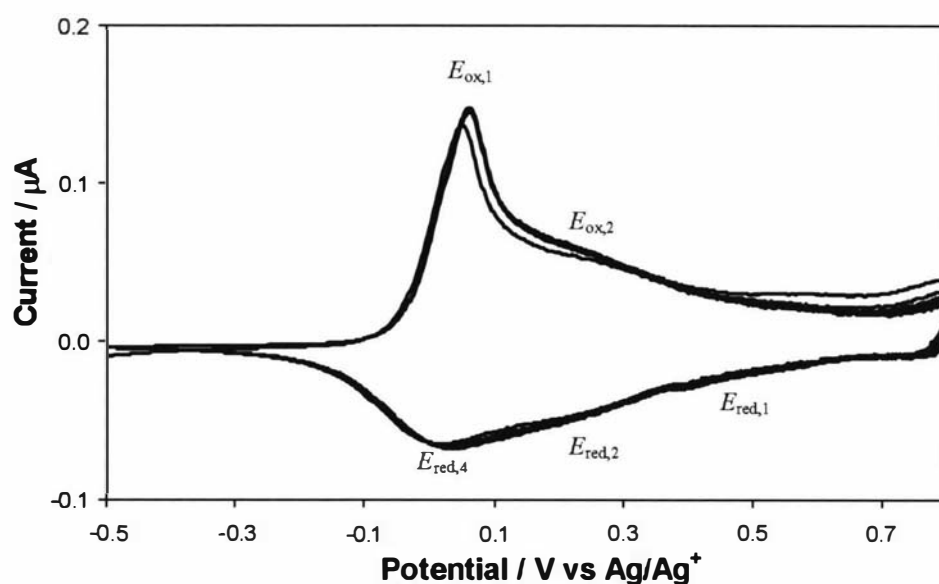


Fig. 5.43. Post growth cycling of polyOC₁₀DASTT which has been deposited potentiostatically on a platinum microelectrode (SA: 10 μm^2). Supporting electrolyte: 0.1 M TBAP/AN. Potential limits: -500/+800 mV. 10 cycles. Scan rate: 100 mV s^{-1} .

The post-growth CVs of the polyOC₆DASTT and polyOC₁₀DASTT films are similar to those reported by Zotti *et al.* of electrochemically grown films of 3'-octyl-4,4''-dipentoxy-2,2':5'2''-polyterthiophene.⁷³ As mentioned previously, the peaks may be due to transitions between the neutral, polaron, bipolaron and quasi-metallic states of the polymer. Further clarification can be gained from the UV-VIS-NIR spectra of the polyOC₁₀DASTT film obtained by varying the potential applied to the film (Fig. 5.44), which shows the different oxidation states of the polymer. An intense polaron/bipolaron band (900 nm) is present between potentials of -0.8 and +0.12 V, consistent with $E_{ox,1}$ in the post-polymerisation CV (Fig. 5.43). At higher potentials, a significant free-carrier tail is displayed in the UV-VIS-NIR spectrum, indicative of the quasi-metallic metallic state. This can be correlated with the broad oxidation peak observed in the post-growth CVs between potentials of ca. 0.1 and 0.5 V ($E_{ox,2}$).

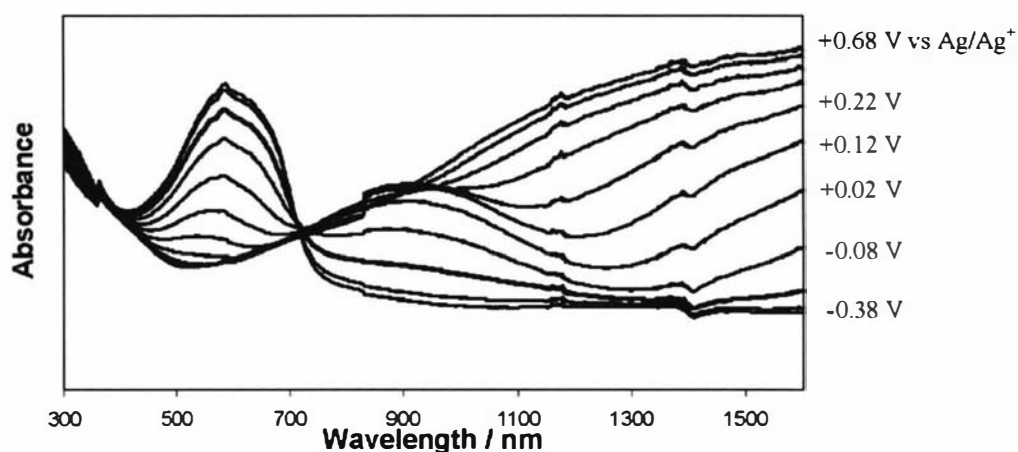


Fig. 5.44. Spectroelectrochemistry of a potentiostatically deposited poly(OC₁₀DASTT) film on ITO-coated glass. The film was initially in a reduced state and was oxidised in steps of 0.1 V. Supporting electrolyte: 0.1 M TBAP/AN. Potentials are reported vs Ag/Ag⁺.

As for polyOC₆DASTT, films of polyOC₁₀DASTT were deposited on ITO-coated glass for analysis by MALDI-TOF MS and SEM imaging. The CV of potentiodynamic growth of polyOC₁₀DASTT (Fig. 5.45) appears similar to that observed for the growth of polyOC₆DASTT on ITO-coated glass (Fig. 5.36), but displays a lower oxidation onset potential of 0.60 V (0.67 V for OC₆DASTT). This is consistent with the lower oxidation onset potential observed by growth of polyOC₁₀DASTT on the platinum microelectrode.

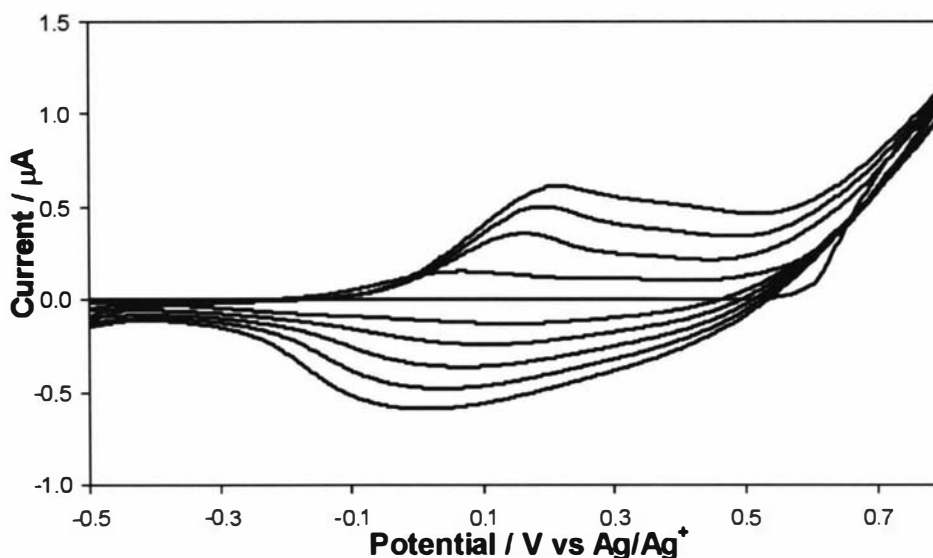


Fig. 5.45. Growth CV of OC₁₀DASTT (5 mM) on an ITO-coated glass electrode (SA: ~1 cm²). Electrolyte solution: 0.1 M TBAP/1:1 AN:DCM. Potential limits: -500/+800 mV. 5 cycles. Scan rate: 100 mVs⁻¹.

The post-growth CV of the resulting film (Fig. 5.46) is similar to that of polyOC₆DASTT, displaying broad oxidation and reduction peaks, but has a higher oxidation onset potential of -0.06 V, compared to -0.22 V. This suggests a decrease in the mean conjugation length of the polyOC₁₀DASTT film compared to the polyOC₆DASTT film,^{114,127} which is also consistent with the observations of growth on the platinum microelectrodes. In comparison to the CV of the cast film of chemically polymerised polyOC₁₀DASTT (Section 5.4.3), the oxidation peak is similar (*ca.* 0.16 V) but the peaks are not as broad, possibly due to a lower polydispersity of the polymer, or a difference in film morphology. A higher oxidation onset potential is also observed (-0.06 V compared to -0.23 V for the cast film), which may again indicate a decrease in the mean conjugation length of the deposited polymer.^{114,127}

The chronoamperogram produced by the potentiostatic growth of polyOC₁₀DASTT on ITO-coated glass is shown in Fig. 5.47, and shows an initial sharp current transient due to non-Faradaic charging of the electrode/solution interface, followed by production of Faradaic current that decreases with time. This decrease in current is most likely due to the depletion of starting material in the vicinity of the electrode, reducing the rate at which polymer can be deposited (and hence current produced).

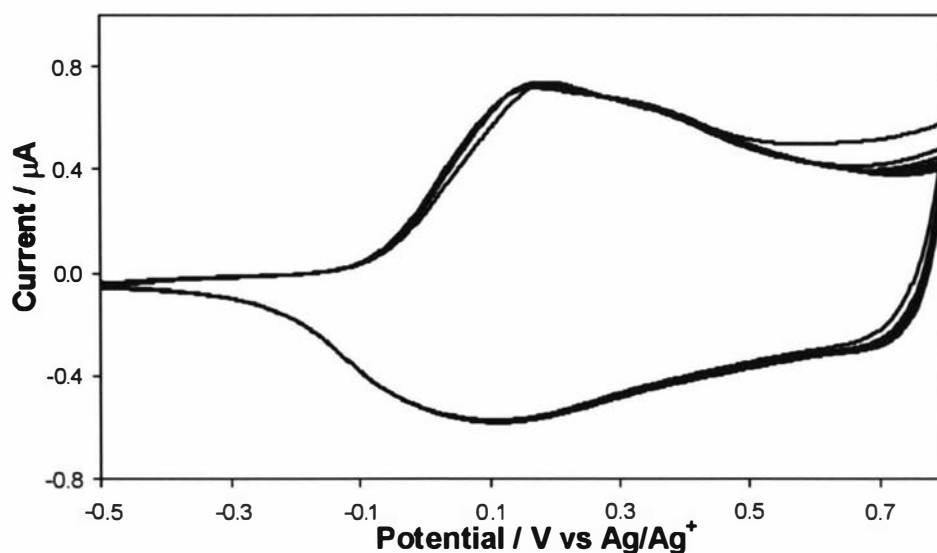


Fig. 5.46. Post growth cycling of poly(OC₁₀DASTT) that has been deposited potentiodynamically on an ITO-coated glass electrode (SA: ~1 cm²). Supporting electrolyte: 0.1 M TBAP/AN. Potential limits: -500/+800 mV. 10 cycles. Scan rate: 100 mV s⁻¹.

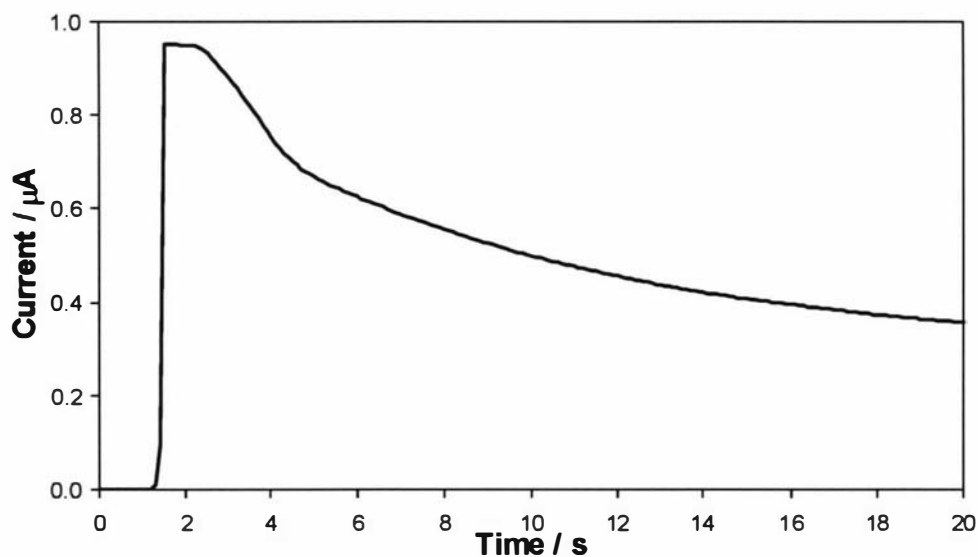


Fig. 5.47. Potentiostatic growth of poly(OC₁₀DASTT) (5 mM) on an ITO-coated glass electrode (SA: ~1 cm²). Electrolyte solution: 0.1 M TBAP/1:1 AN:DCM. Potential held at -500 mV for 1 s, then stepped to 800 mV for 19 s.

The post-growth CV of the resulting film (Fig. 5.48) shows higher oxidation onset and peak potentials (0.11 and 0.42 V respectively) and a higher reduction peak potential (0.15 V) than the post-growth CV of the potentiodynamically deposited film (Fig. 5.46). This may indicate a difference in the mean conjugation length of the

deposited polymer,^{114,127} or be caused by a difference in the morphology of the film, which can affect the mobility of the anion into and out of the polymer film and consequentially oxidation and reduction peak positions.¹⁴⁷

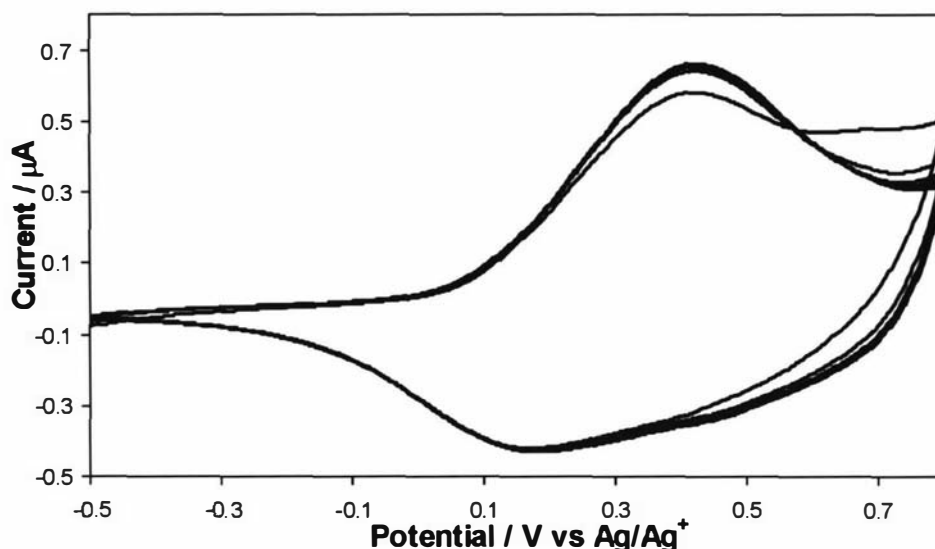


Fig. 5.48. Post growth cycling of polyOC₁₀DASTT that has been deposited potentiostatically on an ITO-coated glass electrode (SA: ~1 cm²). Supporting electrolyte: 0.1 M TBAP/AN. Potential limits: -500/+800 mV. 10 cycles. Scan rate: 100 mV s⁻¹.

SEM images of the polyOC₁₀DASTT films deposited using potentiodynamic and potentiostatic methods are shown in Figs 5.49 and 5.50 respectively. A higher degree of folding is observed in the oxidised films than the films in the neutral state. As for the polyOC₆DASTT films, this is likely to be due to expansion/swelling of the film due to insertion/extraction of bulky anions (and possibly associated solvent molecules), conformational changes of the polymer chains due to delocalisation of the π -electrons, and/or electrostatic repulsion between like-charges.²⁹ SEM images of the potentiostatically deposited film reveals a rougher morphology (with deposition of more precipitous material) and shows a higher degree of folding on oxidation, than the potentiodynamically grown film and the polyOC₆DASTT films. This difference in morphology may be causing the difference in oxidation/reduction peak potentials observed by the post-growth cyclic voltammograms of these films.

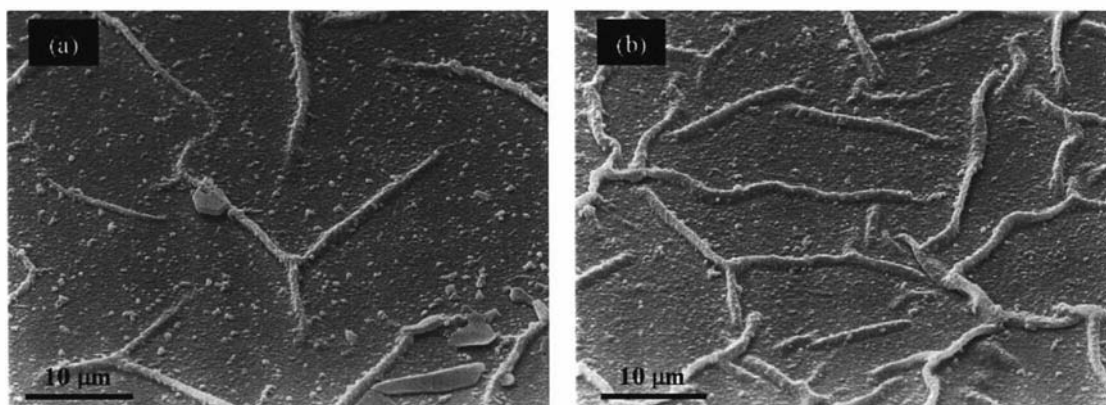


Fig. 5.49. SEM images of potentiodynamically deposited films of OC₁₀DASTT oligomers. (a) Neutral film: x1400, (b) Oxidised film: x1400.

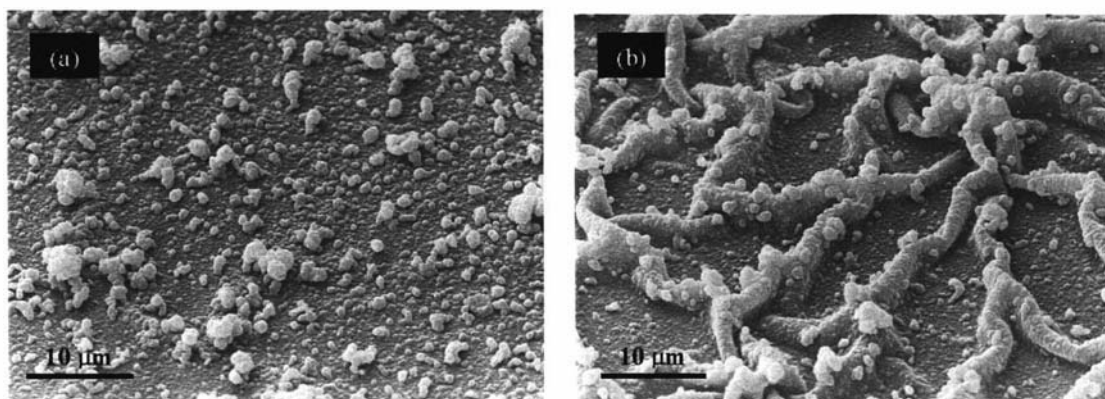


Fig. 5.50. SEM images of potentiostatically deposited films of OC₁₀DASTT oligomers. (a) Neutral film: x1400, (b) Oxidised film: x1400.

A film of polyOC₁₀DASTT was also deposited galvanostatically onto ITO-coated glass by applying a constant current of 2 mA for 30 seconds. SEM images of this film are displayed in Fig. 5.51 and are compared to higher resolution images of the previously grown potentiostatically deposited film (Fig 5.50a). The potentiostatically deposited film appears to consist of a compact film (approximately 300 nm thick). In contrast, the galvanostatically deposited film appears nodular. This is indicative that the films may grow by different types of mechanisms. A similar difference in film morphology was reported by Pringle *et al.* in electrochemically deposited films of polythiophene and polyterthiophene.¹⁴⁷

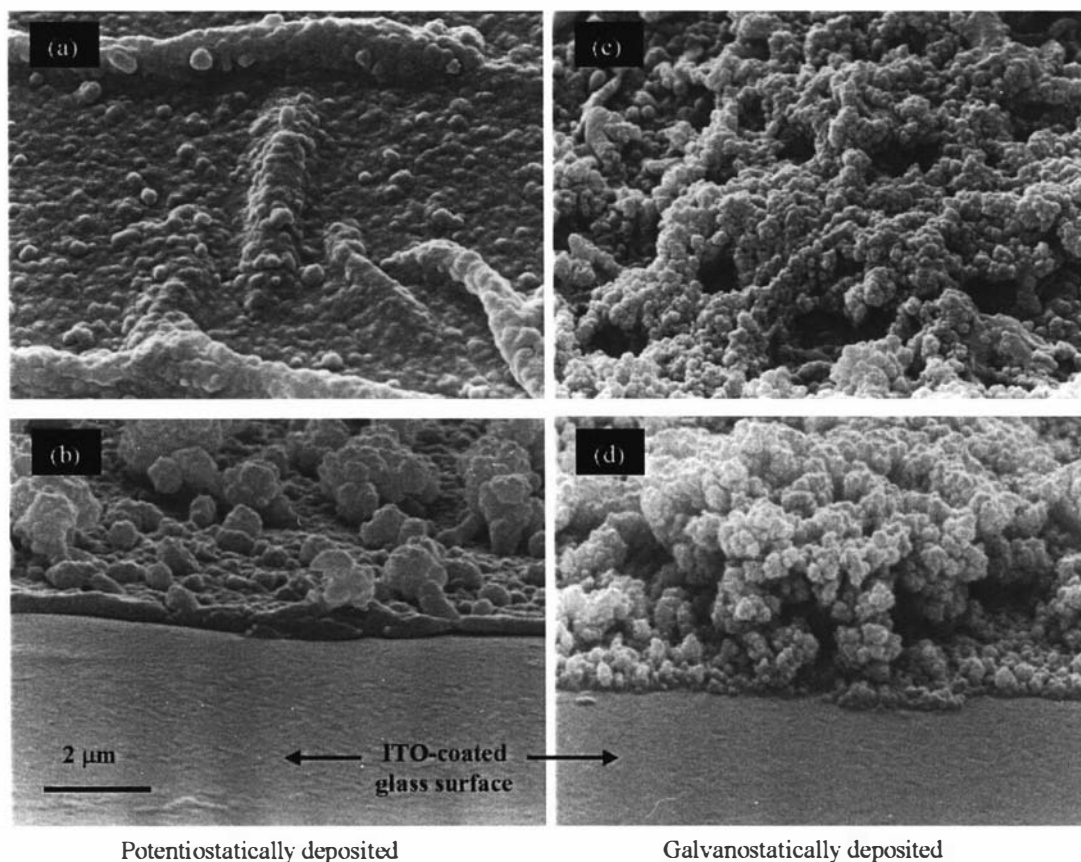


Fig. 5.51. SEM images of (a/b) potentiostatically and (c/d) galvanostatically deposited polyOC₁₀DASTT films on ITO-coated glass. Images (b) and (d) are of the film edges formed at the solution/air interface. All images are displayed at x7000 magnification.

The neutral films were dissolved in chloroform and analysed by MALDI-TOF MS. The spectra (Figs. 5.52, 5.53 and 5.54) appear generally similar to those obtained by the chemically polymerised material (Section 5.4.2) and show the detection of oligomers up to $n = 14$. However, as previously discussed, the large polydispersity apparent by these materials means that the MALDI-TOF mass spectra does not necessarily give an accurate indication of the average chain length and these results should be treated with caution.

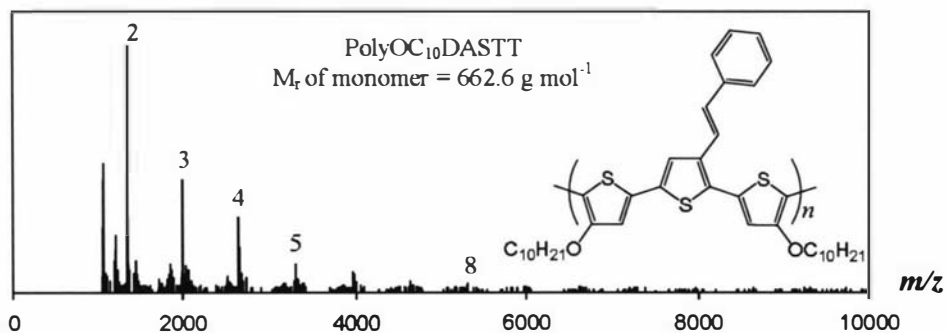


Fig. 5.52. MALDI-TOF MS of polyOC₁₀DASTT, which was polymerised by potentiodynamic deposition onto an ITO-coated glass electrode. Significant signals are labelled with oligomer length in terms of monomer units (*n*). Detection suppression limit: 1000 Da.

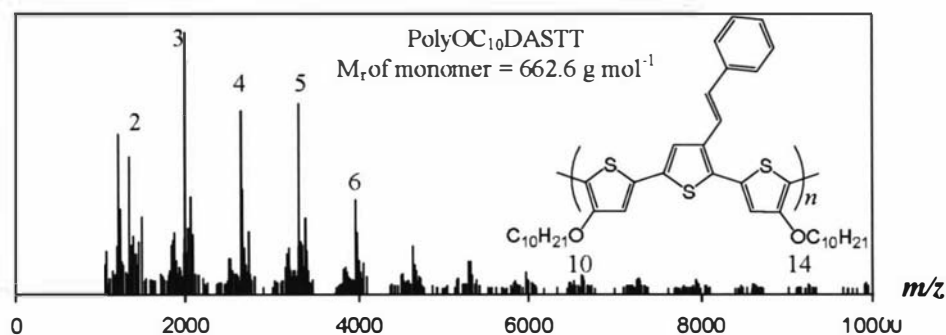


Fig. 5.53. MALDI-TOF MS of polyOC₁₀DASTT, which was polymerised by potentiostatic deposition onto an ITO-coated glass electrode. Significant signals are labelled with oligomer length in terms of monomer units (*n*). Detection suppression limit: 1000 Da.

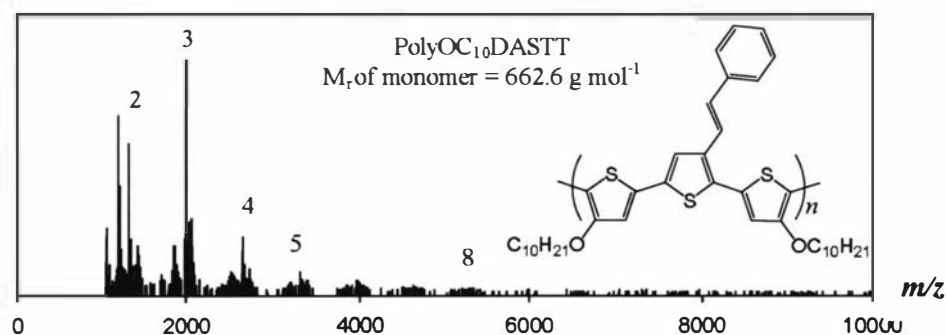


Fig. 5.54. MALDI-TOF MS of polyOC₁₀DASTT, which was polymerised by galvanostatic deposition onto an ITO-coated glass electrode. Significant signals are labelled with oligomer length in terms of monomer units (*n*). Detection suppression limit: 1000 Da.

5.5.5 Summary of electrochemically polymerised material

Films of C₇DASTT, OC₆DASTT and OC₁₀DASTT polymers were successfully grown by potentiostatic and potentiodynamic methods onto platinum microelectrodes. The presence of the alkyl and alkoxy substituents was found to cause a significant reduction in the oxidation onset potential of the monomers compared to STT. The alkoxy substituents were also observed to significantly decrease the oxidation potential of the resulting polymer, consistent with a high stability of these materials in the oxidised state as observed for the chemically polymerised materials.

Films of polyOC₁₀DASTT were observed to produce oxidation onset potentials higher than those of polyOC₆DASTT on both the platinum microelectrode and ITO-coated glass. This suggests a decrease in the mean conjugation length of the polyOC₁₀DASTT films compared to the polyOC₆DASTT films.^{114,127}

Films of these alkoxy-substituted polymers deposited onto ITO-coated glass by potentiodynamic and potentiostatic methods were observed to be reasonably smooth and compact, and showed significant folding on oxidation. In contrast, a film of polyOC₁₀DASTT that was deposited galvanostatically was observed to be nodular.

5.6 Conclusions

C₇DASTT, OC₆DASTT and C₁₀DASTT were successfully polymerised using both chemical and electrochemical methods. Alkyl and alkoxy substitution at the 4 and 4'' positions of styryl-substituted terthiophene was found to significantly reduce the oxidation potential of the monomers investigated in this study. Consequently, the degree of polymerisation was enhanced as evidenced by MALDI-TOF MS and UV-VIS-NIR spectroscopy. As anticipated from previous work by Gallazzi *et al.*⁶² attachment of alkyl and alkoxy chains to the polymer backbone greatly increased the solubility of the (dedoped) product in organic solvents.

Oxidation of OC₆DASTT with iron(III) chloride was found to produce a soluble fraction of 67%, which could be increased to 78% by decreasing the reaction temperature to -10°C. This polymer was found to have an average length of about $n = 11$, and showed a significant free-carrier by UV-VIS-NIR spectroscopy.

An attempt was made to increase the soluble fraction by attachment of C₇-alkyl chains instead of C₆-alkoxy chains. Although this resulted in the production of 100% soluble oligomeric/polymeric material, the product was observed to consist of shorter polymer than obtained by polymerisation of OC₆DASTT. Although polymerisation of C₇DASTT could possibly be enhanced by altering polymerisation conditions such as the oxidant:monomer ratio or the polymerisation temperature, further experimentation was impeded by limited availability of the C₇DASTT monomer. However, it was shown by Sumi *et al.* that polythiophene with a length of 48 thiophene units and substituted by C₈-alkyl chains on two out of every three thiophene units, is only sparingly soluble.¹¹⁴ This suggests that longer chain C₇DASTT polymer may be insoluble.

Since the presence of oxygen atoms at the 4 and 4'' positions appeared to be enhancing polymerisation, consistent with work reported by Giroto *et al.*,¹¹¹ attention was refocused on alkoxy derivatives. It was found that solubility could be increased by the attachment of longer alkoxy chains, as polymerisation of OC₁₀DASTT resulted in a soluble fraction of 97%. No enhancement in polymerisation was shown by addition of

longer alkoxy chains, as an average polymer length of $n = 11$ was estimated for polyOC₁₀DASTT, which is the same as for polyOC₆DASTT. UV-VIS-NIR spectroscopy also indicated that the materials consisted of polymer with a comparable mean conjugation length, by revealing similar λ_{max} due to the $\pi \rightarrow \pi^*$ transition. However, it was found by that cyclic voltammetry a cast film of polyOC₁₀DASTT produced a higher oxidation onset potential than a cast film of polyOC₆DASTT, possibly indicating a slightly lower mean conjugation length.^{114,127} It was also found that electrochemically polymerised polyOC₁₀DASTT films have higher oxidation onset potentials than electrochemically polymerised polyOC₆DASTT films, indicating that the electrochemically polymerised polyOC₁₀DASTT may have a slightly lower mean conjugation length.¹¹⁴

The poorer solubility of alkoxy-substituted polythiophenes compared to analogous alkyl-substituted polythiophenes has been observed by Gallazzi *et al.*⁶² and may be due to higher stability in the oxidised (less soluble) state caused by the better electron-donating properties of the alkoxy substituent. It is also possible that the lower solubility when compared to polyC₇DASTT may be due to the presence of longer oligomers in the alkoxy derivatives, as was shown by MALDI-TOF MS and UV-VIS-NIR spectroscopy.

Experimental conditions during chemical polymerisation, such as the order of addition of reagents (oxidant to monomer or monomer to oxidant), and ethanol impurities were found to have a significant effect on the resulting polymer length, and hence solubility. It was found that addition of the oxidant to monomer produced shorter oligomers, most likely due to a decrease in the initial oxidant:monomer ratio and hence rate of reaction. It was also found that the presence of ethanol decreased the average oligomer length. This may be explained by an effect of the ethanol on the oxidation potential of the iron(III) chloride oxidant.

Oligomers of different lengths were successfully separated using sequential extractions in a series of solvents. The average oligomer length was found to increase with each sequential extraction as determined by MALDI-TOF MS. Cyclic voltammetry revealed that the oxidation onset potential of cast films of the OC₁₀DASTT oligomer/polymer

fractions was also found to reduce with increasing oligomer length. This is consistent with work by Sumi *et al.*¹¹⁴ and Trznadel *et al.*¹²⁷

The CVs of cast films of chemically polymerised polyOC₆DASTT and polyOC₁₀DASTT displayed oxidation and reduction peaks that were much broader than peaks generated by electrochemically polymerised and deposited polyOC₆DASTT and polyOC₁₀DASTT films. This is possibly due to wider polydispersity of the chemically polymerised materials,¹⁵⁹ or a more inconsistent film morphology produced by the casting method.

PolyOC₁₀DASTT films displayed relatively smooth and compact morphologies when deposited by potentiostatic or potentiodynamic methods, and the films showed significant folding due to expansion/swelling of the film on oxidation. In contrast, a polyOC₁₀DASTT film deposited using galvanostatic methods was observed to be very porous.

5.6 Experimental

5.6.1 Reagents and materials

All reagents were used as received from suppliers unless specified otherwise. Chloroform obtained from BDH Laboratory Supplies (London) was used in all reactions unless specified otherwise and contains 0.5 to 1.0% ethanol as a stabiliser. Chloroform obtained from SDS Laboratory Supplies (London), which does not contain ethanol impurities, was used where stated. TBAP (Fluka, Purum) was partially dried under vacuum at 70°C for 48 hrs followed by further drying under vacuum with potassium hydroxide.

Note: As the length of the oligomers can not be accurately measured, the theoretical yield has been calculated without taking into account the loss of α -hydrogens on polymerisation. At most, this leads to an uncertainty of 0.3% in the calculated polymer yields.

5.6.2 Chemical synthesis

Polymerisation of OC₆DASTT

(a) A suspension of anhydrous FeCl₃ (113 mg, 6.77×10^{-4} mol, 4 equiv.) in CHCl₃ (10 mL) was added dropwise over *ca.* 30 mins. to a stirred solution of OC₆DASTT (93 mg, 1.69×10^{-4} mol, 1 equiv.) in CHCl₃ (7 mL). The mixture was stirred for 4 hrs at room temperature. The reaction mixture was then diluted with CHCl₃ (100 mL) and washed with distilled water (2 x 50 ml). The insoluble, oxidised oligomers were reduced by stirring for 24 hrs with 60% hydrazine/H₂O (5 mL). After washing with H₂O (2 x 100 mL), the organic layer and insoluble black mass were separated by filtration to give 24 mg of soluble product. The insoluble fraction was dried, and again stirred with 60% hydrazine/H₂O, added to CHCl₃ (100 mL), washed with H₂O (2 x 100 mL) and the chloroform soluble fraction separated to give a further 39 mg of soluble material, to give a total soluble fraction of 67%.

(b) This reaction was repeated using similar conditions but reducing the oxidant:monomer ratio to 1:1. A suspension of anhydrous FeCl_3 (51 mg, 3.07×10^{-4} mol, 1 equiv.) in CHCl_3 (15 mL) was added dropwise over *ca.* 30 mins. to a stirred solution of OC_6DASTT (169 mg, 3.07×10^{-4} mol, 1 equiv.) in CHCl_3 (15 mL). The mixture was stirred for 60 hrs at room temperature. The reaction mixture was then reduced by stirring with 30% hydrazine/ H_2O for 24 hrs, washed with distilled water (4 x 200 ml) and the organic solvent evaporated. Oligomers from the resulting crude material were extracted using a soxhlet apparatus with methanol to give 52 mg of soluble material followed by hexane to give 9 mg, acetone to give 16 mg, DCM to give 11 mg and finally chloroform to give 5 mg of soluble material, yielding a total soluble fraction of 93 mg (55 %).

(c) The reaction was again repeated but reducing the temperature to -10°C . A suspension of anhydrous FeCl_3 (121 mg, 7.27×10^{-4} mol, 4 equiv.) in CHCl_3 (10 mL) was added dropwise over *ca.* 30 mins. to a stirred solution of OC_6DASTT (100 mg, 1.82×10^{-4} mol, 1 equiv.) in CHCl_3 (8 mL). The mixture was stirred for 4 hrs over a salt/ice bath (-10°C) while constantly being flushed with argon. The reaction was then diluted with CHCl_3 (100 mL) and washed with distilled water (4 x 200 ml). The insoluble, oxidised oligomers were reduced by stirring for 24 hrs with 60% hydrazine/ H_2O (5 mL). The organic layer and insoluble black mass were then washed with H_2O (4 x 200 mL), and the organic solvent evaporated using rotatory evaporation to give the crude oligomeric material (97 mg of a black precipitate and copper film). Soxhlet extractions of 90 mg of the crude material were carried out using methanol, followed by hexane, acetone, dichloromethane and chloroform. The left-over insoluble material (45 mg) was dried and further reduced to give another 28 mg of soluble material, affording a total of 78% soluble material.

Polymerisation of C_7DASTT

A suspension of anhydrous FeCl_3 (183 mg, 1.10×10^{-3} mol, 4 equiv.) in CHCl_3 (10 mL) was added dropwise over *ca.* 30 mins. to a stirred solution of C_7DASTT

(150 mg, 2.75×10^{-4} mol, 1 equiv.) of C₇DASTT in CHCl₃ (7 mL). The mixture was stirred for 4 hrs at room temperature under argon to form a fine black precipitate. The mixture was then washed with H₂O (2 x 100 mL), added to 60% hydrazine/H₂O (50 mL) and stirred overnight. The orange organic layer was separated and washed with water (3 x 100 mL) to give 150 mg of a red, fully soluble gum. Soxhlet extractions of 110 mg of this material were completed using methanol, followed by hexane, acetone, dichloromethane and chloroform. The extraction was continued until no further colour was evident in the extracting solvent.

Polymerisation of OC₁₀DASTT

(a) A suspension of anhydrous FeCl₃ (807 mg, 4.83×10^{-3} mol, 4 equiv.) in CHCl₃ (80 mL) was added dropwise over *ca.* 30 mins to a stirred solution of OC₁₀DASTT (800 mg, 1.21×10^{-3} mol, 1 equiv.) in CHCl₃ (64 mL). The mixture was stirred for 4 hrs over a salt/ice bath (-10°C) while constantly being purged with argon. 43% hydrazine/H₂O (50 mL) was then added to the solution and the mixture stirred for a further 24 hrs. The organic layer (containing a black precipitate) was separated and washed with H₂O (6 x 400 mL) and the organic solvent evaporated to give the crude oligomeric material. This was further washed with methanol using soxhlet extraction apparatus. Using soxhlet extraction apparatus, oligomeric material was then extracted with hexane to give 106 mg of soluble material, followed by CHCl₃ to give a further 378 mg of soluble material. The remaining insoluble material was dried, stirred with 43% hydrazine/H₂O (50 mL) for 5 days followed by 3 days with chloroform added, washed and extracted with chloroform to give 91 mg of soluble material. A third reduction yielded 197 mg to give a total soluble yield of 97%. 50 mg of chloroform soluble material (but not hexane soluble) was extracted in acetone to give 2 mg of soluble material followed by DCM to give 13 mg and chloroform, affording a further 35 mg of soluble material.

(b) This reaction was repeated under similar conditions but the monomer was added to the oxidant. A solution of OC₁₀DASTT (100 mg, 1.51×10^{-4} mol, 1 equiv.) in CHCl₃ (8 mL) was added dropwise over *ca.* 30 mins. to a stirred suspension of

anhydrous FeCl_3 (101 mg, 6.04×10^{-4} mol, 4 equiv.) in CHCl_3 (10 mL). The mixture was stirred for 4 hrs over a salt/ice bath (-10°C) while constantly being purged with argon. The reaction mixture was then washed with water, reduced and dried under vacuum. The resulting black powder was stirred for 24 hrs with 60% hydrazine/ H_2O (30 mL) and then added to 200 mL of CHCl_3 and stirred for a further 24 hrs. The organic layer (containing a black precipitate) was separated, washed with H_2O (6 x 200 mL) and the organic solvent evaporated to give the crude oligomeric material. Soxhlet extraction in hexane followed by chloroform gave a soluble product of 41 mg. The remaining insoluble material was dried, stirred with 60% hydrazine/ H_2O (5 mL) for 2 days followed by 24 hrs with chloroform added, washed and extracted with chloroform to give a further 3 mg of soluble material, yielding a total soluble fraction of 44%.

(c) The reaction was again repeated, but using solvent without ethanol impurities. A suspension of anhydrous FeCl_3 (3.228 g, 1.933×10^{-2} mol, 4 equiv.) in CHCl_3 (320 mL, SDS laboratory supplies, London) was added dropwise (over *ca.* 30 mins.) to a stirred solution of $\text{OC}_{10}\text{DASTT}$ (3.200 g, 4.83×10^{-3} mol, 1 equiv.) in CHCl_3 (256 mL, SDS laboratory supplies, London). The mixture was stirred for 4 hrs over a salt/ice bath while constantly being purged with argon. 10% hydrazine/ H_2O (240 mL) was then added to the solution and the mixture stirred for a further 24 hrs. The organic layer (containing a black precipitate) was separated and washed with H_2O (7 x 500 mL) and the organic solvent evaporated to give the crude oligomeric material. This polymerisation process was repeated, the crude products combined and further washed with methanol using soxhlet extraction apparatus. Using soxhlet extraction apparatus, oligomeric material was then extracted with acetone to give 280 mg of soluble material, followed by DCM to give 753 mg, THF to give 825 mg and chloroform to give 1320 mg of soluble material. The remaining insoluble material was dried and ground to a powder using a blender. The powder was stirred with 10% hydrazine/ H_2O (240 mL) for 24 hrs followed by 24 hrs with chloroform added, washed and extracted with chloroform to give 562 mg soluble material. A third reduction performed in the same way yielded a further 143 mg to give a total soluble yield of 61%. The remaining insoluble material weighed 3.040 g.

5.6.3 Electrochemical synthesis

The electrochemical synthesis of the polymers and their electrochemical analysis were performed with an Ecochemie Autolab system PGSTAT30 potentiostat/galvanostat service, with the associated General Purpose Electrochemical System (GPES) software. Experiments involving microelectrodes were carried out in a Faraday cage.

For analysis of growth and polymer redox processes, either a platinum microelectrode (surface area = $10 \mu\text{m}^2$) consisting of a metal wire sealed within a tempered glass body with a polished, flat end, or a platinum disc electrode (surface area = 1.8mm^2) consisting of a metal rod fitted into a KEL-F polymer sleeve was used. These were both obtained from Bioanalytical Systems Inc., Indiana, USA. Prior to each set of experiments, the electrode was polished with $0.01 \mu\text{m}$ alumina powder (PK-4 polishing kit, Bioanalytical Systems Inc., Indiana, USA). It was then rinsed with de-ionized water followed by acetone then acetonitrile and allowed to dry. Films were also grown or cast onto ITO (indium tin oxide) coated glass (sheet resistance $\leq 10 \Omega \text{cm}^{-2}$) which is transparent between 300 nm and 1600 nm for spectroscopic and microscopic analysis, and for use in photovoltaic cells.

The concentration of monomer for all solutions was 5 mM and an electrolyte concentration of 100 mM. A solvent that allows solubility of the monomer without solvation of the deposited polymerised material is needed to deposit polymer on the electrode surface. A 1:1 mixture of AN:DCM was found to have the required intermediate relative permittivity for the materials in this chapter. All solutions were degassed by sonication prior to uses.

Polymers were electrochemically deposited using both potentiostatic and potentiodynamic methods. Anodic limits were chosen just above the potential at which material was observed to deposit, and cathodic limits just below the reduction potential of the polymer. A scan rate of 100mV s^{-1} was used for all growth cyclic voltammetry. Fifteen cyclic voltammograms were used to grow the polymer. The anodic limit was also used for potentiostatic growth where the chosen potential was held for 20

seconds. Growth of polyOC₁₀DASTT onto ITO-coated glass by constant current methods was performed at 2 mA for 30 seconds. All electrochemical experimentation was performed at a controlled temperature of 22°C.

5.6.4 MALDI-TOF MS

Spectra have been recorded in the linear mode in this study due the higher sensitivity of this technique. Dithranol was used as the matrix. Chloroform was used as the solvent for both the sample and the matrix. The sample was prepared by mixing a sample solution (~500 µg mL⁻¹) monomer solution with equal volume of a 10 mg mL⁻¹ matrix solution. 100 µL of this mixture was spotted onto a target plate. Detection has been suppressed below either 500 or 1000 *m/z* units to prevent overload of the detector by matrix ions.

5.6.5 UV-VIS-NIR instrumentation and spectroelectrochemistry

UV-VIS-NIR spectra were obtained using a Shimadzu UV1601 spectrometer, scanning over the range 300-1500 nm. Neutral samples that were measured in solution were dissolved in chloroform. They were oxidised with excess Cu(ClO₄)₂·H₂O.

Spectroelectrochemistry was carried out using a Shimadzu UV1601 spectrometer and the potential controlled with a BAS CV27 voltammograph. A polymer film on ITO-coated glass was used as the working electrode, with a coiled platinum wire as the counter electrode and silver wire as the reference electrode. The electrolyte consisted of 0.1 M TBAP in acetonitrile. The potential was varied from reducing to oxidising, the reducing limit determined from the post-polymerisation CV of the film. Oxidation was continued until no apparent spectral changes were observed.

5.6.6 SEM imaging

SEM analysis was performed by Mr. Doug Hopcroft at HortResearch, Palmerston North, New Zealand. Samples were mounted on an aluminium specimen stub, sputter coated with approximately 100-150 nm of gold and studied using a Cambridge 250 Mk3 Scanning Electron Microscope in the secondary electron mode. Images were recorded on Ilford FP4 black and white film at the chosen magnifications and printed on Kodak multigrade paper.

Chapter 6

Device Fabrication and Analysis

6.1 Introduction

Soluble materials provide much easier processing since they can be spin-coated, electrospun and cast onto a range of conductive and non-conductive substrates, including fabrics. This provides the possibility of preparing a wide variety of conducting polymer-based electrodes, which would be of use in photovoltaic, actuator (artificial muscle) and organic battery applications. The use of polymeric materials allows the production of light-weight, flexible and cheap devices.¹⁷⁵ Therefore the soluble materials developed in Chapters 3 to 5 were examined for their suitability for use as photovoltaic and battery electrodes, and in actuators.

All of these applications require materials that exhibit good charge transport. For example, organic photovoltaic materials are typically required to be good hole-transport materials, a feature of polythiophenes. In addition, both batteries and actuators require active materials for electrodes that can undergo efficient and sustainable redox cyclability. The electrochemical efficiency in all of these applications is reliant on interfacial charge transfer, and this is most effective with high surface area electrodes.

The aim of the work in this thesis has been to produce conducting polymers with both tailored electronic and physical properties through the use of the appropriate functional groups. The efficacy of the functionalised materials in devices could allow an assessment of the success of this approach. Thus, photovoltaic hole transport may be enhanced by the styryl functionalities of the donor-acceptor dimers in polymers produced in Chapters 3 and 4, and the ready oxidation of polymers such as polyOC₁₀DASTT suggests that it may be useful for battery applications.

Given the promise of some of these materials, the aim of the work in this chapter was to undertake a preliminary study of these functionalised polythiophenes to determine whether the styryl functionality would be advantageous for photovoltaics, actuation or redox cycling in batteries. In addition, the solubilisation of the styryl functionalised materials by the alkoxy substituents provided the opportunity to produce fibrillar, opal and fibre high surface area structures, which may also enhance electrochemical efficiency in the devices.

6.2 Photoelectrochemical cells

6.2.1 Introduction

At present, most commercial photovoltaic (solar) devices are made from inorganic semiconductors.^{176,177} These devices contain inorganic materials which are toxic, expensive and/or have limited availability. Organic semiconductors provide an alternative to silicon devices with the prospect of cheap solar devices. Polythiophene derivatives are often studied for use in organic photovoltaic cells since their properties can be readily tailored through functionalisation, and are typically environmentally stable.^{91,132,178} However, unless substituted with alkyl or alkoxy substituents, polythiophene and its derivatives are often difficult to process and frequently require polymerisation and deposition by electrochemical methods.

Conducting polymers have been incorporated into two types of all-organic photovoltaic devices, Schottky (solid state) or photoelectrochemical (PEC) devices.^{175,176} Schottky devices require sophisticated fabrication techniques. Photoelectrochemical devices are simple to make and were chosen in this study as a medium to provide insight into the utility of these materials for photovoltaics.

PEC cells use a liquid electrolyte to transfer charge carriers between the active layer and the cathode. The active layer of PEC cells may consist of either a dye on an inorganic semiconductor or semiconducting polymer (referred to in this study as polymer-based PEC cells).¹³² Although inorganic-based PEC devices have energy conversion efficiencies of up to 11%,¹⁷⁹ polymer-based PEC cell efficiencies typically lie in the range 0.01 – 0.1%.¹⁸⁰ This is due to low charge mobility in the polymer and electrolyte, poor exciton generation and/or large interface distances (exceeding exciton diffusion lengths).

Polythiophene derivatives are often investigated for use as the active material in solar devices as they are typically good hole transport materials.¹⁸¹ Regioregular poly(3-alkylthiophene), for example, has been shown to produce relatively high hole mobilities of $0.1 \text{ cm}^2 \text{ V}^{-1} \text{ s}^{-1}$.^{182,183} One approach to increase energy conversion efficiency (ECE)

values is to attach functional groups to the polymer backbone with the purpose of broadening the range of wavelengths that is absorbed by the active layer.¹⁰⁴ This can be achieved by attachment of substituents that affect the electron density in the polymer and reduce the bandgap between the HOMO and LUMO energy levels. Greenwald *et al.* found that photocurrents of polythiophene-based cells can be increased by attaching electron-withdrawing groups, such as nitrobenzene, to the polymer backbone.⁹⁰

In 2001, Cutler *et al.* reported an ECE value of 0.0153% for a PEC device using an electrodeposited film of polyterthiophene.⁹¹ They also investigated the photovoltaic properties of a device comprising NO₂STT homopolymer, and copolymer with terthiophene. Although, these materials gave slightly better open circuit voltages (V_{OC}), very low short circuit currents (I_{SC}) meant their ECE values were inferior to those obtained for polyterthiophene. Cutler *et al.* also reported photovoltaic responses for devices comprising films of styrylthiophene/bithiophene copolymers (with a ratio of thiophene units to bithiophene units of ~1:8) that were substituted at the *para*-position on the phenyl ring by dimethylamino, cyano and nitro substituents.⁷⁹

A selection of similar styryl-substituted polythiophene materials that were discussed in Chapters 3-5 were investigated for photovoltaic activity. Soluble, chemically synthesised NMe₂STT dimer, STV dimer and polyOC₁₀DASTT were incorporated into PEC devices by spin-coating and casting methods. PEC devices incorporating electrochemically deposited films of the STV series (Chapter 4) were also assembled and tested to investigate this lower band-gap material and compare the effect of the electron withdrawing/donating substituents.

This work was carried out in the Intelligent Polymer Research Institute (IPRI) at the University of Wollongong, with the assistance of Dr. Jun Chen and Mr. George Tsekouras.

6.2.2 Device assembly and materials

Photoelectrochemical devices were assembled by sandwiching an I/I_3^- liquid electrolyte between a platinum sputter-coated ITO-coated glass electrode (cathode) and a polymer-coated ITO-coated glass electrode (anode) as shown in Fig. 6.1. A parafilm gasket was used to contain the liquid electrolyte and separate the electrodes to prevent short circuiting.

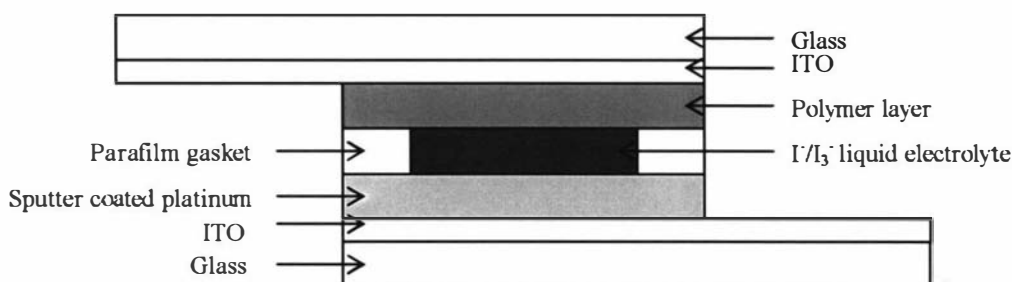


Fig. 6.1. Construction of a PEC cell.

The counter electrode (cathode) was produced by sputter coating a thin (10 Å) layer of platinum onto ITO-coated glass. The platinum is necessary because the I/I_3^- redox process is irreversible on ITO electrodes.¹⁸⁴ The polymer was deposited onto ITO-coated glass either electrochemically from the monomer, or by casting or spin-coating the soluble polymer. The devices were tested in a large dark box containing a broad spectrum halogen lamp (500 W m^{-2}). The $I - V$ data was obtained and analysed as described in Chapter 2, Section 2.8.

Films of oligoNMe₂STT (Chapter 3), polyOC₁₀DASTT (Chapter 5) and the oligo(terthiylenevinylene) materials (Chapter 4) were prepared by casting and/or spin-coating chemically polymerised materials and/or by electrochemical deposition.

6.2.3 NMe₂STT oligomer films

Films of NMe₂STT oligomers were prepared both by drop-casting from a solution of chemically dimerised material (synthesis and characterisation discussed in Chapter 3, Section 3.3), and by electrochemical deposition.

A solution containing NMe₂STT dimer (in the neutral state) was cast onto ITO-coated glass to give a very uneven, thin red film. The $I - V$ curve for this film is given in Fig. 6.2.

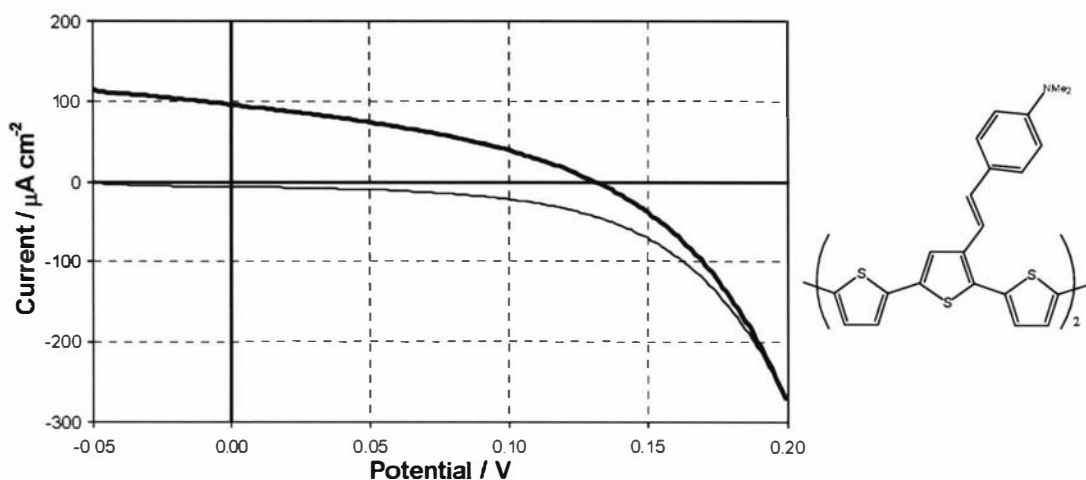


Fig 6.2. $I - V$ curve of a cast film of chemically dimerised NMe₂STT in the dark (thin line) and under illumination (thick line).

This material is somewhat soluble in the electrolyte solvent and the film was observed to slightly dissolve. Even so, it gave an ECE of 0.0089% as determined from V_{OC} , I_{SC} and FF (Table 6.1). The photoelectric responses reported for a *p*-dimethylaminostyryl-substituted thiophene/bithiophene copolymer synthesised by Cutler *et al.*⁷⁹ are shown for comparison. Although the FF is identical for both cells, the I_{SC} and ECE are much better for the cast film.

A film of oligoNMe₂STT was electrochemically deposited using a constant potential (and then reduced to a neutral state) and tested to compare to the chemically synthesised cast film. This electrochemically deposited film was not soluble in the electrolyte solvent. The insolubility of the electrochemically deposited film in comparison to the chemically prepared and cast film could be due to a number of reasons. The electrochemically synthesised film may be composed of oligomers which are longer (and therefore less soluble) than the dimer oligomers used for the cast film. Alternatively, the reduced solubility could be a result of differences in the

polymerisation route (Sections 3.3.1 and 3.4.2, Chapter 3), including perhaps crosslinking of chains.

A cell comprising this electrochemically deposited film showed no detectable photovoltaic activity. The lack of photovoltaic activity of the electrochemically deposited films in comparison to the cast film could also be a result of differences in oligomer length and defects. In addition, casting the film rather than forming it electrochemically could result in a difference in film morphology, possibly influencing the electrical contact with the ITO and/or nature of the polymer-electrolyte interface. Some thiophene oligomers with a well-ordered closely-packed structure have been shown in some cases to possess greater charge carrier mobility.¹⁸⁵

Table 6.1. Photovoltaic characteristics of a cast film of NMe₂STT dimer

Material	Preparation method	V_{OC} (mV)	I_{sc} ($\mu\text{A cm}^{-2}$)	FF (%)	ECE (%)
NMe ₂ STT dimer	Drop-cast	132	95.6	35	0.0089
OligoNMe ₂ STT	Electrochemical	—	—	—	—
Co-polymer ^a	Electrochemical	146	24.6	35	0.0030

^aDimethylaminostyryl-substituted thiophene/bithiophene copolymer synthesised by Cutler.⁷⁹

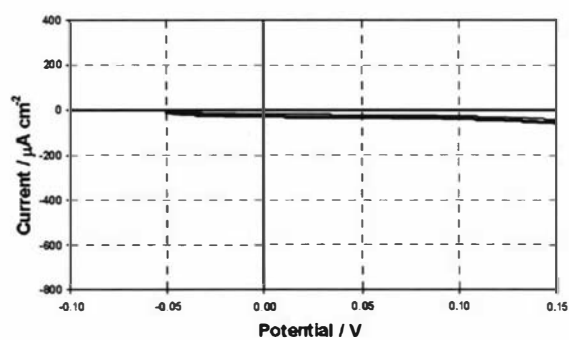
6.2.4 PolyOC₁₀DASTT films

Films of polyOC₁₀DASTT were prepared by casting and spin-coating chemically polymerised materials (polymerised as described in Chapter 5 and washed with hexane to remove short oligomers with $n < 3$), and by electrochemical methods (cyclic voltammetry and potentiostatic) and assembled into PEC devices. However, none of the devices showed any detectable photovoltaic activity. This is possibly due to a partial oxidation of this material. Cutler *et al.* reported that PEC cells incorporating polyterthiophene perform best when the polymer is fully reduced.⁹¹

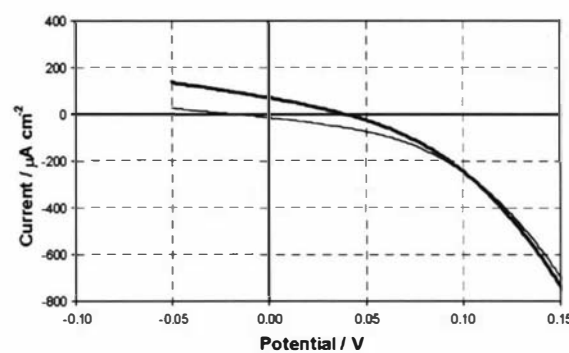
6.2.5 Styryl thienylenevinylene derivatives

There has been reported interest in polythienylenevinylene derivatives for use in photovoltaic devices due to their low band gaps, which allows their spectral absorption to be extended into the infra-red.¹⁰⁴ Films of NO₂STV, CNSTV, STV, OMeSTV and NMe₂STV oligomers were electrodeposited onto ITO-coated glass and then reduced. The $I - V$ curves obtained from PEC cells using these films are displayed in Fig. 6.3, except for the polySTV film, which was observed to dissolve in the electrolyte solvent. Both the curves obtained in the dark and in the light are displayed. In an ideal cell, the scan obtained in the dark should pass through the origin. However, all the scans obtained in the dark have an I_{SC} at a negative value indicating the current is moving in the opposite direction to the desired cell current. As this negative current is produced in the dark, without any light energy source, it must be due to a non-photochemical reaction. A possible reaction that could be occurring is oxidation or reduction of the polymer film by the I/I_3^- electrolyte. A deterioration of TiO₂-bound STV derivative has been observed by Campbell in dye-sensitised PEC devices.¹⁸⁶

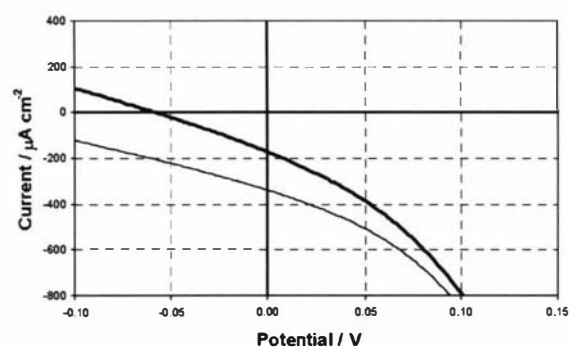
The difference in current (ΔI_E) between the light and dark scans ($I_{light,E}$ and $I_{dark,E}$ respectively) gives an indication of photovoltaic activity. It appears that there is an increase in photovoltaic activity at short circuit current (ΔI_{SC}) on illumination, with increasing electron-withdrawing capability of substituent (Fig. 6.4). This may be due to the increased charge separation between the polymer layer and platinum counter electrode caused by the more electron-withdrawing substituents.⁹¹



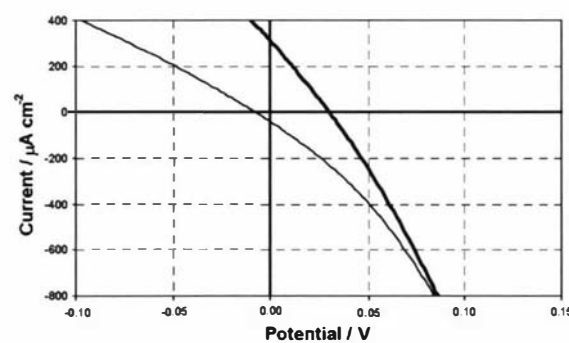
(a) NMe₂STV



(b) OMeSTV



(c) CNSTV



(d) NO₂STV

Fig. 6.3. $I-V$ curves of electrochemically grown films of styryl thienylenevinylene derivatives, (a) NMe₂STV, (b) OMeSTV, (c) CNSTV and (d) NO₂STV, in the dark (thin line) and under illumination (thick line).

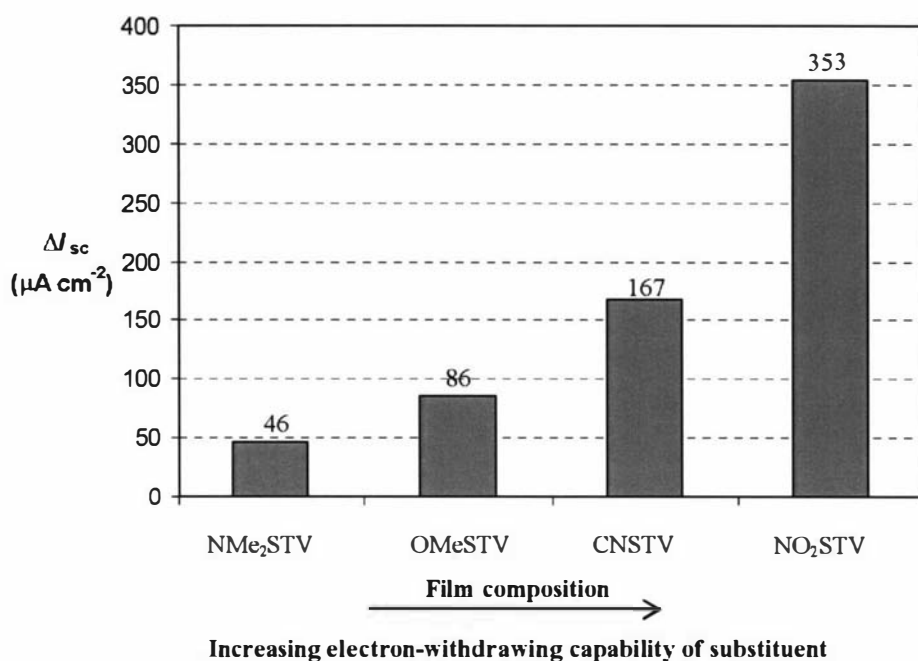


Fig. 6.4. The relationship between the photovoltaic activity at I_{sc} (ΔI_{sc} , where $\Delta I_{sc} = I_{light,sc} - I_{dark,sc}$) and the electron-withdrawing capability of substituents on films of thienylenevinylene oligomers.

The device comprising oligoNO₂STV produces the highest short circuit current of this series. This is consistent with results obtained by Greenwald *et al.*⁹⁰ on substituted polythiophenes, and may be accounted for by an increase in charge separation due to the electron-withdrawing effect of the nitro group.⁹¹ However, it does display a low open circuit voltage and low FF compared to terthiophene and NO₂STT films (Table 6.2).

Table 6.2. Photovoltaic characteristics of PEC devices constituting nitrostyryl-substituted terthiophene and thienylenevinylene oligomer films.

Material	Preparation method	V_{oc} (mV)	I_{sc} ($\mu\text{A cm}^{-2}$)	FF (%)	ECE (%)
Terthiophene ^a	Electrochemical	142	141.8	35	0.0513
NO ₂ STT ^a	Electrochemical	166	21.6	48	0.0037
NO ₂ STV	Electrochemical	31	312.5	25	0.0049

^aResults obtained by Cutler *et al.*⁹¹

Since the electrodeposited oligoSTV film was observed to dissolve in the electrolyte solution, a cast film of chemically synthesised STV dimer (in the neutral state) was tested for photovoltaic activity. In comparison to the electrochemically synthesised

film, this film did not dissolve in the electrolyte solution, and the $I - V$ curve of a PEC device incorporating this film is shown in Fig. 6.5. Significant photovoltaic activity is observed with an increase in I_{SC} on illumination of $367 \mu\text{A cm}^{-2}$ (Table 6.3). As this is greater than might be expected from the electrochemically deposited STV material ($\sim 125 \mu\text{A cm}^{-2}$ by interpolation of Fig. 6.4), it appears that there may be an improvement in photovoltaic activity with a cast film rather than an electrodeposited film, as was observed for the cast and electrochemically deposited NMe_2STT films (Section 6.2.3).

Table 6.3. Photovoltaic characteristics of a cast film of chemically synthesised STV dimer.

Material	Preparation method	V_{oc} (mV)	I_{sc} ($\mu\text{A cm}^{-2}$)	FF (%)	ECE (%)
STV dimer	Casting	94	237	32	0.0014

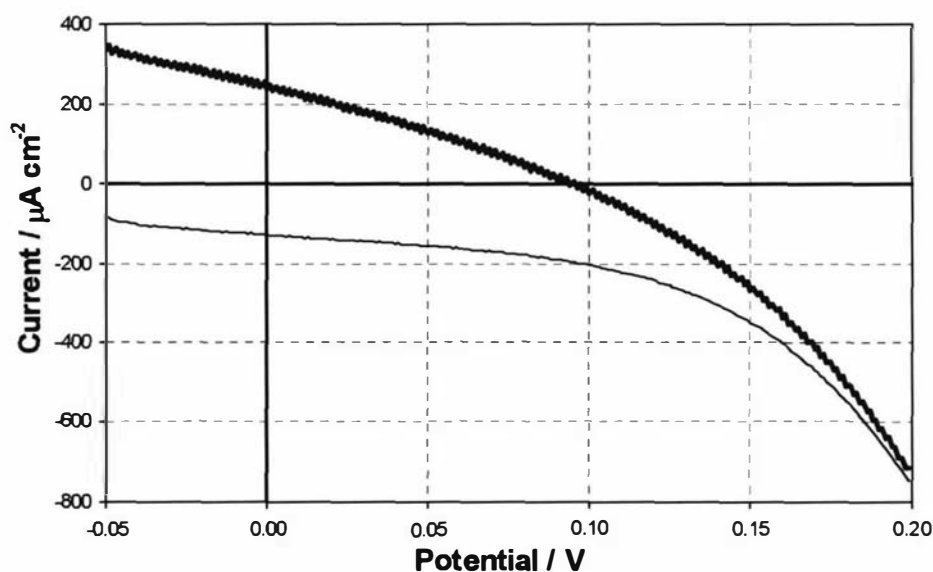


Fig 6.5. $I - V$ curve of a PEC device comprising a cast film of STV dimer in the dark (thin line) and under illumination (thick line).

6.2.6 Conclusions

It was observed that cast films of chemically oxidised NMe₂STT dimer and STV dimer, gave better photovoltaic performances than electrochemically deposited films. This may be due to either a difference in the morphology of the films depending upon the deposition technique, or to an increase in the oligomer length of the electrochemically deposited materials. Electron-withdrawing substituents on styryl-thienylenevinylenes films showed greater photovoltaic activity at short circuit current (ΔI_{sc}) than electron-donating substituents. Devices made from OC₁₀DASTT gave no discernable photovoltaic activity. This may be caused by a high stability of this polymer in the oxidised state, and possible oxidation of this material by air or the electrolyte.

6.3 Electromechanical actuators

6.3.1 Introduction

Electromechanical actuators are materials that display mechanical movement or produce a force with an electrical stimulus.³⁸ A number of conducting polymers show electromechanical actuation by expanding in volume when doped, and contracting when de-doped.^{29,187-190} It has been proposed that expansion/contraction is due to (1) the incorporation/expulsion of anions/cations, possibly together with associated solvent molecules, (2) a conformation change due to delocalisation of π -electrons,²¹ and/or (3) electrostatic repulsion between charges.²⁹

Actuators prepared from conducting polymers show potential for use in a range of medical, electronic and industrial applications, such as micromachines,³⁸ microscopic valves and pumps,³⁸ and artificial muscles for robotic and prosthetic devices.^{189,191} Polypyrrole fibre actuators have been investigated by Spinks *et al.* to be used in a glove that can open and close a human hand.¹⁹¹ For this application, the polypyrrole fibres need to have a high tensile strength, be able to generate 16 mm of contractile movement (created by an expansion of the fibre (strain) of ~4.5%) while creating 2.9 N of force, and produce a rate of movement (strain rate) of about 10 mm s⁻¹. Although polypyrrole fibres have been shown to produce strains of up to 5%, these are only under very low loads (<0.1 MPa).¹⁹¹

Most actuator work has focussed on polypyrrole and polyaniline due to their large strains (typically 3-30%), but actuators based on polythiophene and polythiophene derivatives (including poly(3,4-ethylenedioxythiophene),¹⁹² poly(3-methylthiophene)¹⁹³ and poly(3-alkylthiophene).¹⁹⁴) have also been demonstrated.¹⁹⁵

In this study, the electromechanical properties displayed by materials fabricated from polyOC₁₀DASTT were investigated. Conducting polymers prepared for use in actuator materials are typically electrochemically polymerised due to their low solubility and processability.^{29,174} The solubility of polyOC₁₀DASTT, however, allows polymer films to be cast onto a wide variety of substrate types and shapes. Three different sample

types have been constructed and tested to determine the electromechanical performance of this material: benders (produced by deposition onto a flat, non-conductive, porous polyvinylidene fluoride (PVDF) membrane), fibres (cylindrical shaped samples) and a flat, rectangular-shaped free-standing film.

6.3.2 Testing procedures and terminology

This work was done in collaboration with Yanzhe Wu in the IPRI at the University of Wollongong.

Samples were tested using a Dual Mode Lever System (Fig. 6.6). The bottom of the sample was held stationary by a clamp with a platinum wire wound around it, which also functioned as the working electrode connection. The top of the sample was held by a silicon rubber clamp which was connected to the lever by a stiff wire. The entire sample was submerged in the electrolyte solution. A stainless steel mesh sheet was used as the counter electrode, and a Ag/Ag^+ electrode used as the reference electrode.

Actuation is produced by expansion or contraction of the sample as the polymer is electrochemically cycled between oxidised and reduced states, and can be measured by two methods using the Dual Mode Lever System. The lever can apply a constant force while the change in the displacement of the lever is measured (isotonic measurements), or alternatively, the lever can be maintained stationary while the change in force on the lever is measured (isometric measurements). Although an optimum force can be determined by investigating the strength of the sample, for this preliminary study, a force slightly above the minimum force that will keep the sample material visibly taut has been selected.

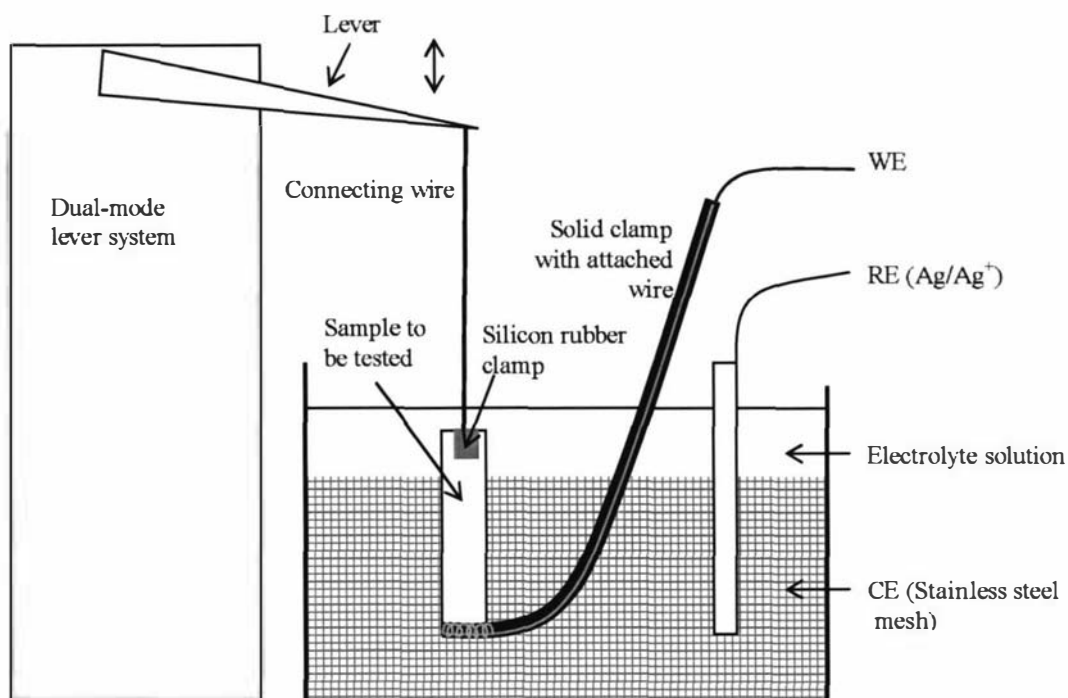


Fig. 6.6. Experimental setup using a Dual Mode Lever System for measuring electromechanical properties of a sample.

The electrochemical efficiency (EE , %) on oxidation (EE_{ox}) and reduction (EE_{red}) is defined as:

$$EE_{ox} = \frac{\text{Charge passed during oxidation}}{\text{Charge for complete oxidation}} \times 100\%$$

and

$$EE_{red} = \frac{\text{Charge passed during reduction}}{\text{Charge for complete reduction}} \times 100\%$$

The theoretical charge (C) for complete oxidation/reduction of the film was estimated using an assumption of 1 charge per terthiophene monomer repeat unit (which has been shown to be a typical charge:thiophene unit ratio found for polythiophenes)⁹¹ and is calculated as:

$$\text{Theoretical Charge} = \frac{m F}{M_r}$$

Where:

m = mass of polymer film (g)

F = Faraday's constant (96490 C mol⁻¹)

M_r = molar mass of polymer functionalised terthiophene repeat unit (660.48 g mol⁻¹)

Typical polymer masses used in materials investigated in this study range from 528 µg (for a bender) to 11 mg (for a free-standing film), with corresponding theoretical charges of 77 mC and 1.6 C respectively.

The displacement (mm) is the change in length of the sample under isotonic conditions. In this report, a more negative value for displacement is used to indicate that the fibre is contracted (reduced) and a less negative value means it is expanded (oxidised).

The strain (%) relates the displacement to the original length of the film (measured between the two clamps) and is defined as:

$$\text{Strain} = \frac{\text{Displacement}}{\text{Original length of film}} \times 100\%$$

The strain rate (% s⁻¹) is defined as:

$$\text{Strain rate} = \frac{\text{Strain}}{\text{Time}}$$

Stress (Pa) is measured under isometric conditions and is the force applied to a film or produced by a film. 1 Pa = 1 N m⁻²

6.3.3 Bilayer benders

One method to investigate actuation properties of a material is by producing a ‘bender’ by coating an inert material with a material which expands/contracts creating a bending motion.

Sample fabrication

A very shiny (near mirror quality) bronze-coloured film was produced by applying drops of a chloroform solution of polyOC₁₀DASTT polymer evenly over the surface of an inert porous polyvinylidene fluoride (PVDF) membrane sheet (Fig. 6.7). Although the average pore size of porous PVDF membrane is about 0.45 μm, the polymer solution was observed to only partially permeate through the membrane to leave a 5 μm thick film on top of the membrane (measured with a micrometer and taking the difference of the PVDF membrane with and without the polymer layer).



Fig. 6.7. Schematic of a bender made by casting polymer as a solution in chloroform on a PVDF membrane strip.

Sample characterisation

The conductivity of the polyOC₁₀DASTT film immediately after casting on PVDF was measured as $1.15 \times 10^{-4} \text{ S cm}^{-1}$, which is relatively high compared to fully de-doped polythiophene for example that has a conductivity in the range of $10^{-10} \text{ S cm}^{-1}$. This indicates that this material is unlikely to be fully reduced to the neutral state.

Electrochemical analysis was used to investigate the redox potentials and cycle stability of polyOC₁₀DASTT on the PVDF membrane. A CV of a polyOC₁₀DASTT coated PVDF sample ($2 \mu\text{g mm}^{-2}$) is displayed in Fig. 6.8. Ten cycles are shown, the first of which is unique as typically seen for polythiophene samples for reasons discussed previously (Chapter 3, Section 3.4.3.1). Further scans are similar, indicating that the film is

relatively stable during oxidation-reduction between -0.5 V and 0.8 V in the given conditions (electrolyte solution consisting of TBAP in acetonitrile, at room temperature and a scan rate of 100 mV s^{-1}). The CV displays an oxidation peak at 0.59 V, and reduction peak at 0.53 V, both of which are relatively sharp compared to the cast polyOC₁₀DASTT film on ITO-coated glass displayed in Chapter 5, Section 5.4.2.

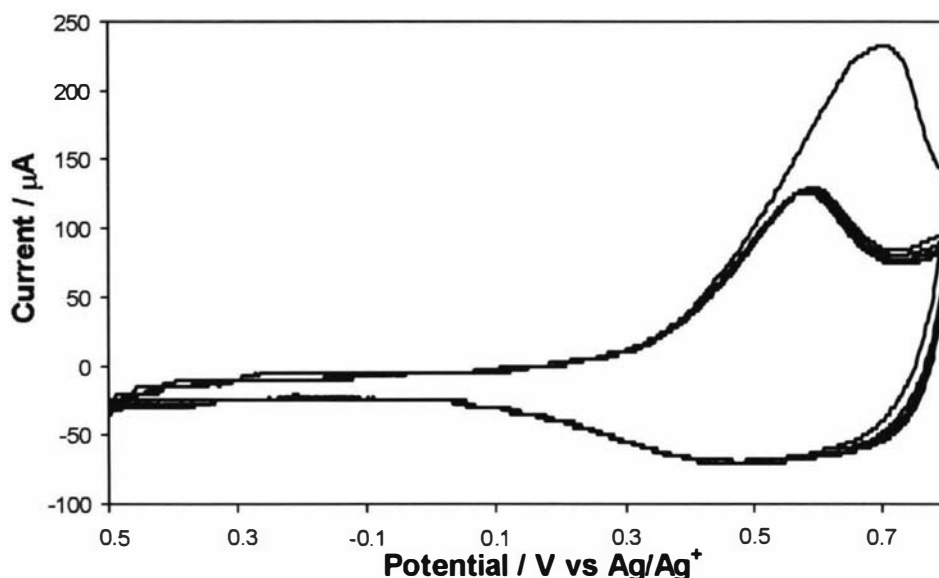


Fig. 6.8. CV of a cast polyOC₁₀DASTT film on a PVDF membrane substrate. Surface area of substrate: 7 mm^2 . Amount of polymer cast: 15 μg . Supporting electrolyte: 0.1 M TPAP/AN. Ten cycles. Scan rate: 100 mV s^{-1} .

The UV-VIS-NIR absorbance spectrum of a polyOC₁₀DASTT film on PVDF in different oxidation states is shown in Fig. 6.9. The oxidised films (Curves (a) and (b)) show free-carrier tails that rise at wavelengths beyond 1200 nm, indicating a high degree of conjugation.¹²⁶ The absorbance spectra of the film immediately after it was cast from solution (in 'neutral' state, curve (c)) shows two peaks at 720 nm and at 1312 nm. The peak at 1312 nm may be due to the presence of polaron or bipolaron species, consistent with the relatively high conductivity (mentioned above) and partial oxidation of the film, discussed in Chapter 5, Section 5.4.2.

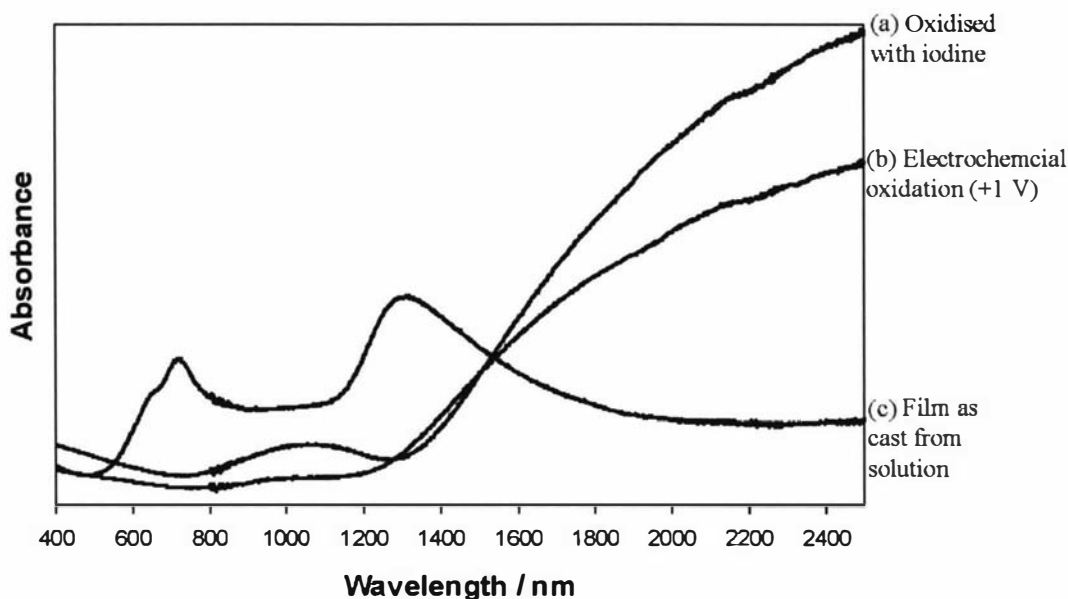


Fig. 6.9. Absorbance of a polyOC₁₀DASTT film on PVDF (a) immediately after being cast from solution, (b) after electrochemical oxidation (+1 V vs Ag/Ag⁺) and (c) after oxidation with iodine.

The film could not be fully de-doped by using electrochemical methods either, as indicated by the free-carrier tail in UV-VIS-NIR spectra (Fig. 6.10). From inspection of a CV of the polymer, the reduction potential was chosen at -0.6 V, and was held at that potential for 30 minutes. An incomplete reduction is suggested by the enduring free-carrier tail, and by a charge efficiency of only 28% on reduction from a fully oxidised state to -0.6 V. The incomplete reduction may be due to the low conductivity of the polymer in the reduced state hindering electron injection back into the oxidised polymer, inaccessible material, an inability to reduce completely due to occlusion, or incomplete oxidation to begin with.

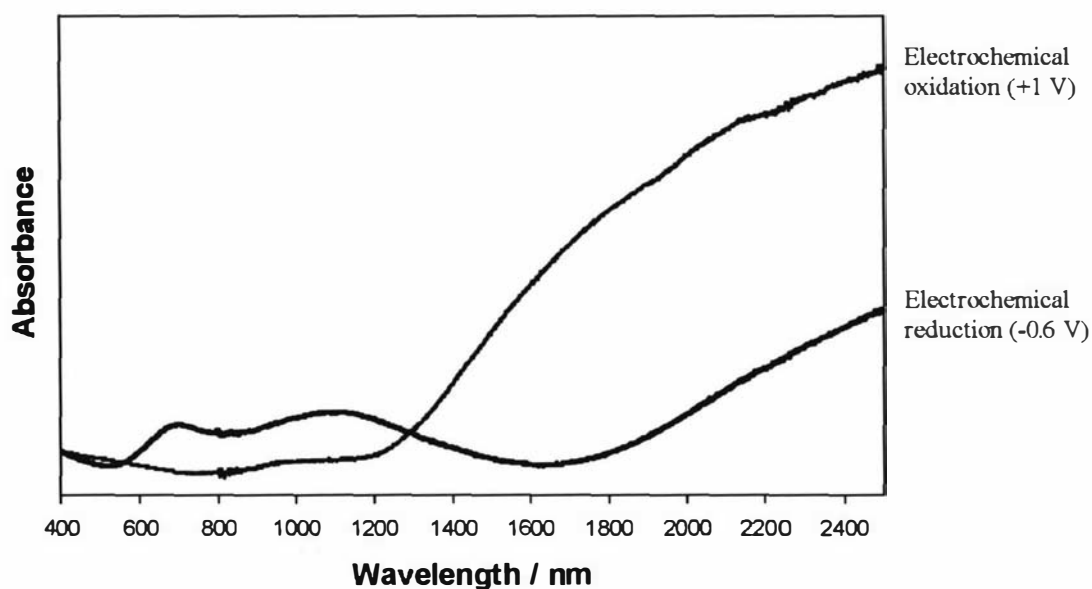


Fig. 6.10. UV-VIS-NIR spectra of a cast polymer/PVDF strip which has been reduced and oxidised potentiostatically at -0.6V and $+1.0\text{V}$. Supporting electrolyte: $0.25\text{M TBAPF}_6/\text{PC}$. A piece of platinum coil was used to wrap around the polymer/PVDF film to increase charge accessibility, and the potential was applied for 30 minutes.

Strips of PVDF membrane coated in polyOC₁₀DASTT ($12\ \mu\text{g mm}^{-2}$) were tested for electromechanical properties.

Electromechanical testing and results

Photographs showing the experimental setup for testing the actuation of a PVDF/polymer strip ($30 \times 2\text{ mm}$) are shown in Fig. 6.11. A TBAPF₆/propylene carbonate (PC) electrolyte was used. The polymer could be oxidised (doped) and reduced (dedoped) by altering the potential applied to the strip. When initially submerged in the electrolyte, the strip curved towards the polymer-coated side, as the PVDF membrane soaked up solvent and expanded (Fig. 6.11a). By applying an oxidising potential of $+0.8\text{ V}$, the polymer was induced to incorporate anions (possibly with associated solvent molecules) to balance the charge. As the polymer film increased in volume, the strip bended towards its uncoated side, causing the strip to straighten (Fig. 6.11b). When a potential of -0.6 V was applied, anions were expelled, which caused the polymer layer to contract and the strip to bend back towards the polymer-coated side (Fig. 6.11a). A schematic of the mechanism is illustrated in Fig. 6.12.

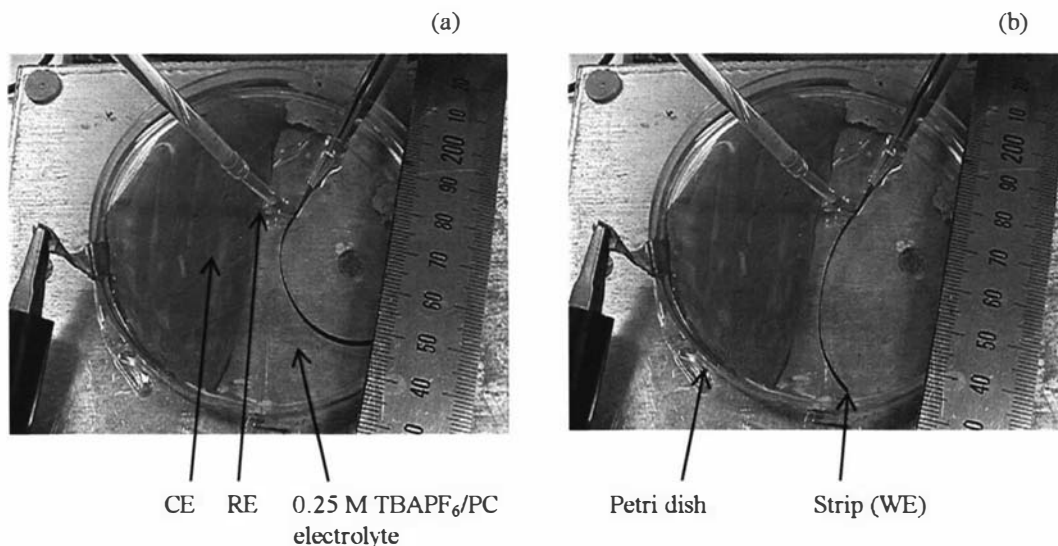


Fig. 6.11. Experimental setup for testing a polymer/PVDF strip. Electrolyte: 0.25 M TBAPF₆/PC electrolyte. Counter electrode: stainless steel mesh. Reference electrode: Ag/Ag⁺. The strip is shown in both an (a) reduced and (b) oxidised state.

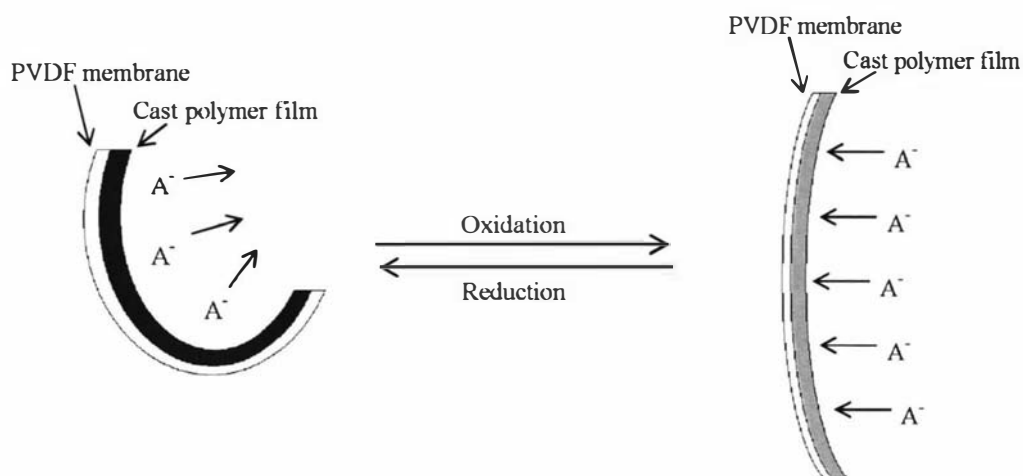


Fig. 6.12. Schematic showing the expansion of the polymer film on oxidation by incorporation of the anion, and contraction on reduction due to expulsion of the anion.

The tip of the polymer/PVDF strip was observed to move 23 mm, however, contraction took *ca.* 7 seconds and expansion *ca.* 21 seconds. This indicated that there is a difference in the rate of oxidation and reduction.

One way of probing this is to examine the chronoamperometry of the bilayer bender. A chronoamperogram of a 2 x 22 mm strip is shown in Fig. 6.13. This shows that the charge passed during the oxidation and reduction processes are similar (31.4 and

36.9 mC respectively) as would be expected for a reversible process. However, a significant difference in the current distribution and peak current produced by the film during oxidation and reduction is observed. The charging current produced during oxidation of the film shows a broad peak which reaches 0.45 mA, whereas the peak charging current during reduction is very sharp and reaches 3.7 mA (more than seven times larger than the oxidising charging current). It is possible that the difference in the rate of the redox processes is due to a difference in the conductivity of the film. The rate of oxidation of the neutral (poorly conducting) film appears to be limited by the mass transport of the anions/cations into/out of the polymer film.

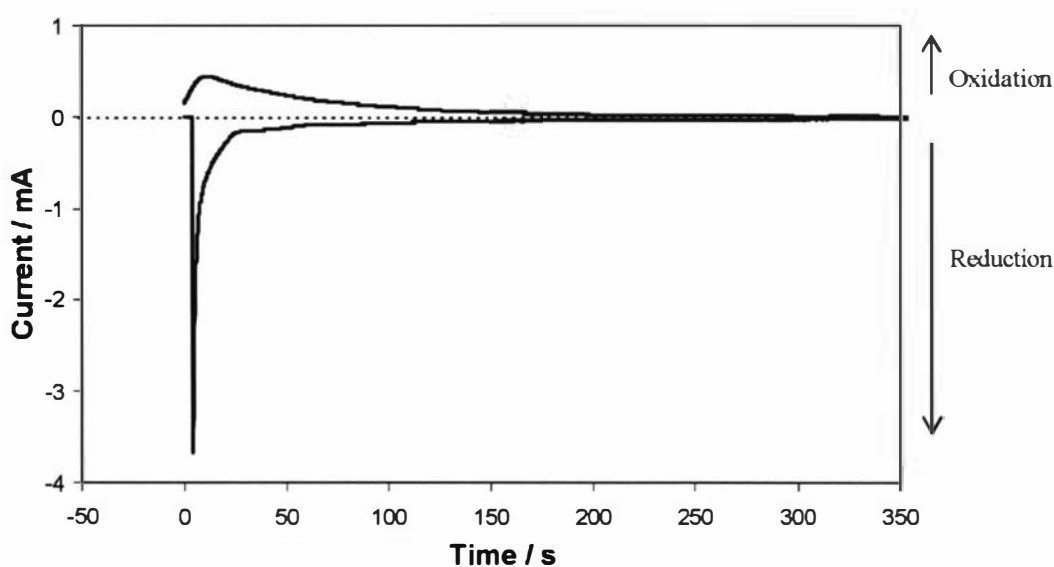


Fig. 6.13. Chronoamperometry of polyOC₁₀DASTT/PVDF strip in 0.25 M TBAPF₆/PC. Oxidation potentials: switching from -0.6 V to 0.8 V. Reduction potentials: switching from 0.8 V to -0.6 V.

After an initial increase in charge of 14 mC, a linear correlation between redox charge and expansion of the film (measured by displacement of the free end) is observed (Fig. 6.14). The initial increase in charge may be partially due to non-Faradaic charge due to charging of the double layer. The electrochemical efficiency (including any non-Faradaic charge as this can not be determined) for this process is calculated as 41%. This low value compared to polypyrrole actuators that have been shown to produce electrochemical efficiencies of up to 56%,¹⁹⁶ may be due to low conductivity of the film.

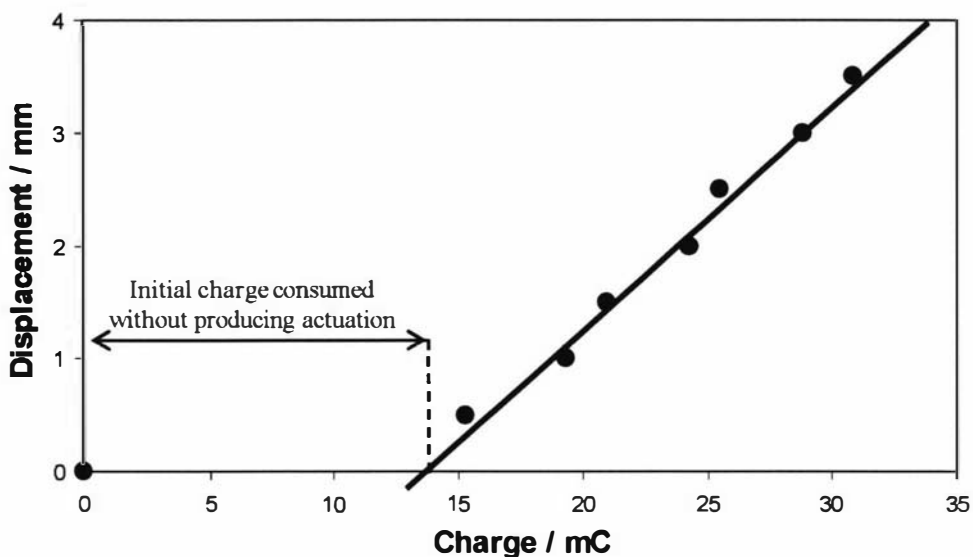


Fig. 6.14. Correlation between the injected charge and the displacement of the free end of the film.

Deposition onto platinum-coated PVDF

The rate of movement of the bilayer bender was observed to be slow compared to analogous devices prepared from polypyrrole.¹⁹⁷ Deposition of the polymer on a conductive surface is expected to increase the rate of actuation by increasing charge accessibility to the polymer in its semi-conducting, neutral state.

The polymer was cast onto a PVDF sheet which had been sputter coated with platinum. While the purpose was to form a polymer layer on the platinum coating, the polymer soaked through the platinum coating to the PVDF membrane leaving the platinum layer completely un-coated.

Since poor adhesion was observed for cast films of polyOC₁₀DASTT films on platinum-coated surfaces, an attempt was made to increase the thickness and quality of the polymer film by electrochemical deposition onto a platinum sputter-coated PVDF membrane. As polyterthiophene and its derivatives are renowned for forming porous, powdery films when grown thicker than a few microns,⁸ the growth of a smoother and more robust film was explored by decreasing the rate of polymerisation. Deposition of the polymer over 12 hours by potentiostatic and galvanostatic methods at low

temperatures (4°C) nevertheless resulted only in coatings of black, non-adherent, finely divided precipitate.

An attempt was made to improve the morphology of the electrochemically deposited polyOC₁₀DASTT films by using polyhydroxyether as an electrolyte. Ding¹⁹⁸ reported making smooth, robust polyterthiophenes films by electrochemical growth with this electrolyte. Growth of polyOC₁₀DASTT using the method reported by Ding resulted in a very smooth, tough film but with a very high resistance (> 1 MΩ cm⁻¹).

6.3.4 Fibres

Spinks *et al.*¹⁹¹ demonstrated that polypyrrole actuators in the form of hollow polymer fibres, have better strain and strain-rate properties than flat films, attributed to a higher electrical conductivity of the tubes. Accordingly, an attempt was made to construct three different types of fibre structures coated with polyOC₁₀DASTT. Schematics of the fibre structures prior to coating are shown in Fig. 6.15. Fig. 6.15(a) displays a schematic of a hollow PVDF fibre wrapped with a 50 μm platinum wire. The purpose of the wire is to increase the electrical connectivity through the entire length of the polymer tube when it is in the low conducting, neutral state to increase the rate of actuation. Platinum coating of the PVDF fibre (Fig. 6.15b) was also intended to increase the charge distribution but unfortunately the polymer did not adhere well to the platinum coating and peeled off when the thickness was increased.

As the PVDF membrane is not very pliable and restricts expansion and contraction, it was attempted to create a hollow polymer fibre wrapped in a platinum coil without the PVDF membrane. With polypyrrole, this is normally achieved by electrochemically growing a thick film onto a thick (250 μm diameter) platinum wire that is coiled in a fine platinum wire (Fig. 6.15c). The inner wire is then removed to leave a hollow polymer fibre incorporating a platinum coil. Unfortunately, poor adhesion of the polymer to the platinum wire meant the coating could not be made thick enough by casting or electrochemical deposition methods to produce a free-standing polymer fibre.

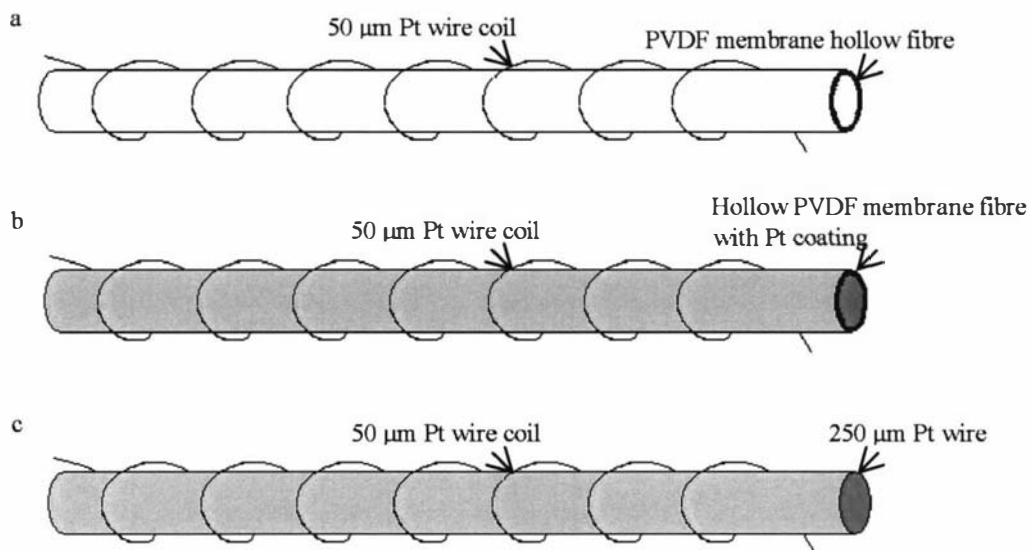


Fig. 6.15. Schematic of fibres on which polyOC₁₀DASTT was deposited. (a) Hollow PVDF membrane fibre wrapped with a 50 μm platinum wire. (b) Hollow PVDF membrane fibre which has been sputter-coated with platinum and wrapped with a 50 μm platinum wire. (c) 250 μm wire wrapped in a 50 μm wire.

Since polyOC₁₀DASTT could be successfully deposited only on the PVDF fibre coiled in platinum (Fig. 6.15a), this type of fibre was selected for further experimentation. Isotonic electromechanical measurements of a fibre that was 49 mm long and supported a polymer coating of 39 μg mm⁻¹ length of fibre, are given in Fig. 6.16. The force stretching the fibre (stress) was held constant while the potential was alternated between -0.6 V and +0.8 V. The current, and the distance the fibre stretched/contracted (displacement) were measured. In this study, a more negative value for displacement is used to indicate that the fibre contracted and a less negative value indicates it expanded. Total expansion of the sample between the oxidised and neutral state was 10.8 μm, giving a strain of 0.0002%.

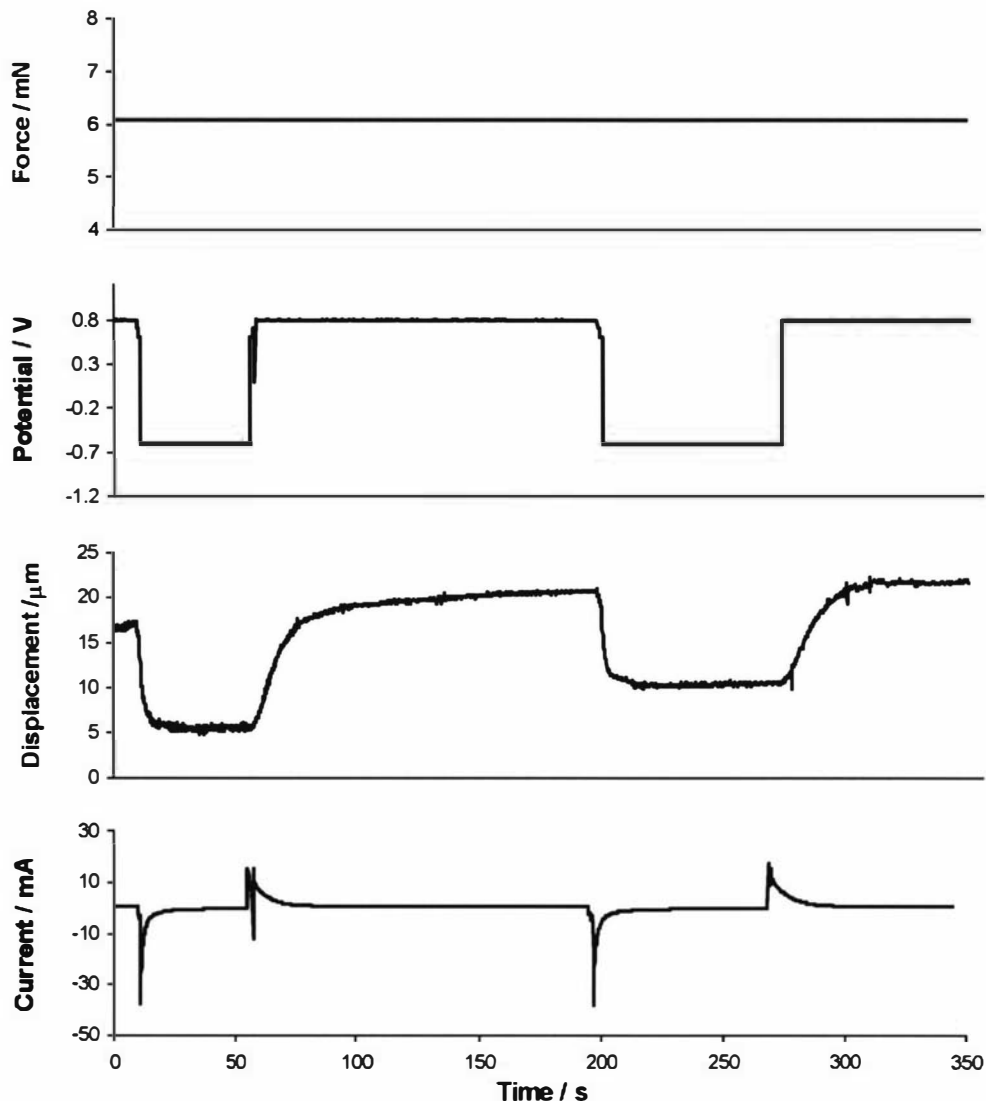


Fig. 6.16. Actuation of a hollow PVDF membrane fibre (49 mm long) wrapped in a 50 μm wire and coated with polymer ($39 \mu\text{g mm}^{-1}$). The force was held constant at 6 mN while the potential was alternated between -0.6 V and +0.8 V. The distance the fibre stretches and the current produced were measured.

Fig. 6.17 shows the relationship between the charge injected into the sample and the change in length of the sample (displacement). Reduction and contraction are represented by negative values, and oxidation and expansion by positive values. Although an ideal actuation system would display a linear relationship to indicate efficient power consumption, in this case, the response is clearly not linear. The non-linear relationship may be due to an impedance of the expansion and contraction by the non-pliable PVDF membrane substrate.

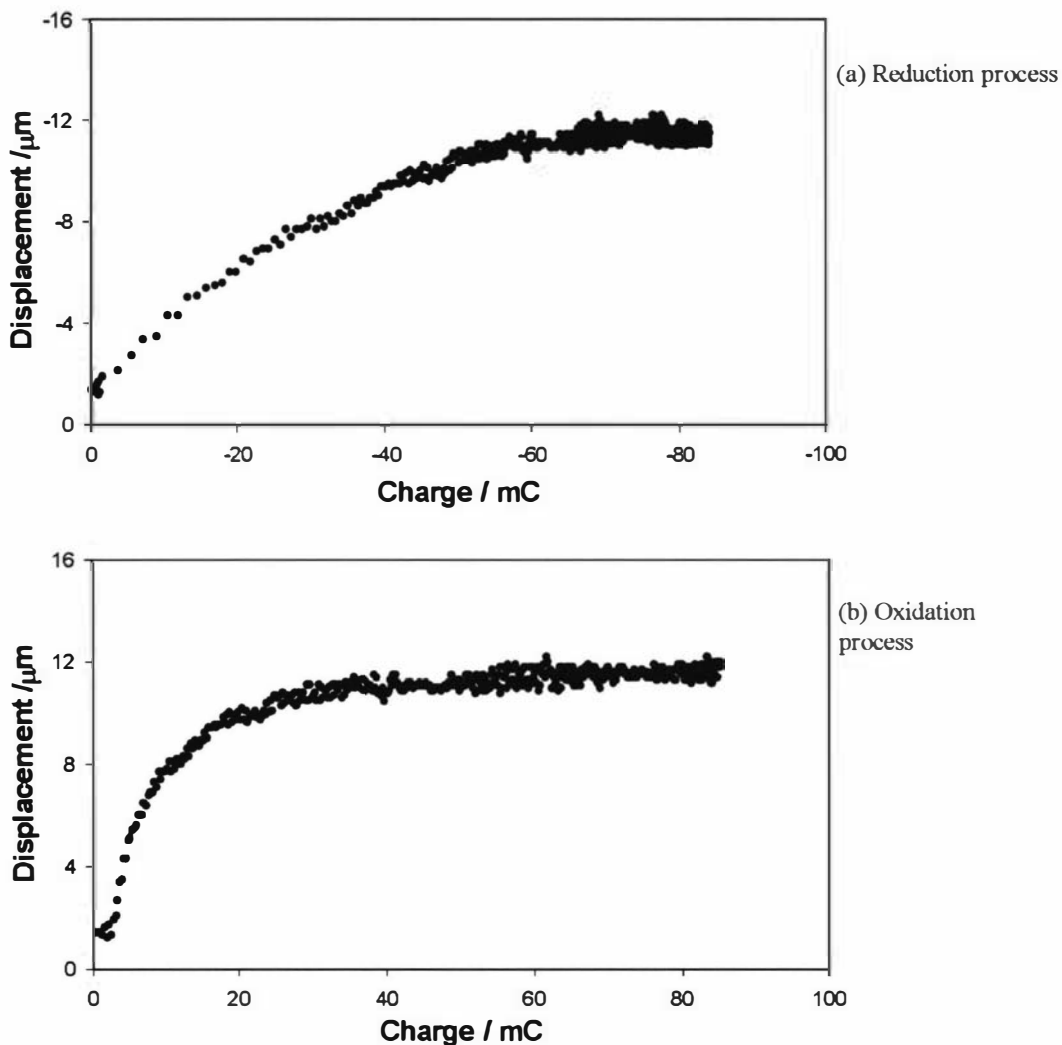


Fig. 6.17. Relationship between displacement and charge injected into a PVDF membrane fibre coated with polyOC₁₀DASTT during (a) reduction and (b) oxidation of one typical pulse. A negative charge is used to indicate reduction, a negative displacement to indicate contraction, a positive charge to indicate oxidation and positive displacement to indicate expansion.

Fig. 6.18 shows the displacement with time that is displayed by the fibre during oxidation and reduction. The slope represents the rate at which the fibre is expanding or contracting. This diagram reveals that the rate at which the fibre is contracting on reduction is much quicker than the rate of expansion on oxidation. Again, this is most likely due to the higher conductivity of the polymer in the oxidised state.

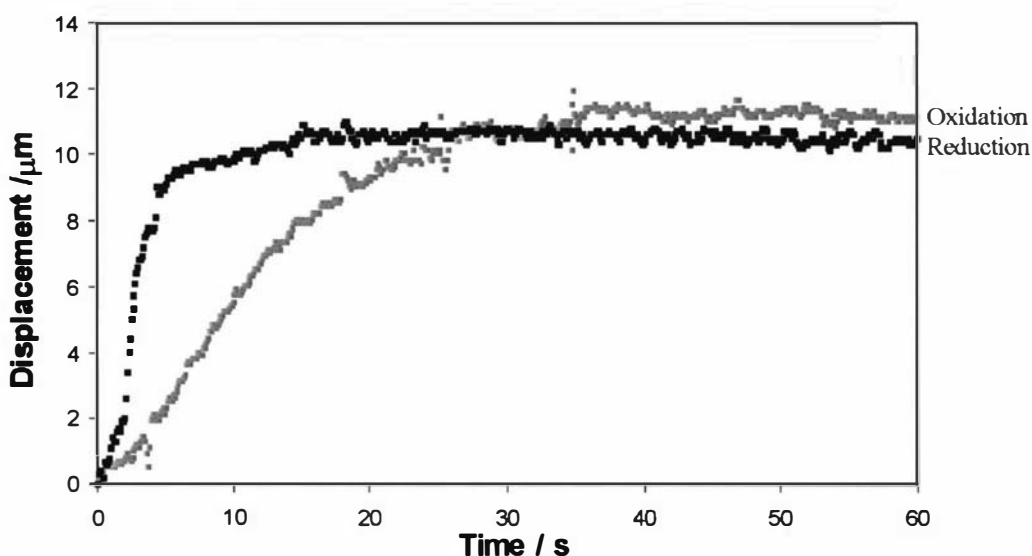


Fig. 6.18. Comparison of the rate of contraction/expansion during oxidation and reduction of one typical pulse. The slope represents the rate at which the fibre is expanding or contracting.

In comparison to polypyrrole actuators that typically display strains of 3-30% and strain-rates up to $3.2\% \text{ s}^{-1}$, this polyOC₁₀DASTT/PVDF fibre displays a very low strain (0.0002%) and strain-rate (*ca.* $0.00001\% \text{ s}^{-1}$).

6.3.5 Free-standing film with incorporated wire

The non-linear relationship between time and displacement shown by the PVDF membrane fibre suggests that the actuation performance is hindered by the relatively inflexible PVDF membrane. To prevent this problem, a free-standing polymer film was cast and tested. A 50 µm wire was zigzagged through the film in an attempt to increase the actuation response by improving the accessibility of charge to the polymer when in its semi-conducting undoped state ($<1.1 \times 10^{-4} \text{ S cm}^{-1}$) as shown in Fig. 6.19. The conductivity of this film when doped with iodine was 1.1 S cm^{-1} , i.e. a 10000 fold change.

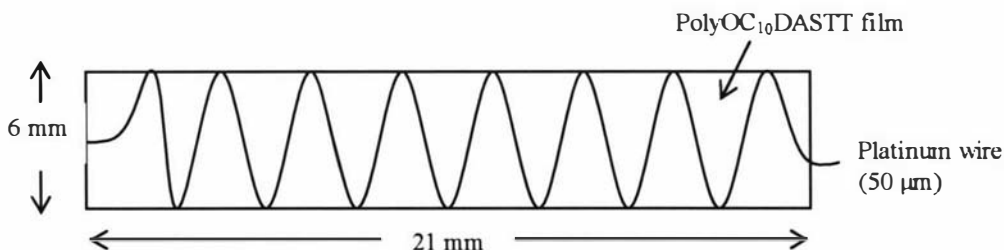


Fig. 6.19. Free-standing film of polyOC₁₀DASTT incorporating a zigzagged (50 μm diameter) wire. Dimensions of film: 6 mm x 21 mm with a thickness of 81 μm. Mass = 16.1 mg.

The film was tested isotonicly using the dual-mode lever system with a constant tensile stress of 44 KPa (40 mN tensile loading). Before performing electromechanical measurements, the film was pre-conditioned. The constant stretching force (40 mN) was applied to the film in order to keep it straight, and 4 hour square wave potential function which pulsed between +1 V and -0.6 V (*vs* Ag/Ag⁺) was applied from the electrical contact at the bottom of the film. This process was conducted for 24 hours until consistent displacement and current measurements were obtained.

After pre-conditioning, the film was oxidised and reduced under isotonic conditions to and from various oxidation potentials as shown in Fig. 6.20. In each case, the initial/final reduction potential was -0.6 V. As the potential was switched from a reducing potential to an oxidising potential, a rapid initial strain-rate (rate of expansion) was observed as the polymer became positively charged and anions were inserted into the polymer matrix. This initially relatively rapid expansion was followed by a slower rate of expansion as the film approached a neutral state, possibly due to further chain relaxation. A similar process seemed to happen on reduction as the change in potential of the polymer forced out anions to give a relatively fast initial contraction. This was again followed by a slower rate of contraction as the film approached a neutral state. An exception is the oxidation at +0.2 V, which shows an initial slight contraction on application of this potential, possibly due to an initial reduction of the film which may have been partially oxidised.

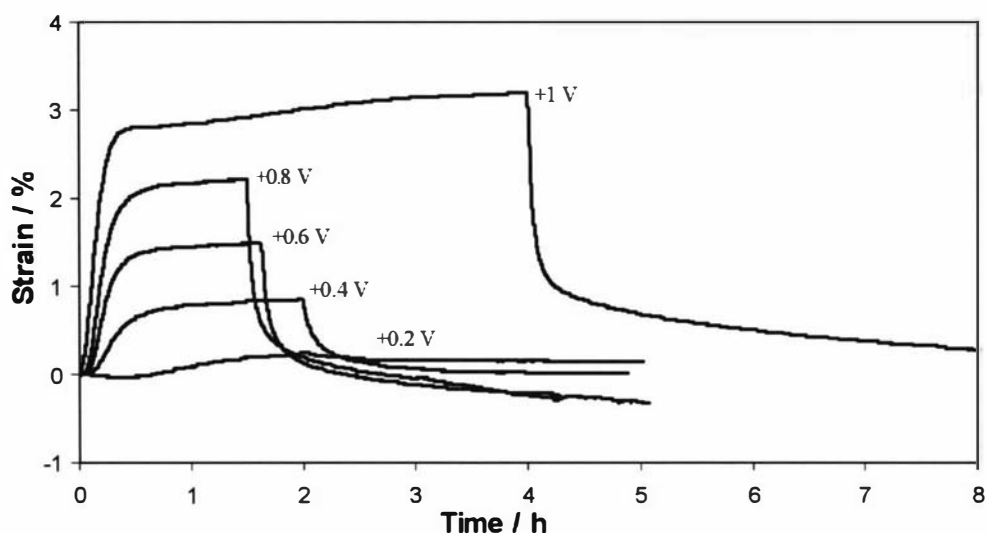


Fig. 6.20. Strain created by the polyOC₁₀DASTT film over time as it is doped (oxidised) and then dedoped (reduced at -0.6 V) to and from various oxidation potentials.

The maximum strain rates for the oxidation and reduction of films at different oxidation potentials are given in Table 6.4. The strain rate was observed to increase with applied oxidation potential. This was expected as the higher potential differences at the interface between the film and solution should induce faster anion absorption/expulsion and therefore expansion/contraction of the film.

The strain-rate of the film was measured to be about three times higher during reduction than during expansion. This may be due to two possible reasons. The low conductivity of the film in the neutral state may be impeding the accessibility of charge through the film, thus hindering oxidation and expansion of the film. A second possibility is a difference in anion accessibility into the neutral and oxidised polymer matrix. A higher strain rate during oxidation is often reported in literature^{188,199} due to a higher energy requirement to open the molecular entanglement and allow the penetration of counterions. During reduction, however, counterions are able to diffuse along the opened structure to the solution without any resistance, giving rise to a faster contraction behaviour.

Table 6.4. Maximum strain rate on oxidation and reduction of films which are oxidised at various potentials. The reduction potential is kept constant at -0.6 V.

Upper potential limit	+0.2 V	+0.4 V	+0.6 V	+0.8 V	+1.0 V
Maximum strain rate on oxidation ($\% s^{-1}$)	0.001	0.0013	0.0040	0.0033	0.0042
Maximum strain rate on Reduction ($\% s^{-1}$)	N/A	0.0023	0.0056	0.010	0.011

A linear correlation is revealed between the oxidation potential and the strain measured after 1.4 hours of oxidation (Fig. 6.21). This can be explained by a higher level of doping (and hence film expansion) at more positive oxidation potentials. The doping level is measured by the charge passed, and is used to calculate the electrochemical efficiency. The increase in strain generated by the film with the increase in electrochemical efficiency and charge passed is shown in Fig. 6.22.

The maximum strain obtained from the polyOC₁₀DASTT film (at an oxidation state of +1 V after 4.2 hours as determined by Fig. 6.22) is about 3.2%. This measurement is twice that displayed by another example of solution processable ICP actuator film based on a polyaniline film plasticized with di-2-butoxy-ethyl ester of sulfosuccinic acid (about 1.5% at 0 tensile loading).²⁰⁰

At a constant tensile stress of 44 KPa, reversible strain was observed in the potential range from +1 V to 0.6 V without significant creeping during a 48 hour experimental period. One possibility for this result is favourable interactions between the polymer substituents (involving either interdigitation of the alkoxy substituents, or π - π interactions between the styryl substituents), which may prevent the polymer chains from slipping and causing irreversible chain relaxation during the electrochemical doping process.

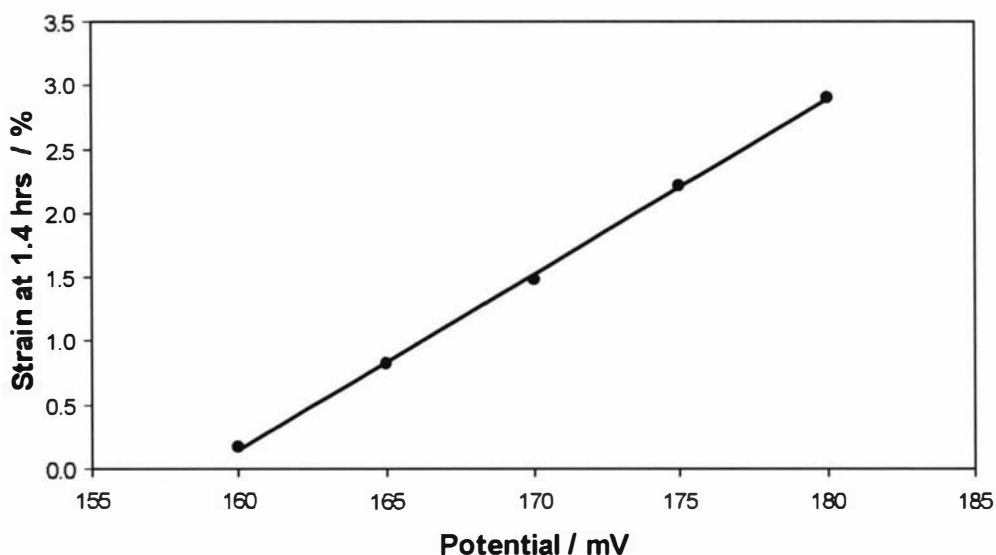


Fig. 6.21. The effect of the oxidation potential on the strain measured after 5000 seconds of oxidation.

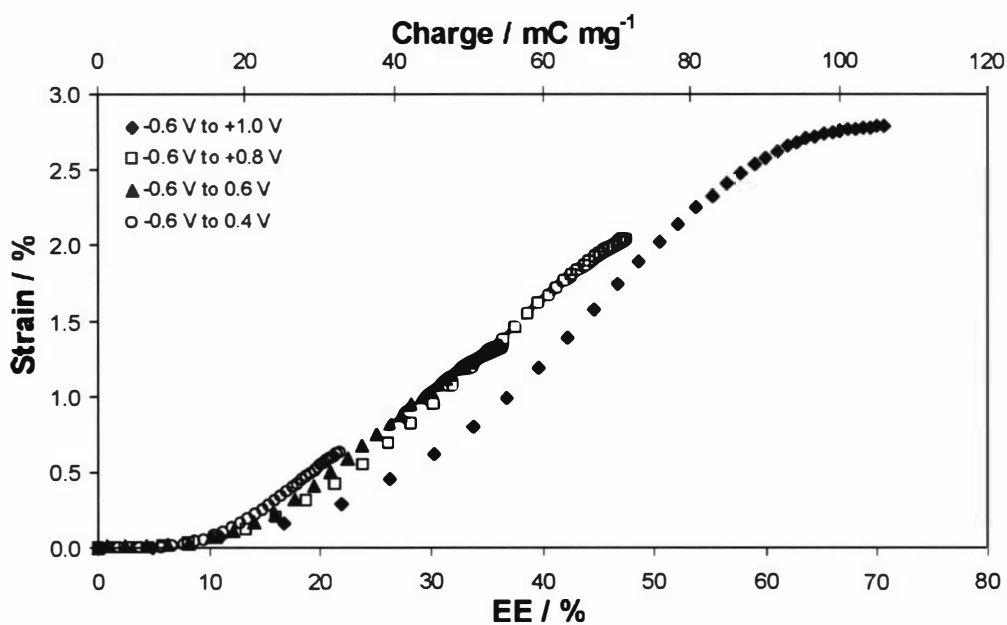


Fig. 6.22 Relationship between the strain generated at different oxidation potentials and the electrochemical efficiency (EE).

The electromechanical tensile performance was evaluated under isometric conditions. The polymer film was oxidised and pre-conditioned at +1 V to allow full expansion before the lever arm was fixed. The force applied on the lever by the film due to contraction was then measured as the film was reduced from the oxidised state to the

neutral state (+1 V to -0.6 V). The stress generated by the film in relation to the charge density passed into the film was calculated and is shown in Fig. 6.23. The contraction force (stress) is observed to increase almost linearly to the reduction charge, as expected if the charge is balanced by removal of anions rather than insertion of cations. Although the polyOC₁₀DASTT film broke at 111 KPa, extrapolation of this linear trend line to the maximum redox charge density at 105 mC mg⁻¹ yields a tensile stress of about 260 KPa. This lies in the range shown by natural skeletal muscles, which usually display tensile stresses of between 0.1 MPa and 0.5 MPa.¹⁹⁰ However, failure of the film at 111 KPa reveals that the largest tensile loading must be less than this value. Further structural strengthening is required to make a tougher film with a higher tensile modulus (ability to elongate) when submerged in an electrolytic medium.

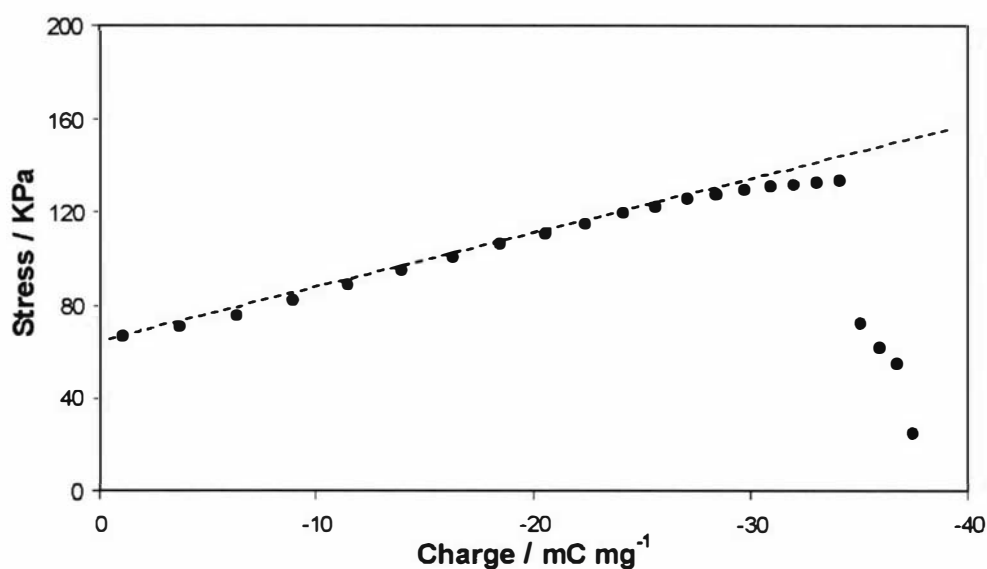


Fig. 6.23. Relationship between the isometric stress generated on the film and the charge density passed as the film is reduced. The film was pre-conditioned at +1 V to obtain the fully expanded state and then isometric measurements were performed as the potential was switched to -0.6 V.

6.3.6 Conclusions

PVDF membrane benders and fibres, as well as a stand-alone film have been prepared by solution casting of polyOC₁₀DASTT. These structures have been shown to possess electromechanical properties by undergoing a reversible volume change in response to a repetitive potential pulse in an electrolytic media.

Although the PVDF substrate appeared to hinder the expansion/contraction of the polyOC₁₀DASTT/PVDF fibre giving a very low strain, it was shown that the stand alone polyOC₁₀DASTT film actuator could achieve a strain of up to 3.2% under a stress level of 44 kPa. However, a relatively low strain rate of about 0.011% s⁻¹ was observed for this film. This modest result may be due to the electrolyte struggling to penetrate the film and/or poor accessibility of charge due to the low conductivity of the material. Although this strain rate may be improved by using a metallic substrate, casting or electrochemical growth of a polyOC₁₀DASTT film of suitable thickness onto a platinum surface proved difficult.

Although some aspects, including the electrochemical efficiencies, mechanical toughness and long-term durability of polymer actuators still need to be improved, the versatility of polythiophene materials, created by easy functionalisation of the polymer backbone, provides possibilities for overcoming these problems. Although PVDF membrane was suitable as a substrate for the preliminary investigations discussed in this report, further work would require substrates that show a higher elasticity as the PVDF membrane does not appear to allow full contraction/expansion of the polymer.

6.4 Batteries

6.4.1 Introduction

Batteries incorporating polymeric materials are potentially a form of energy storage, which is low in weight, flexible and environmentally safe. Although polymer batteries currently show modest voltages compared to metal-based secondary batteries, they have high specific capacities due to possible fabrication of high surface area electrodes. Gofer *et al.*²⁰¹ reported a polythiophene based battery, where both cathode and anode were made from fluoro-substituted phenyl thiophene polymers, which produced a discharge voltage of about 2.4 V and capacities of 9.5 to 11.5 mAh g⁻¹. Batteries consisting of these materials were reported by Ferraris *et al.* to exhibit a cycle efficiency (ratio of the recovered charge:injected charge) of 96±1%.⁸⁶

An all-polymer battery reported by Rehan,²⁰² where the anode and cathode consisted of poly-1-naphthol and polyaniline respectively, was reported to have a specific capacity of 150 mAh g⁻¹ with an open-circuit potential of 1.4 V. However, since the reported specific capacity is higher than the theoretical capacity for the two electrodes (108 mAh g⁻¹, calculation shown below, the theoretical capacities of the polyaniline and poly(1-naphthol) electrodes were reported as 298 and 171 Ah kg⁻¹ respectively), there must be an error with their Ah or mass measurements, or additional reactions are taking place possibly involving impurities. This paper also contains an error in the calculation for the theoretical capacity of poly(1-naphthanol). From Fig. 2 of the paper, which shows one electron transferring for every two naphthanol units (280 g mol⁻¹), a capacity for polynaphthol of 96 mAh g⁻¹ is calculated (using the equation for calculating theoretical charge given in Section 6.3.2 and dividing by 3600 to convert units to hours) rather than 171 mAh g⁻¹ reported by Rehan for this material. Using this corrected value of 96 mAh g⁻¹ for the capacity of poly(1-naphthanol), an even lower value of 74 mAh g⁻¹ is calculated for the specific capacity.

$$\text{Theoretical capacity of two battery electrodes} = \frac{1}{\frac{1}{\text{Theoretical capacity of first electrode}} + \frac{1}{\text{Theoretical capacity of second electrode}}}$$

The development of electrochemical devices for applications involving charge storage usually requires polymers with a high doping level and good redox reversibility.²⁸ Many polymers including polypyrrole and polyacetylene²⁰³ have been found to perform as promising cathodes. However, a suitable material for an organic anode has not been reported.

In this study, polyOC₁₀DASTT was investigated for use as an anode-active material. The low HOMO level shown by polyOC₁₀DASTT (oxidation onset potential of approximately -0.34 V, Chapter 5, Section 5.4.2), and the high redox stability of this material, indicated that polyOC₁₀DASTT might be a useful material as an anode-active material. Chemically polymerised polyOC₁₀DASTT was cast onto two different substrates for comparison: carbon fibre mat (carbon fibre substrate) and Ni/Cu coated nonwoven polyester (Ni/Cu substrate). These conductive materials were chosen for their high surface area and the ability of the polymer to adhere to the fibres. Polypyrrole electrodeposited on stainless steel mesh was employed as cathodes.

6.4.2 Cell construction, testing procedures and terminology

This work was carried out in collaboration with Dr. Caiyun Wang at IPRI, University of Wollongong using their well established battery testing facilities.

A schematic of the test cell used in this study is given in Fig. 6.24. The anode consists of polyOC₁₀DASTT, which was drop-cast onto either carbon fibre mat or Ni/Cu-coated nonwoven polyester fabric to give a polymer coating of about 1 mg cm⁻². The cathode was prepared by electrodeposition of polypyrrole onto stainless steel mesh and is separated from the anode by a microporous polypropylene membrane. The

electrodes were submerged in a LiPF_6 (1.0 M), 1:1 ethylene carbonate:dimethylcarbonate solution, and are kept adjacent through use of a spring. The cells were designed to be anode-limited (the theoretical capacity of the cathode was 6.7 times that of the anode) to allow the features of this electrode to be investigated since polyOC₁₀DASTT is the material of interest.

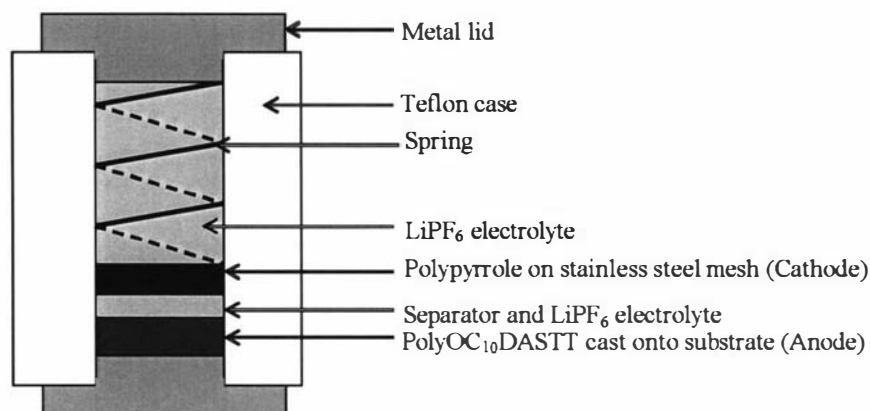


Fig. 6.24. Schematic of the test cell in this study.

Cells were tested by Dr. Caiyun Wang using a battery testing device. The cells were galvanostatically charged to a cell voltage of 1.65 V, and then discharged at the same current density to a cut-off voltage of 0.2 V. A range of current densities were employed to investigate the properties of the cell. Cycle life testing was then performed under a charge/discharge current density of 0.05 mA cm⁻² of electrode support area.

The coulometric efficiency (η) is defined as:

$$\text{Coulometric efficiency} = \frac{\text{Discharge capacity}}{\text{Charge capacity}} \times 100\%$$

The discharge capacity is defined as:

$$\text{Discharge capacity} = \frac{\text{Charge passed while discharging}}{\text{Mass of active material (polyOC}_{10}\text{DASTT)}}$$

The charge capacity is defined as:

$$\text{Charge capacity} = \frac{\text{Charge passed while charging}}{\text{Mass of active material (polyOC}_{10}\text{DASTT)}}$$

6.4.3 Analysis of electrodes

SEM images showing the surface morphologies of the Ni/Cu substrate and carbon fibre substrate after coating with polyOC₁₀DASTT are shown in Fig. 6.25a and b respectively. The blank substrates before polymer deposition are displayed as insets so the polymer can be distinguished. It can be observed that the polymer completely coats the fibres as a smooth film, forming a web between them which results in a very high surface area. The cathode formed from electrodeposited polypyrrole on stainless steel mesh is shown in Fig 6.25c. The polymer is observed to grow uniformly on the substrate and has a cauliflower-like morphology.

Cyclic voltammetry using samples of polyOC₁₀DASTT on the Ni/Cu and carbon fibre substrates as working electrodes, revealed that the redox potentials of the polymer sample is affected by the substrate (Fig. 6.26). The oxidation peak occurs at a higher potential, and the reduction peak at a slightly lower potential, when the polymer is cast on the Ni/Cu substrate compared to carbon fibre substrate. This is possibly due to more accessible charge to the polymer cast on the carbon fibre substrate due to less webbing between the fibres.

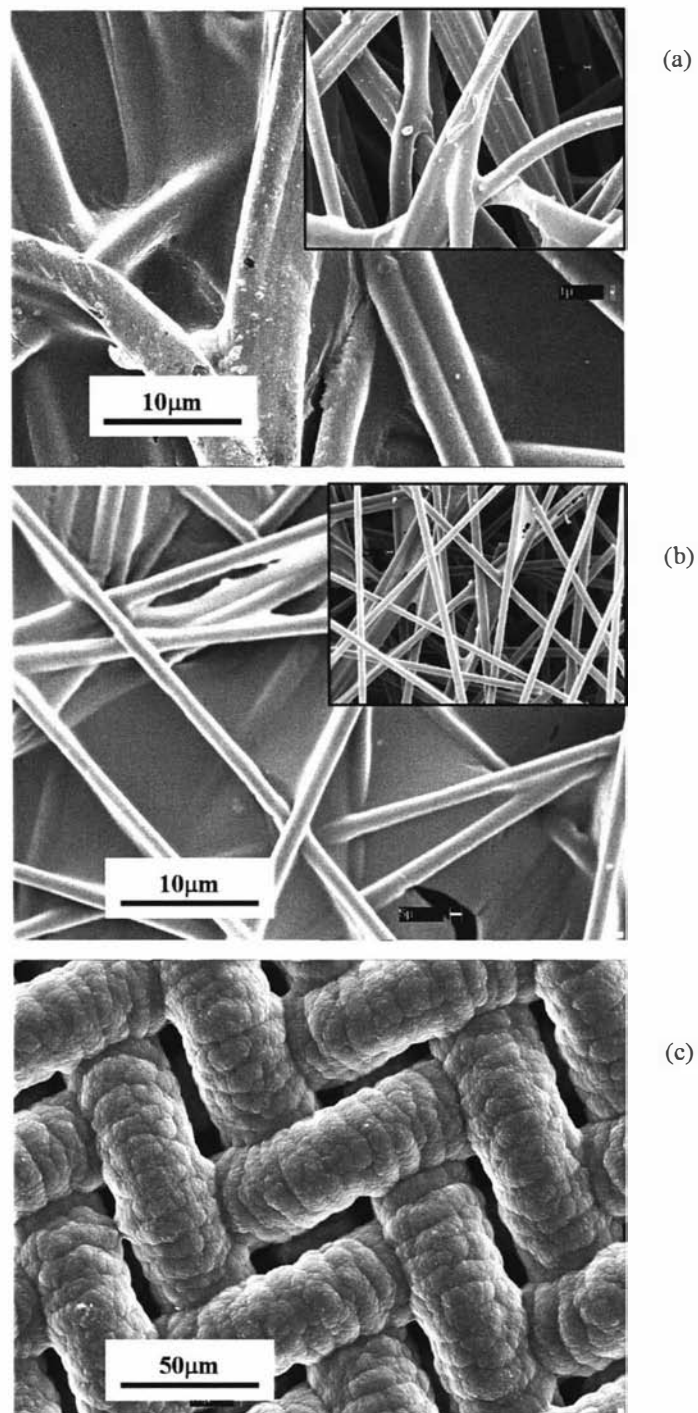


Fig. 6.25. SEM images of the electrodes. Anodes prepared by casting poly(OC₁₀DASTT) onto (a) Ni/Cu substrate (b) carbon fibre substrate. The blank substrates before polymer deposition are given for comparison as insets in the top right hand corner. (c) Cathode prepared by electrodepositon of polypyrrole on stainless steel mesh. Images are displayed at x400 magnification with insets at x100 magnification.

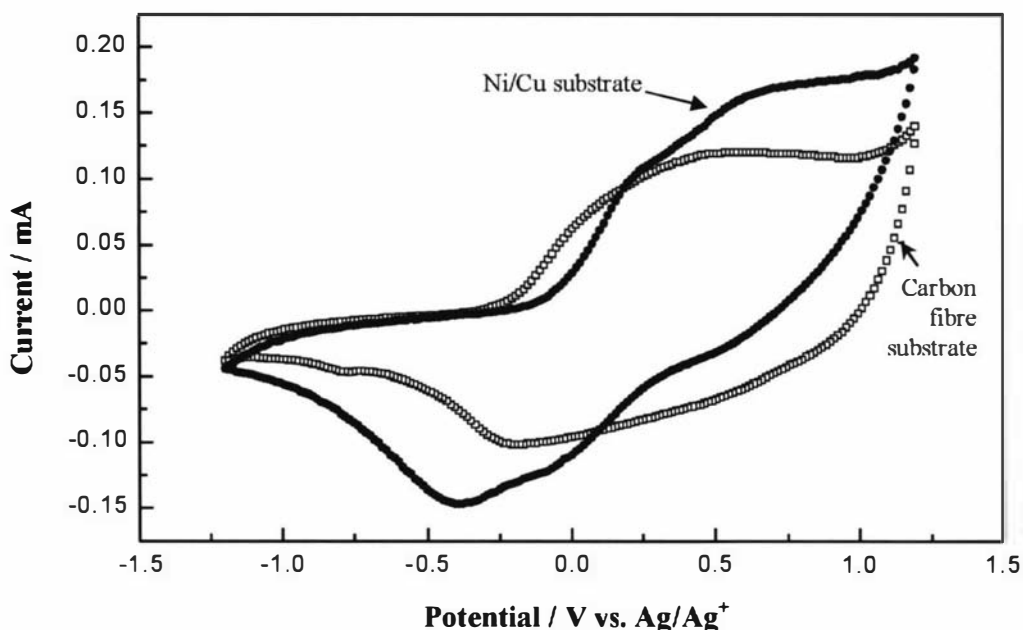


Fig 6.26. Cyclic voltammograms of polyOC₁₀DASTT cast on carbon fibre substrate and Ni/Cu substrate. Electrolyte solution: 60 mM TBAPF₆/PC. Scan rate: 10 mV s⁻¹.

6.4.4 Charge/discharge characteristics

Galvanostatic charging and discharging was used to evaluate the capacities of the prepared cells. Fig. 6.27 displays the charge and discharge curves for a cell with the anode comprising polyOC₁₀DASTT on Ni/Cu substrate (curves A and B) and carbon fibres (curves C and D). The cells were galvanostatically charged at a current density of 0.02 mA cm⁻² to 1.65 V, and then discharged at the same current density to a cut-off voltage of 0.2 V. The charge/discharge capacity was calculated based on the amount of the active material (polyOC₁₀DASTT, measured by weighing the sample) in the anode electrode. Much higher charge and discharge capacities were obtained for the cell with the anode comprising the Ni/Cu substrate (41.1 and 39.1 mA h g⁻¹ respectively) than the carbon fibre substrate (19.1 and 18.0 mA h g⁻¹ respectively). It was also observed that the anode comprising the Ni/Cu substrate exhibited a lower cell voltage before charging, and a higher cell voltage prior to discharging.

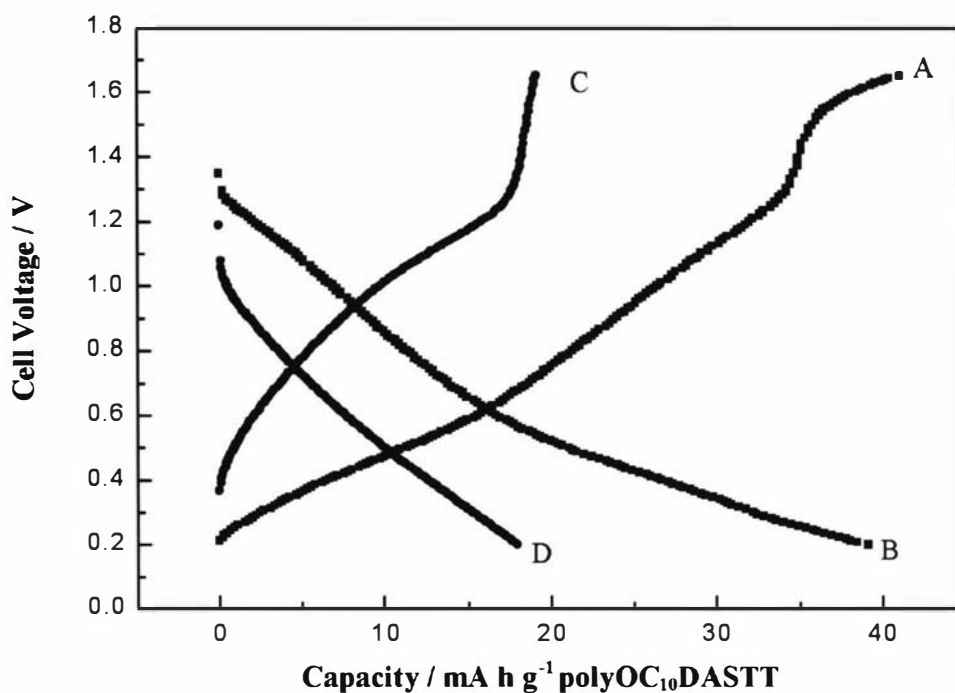


Fig. 6.27. Charge (A,C) and discharge (B,D) curves of cells with anodes comprising Ni/Cu substrate (A,B) and carbon fibre (C,D). The charge/discharge current density is 0.02 mA cm^{-2} .

Higher charge/discharge current densities were used to investigate the properties of the cell. The discharge capacities are observed to decrease with increasing discharge current density as displayed in Fig. 6.28. The cell containing polyOC₁₀DASTT on the carbon fibre substrate showed significant reduction in discharge capacity with increasing current density and was therefore not investigated at current densities above 0.1 mA cm^{-2} . In comparison, the cell comprising polyOC₁₀DASTT on Ni/Cu substrate showed a much lower reduction in discharge capacity with increasing discharge current density. At 0.5 mA cm^{-2} the discharge capacity was measured to be 53.4% that of the discharge capacity at 0.02 mA cm^{-2} .

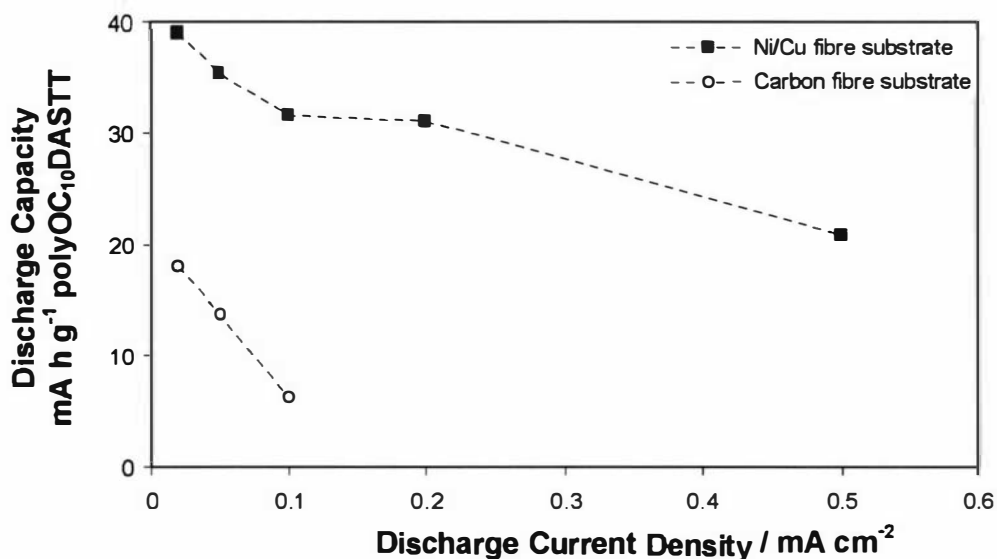


Fig. 6.28. Discharge capacities at different discharge current densities obtained for the Teflon cell using Ni/Cu and carbon fibre anode substrates.

6.4.5 Cycle life

The discharge capacity as a function of cycle number is shown in Fig. 6.29 for cells with anodes comprising polyOC₁₀DASTT on Ni/Cu substrate and carbon fibre substrate. No deterioration in discharge capacity after 50 cycles was displayed by this cell. When using the anode comprising the carbon fibre substrate, however, the discharge capacity was observed to drop to 71.5% of the initial capacity after 50 cycles.

The coulometric efficiency (η) was also measured to remain relatively stable over 50 cycles. Both cells showed a high discharge efficiency of $\sim 93\%$ for cells employing the carbon-fibre substrate, and $\sim 99\%$ for cells employing the Ni/Cu substrate.

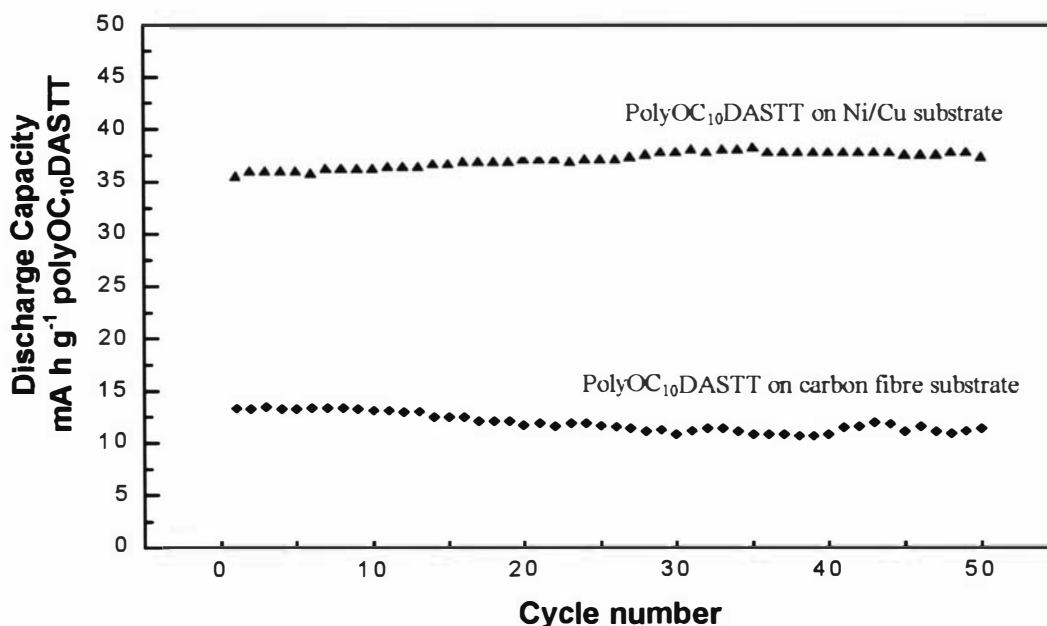


Fig 6.29. Variation of discharge capacity with cycle number for cells with an anode comprising polyOC₁₀DASTT on Ni/Cu substrate and carbon fibre substrate. Current density: 0.02 mA cm⁻².

6.4.6 Conclusions

The good discharge capacity and excellent cycle life shown by the Teflon batteries described in this study, reveals potential for polyOC₁₀DASTT as an active anode material for all-polymer batteries. The substrate that the polyOC₁₀DASTT was cast onto was shown to have a significant effect upon the performance of the cell. Ni/Cu coated nonwoven polyester fabric was found to produce significantly improved discharge capacity compared to anodes comprising carbon fibre mat as a substrate. A high coulometric efficiency of >94% was generated by both types of cells with anodes employing polyOC₁₀DASTT.

6.5 Micro- and nano-structured surfaces

6.5.1 Introduction

In this section, it is described how polyOC₁₀DASTT may be processed into a variety of structures with a high surface area. High surface areas are desirable in some applications, such as solar cells, molecular sensors and batteries. This is because they provide a high interfacial area for reactions to occur (for example charge separation at solar cell electrode interfaces or interactions of the polymer with atmospheric molecules), and hence allow the production of more efficient devices.

Since most conducting polymers are insoluble, high surface area structuring is often achieved by electrochemical growth and deposition onto a template.²⁰⁴ For example, Misoska²⁰⁴ prepared a polypyrrole inverse-opal by electrochemical deposition through the void spaces in polystyrene synthetic opal crystal on an electrode. One limitation of this technique is that an electroactive surface is required for electrochemical growth.

The solubility of the materials produced in this study allows them to be processed by techniques such as casting, spin-coating and electrospinning. This means they can be deposited onto a variety of conductive and non-conductive substrates. In this study, polyOC₁₀DASTT has been cast onto templates, which are then removed to produce fibrillar, opal and inverse-opal polymer structures. This work was undertaken in the IPRI at the University of Wollongong with the assistance of Dr. Violeta Misoska.

In addition, polyOC₁₀DASTT fibres have been produced by electrospinning.

6.5.2 Fibrils

Fibrils are fine, thread-like structures. Their small diameter (typically <500 nm) means they have a very high specific surface area. Fibrils of conducting polymers, such as polypyrrole, can be made by electrochemical deposition onto a porous alumina template which has one side sputter coated with platinum.²⁰⁵ The polymer grows from the platinum electrode through the pores in the template. The template is then dissolved to leave polymer fibrils adhered to the platinum film.

In this study, however, fibrils have been prepared by casting dissolved OC₁₀DASTT polymer directly onto the template without any platinum backing. The advantage of casting the polymer, rather than by electrochemical growth, is that it is a much simpler technique, and eliminates the possibility of monomer or short oligomers becoming merely trapped in the template pores and not contributing to a polymeric structure.

The template used in this study was composed of alumina (Anodic Aluminium Oxide, AAO), and had honeycomb shaped pores 200 nm in diameter. The template was soaked in a solution of polymer (about 2 mg mL⁻¹) for one hour. The template containing the fibrils was then removed from the solution and drip-dried.

Templates are typically dissolved by soaking in 1 M NaOH for 20 minutes.^{206,207} However, electrochemical analysis of a poly(OC₁₀DASTT) cast film, which had been exposed to these conditions, showed that the film was severely damaged. Soaking in 0.5 M NaOH for 50 minutes at room temperature, however, completely dissolved the template while having no effect on the electrochemical properties of the polymer. The template was either fully dissolved (by soaking for 50 minutes) to leave a very fragile film of polymer fibrils, or partially dissolved (by soaking for 25 minutes) so the remaining template structure could operate as support. To further increase the robustness of the fragile fibrils, templates could be sputter-coated on one side with platinum prior to soaking in polymer. The resulting conducting platinum film (with fibrils attached) could be used as an electrode to investigate the properties of the polymer fibrils.

SEM images (Fig. 6.30) show polyOC₁₀DASTT fibrils, held together by (a) a thin polymer film and (b/c) a platinum film and partially remaining template as support. The fibrils appear to be more structured near the platinum-coated side, and tangled at the unsupported end. They appear to be about 200 nm in diameter, which is expected from the 200 nm pore size in the template.

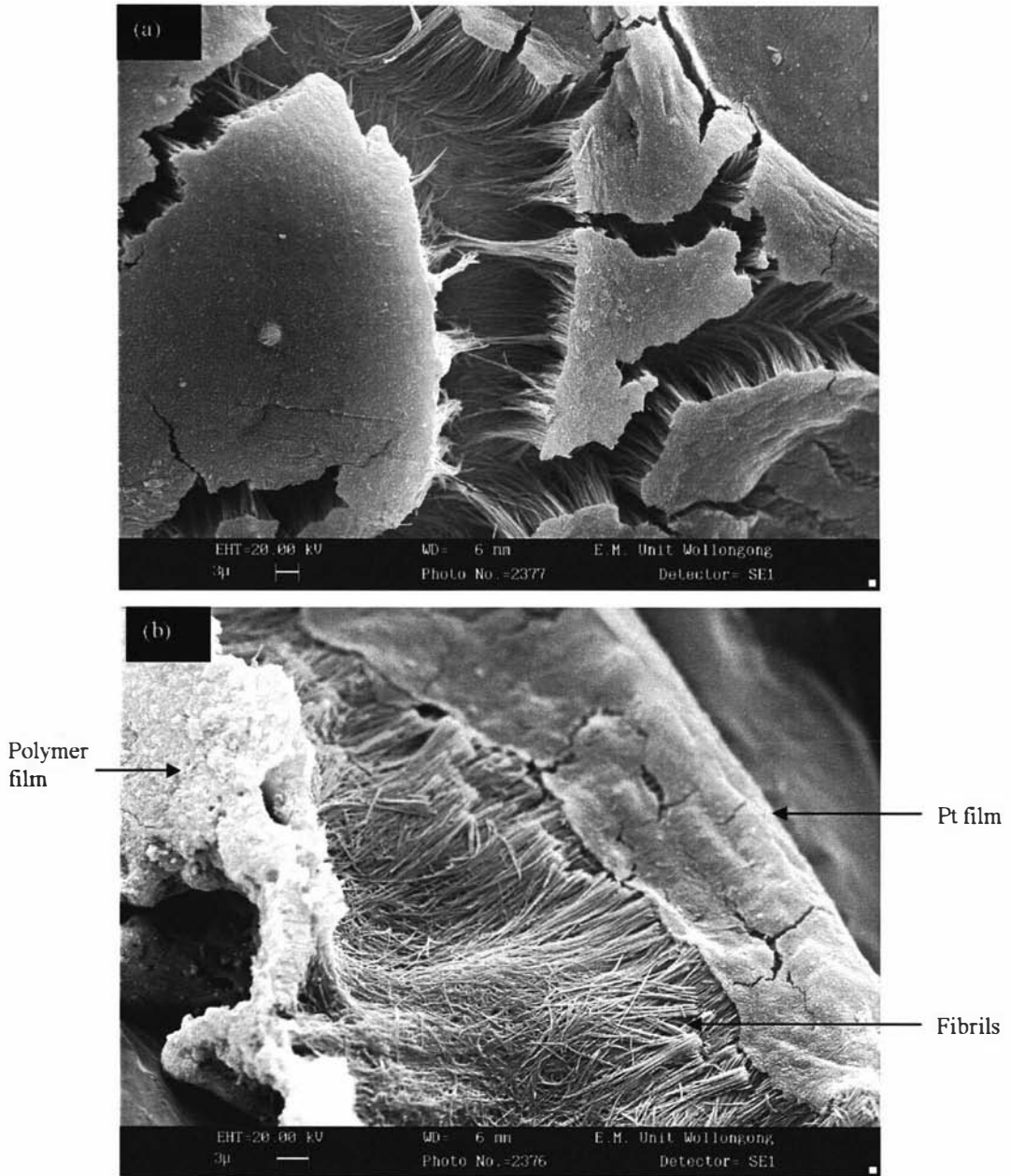


Fig. 6.30. SEM images showing polyOC₁₀DASTT fibrils with a platinum film as a support. (a) Partially dissolved template and viewed from platinum coated side, and (b) cross-section of the fibrils with a polymer film on left and platinum film on the right.

By drying the fibrils on ITO-coated glass (with the platinum side contacting the ITO), a satisfactory contact could be made. Electrochemical analysis of fibrils on ITO-coated glass is given in Fig. 6.31. The polymer fibrils appear to be very stable, showing negligible change in current on cycling.

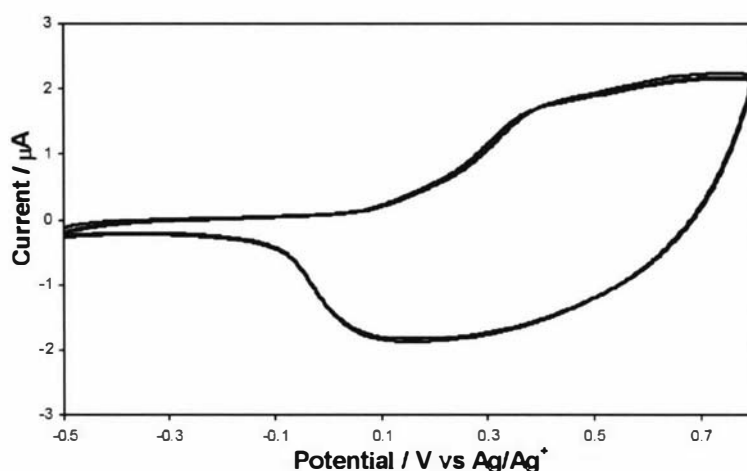


Fig. 6.31. CV of fibrils in a partially dissolved template with a platinum backing stuck on ITO coated glass. Supporting electrolyte: 0.1 M TBAP/AN. Scan rate: 100 mV s^{-1} .

In summary, fibrils of polyOC₁₀DASTT were successfully made by using an alumina template. The fibrils appeared to be stable during repetitive oxidation, and reduction back to a neutral state.

6.5.3 Inverse opal and opal structures

6.5.3.1 Introduction

Films of synthetic opal crystals can be made by sedimentation of colloidal polystyrene (0.2 – 1 μm diameter) onto a substrate. This results in a highly ordered, self-assembled beaded structure with a high surface area. Using this template, opal (bead morphology) and inverse opal (honeycomb morphology) polymer structures can be made. The opal template can be removed by either soaking in an organic solvent such as acetone, or heating in a furnace (450°C). As both these methods may damage a fine layer of polyOC₁₀DASTT, platinum opal and inverse opal structures were made. After removal of the polystyrene, the remaining platinum structure was coated with polymer.

The polystyrene opal was deposited onto ITO-coated glass by evaporation of a emulsion droplet, containing 200 nm or 920 nm polystyrene microspheres in water, at room temperature. Films were also made by spin-coating methods using the same polystyrene emulsion. Although drop-casting resulted in uneven films (even when using gaskets), the films generally resulted in a high degree of ordering. Spin-coating of the polystyrene bead solution onto ITO-coated glass allowed the production of thin films with a larger area than cast films ($\sim 2 \text{ cm}^2$), but with an inferior degree of ordering.

6.5.3.2 Platinum inverse opals (honeycomb structure).

Platinum opals are made by electrochemical deposition of platinum on the ITO-coated glass through the spaces between the opal beads. The opal is then removed (by heating in a furnace at 450°C) to leave a platinum honey-comb inverse-opal structure as shown by SEM in Fig. 6.32.

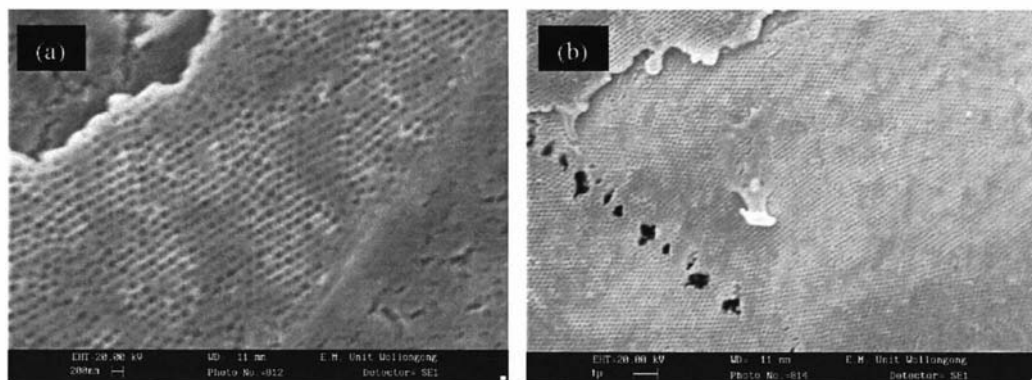


Fig. 6.32. Platinum inverse opals showing the honey comb structure. (a) $\times 7500$ and (b) $\times 3000$ magnification.

6.5.3.3 Platinum, gold and ITO opals (bead structure).

The polystyrene opal (cast onto ITO-coated glass) was sputter-coated with platinum, to give platinum films which retained the iridescent sheen of the underlying opal surface. These films were then heated in a furnace 450°C for 2 hours in an attempt to remove the polystyrene support. SEM images of the resulting platinum opal structures are shown in Figs. 6.33. The metal coating appears to have completely encapsulated

the polystyrene beads, retaining the bead-like morphology and forming a platinum opal structure. This explains the enduring opalescent appearance of these films. Samples showed close-packed (hexagonal) and/or square-packed structuring.

Although these materials were heated in a furnace at 450°C to burn out the polystyrene (melting point: ~240°C), it is unclear whether the polystyrene was completely removed.

The platinum opal films (after heating in the furnace) were removed from the glass slides using adhesive tape. Inspection of the under-side (glass side) of the opal by AFM reveals 'pits', which appear to be left after the polystyrene has been removed (Fig 6.34). The six prominent protrusions observed around each pit is most likely due to filling of the spaces left between opals colloids that are hexagonally (close) packed. The pits indicate that the polystyrene colloids may have been removed.

The platinum opal films were coated with polymer by drop-casting from a chloroform solution. However, poor adhesion of the polymer to the platinum surface created a very uneven film. An attempt was made to improve the quality of the film by synthesising gold and ITO sputter-coated opals. These opals were produced in the same way that the platinum opals were made. SEM images of the resulting gold and ITO opals (after heating in the furnace at 450°C) are displayed in Figs. 6.35 and 6.36 respectively. The gold opal structure (Fig. 6.35) shows uneven bead sizes and non-spherical shapes, possibly due to partial collapsing of the beads by removal of the polystyrene support, and is further evidence that the polystyrene has been removed.

As for the platinum opal film, it was found that polyOC₁₀DASTT did not adhere well to these ITO and gold opal structures.

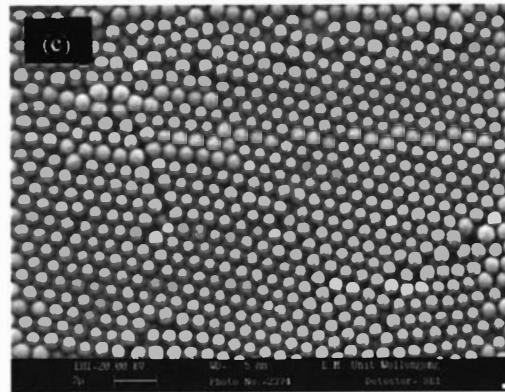
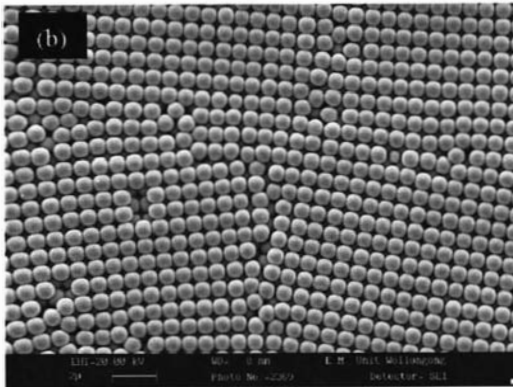
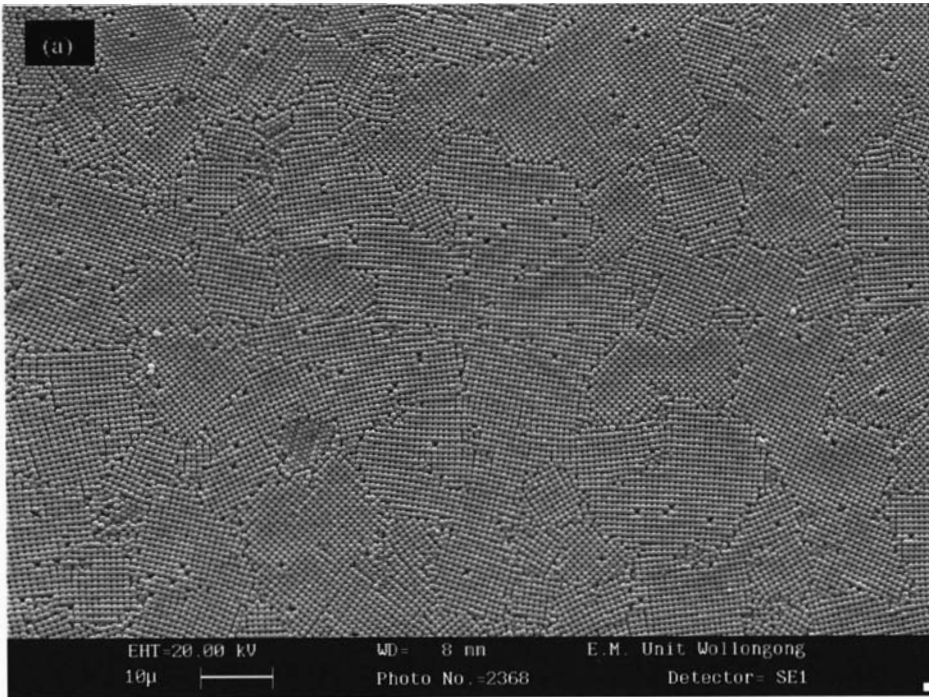


Fig. 6.33. (a) Platinum opal structure produced by sputter-coating the polystyrene opal with platinum, (b) opal showing predominantly body-centred cubic square-packing and (c) opal showing predominantly hexagonal close-packing with polymer coating.

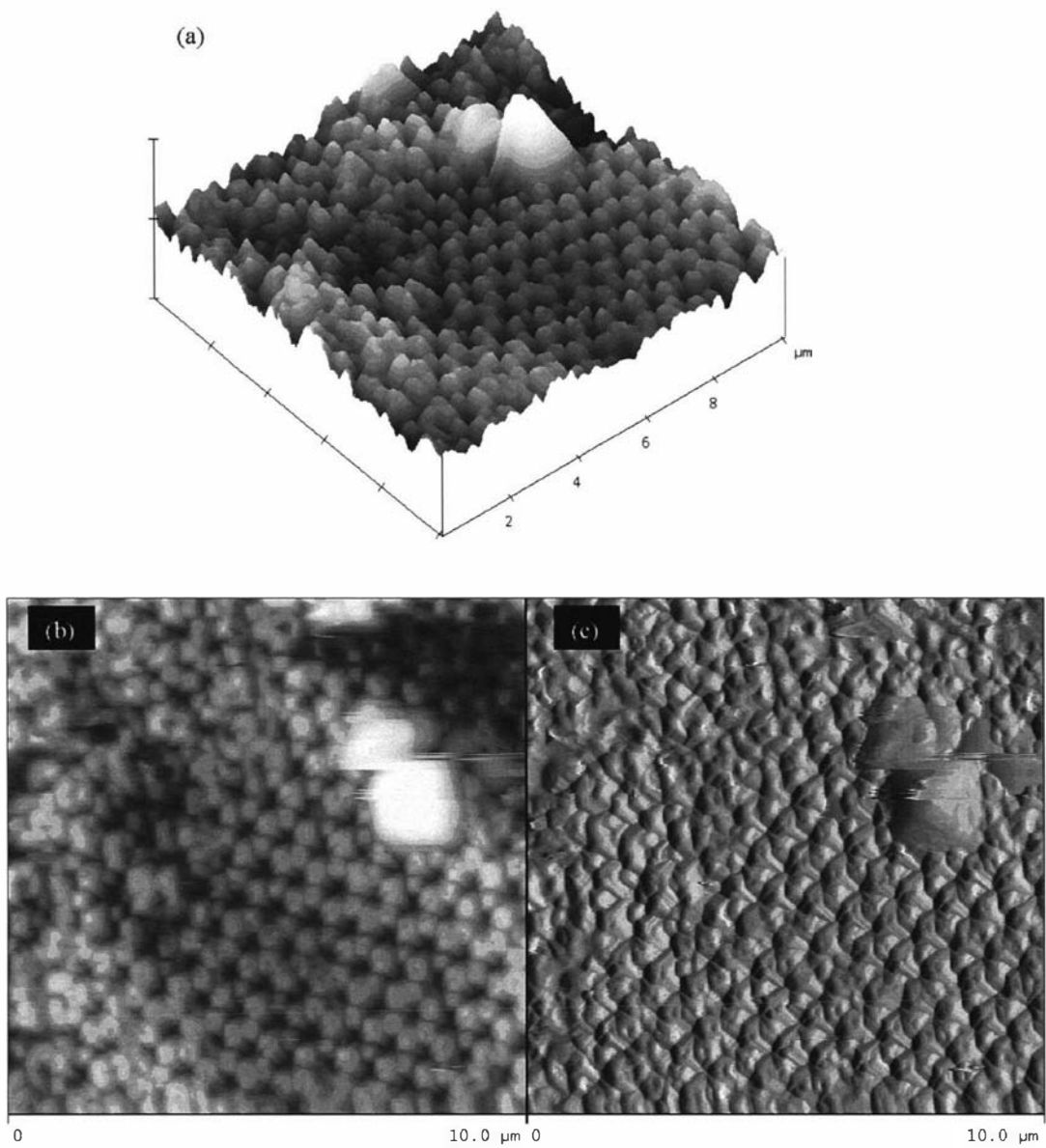


Fig. 6.34. AFM images of the underside of a platinum opal structure. (a) 3-Dimensional image, (b) height data and (c) deflection data. Scan size: 10.00 μm .

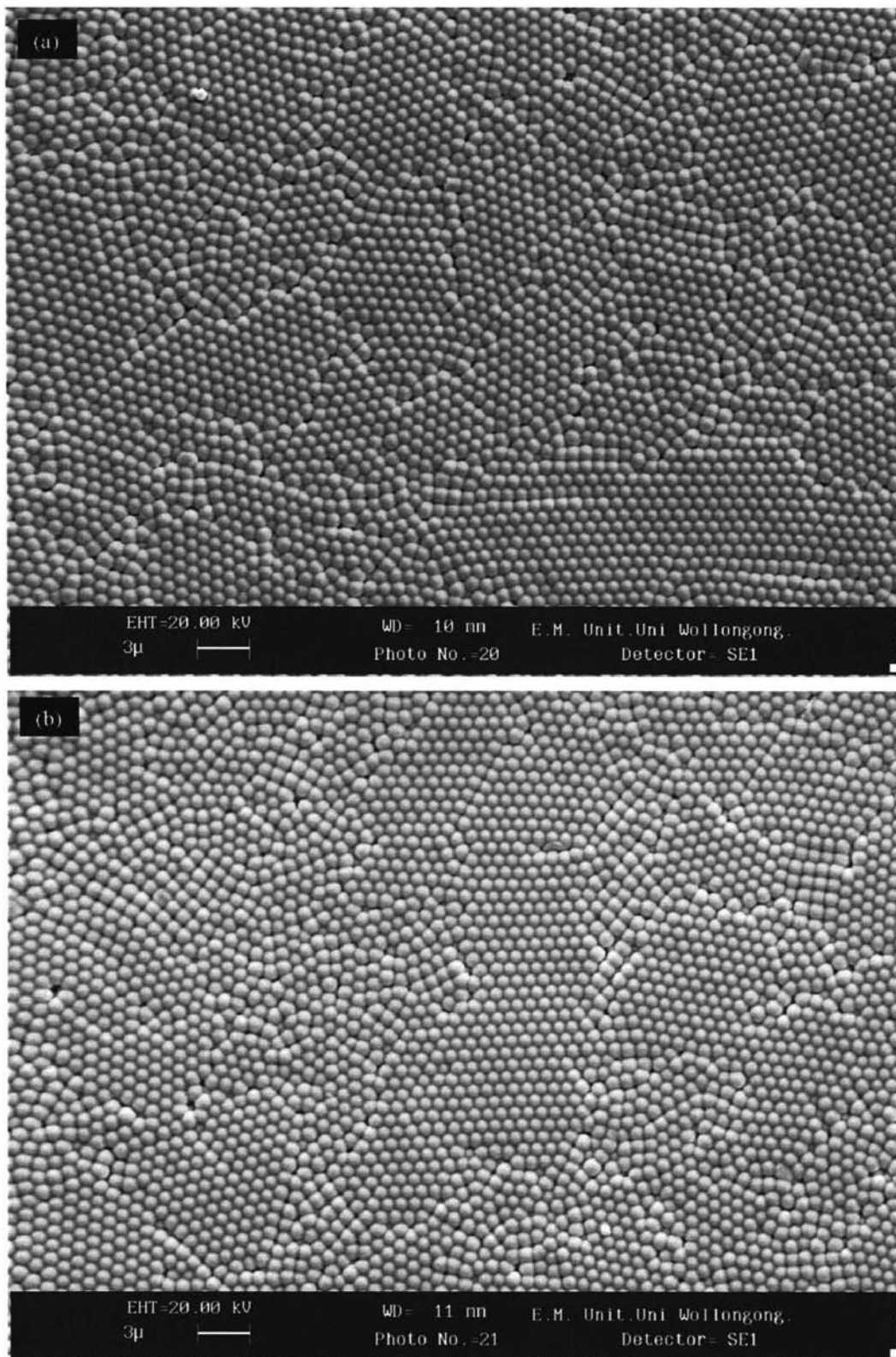


Fig. 6.35. (a) Gold opal surface on ITO-coated glass and (b) poly(OC₁₀DASTT) cast on a gold opal surface.

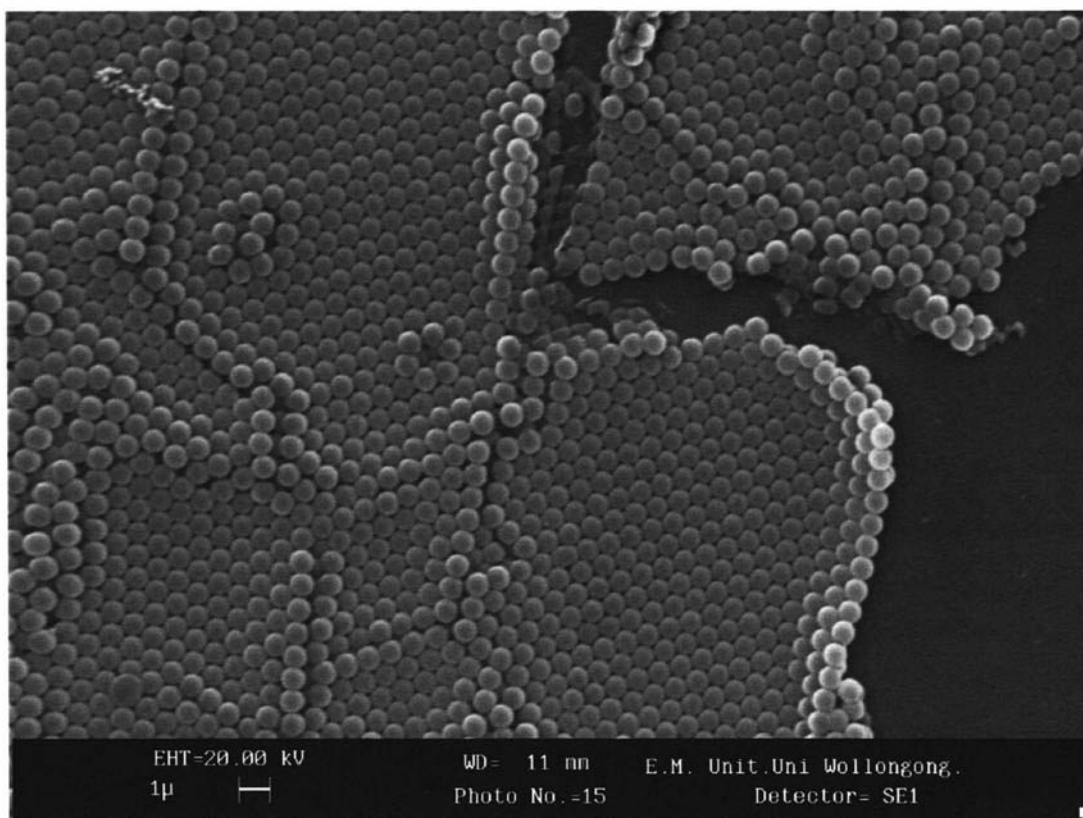


Fig. 6.36. Edge of ITO opal structure on ITO-coated glass.

6.5.3.4 Summary

Platinum opal and inverse opal structured films were successfully made by electrodeposition and sputter-coating of the platinum metal. It was found, however, that polyOC₁₀DASTT did not adhere well to the platinum surfaces. Gold and ITO opal films were made in an attempt to improve the polymer film quality, but this did not work.

6.5.4 Electrospinning

Fibres are fibrils that are entwined to form rope-like structures. Fibres of conducting polymers show potential for applications such as nanowires,¹³ high surface area conducting materials,²⁰⁸ electrodes and sensors.

Electrospinning is one technique used for the formation of polymer fibres.^{13,208,209} By applying a potential difference (typically 30 kV) between a polymer-containing droplet and a target plate, the polymer particles are induced to fly towards the target. Fine polymer fibres are generated as the solvent evaporates.

The electrospinning of chemically synthesised polyOC₁₀DASTT was investigated in this study. Although attempts at electrospinning a pure solution of polyOC₁₀DASTT (50 mg mL⁻¹) in chloroform resulted only in a spray of fine droplets, addition of 5% polyethyleneoxide (PEO) allowed the production of blue/black fibres. SEM images of these fibres (Fig. 6.37) show that they range between 400 and 600 nm in diameter.

Pure PEO fibres were established to be white in colour, and soluble in methanol. The polyOC₁₀DASTT/PEO fibres produced in this study were blue/black and not soluble in methanol. This suggests that the fibres contain polyOC₁₀DASTT, although further analysis would be required to reveal the actual polyOC₁₀DASTT to PEO proportion. PEO does, however, appear necessary for the formation of polyOC₁₀DASTT fibres. Solution viscosity has been found to be a significant parameter in fibre formation.¹²⁹ Since it was observed that addition of PEO to the solutions (in amounts as low as 5%) dramatically increased the viscosity of the solution, this may be a significant role of PEO.

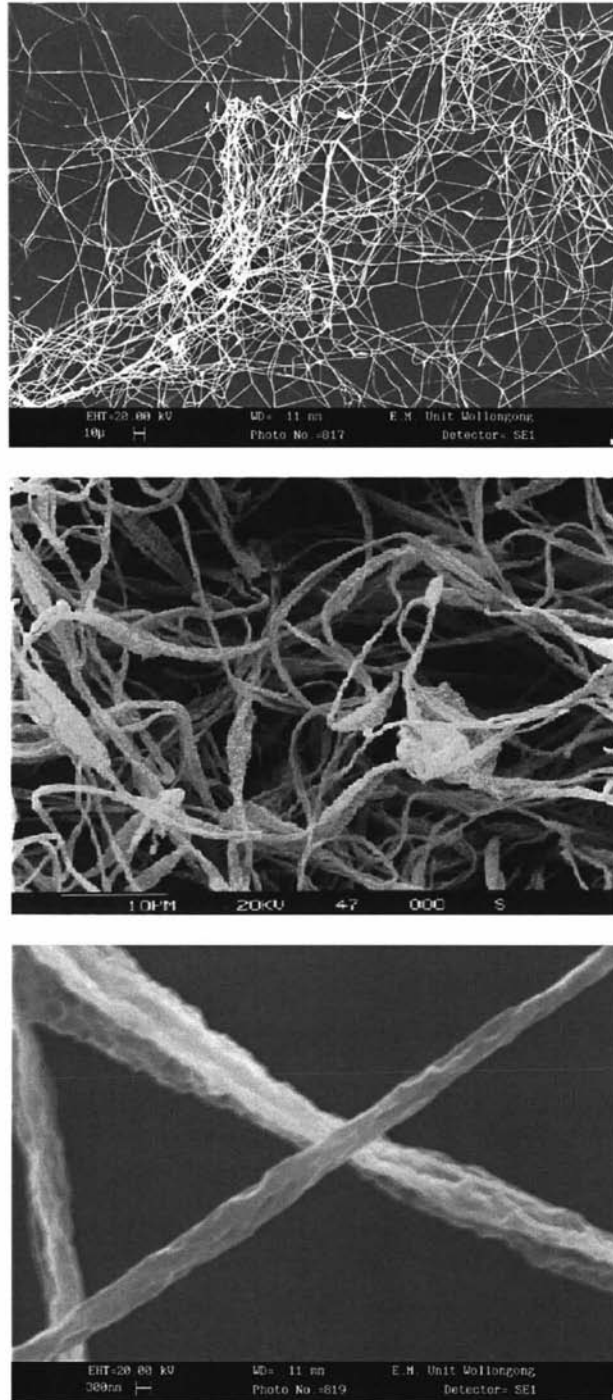


Fig. 6.37. SEM images at different magnifications of electrospun poly(OC₁₀DASTT) fibres.

6.5.5 Conclusions

The solubility of polyOC₁₀DASTT allowed preparation of nanostructured surfaces by casting and electrospinning methods. This material was successfully made into fibrillar structures by casting onto a template, and fibres by electrospinning. Both of these structures display a high surface area that should be useful for improving the efficiency of devices.

Platinum, gold and ITO opal structured films were successfully made by sputter-coating polystyrene opal surfaces. Platinum inverse-opal surfaces on ITO-coated glass could also be made by electrodeposition through the polystyrene opal beads, followed by removal of the polystyrene. Unfortunately, it was found that polyOC₁₀DASTT did not adhere well to these surfaces.

6.6 Conclusions

A selection of the styryl-substituted oligo- and polythiophenes reported in Chapter 3-5 were incorporated and tested in PEC cells. A cell incorporating a cast film of chemically dimerised NMe₂STT produced a FF of 35%, the same as that reported by Cutler *et al.* for a similar cell incorporating a dimethylaminostyryl-substituted thiophene/bithiophene copolymer. Photoelectrochemical devices made from polyOC₁₀DASTT did not give any detectable photovoltaic activity, possibly due to the high stability of this polymer in the oxidised state. PEC cells incorporating films of styryl-thienylenevinylene derivatives showed an increase in photovoltaic activity with an increasing electron-donating effect of the *p*-phenyl substituent.

PVDF membrane benders and fibres, as well as a stand-alone film were synthesised from simple solution casting of polyOC₁₀DASTT. These structures have been shown to possess electromechanical properties by undergoing a reversible volume change in response to a repetitive potential pulse in an electrolytic media. It was shown that a stand alone polyOC₁₀DASTT film actuator could achieve a strain of up to 3.3% under a stress level of 44 kPa. A relatively low strain rate of about 0.011% was observed for a stand-alone film. This modest result may be due to the electrolyte struggling to penetrate the film and/or poor accessibility of charge due to the low conductivity of the material. Although this strain rate may be improved by using a conductive substrate, casting or electrochemical growth of a polyOC₁₀DASTT film of suitable thickness onto a platinum surface proved difficult.

The good discharge capacity and excellent cycle life shown by the Teflon test batteries described in this study, reveals potential for polyOC₁₀DASTT as an active anode material for all-polymer batteries. The substrate that the polyOC₁₀DASTT was cast onto was shown to have a significant effect upon the performance of the cell. Ni/Cu coated nonwoven polyester fabric was found to produce significantly improved discharge capacity compared to anodes comprising carbon fibre mat as a substrate. A high discharge efficiency of >94% was generated by both types of cells with anodes employing polyOC₁₀DASTT.

Soluble polyOC₁₀DASTT was successfully fabricated into fibrillar structures by casting onto templates, and fine fibres by electrospinning. These materials were observed by microscopy to have high surface areas.

6.7 Experimental Procedures

6.7.1 PEC devices

Tetrabutylammonium perchlorate (TBAP, Fluka), iodine (Univar, Ajax or Aldrich 99.8%), methanol (Univar, Ajax), acetonitrile (AN, Univar, Ajax), dichloromethane (DCM, Univar, Ajax), isopropanol (Univar, Ajax), tetrapropylammonium iodide (Sigma-Aldrich, $\geq 98\%$), ethylene carbonate (Sigma-Aldrich 99%), propylene carbonate (Sigma-Aldrich 99%) and chloroform (Sigma-Aldrich) were used without further purification. ITO (indium tin oxide) coated glass ($\leq 10 \Omega \text{ cm}^{-2}$) was purchased from Delta Technologies Limited (USA), cut into required sizes, washed with liquid detergent, rinsed thoroughly with Milli-Q water followed by acetone, and allowed to dry. Before coating with polymers, the ITO coated glass was treated in an UVO-cleaner (Model No. 42-220, Jelight Co. Inc., USA).

Electrochemical synthesis of films, and photovoltaic testing was performed using an EG&G PAR 363 Potentiostat/Galvanostat, a MacLab 400, and EChem v 1.3.2 software (ADInstruments).

The counter electrode (cathode) was produced by sputter coating a thin layer of platinum onto ITO coated glass. The sputter coating was done using a Dynavac Magnetron Sputter Coater Model SC100MS at a current of 50mA and argon pressure of 2×10^{-3} mbar. A Pt thickness of 10Å was sputter coated.

Liquid electrolyte was prepared by dissolving Iodine (60 mM) and tetrapropylammonium iodide (500 mM) in a 1:1 (by weight) mixture solution of ethylene carbonate and propylene carbonate. This results in a I_3^-/I^- redox couple being formed in solution.

The polymer was deposited onto ITO coated glass either electrochemically from the monomer, by casting, or by spin-coating. Electrochemically produced films were reduced at -0.5 V vs. Ag/Ag^+ in 0.1 M TBAP/AN, rinsed with acetonitrile and allowed

to dry. The device was assembled by sandwiching the I/I_3^- liquid electrolyte between the platinum sputter coated ITO coated glass electrode (cathode) and the polymer coated ITO glass electrode (anode) as shown in Fig. 6.1. A gasket made of parafilm was used to separate the electrodes to avoid short circuits and to contain the liquid electrolyte.

The devices were tested immediately after fabrication in a large dark box containing a broad spectrum halogen lamp (500 W m^{-2} , SOLUX, 4700K, Wiko Ltd.) The polymer coated side was faced to the lamp. Linear sweep voltammetry with a lower limit of -50 mV , an upper limit of 250 mV and a scan rate of 100 mV s^{-1} was used to record the $I-V$ curve. This potential range was scanned first in the dark then under illumination to record the change in current due to the absorption of light.

Films of NO_2STV , CNSTV and STV oligomers were electrodeposited onto ITO-coated glass using cyclic voltammetry (-0.5 V to 0.8 V), and OMeSTV and NMe_2STV oligomers by constant potential (0.8 V) due to their high solubility in the neutral state. The films were then reduced at -0.5 V in monomer free 0.1 M TBAP/AN. A film of oligo NMe_2STT was electrochemically deposited using a constant potential (0.9 V for 30 seconds) and then reduced (-0.5 V in monomer free solution) to a neutral state.

6.7.2 Actuator fabrication and experimental procedures

Chloroform, tetrabutylammonium hexafluorophosphate (TBAPF_6) and propylene carbonate (PC) were obtained from Sigma-Aldrich and used without further purification. Inert porous polyvinylidene fluoride (PVDF) membrane sheets and fibres were obtained from Millipore, MA01730. Platinum sputter-coating of the sheets was performed using a Magnetron Sputter Coater, DYNAVAC Sc 100MS using a constant current of 50 mA for 20 minutes.

Poly $\text{OC}_{10}\text{DASTT}$ ($12 \mu\text{g mm}^{-2}$) was cast onto both platinum coated, and non-coated PVDF membranes. These membranes were cut into $30 \times 2 \text{ mm}$ strips which were $115 \mu\text{m}$ thick. The strips were tested using a 3 electrode cell in a Petri-dish. An

electrolyte consisting of 0.25 M TBAPF₆/PC was used with a stainless steel mesh counter electrode and a Ag/Ag⁺ reference electrode.

Electrochemical deposition of OC₁₀DASTT onto platinum sputter-coated PVDF membrane was attempted using galvanostatic methods by applying constant current (0.5 mA cm⁻²) for twelve hours in a 1:1 AN:DCM solution containing 10 mM monomer and 0.1 M TBAP. This solvent mix is required to dissolve the monomer without solvation of the resulting polymer. The deposition was carried out at 4°C to further slow polymerisation, and the reaction vessel sealed to reduce evaporation of the dichloromethane. Electrochemical deposition was also attempted from a 2:1 PC:DCM solution containing 5 mM OC₁₀DASTT and 2% polyhydroxy ether /propylene carbonate. Both galvanostatic methods (0.05 mA cm⁻² for four hours) and potentiostatic methods (0.8 V for 1.5 hrs) were performed at 4°C.

A free-standing film was produced by casting a chloroform solution of polyOC₁₀DASTT evenly over a glass surface on which a zigzagged wire (50 μm diameter) was placed. The resulting film with incorporated wire was peeled off and cut to appropriate dimensions: 6 mm wide and 14.5 mm in length.

Spectra were measured using a Cary 500 UV-VIS-NIR spectrophotometer (Varian) in the reflectance mode and the data recalculated to show absorbance. Cyclic voltammetry of cast poly(OC₁₀DASTT) films on glassy carbon electrodes or PVDF membranes was performed using a 3-electrode, 1-compartment cell setup. A platinum mesh counter electrode and Ag/Ag⁺ reference electrode was used with an electrolyte solution of 0.1 M TPAP/AN. A scan-rate of 10 mV s⁻¹ or 100 mV s⁻¹ was used as indicated. Conductivity measurements were made using a multiheight four-point probe with a Jandel raising and lowering mechanism and a cylindrical probe.

Samples were tested using a 305B Dual Mode Lever System (Aurora Scientific Inc.). The bottom of the sample was held stationary with a platinum wire wound around a clamp which also functioned as the working electrode connection. The top of the sample was held by a silicon rubber clamp which was connected to the lever by a stiff

wire. The entire sample was submerged in a 0.25 M TBAPF₆/PC electrolyte solution. A high surface area stainless steel mesh sheet and a Ag/Ag⁺ reference electrode were employed as the counter and reference electrodes respectively to complete a 3-electrode cell setup. The potential was controlled, and data measured by an EG&G PAR model 363 potentiostat/galvanostat with a MacLab 400 electrical interface. The data was recorded by Chart software (V3.3.7, ADInstruments). All measurements were made at room temperature.

Before performing electromechanical measurements, the free-standing film was pre-conditioned. A small constant 40 mN stretching force was loaded to on the top of film in order to keep it straight and 4 hour square wave pulsed potential between +1/-0.6 V (vs Ag/Ag⁺) was applied from the electrical contact at the bottom of the film. This process was conducted for 24 hrs until a steady equilibration state was obtained.

6.7.3 Details of battery fabrication and testing procedures

The anode was prepared by drop-casting a solution of polyOC₁₀DASTT in chloroform onto either a carbon fibre mat substrate (resistance of ~10.5 Ω cm⁻¹) or Ni/Cu coated nonwoven polyester substrate (resistance of <0.5 Ω cm⁻¹). Several coats were applied to give a polymer coating of about 1 mg cm⁻².

The cathode was prepared by galvanostatic electro-deposition of polypyrrole onto stainless steel mesh. A current density of 1.0 mA cm⁻² was employed with a propylene carbonate (PC) solution containing 0.06 M monomer (pyrrole) and 0.05M tetrabutylammonium hexafluorophosphate (TBAPF₆). Prior to the experiment, the solution was deaerated with N₂. A total charge density of 3.0 C cm⁻² was consumed in the deposition of the polypyrrole film.

Cyclic voltammetry of the polymer was performed using an EG&G PAR 363 potentiostat/galvanostat, a MacLab 400, and EChem v 1.3.2 software (ADInstruments). The electrochemistry was performed using a standard one

compartment, three-electrode cell with a stainless steel mesh counter electrode, Ag/Ag⁺ reference electrode and a 0.05 M TBAPF₆/PC electrolyte.

The surface morphologies of the electrodes were investigated using a scanning electron microscope (SEM, Leica Model Stereoscan 440) with a secondary electron detector. All materials were sputter coated with gold prior to scanning.

The test cells were assembled in an argon-filled glove box (Unilab, Mbraun, USA). For fabrication of the test cell, the anode and cathode material were cut into 1 x 1 cm² squares. These were separated by a Celgard 2500 (microporous polypropylene membrane) and submerged in an electrolyte consisting of 1.0 M LiPF₆ in 1:1 ethylene carbonate:dimethylcarbonate solution. In order to let the electrolyte penetrate into the inner part of the active material in the electrodes, the Teflon cells were kept at room temperature for 2 hours after the assembly.

Cells were tested using a battery testing device (Neware Electronic Co. China). Different current densities were employed to investigate the properties of the cell. The cells were galvanostatically charged to a cell voltage of 1.65 V, and then discharged at the same current density to a cut-off voltage of 0.2 V. For the cycle life test, the cell was initially activated by cycling at a current density of 0.02 mA cm⁻² for several cycles until a steady charge/discharge capacity was obtained. Cycle life testing was then performed under a charge/discharge current density of 0.05 mA cm⁻².

6.7.4 Fabrication and evaluation of nanostructures

General

Tetrabutylammonium perchlorate (TBAP, Fluka), methanol (Univar, Ajax), acetonitrile (AN, Univar, Ajax), dichloromethane (DCM, Univar, Ajax), chloroform (Sigma-Aldrich), propylene carbonate (Aldrich 99%) were used without further purification. ITO (indium tin oxide) coated glass ($\leq 10 \Omega \text{ cm}^{-2}$) was purchased from Delta Technologies Limited (USA), cut into required sizes, washed with liquid detergent,

rinsed thoroughly with Milli-Q water followed by acetone, and allowed to dry. Before coating with polymer, the ITO-coated glass was treated in an UVO-cleaner (Model No. 42-220, Jelight Co. Inc., USA) for 15 mins.

Electrochemistry was generally performed using an EG&G PAR 363 potentiostat/galvanostat, a MacLab 400, and EChem v 1.3.2 software (ADInstruments). Charge measurements were made using a BAS CV27 voltammograph. A standard one compartment, three-electrode cell with a stainless steel mesh or platinum mesh counter electrode and a Ag/Ag⁺ reference electrode with 0.1 M TBAP/AN salt bridge was used. An electrolyte solution of 0.1 M TBAP/AN was employed for analysis of polymeric samples using cyclic voltammetry.

Imaging by scanning electron microscopy (SEM) was carried out using a Leica-stereoscan SS 440 Microscope. Non-conductive surfaces were sputter-coated with gold prior to imaging. Atomic force microscopy (AFM) was performed on a DI (Digital Instruments) 3100 NanoMan. A tapping mode was used for all imaging.

Sputter-coating of gold, platinum or ITO was performed using a Dynavac Magnetron Sputter Coater Model SC100MS.

Fabrication of fibrillar structures

The template used in this study to fabricate fibrillar structures was a Whatman anodisc 13 membrane composed of alumina, with honeycomb shaped pores of 200 nm diameter. Sputter-coating of the template with platinum was achieved at a current of 30mA and argon pressure of 2×10^{-3} mbar for 10 mins. A film thickness of 10 Å was sputter coated. The template was soaked in a solution of polymer (about 2 mg mL⁻¹) for one hour. The template containing the fibrils was then removed from the solution and drip dried.

The template was either fully dissolved by soaking in 0.5 M NaOH for 50 minutes to leave a very fragile film of polymer fibrils, or partially dissolved by soaking in 0.5 M NaOH for 25 minutes to leave an alumina support. Finally, the fibrils were rinsed with deionised water.

Fabrication of opal and inverse opal surfaces

Polystyrene opals were prepared by air drying a drop-cast film or spin-coated film of polybead[®] dyed blue solution (0.20 micron microspheres, 2.63% solids-latex, Polysciences Inc., Warrington PA) or polystyrene particles (0.92 $\mu\text{m} \pm 0.07 \mu\text{m}$ diameter, Microparticles, GmbH, Germany) on ITO-coated glass ($\sim 2 \text{ cm}^2$ area). This was allowed to dry and pack for at least 24 hours to form an organized structure.

Platinum inverse opals (honey comb structure) were created by electrochemically depositing platinum from a solution containing hexachloroplatinic (IV) acid, concentrated nitric acid and concentrated hydrochloric acid. This solution was made by stirring platinum granules (1 g) in 10 mL of aqua regia (2:1 v/v HCl:HNO₃) for 48 hrs while heating at 70°C.

Both cyclic voltammetry growth methods (five or ten cycles at scan rates of 50 or 100 mVs^{-1} between the limits of -400 to 1600 mV vs. Ag/Ag⁺) and potentiostatic growth methods (-0.4 V at 100 seconds) were investigated. It was found that inverse opal adhered very poorly to the ITO surface and peeled away when the slide was removed from solution. In addition, platinum did not always deposit properly and there was a problem of 'beading' which covered the opal structure. The best films were obtained using cyclic voltammetry (either 10 cycles at 100 mVs^{-1} or five cycles at 50 mVs^{-1}). The growth CV for platinum deposition at 100 mVs^{-1} is shown below in Fig. 6.38. The voltammograms at 50 mVs^{-1} are similar but display a slightly higher current.

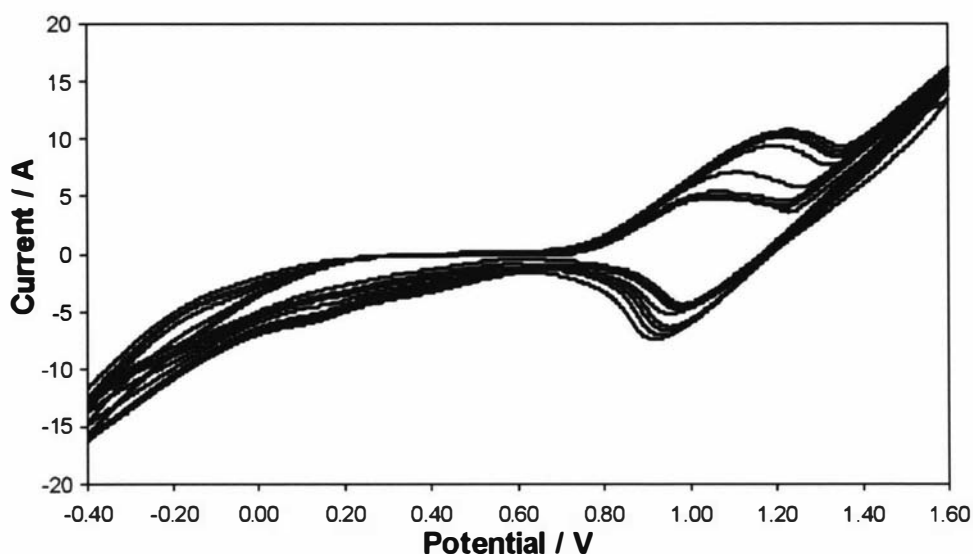


Fig. 6.38. Growth of platinum on opal coated ITO coated glass. 10 cycles. Scan rate: 100 mV s^{-1} .

Platinum, gold or ITO opal structures (beads) were prepared by sputter-coating the polystyrene opal with platinum. A film thickness of $\sim 120 \text{ nm}$ was deposited by applying a current of 50 mA and argon pressure of $2 \times 10^{-3} \text{ mbar}$ for 10 mins.

The polystyrene opal was then removed from the structure by heating in a furnace at 450°C for two hours, or by soaking in chloroform for 24 hrs. The remaining metal or ITO opal structures were subjected to an ozone atmosphere for 15 minutes. PolyOC₁₀DASTT was then drop cast onto a 27 mm^2 area of the remaining metal or ITO opal structure by using a circular shaped gasket.

Electrospinning

PolyOC₁₀DASTT fibres were synthesised by electrospinning a solution of chemically synthesised polyOC₁₀DASTT (50 mg mL^{-1}) with 5% PEO in chloroform (1 mL).

The solution to be electrospun was filtered through a 0.45 mm filter and placed in a hypodermic syringe 20 – 30 cm from a galvanized steel target place covered with aluminium foil. The positive (anode) electrode of a variable high voltage transformer (Gamma High Voltage Research, Ormond, Florida 32174) was attached to the metal needle of the syringe and the negative terminal was attached to the target electrode. A 20 kV differential was applied across the electrodes. Fibres were collected by passing a

glass slide or silicon wafer between the electrodes and washed with methanol to remove any residue PEO.

Chapter 7

Conclusions

This work demonstrates that, although oxidation of styryl-terthiophene results in insoluble and short-chain material, the attachment of alkoxy substituents allows the synthesis of soluble polymer. Although not suitable as an active material in photovoltaics, alkoxy-substituted styrylterthiophene (polyOC₁₀DASTT) exhibits potential as an active material for use in actuators and battery anodes.

Styryl-substituted terthiophenes (Chapter 3)

The chemical oxidation of a series of styryl terthiophene derivatives, functionalised by electron-withdrawing or donating substituents, resulted in the production of mostly insoluble materials. Although the insoluble fraction was difficult to characterise and further process, analysis of the soluble fraction revealed predominantly dimer with traces of short oligomers ($n < 4$). It was shown by NMR spectroscopy that the dimeric materials produced are predominantly of the head-to-head isomer, which is consistent with reports by Grant *et al.* who studied ether-substituted styrylterthiophene derivatives,¹¹ and theoretical calculations of similar materials by Clarke *et al.*¹⁴⁰ However, it was found to be difficult to isolate the head-to-head isomers of these materials.

It was then demonstrated that films of these materials could be grown both potentiostatically and electrodynamically. UV-VIS-NIR spectra of these films indicated that they consisted predominantly of oligomers with a short effective conjugation length. SEMs of the films showed evidence of crystallinity, consistent with films of styrylsexithiophene derivatives reported by Grant.¹¹

Styryl-substituted terthienylenevinylene (Chapter 4)

The electrochemical oxidation of a series of styryl-substituted terthienylenevinylene derivatives was also found to generate films consisting predominantly of dimer. This is consistent with the chemical oxidation of these materials that was reported by Wagner

*et al.*¹⁵⁶ The low degree of polymerisation of these materials may be due to a low reactivity of the terminal 'α' positions of the monomers due to their extended π-conjugation.²³

Films of terthiénylenevinylene oligomers were observed to generate absorption maxima (due to the $\pi \rightarrow \pi^*$ transition), at higher wavelengths than those of films of terthiophene oligomers with the same substituent. This is consistent with reports in the literature of smaller bandgaps produced by polythiénylenevinylenes than polythiophenes,¹⁰² and is most likely due to an increase in the effective conjugation length provided by the addition of the vinyl linker and/or increased planarity of the oligomer chain allowing enhanced π -orbital overlap.

Alkyl and alkoxy substituted styryl terthiophenes (Chapter 5)

The chemical and electrochemical polymerisation of alkyl- and alkoxy-substituted styrylterthiophenes was investigated. It was found that attachment of these substituents at the 4 and 4' positions enhanced polymerisation of styrylterthiophene and improved the solubility of the resulting materials.

The chemical polymerisation of C₇-dialkyl-substituted styrylterthiophene (C₇DASTT) was found to produce a polymer with an average chain length of *ca.* $n = 6$ and maximum detectable length (by MALDI-TOF MS) of *ca.* $n = 12$. This material (polyC₇DASTT) appeared to be very stable in the neutral state and readily reduced to the neutral state. PolyC₇DASTT was found to be completely soluble in chloroform.

In comparison, polymerisation of C₆-dialkoxy-substituted styrylterthiophene (OC₆DASTT) generated longer oligomers, with an average polymer length of *ca.* $n = 11$ and maximum detectable length of *ca.* $n = 35$ (indicated by MALDI-TOF). PolyOC₆DASTT was shown to be very stable in the oxidised state, and chemical reduction proved difficult. The high stability of the polymer in the oxidised state may be explained by the strong electron-donating properties of the alkoxy substituent, which stabilises the positive charge. Only 78% of polyOC₆DASTT was soluble. The poorer solubility of polyOC₆DASTT compared to polyC₇DASTT may be due to a much higher stability of the alkoxy derivative in the oxidised (less soluble) state. It is

also possible that the lower solubility when compared to polyC₇DASTT may be due to the presence of longer chain OC₆DASTT polymer.

Lengthening the alkoxy chain from 6 carbons (polyOC₆DASTT) to 10 carbons (polyOC₁₀DASTT) did not appear to affect the resulting length of the polymer (which also showed an average polymer length of *ca.* $n = 11$ by MALDI-TOF MS), but did increase the solubility to provide a chloroform soluble fraction of 97% of the total expected polymer yield. UV-VIS-NIR spectroscopy indicated that more of the soluble polyOC₁₀DASTT material appeared to be in a partially oxidised state. Therefore, the higher fraction of soluble material compared to polyOC₆DASTT may be due to the fact that partially oxidised material is soluble.

The presence of the alkyl and alkoxy substituents was found to cause a significant reduction in the oxidation onset potential of the monomers compared to STT, which may account for their higher degree of polymerisation. The alkoxy substituents were also observed to significantly decrease the oxidation potential of the resulting polymer, consistent with the high stability observed by chemically polymerised polyOC₆DASTT and polyOC₁₀DASTT in the oxidised state. Electrochemically deposited films of these alkoxy-DASTT materials on ITO-coated glass were observed to show folding on oxidation, most likely due to the incorporation of dopant ions into the polymer matrix.

Experimental conditions during the chemical polymerisation of OC₆DASTT and OC₁₀DASTT were found to have a significant effect on the resulting polymer length, and hence solubility. It was found that addition of the oxidant to monomer produced shorter oligomers, most likely due to a decrease in the initial oxidant:monomer ratio and hence rate of reaction. It was also found that the presence of ethanol decreased the average oligomer length, which may be explained by an effect of the ethanol on the oxidation potential of the iron(III) chloride oxidant.

Polymers of different lengths were successfully separated using sequential extractions in a series of solvents. The average polymer length was found to increase with each sequential extraction as determined by MALDI-TOF MS. A bathochromic shift of the absorbance maxima, and reduction in oxidation onset potential of cast films of the

OC₁₀DASTT oligomer/polymer fractions was observed with increasing polymer length, indicating a corresponding increase in the mean conjugation length.^{114,127}

The CVs of cast films of chemically polymerised polyOC₆DASTT and polyOC₁₀DASTT displayed oxidation and reduction peaks that were much broader than peaks generated by electrochemically polymerised and deposited polyOC₆DASTT and polyOC₁₀DASTT films. This may be due to a wider polydispersity of the chemically polymerised materials,¹⁵⁹ and/or a less consistent film morphology produced by the casting method compared to electrochemical deposition.

The use of substituted terthiophene and terthienylenevinylene oligomeric/polymeric materials in photovoltaic devices (Chapter 6)

Photoelectrochemical cells with anodes comprising electrochemically deposited films of styryl-thienylenevinylene derivatives showed an increase in photovoltaic activity with an increasing electron-donating effect of the *p*-phenyl substituent.

Photoelectrochemical devices made from polyOC₁₀DASTT did not give any detectable photovoltaic activity. This may be caused by a high stability of this polymer in the oxidised state. Schottky devices using polyOC₁₀DASTT also produced poor photovoltaic results, with low I_{sc} and V_{oc} values. However, polyOC₁₀DASTT was found to produce a spectral response that extended to 750 nm. Addition of PPV to the polymer mixture appears to add to the SR and photovoltaic performance.

Use of polyOC₁₀DASTT in actuator devices (Chapter 6)

PolyOC₁₀DASTT actuators were shown to generate a moderate strain, although a low strain rate. This is possibly due to difficulty in diffusion of the anion molecules through the compact polymer matrix. It could also be due to poor charge accessibility throughout the film in the neutral state. However, the simple preparation of actuator materials using this polymer provides potential for some applications where a low strain rate is required.

Use of polyOC₁₀DASTT as an anode in all-polymer batteries (Chapter 6)

PolyOC₁₀DASTT showed promise as a good anode active material for an all-polymer battery. A battery comprised of polypyrrole (cathode-active material), polyOC₁₀DASTT (anode-active material) and LiPF₆ as an electrolyte displayed an excellent discharge capacity, discharge efficiency and cycle life over fifty cycles. The substrate on which polyOC₁₀DASTT was cast was found to affect the performance of the cell, suggesting that more work is required to find an optimum anode substrate.

Micro- and nanostructured surfaces (Chapter 6)

The solubility of polyOC₁₀DASTT allows this material to be prepared by simple casting or spin-coating methods to produce films and surfaces for applications such as photovoltaic cells, actuator materials and battery electrodes. PolyOC₁₀DASTT can be moulded into nanostructured surfaces (fibrils, opals and fibres), which have high surface areas. These surfaces can now be used in device fabrication to increase device efficiency.

The ease of functionalising terthiophene with an assortment of substituents via a styryl linker presents the opportunity to supply a large range of polymer properties. By attachment of the alkoxy substituents to allow the preparation of processable polymer, the door is opened for use of these polymers in a variety of applications. Continuation of the work presented in this thesis could include reducing the alkoxy chain length to generate anode active materials with higher charge/discharge capacities. The effect of electron-withdrawing/donating substituents on the ability of poly(dialkoxy-substituted styrylterthiophene) to perform as an anode active material could also be investigated. Finally, it would be interesting to see if the tensile strength and strain rate of actuators constructed using poly(OC₁₀DASTT) could be improved, possibly by blending the polymer with a conducting and strengthening material.

Bibliography

- (1) Wallace, G. G.; Spinks, G. M.; Kane-Maguire, L. A. P.; Teasdale, P. R. *Conductive electroactive polymers*, 2nd Ed.; CRC Press: Boca Raton, 2003.
- (2) Allcock, H. R.; Lampe, F. W.; Mark, J. E. *Contemporary polymer chemistry*, 3rd Ed.; Pearson Education Inc.: New Jersey, 2003.
- (3) Shirakawa, H. *Synth. Met.* **2001**, *125*, 3-10.
- (4) MacDiarmid, A. G. *Synth. Met.* **2001**, *125*, 11-22.
- (5) Biserni, M.; Marinangeli, A.; Mastragostino, M. *J. Electrochem. Soc.* **1985**, *132*, 1597-1601.
- (6) Kaufman, J. H.; Chung, T. C.; Heeger, A. J.; Wudl, F. *J. Electrochem. Soc.* **1984**, *131*, 2092-2093.
- (7) Kraft, A.; Grimsdale, A. C.; Holmes, A. B. *Angew. Chem., Int. Ed.* **1998**, *37*, 403-428.
- (8) Roncali, J. *Chem. Rev.* **1992**, *92*, 711-738.
- (9) Beaupre, S.; Leclerc, M. *Adv. Funct. Mater.* **2002**, *12*, 192-196.
- (10) Reddinger, J. L.; Reynolds, J. R. *Polym. Prepr. (Am. Chem. Soc., Div. Polym. Chem.)* **1997**, *38*, 321-322.
- (11) Grant, D. K., *The synthesis and properties of polyether substituted oligothiophenes*. Ph.D. Thesis, Institute of Fundamental Sciences, Massey University, **2003**.
- (12) Garnier, F. *Angew. Chem.* **1989**, *101*, 529-533.
- (13) Jones, W. E., Jr.; Dong, H.; Nyame, V.; Ochanda, F. *Annual Technical Conference - Society of Plastics Engineers* **2003**, Vol. 2, 1948-1950.
- (14) Higgins, S. J. *Chem. Soc. Rev.* **1997**, *26*, 247-258.
- (15) Higgins, S. J.; Pounds, T. J.; Christensen, P. A. *J. Mater. Chem.* **2001**, *11*, 2253-2261.
- (16) Shi, G.; Yu, B.; Xue, G.; Jin, S.; Li, C. *J. Chem. Soc., Chem. Commun.* **1994**, 2549-2550.
- (17) Arbizzani, C.; Gallazzi, M. C.; Mastragostino, M.; Rossi, M.; Soavi, F. *Electrochem. Commun.* **2001**, *3*, 16-19.
- (18) Fusalba, F.; Ho, H. A.; Breau, L.; Belanger, D. *Chem. Mater.* **2000**, *12*, 2581-2589.
- (19) Soudan, P.; Lucas, P.; Ho, H. A.; Jobin, D.; Breau, L.; Belanger, D. *J. Mater. Chem.* **2001**, *11*, 773-782.

- (20) Fichou, D. *J. Mater. Chem.* **2000**, *10*, 571-588.
- (21) Anquetil, P. A.; Hunter, I.; Madden, J. D.; Madden, P. G.; Pullen, A.; Swager, T. M.; Xu, B.; Yu, H.-H.; (Massachusetts Institute of Technology, USA). Application: WO2003101955, 2003; 135 pp.
- (22) Gadisa, A.; Workalemahu, B. *Synth. Met.* **2002**, *129*, 179-185.
- (23) Roncali, J. *Chem. Rev.* **1997**, *97*, 173-205.
- (24) Sato, M.; Tanaka, S.; Kaeriyama, K. *Synth. Met.* **1986**, *14*, 279 - 288.
- (25) Cutler, C. A., *Electrochemical and photoelectrochemical studies of functionalised polythiophenes*. PhD Thesis, Department of Chemistry, University of Wollongong, **2000**.
- (26) McQuade, D. T.; Pullen, A. E.; Swager, T. M. *Chem. Rev.* **2000**, *100*, 2537-2574.
- (27) McCullough, R. D. *Adv. Mater.* **1998**, *10*, 93-116.
- (28) Roncali, J. *J. Mater. Chem.* **1999**, *9*, 1875-1893.
- (29) Fuchiwaki, M.; Takashima, W.; Pandey, S. S.; Kaneto, K. *Synth. Met.* **2003**, *135-136*, 135-136.
- (30) Epstein, A. J.; Yang, Y. *MRS Bull.* **1997**, *22*, 13-14.
- (31) Pratt, C. *Conducting polymers*. Electronic source. **2002**.
- (32) Child, A. D.; Sankaran, B.; Larmat, F.; Reynolds, J. R. *Macromolecules* **1995**, *28*, 6571-6578.
- (33) Pron, A.; Rannou, P. *Prog. Polym. Sci.* **2001**, *27*, 135-190.
- (34) Pickup, P. G. In *Modern aspects of electrochemistry*; White, R. E., Ed.; Kluwer Academic/Plenum Publishers: New York, 1999; Vol. 33, pp 549-597.
- (35) Swager, T. M. *Acc. Chem. Res.* **1998**, *31*, 201-207.
- (36) Roncali, J. *Annu. Rep. Prog. Chem., Sect. C, Phys. Chem.* **1999**, *95*, 47-88.
- (37) Elandaloussi, E. H.; Frere, P.; Richomme, P.; Orduna, J.; Garin, J.; Roncali, J. *J. Am. Chem. Soc.* **1997**, *119*, 10774-10784.
- (38) Baughman, R. H. *Synth. Met.* **1996**, *78*, 339-353.
- (39) Shirota, Y. *J. Mater. Chem.* **2000**, *10*, 1-25.
- (40) Gallazzi, M. C.; Toscano, F.; Paganuzzi, D.; Bertarelli, C.; Farina, A.; Zotti, G. *Macromol. Chem. and Phys.* **2001**, *202*, 2074-2085.
- (41) Elsenbaumer, R. L.; Jen, K. Y.; Miller, G. G.; Shacklette, L. W. *Synth. Met.* **1987**, *18*, 277-282.

- (42) Chen, J.; Burrell, A. K.; Campbell, W. M.; Officer, D. L.; Too, C. O.; Wallace, G. G. *Electrochim. Acta* **2004**, *49*, 329-337.
- (43) Waltman, R. J.; Bargon, J.; Diaz, A. F. *J. Phys. Chem.* **1983**, *87*, 1459-1463.
- (44) Wang, C.; Benz, M. E.; LeGoff, E.; Schindler, J. L.; Allbritton-Thomas, J.; Kannewurf, C. R.; Kanatzidis, M. G. *Chem. Mater.* **1994**, *6*, 401-411.
- (45) Loewe, R. S.; Ewbank, P. C.; Liu, J.; Zhai, L.; McCullough, R. D. *Macromolecules* **2001**, *34*, 4324-4333.
- (46) Roncali, J. *Acc. Chem. Res.* **2000**, *33*, 147-156.
- (47) Tourillon, G. *Handbook of conducting polymers*; Marcel Dekker, Inc.: New York, 1986; Vol. 1.
- (48) Smith, J. R.; Cox, P. A.; Campbell, S. A.; Ratcliffe, N. M. *J. Chem. Soc., Faraday Trans.* **1995**, *91*, 2331-2338.
- (49) Krische, B.; Zagorska, M. *Synth. Met.* **1989**, *28*, C263-C268.
- (50) Jerome, C.; Maertens, C.; Mertens, M.; Jerome, R.; Quattrocchi, C.; Lazzaroni, R.; Bredas, J. L. *Synth. Met.* **1996**, *83*, 103-109.
- (51) Smith, J. R.; Campbell, S. A.; Ratcliffe, N. M. *Bull. Electrochem.* **1995**, *11*, 378-386.
- (52) Higgins, T. B.; Mirkin, C. A. *Chem. Mater.* **1998**, *10*, 1589-1595.
- (53) Wei, Y.; Tian, J. *Macromolecules* **1993**, *26*, 457-463.
- (54) Visy, C.; Lukkari, J.; Kankare, J. *Macromolecules* **1994**, *27*, 3322-3329.
- (55) Demanze, F.; Yassar, A.; Garnier, F. *Macromolecules* **1996**, *29*, 4267-4273.
- (56) Randriamahazaka, H.; Noel, V.; Chevrot, C. *J. Electroanal. Chem.* **2002**, *521*, 107-116.
- (57) McCullough, R. D.; Tristram-Nagle, S.; Williams, S. P.; Lowe, R. D.; Jayaraman, M. *J. Am. Chem. Soc.* **1993**, *115*, 4910-4911.
- (58) McCullough, R. D.; Williams, S. P.; Tristram-Nagle, S.; Jayaraman, M.; Ewbank, P. C.; Miller, L. *Synth. Met.* **1995**, *69*, 279-282.
- (59) Daoust, G.; Leclerc, M. *Macromolecules* **1991**, *24*, 455-459.
- (60) Krische, B.; Zagorska, M. *Synth. Met.* **1989**, *33*, 257-267.
- (61) Chandrasekhar, P. *Conducting polymers: fundamentals and applications*; Kluwer Academic Publishers: Boston, 1999.
- (62) Gallazzi, M. C.; Castellani, L.; Marin, R. A.; Zerbi, G. *J. Polym. Sci., Part A: Polym. Chem.* **1993**, *31*, 3339-3349.
- (63) Xu, J. M.; Chan, H. S. O.; Ng, S. C.; Chung, T. S. *Synth. Met.* **2002**, *132*, 63-69.

- (64) McCarley, T. D.; Noble, C. O.; DuBois, C. J., Jr.; McCarley, R. L. *Macromolecules* **2001**, *34*, 7999-8004.
- (65) Leclerc, M.; Martinez Diaz, F.; Wegner, G. *Makromol. Chem.* **1989**, *190*, 3105-3116.
- (66) Johansson, T.; Mammo, W.; Andersson, M. R.; Inganaes, O. *Chem. Mater.* **1999**, *11*, 3133-3139.
- (67) Martinez, F.; Neculqueo, G. *Int. J. Polym. Mater.* **1999**, *44*, 265-274.
- (68) Kowalik, J.; Tolbert, L. M.; Narayan, S.; Abhiraman, A. S. *Macromolecules* **2001**, *34*, 5471-5479.
- (69) Watson, K. J.; Wolfe, P. S.; Nguyen, S. T.; Zhu, J.; Mirkin, C. A. *Macromolecules* **2000**, *33*, 4628-4633.
- (70) Andersson, M. R.; Selse, D.; Berggren, M.; Jaervinen, H.; Hjertberg, T.; Inganaes, O.; Wennerstroem, O.; Oesterholm, J. E. *Macromolecules* **1994**, *27*, 6503-6506.
- (71) Stein, P. C.; Botta, C.; Bolognesi, A.; Catellani, M. *Synth. Met.* **1995**, *69*, 305-306.
- (72) Waltman, R. J.; Bargon, J. *Can. J. Chem.* **1986**, *64*, 76-95.
- (73) Zotti, G.; Marin, R. A.; Gallazzi, M. C. *Chem. Mater.* **1997**, *9*, 2945-2950.
- (74) Irvin, J. A.; Reynolds, J. R. *Polymer* **1998**, *39*, 2339-2347.
- (75) Casalbore-Miceli, G.; Gallazzi, M. C.; Zecchin, S.; Camaioni, N.; Geri, A.; Bertarelli, C. *Adv. Funct. Mater.* **2003**, *13*, 307-312.
- (76) Bredas, J. L.; Street, G. B.; Themans, B.; Andre, J. M. *J. Chem. Phys.* **1985**, *83*, 1323-1329.
- (77) Bredas, J. L. *J. Chem. Phys.* **1985**, *82*, 3808-3811.
- (78) Burrell, A. K.; Chen, J.; Collis, G. E.; Grant, D. K.; Officer, D. L.; Too, C. O.; Wallace, G. G. *Synth. Met.* **2003**, *135-136*, 97-98.
- (79) Cutler, C. A.; Burrell, A. K.; Officer, D. L.; Too, C. O.; Wallace, G. G. *Synth. Met.* **2002**, *128*, 35-42.
- (80) Collis, G. E.; Burrell, A. K.; Scott, S. M.; Officer, D. L. *J. Org. Chem.* **2003**, *68*, 8974-8983.
- (81) Roncali, J. *J. Mater. Chem.* **1997**, *7*, 2307-2321.
- (82) Giaccai, J.; Killian, J. G.; Gofer, Y.; Poehler, T. O.; Searson, P. C. *Corrosion in Advanced Materials and Systems, Proceedings of Corrosion'98 Research Topical Symposium, San Diego, Mar. 22-27, 1998*, 15-23.
- (83) Martinez, F.; Retuert, J.; Neculqueo, G. *Int. J. Polym. Mater.* **1995**, *28*, 51-59.
- (84) Searson, P.; Killian, J. G.; Sarker, H.; Giaccai, J.; Gofer, Y.; Poehler, T. O.; (Johns Hopkins University, USA). Application: US5733683, 1998, 13 pp.

- (85) Kinbara, E.; Kunugi, Y.; Harima, Y.; Yamashita, K. *Synth. Met.* **2000**, *114*, 295-303.
- (86) Ferraris, J. P.; Eissa, M. M.; Brotherston, I. D.; Loveday, D. C. *Chem. Mater.* **1998**, *10*, 3528-3535.
- (87) Rudge, A.; Raistrick, I.; Gottesfeld, S.; Ferraris, J. P. *Electrochim. Acta* **1994**, *39*, 273-287.
- (88) Smith, J. R.; Campbell, S. A.; Ratcliffe, N. M.; Dunleavy, M. *Synth. Met.* **1994**, *63*, 233-243.
- (89) Welzel, H.-P.; Kossmehl, G.; Engelmann, G.; Plieth, W. *Eur. Polym. J.* **1997**, *33*, 299-301.
- (90) Greenwald, Y.; Cohen, G.; Poplawski, J.; Ehrenfreund, E.; Speiser, S.; Davidov, D. *J. Am. Chem. Soc.* **1996**, *118*, 2980-2984.
- (91) Cutler, C. A.; Burrell, A. K.; Collis, G. E.; Dastoor, P. C.; Officer, D. L.; Too, C. O.; Wallace, G. G. *Synth. Met.* **2001**, *123*, 225-237.
- (92) Collis, G. E.; Burrell, A. K.; Officer, D. L. *Tetrahedron Lett.* **2001**, *42*, 8733-8735.
- (93) Mukoyama, I.; Aoki, K.; Chen, J. *J. Electroanal. Chem.* **2002**, *531*, 133-139.
- (94) Feldhues, M.; Kaempf, G.; Litterer, H.; Mecklenburg, T.; Wegener, P. *Synth. Met.* **1989**, *28*, C487-C493.
- (95) McCullough, R. D.; Lowe, R. D. *J. Chem. Soc., Chem. Commun.* **1992**, 70-72.
- (96) Liu, J.; Loewe, R. S.; McCullough, R. D. *Macromolecules* **1999**, *32*, 5777-5785.
- (97) McCullough, R. D.; Lowe, R. D.; Jayaraman, M.; Anderson, D. L. *J. Org. Chem.* **1993**, *58*, 904-912.
- (98) Gallazzi, M. C.; Bertarelli, C.; Montoneri, E. *Synth. Met.* **2002**, *128*, 91-95.
- (99) Zotti, G.; Gallazzi, M. C.; Zerbi, G.; Meille, S. V. *Synth. Met.* **1995**, *73*, 217-225.
- (100) Ono, N.; Okumura, H.; Murashima, T. *Heteroat. Chem.* **2001**, *12*, 414-417.
- (101) Luo, Y.; Ruud, K.; Norman, P.; Jonsson, D.; Agren, H. *J. Phys. Chem. B* **1998**, *102*, 1710-1712.
- (102) Elandalousi, E. H.; Frere, P.; Roncali, J. *Chem. Commun. (Cambridge)* **1997**, 301-302.
- (103) Wagner, P.; Aubert, P.-H.; Lutsen, L.; Vanderzande, D. *Electrochem. Commun.* **2002**, *4*, 912-916.
- (104) Henckens, A.; Knipper, M.; Polec, I.; Manca, J.; Lutsen, L.; Vanderzande, D. *Thin Solid Films* **2004**, *451-452*, 572-579.
- (105) Videlot, C.; Ackermann, J.; Blanchard, P.; Raimundo, J.-M.; Frere, P.; Allain, M.; de Bettignies, R.; Levillain, E.; Roncali, J. *Adv. Mater.* **2003**, *15*, 306-310.

- (106) Jestin, I.; Frere, P.; Blanchard, P.; Roncali, J. *Angew. Chem., Int. Ed.* **1998**, *37*, 942-945.
- (107) Levillain, E.; Roncali, J. *J. Am. Chem. Soc.* **1999**, *121*, 8760-8765.
- (108) Montenegro, M. I.; Queiros, M. A.; Daschbach, J. L., Eds. *Microelectrodes: theory and applications*; Kluwer Academic Publishers: London, 1991; Vol. 197.
- (109) Michalitsch, R.; El Kassmi, A.; Yassar, A.; Lang, P.; Garnier, F. *J. Electroanal. Chem.* **1998**, *457*, 129-139.
- (110) Sezai Sarac, A.; Evans, U.; Serantoni, M.; Clohessy, J.; Cunnane, V. J. *Surf. Coat. Technol.* **2004**, *182*, 7-13.
- (111) Giroto, E. M.; Casalbore-Miceli, G.; Camaioni, N.; de Paoli, M. A.; Fichera, A. M.; Belobrveckaja, L.; Gallazzi, M. C. *J. Mater. Chem.* **2001**, *11*, 1072-1076.
- (112) Schenning, A. P. H. J.; Kilbinger, A. F. M.; Biscarini, F.; Cavallini, M.; Cooper, H. J.; Derrick, P. J.; Feast, W. J.; Lazzaroni, R.; Leclere, P.; McDonell, L. A.; Meijer, E. W.; Meskers, S. C. J. *J. Am. Chem. Soc.* **2002**, *124*, 1269-1275.
- (113) Smith, J. R.; Ratcliffe, N. M.; Campbell, S. A. *Synth. Met.* **1995**, *73*, 171-182.
- (114) Sumi, N.; Nakanishi, H.; Ueno, S.; Takimiya, K.; Aso, Y.; Otsubo, T. *Bull. Chem. Soc. Jpn.* **2001**, *74*, 979-988.
- (115) Folch, I.; Borros, S.; Amabilino, D. B.; Veciana, J. *J. Mass Spectrom.* **2000**, *35*, 550-555.
- (116) Siuzdak, G. *Mass spectroscopy for biotechnology*; Academic Press: San Diego, 1996.
- (117) Byrd, H. C. M.; McEwen, C. N. *Anal. Chem.* **2000**, *72*, 4568-4576.
- (118) Chaudhary, A. K.; Critchley, G.; Diaf, A.; Beckman, E. J.; Russell, A. J. *Macromolecules* **1996**, *29*, 2213-2221.
- (119) Dey, M.; Castoro, J. A.; Wilkins, C. L. *Anal. Chem.* **1995**, *67*, 1575-1579.
- (120) Montaudo, G.; Garozzo, D.; Montaudo, M. S.; Puglisi, C.; Samperi, F. *Macromolecules* **1995**, *28*, 7983-7989.
- (121) Nielen, M. W. F. *Mass Spectrom. Rev.* **1999**, *18*, 309-344.
- (122) Axelsson, J.; Scrivener, E.; Haddleton, D. M.; Derrick, P. J. *Macromolecules* **1996**, *29*, 8875-8882.
- (123) De Paoli, M.-A.; Nogueira, A. F.; Machado, D. A.; Longo, C. *Electrochim. Acta* **2001**, *46*, 4243-4249.
- (124) Leclerc, M. *Can. Chem. News* **2001**, *53*, 26-27.
- (125) Skompska, M.; Szkurlat, A. *Electrochim. Acta* **2001**, *46*, 4007-4015.

- (126) Lee, W. J.; Kim, Y. J.; Jung, M. O.; Kim, D. H.; Cho, D. L.; Kaang, S. *Synth. Met.* **2001**, *123*, 327-333.
- (127) Trznadel, M.; Pron, A.; Zagorska, M.; Chrzaszcz, R.; Pielichowski, J. *Macromolecules* **1998**, *31*, 5051-5058.
- (128) Gambhir, S.; Wagner, K.; Officer, D. L. *Synth. Met.* **2005**, *Submitted for Publication*.
- (129) Doshi, J.; Reneker, D. H. *J. Electrostatics* **1995**, *35*, 151-160.
- (130) Fong, H.; Chun, I.; Reneker, D. H. *Polymer* **1999**, *40*, 4585-4592.
- (131) Granstrom, M.; Petritsch, K.; Arias, A. C.; Lux, A.; Andersson, M. R.; Friend, R. H. *Nature (London)* **1998**, *395*, 257-260.
- (132) Wallace, G. G.; Too, C. O.; Officer, D. L.; Dastoor, P. C. *MRS Bull.* **2005**, *30*, 46-49.
- (133) Lemaire, M.; Garreau, R.; Delabouglise, D.; Roncali, J.; Youssoufi, H. K.; Garnier, F. *New J. Chem.* **1990**, *14*, 359-364.
- (134) Andreani, F.; Salatelli, E.; Lanzi, M. *Polymer* **1996**, *37*, 661-665.
- (135) Amou, S.; Haba, O.; Shirato, K.; Hayakawa, T.; Ueda, M.; Takeuchi, K.; Asai, M. *J. Polym. Sci., Part A: Polym. Chem.* **1999**, *37*, 1943-1948.
- (136) Laakso, J.; Jarvinen, H.; Skagerberg, B. *Synth. Met.* **1993**, *55*, 1204-1208.
- (137) Bauer, B. J.; Flynn, K. M.; Vogt, B. D. *Polym. Mater. Sci. Eng.* **2004**, *90*, 457-458.
- (138) Bier, M. E. *Polym. Mater. Sci. Eng.* **2003**, *88*, 17-18.
- (139) Grant, D. K.; Jolley, K. W.; Officer, D. L.; Gordon, K. C.; Clarke, T. M. *Org. Biomol. Chem.* **2005**, *3*, 2008-2015.
- (140) Clarke, T. M.; Gordon, K. C.; Officer, D. L.; Grant, D. K. *Manuscript in preparation*.
- (141) Audebert, P.; Catel, J. M.; Le Coustumer, G.; Duchenet, V.; Hapiot, P. *J. Phys. Chem. B* **1998**, *102*, 8661-8669.
- (142) Wei, Y.; Chan, C. C.; Tian, J.; Jang, G. W.; Hsueh, K. F. *Chem. Mater.* **1991**, *3*, 888-897.
- (143) Xu, Z. G.; Horowitz, G. *J. Electroanal. Chem.* **1992**, *335*, 123-134.
- (144) Roncali, J.; Gorgues, A.; Jubault, M. *Chem. Mater.* **1993**, *5*, 1456-1464.
- (145) Harada, H.; Fuchigami, T.; Nonaka, T. *J. Electroanal. Chem. Interfacial Electrochem.* **1991**, *303*, 139-150.
- (146) MacDiarmid, A. G.; Zheng, W. *MRS Bull.* **1997**, *22*, 24-30.
- (147) Pringle, J. M.; Forsyth, M.; MacFarlane, D. R.; Wagner, K.; Hall, S. B.; Officer, D. L. *Polymer* **2005**, *46*, 2047-2058.

- (148) Rapta, P.; Petr, A.; Dunsch, L. *Synth. Met.* **2001**, *119*, 409-410.
- (149) Zotti, G.; Schiavon, G. *Synth. Met.* **1989**, *31*, 347-357.
- (150) Yoshino, K.; Onoda, M.; Manda, Y.; Yokoyama, M. *Jpn. J. Appl. Phys., Part 2.* **1988**, *27*, L1606-L1608.
- (151) Zotti, G.; Schiavon, G.; Zecchin, S. *Synth. Met.* **1995**, *72*, 275-281.
- (152) Domagala, W.; Lapkowski, M.; Guillerez, S.; Bidan, G. *Electrochim. Acta* **2003**, *48*, 2379-2388.
- (153) Sun, L.; Goerner, H. *J. Phys. Chem.* **1993**, *97*, 11186-11193.
- (154) Wagner, P.; Officer, D. L. *Synth. Met.* **2005**, Accepted for publication.
- (155) Clarke, T. M. **2004**, Unpublished work.
- (156) Wagner, P.; Ballantyne, A. M.; Jolley, K. W.; Officer, D. L. *Manuscript in preparation* **2005**.
- (157) Wagner, P.; Officer, D. L. **2004**, Unpublished work.
- (158) Kitani, A.; Yano, J.; Sasaki, K. *Chem. Lett.* **1984**, 1565-1566.
- (159) Yassar, A.; Roncali, J.; Garnier, F. *Macromolecules* **1989**, *22*, 804-809.
- (160) Casado, J.; Miller, L. L.; Mann, K. R.; Pappenfus, T. M.; Kanemitsu, Y.; Orti, E.; Viruela, P. M.; Pou-Amerigo, R.; Hernandez, V.; Lopez Navarrete, J. T. *J. Phys. Chem. B* **2002**, *106*, 3872-3881.
- (161) Andersson, M. R.; Mammo, W.; Olinga, T.; Svermsson, M.; Theander, M.; Inganas, O. *Synth. Met.* **1999**, *101*, 11-12.
- (162) Casalbore-Miceli, G.; Camaioni, N.; Gallazzi, M. C.; Albertin, L.; Fichera, A. M.; Geri, A.; Girotto, E. M. *Synth. Met.* **2001**, *125*, 307-311.
- (163) Yamamoto, T.; Kashiwazaki, A.; Kato, K. *Makromol. Chem.* **1989**, *190*, 1649-1654.
- (164) Bredas, J. L.; Silbey, R.; Boudreaux, D. S.; Chance, R. R. *J. Am. Chem. Soc.* **1983**, *105*, 6555-6559.
- (165) Casalbore-Miceli, G.; Camaioni, N.; Catellani, M.; Gallazzi, M. C. *Synth. Met.* **1998**, *95*, 211-215.
- (166) Rasch, B.; Vielstich, W. *J. Electroanal. Chem.* **1994**, *370*, 109-117.
- (167) Kumar, A.; Reynolds, J. R. *Macromolecules* **1996**, *29*, 7629-7630.
- (168) Andersson, M. R.; Pei, Q.; Hjertberg, T.; Inganaes, O.; Wennerstroem, O.; Osterholm, J. E. *Synth. Met.* **1993**, *55*, 1227-1231.
- (169) Kemp, W. *Organic spectroscopy*, 3rd Ed.; Macmillan Education Ltd.: London, 1991.

- (170) Groenendaal, L. B.; Zotti, G.; Aubert, P.-H.; Waybright, S. M.; Reynolds, J. R. *Adv. Mater.* **2003**, *15*, 855-879.
- (171) Eales, R. M.; Hillman, A. R. *J. Mater. Sci.* **1990**, *25*, 3806-3813.
- (172) Tourillon, G.; Garnier, F. J. *Electroanal. Chem. Interfacial Electrochem.* **1984**, *161*, 407-414.
- (173) Cotton, F. A.; Wilkinson, G. *Advanced inorganic chemistry*, 5th Ed.; John Wiley and Sons: New York, 1988.
- (174) Onoda, M.; Okamoto, T.; Tada, K.; Nakayama, H. *Jpn. J. Appl. Phys., Part 2.* **1999**, *38*, L1070-L1072.
- (175) Shaheen, S. E.; Ginley, D. S.; Jabbour, G. E. *MRS Bull.* **1995**, *30*, 10-15.
- (176) Brabec, C. J. *Sol. Energy Mater.* **2004**, *83*, 273-292.
- (177) Green, M. A.; Emery, K.; King, D. L.; Igari, S.; Warta, W. *Progress in Photovoltaics* **2003**, *11*, 347-352.
- (178) Janssen, R. A. J.; Hummelen, J. C.; Sariciftci, N. S. *MRS Bull.* **2005**, *30*, 33-36.
- (179) Gratzel, M. J. *Photochem. Photobiol., A* **2004**, *164*, 3-14.
- (180) Too, C. O.; Wallace, G. G.; Burrell, A. K.; Collis, G. E.; Officer, D. L.; Boge, E. W.; Brodie, S. G.; Evans, E. J. *Synth. Met.* **2001**, *123*, 53-60.
- (181) Brabec, C. J.; Sariciftci, S. N. *Monatsh. Chem.* **2001**, *132*, 421-431.
- (182) Li, A. D. Q.; Li, L. S. *J. Phys. Chem. B* **2004**, *108*, 12842-12850.
- (183) Ho, P. K. H.; Thomas, D. S.; Friend, R. H.; Tessler, N. *Science (Washington, D. C.)* **1999**, *285*, 233-236.
- (184) Skotheim, T. A.; Feldberg, S. W.; Armand, M. B. *Journal de Physique, Colloque* **1983**, 615-620.
- (185) Wallace, G. G.; Dastoor, P. C.; Officer, D. L.; Too, C. O. *Chem. Innovation* **2000**, *30*, 14-22.
- (186) Campbell, W. M. **2005**. Personal communication.
- (187) Spinks, G. M.; Liu, L.; Wallace, G. G.; Zhou, D. *Adv. Funct. Mater.* **2002**, *12*, 437-440.
- (188) Otero, T. F.; Sansinena, J. M. *Bioelectrochemistry and Bioenergetics* **1995**, *38*, 411-414.
- (189) Zhou, D.; Wallace, G. G.; Spinks, G. M.; Liu, L.; Cowan, R.; Saunders, E.; Newbold, C. *Synth. Met.* **2003**, *135-136*, 39-40.
- (190) Della Santa, A.; De Rossi, D.; Mazzoldi, A. *Synth. Met.* **1997**, *90*, 93-100.

- (191) Spinks, G. M.; Wallace, G. G.; Liu, L.; Zhou, D. *Macromol. Symp.* **2003**, *192*, 161-169.
- (192) Chen, X.; Xing, K.-Z.; Inganaes, O. *Chem. Mater.* **1996**, *8*, 2439-2443.
- (193) Xi, B.; Truong, V.-T.; Whitten, P.; Ding, J.; Spinks, G. M.; Wallace, G. G. *Proceedings of SPIE-The International Society for Optical Engineering* **2005**, 5649, 137-144.
- (194) Fuchiwaki, M.; Takashima, W.; Kaneto, K. *Molecular Crystals and Liquid Crystals Science and Technology, Section A: Molecular Crystals and Liquid Crystals* **2002**, *374*, 513-520.
- (195) Smela, E. *Advanced Materials (Weinheim, Germany)* **2003**, *15*, 481-494.
- (196) Ding, J.; Liu, L.; Spinks, G. M.; Zhou, D.; Wallace, G. G.; Gillespie, J. *Synth. Met.* **2003**, *138*, 391-398.
- (197) Wu, Y. **2004**. Personal communication.
- (198) Ding, J. PhD Thesis, IPRI, University of Wollongong, **2001**.
- (199) Otero, T. F.; Angulo, E.; Rodriguez, J.; Santamaria, C. *J. Electroanal. Chem.* **1992**, *341*, 369-375.
- (200) Takashima, W.; Dufour, B.; Pandey, S. S.; Kaneto, K.; Pron, A. *Sensors and Actuators, B: Chemical* **2004**, *B99*, 601-607.
- (201) Gofer, Y.; Sarker, H.; Killian, J. G.; Giaccari, J.; Poehler, T. O.; Searson, P. C. *Biomedical instrumentation & technology / Association for the Advancement of Medical Instrumentation* **1998**, *32*, 33-38.
- (202) Rehan, H. H. *J. Power Sources* **2003**, *113*, 57-61.
- (203) MacInnes, D., Jr.; Druy, M. A.; Nigrey, P. J.; Nairns, D. P.; MacDiarmid, A. G.; Hoeger, A. J. *J. Chem. Soc., Chem. Commun.* **1981**, 317-319.
- (204) Misoska, V.; Price, W.; Ralph, S.; Wallace, G. *Synth. Met.* **2001**, *121*, 1501-1502.
- (205) Misoska, V. **2004**. Personal communication.
- (206) Rajesh, B.; Ravindranathan Thampi, K.; Bonard, J. M.; Viswanathan, B. *J. Mater. Chem.* **2000**, *10*, 1757-1759.
- (207) Wilson, J. N.; Bangcuyo, C. G.; Erdogan, B.; Myrick, M. L.; Bunz, U. H. F. *Macromolecules* **2003**, *36*, 1426-1428.
- (208) MacDiarmid, A. G.; Jones, W. E.; Norris, I. D.; Gao, J.; Johnson, A. T.; Pinto, N. J.; Hone, J.; Han, B.; Ko, F. K.; Okuzaki, H.; Llaguno, M. *Synth. Met.* **2001**, *119*, 27-30.
- (209) Kameoka, J.; Craighead, H. G. *Appl. Phys. Lett.* **2003**, *83*, 371-373.